256
3/7/92
Chem Lib
3/7/92

Indian J Chem
JULY 1992

CODEN : IJOCAP 31A(7) 393-482 (1992)
ISSN : 0376-4710

INDIAN JOURNAL OF CHEMISTRY

SECTION A

(Inorganic, Bio-inorganic, Physical, Theoretical & Analytical Chemistry)

6 JUL 1992
C.F.T.R.I. REGIONAL CENTRE

Published by
PUBLICATIONS & INFORMATION DIRECTORATE, CSIR, NEW DELHI
in association with
THE INDIAN NATIONAL SCIENCE ACADEMY, NEW DELHI

GOLDEN OFFER

You can now book your copies of the attractive, lavishly illustrated popular science titles under CSIR GOLDEN JUBILEE SERIES in advance and also get a FREE GIFT

Titles in print

BODY'S BATTLES
By **Bal Phondke**
Unfolds the story of the inner defence organisation of the body, the diversity and specificity of its armament and its round the clock vigil that meets every threat to it.
84 pages;
Price: Rs. 9 (Paperback), Rs. 18 (Hardcover)

MINING THE OCEAN
By **T K S Murthy**
Reveals, the timeless secrets of the seas and the secret bounty that they hold in reserve
106 pages;
Price: Rs. 12 (Paperback), Rs. 20 (Hardcover)

HIS MASTER'S SLAVE
By **Tapan Bhattacharya**
Tells the non-specialist the riveting story of the modern day genie of the bottle, the PC.
88 pages;
Price: Rs. 10 (Paperback), Rs. 18 (Hardcover)

INSIDE STARS
By **Biman Basu**
Provides a privileged glimpse into star nurseries, tracking the luminescent trail to fiery senescence and death of stars to reveal the mysteries and marvels of cosmic drama.
90 pages;
Price: Rs. 10 (Paperback), Rs. 18 (Hardcover)

PLASTIC FEAST
By **Subodh Jawadekar**
Celebrates the dawn of the plastics era and elaborates the myriad ways in which plastics touch our lives. A veritable feast of plastics, very palatable to the readers.
96 pages;
Price: Rs. 12 (Paperback) Rs. 20 (Hardcover)

CERAMICS ARE FOREVER
By **B C Sharma**
Highlights the fascinating versatility of ceramics and provides an excellent close-up of the symbiotic relationship between man and materials.
84 pages;
Price: Rs. 11 (Paperback), Rs. 20 (Hardcover)

Forthcoming Titles

ARTIFICIAL INTELLIGENCE

HARDY COMPOSITES

MAN IN SPACE

MIND MASTER

You may place an order for all 10 titles by sending Rs.120.00 (for paperback) or Rs.200.00 (for Hard-cover) including postage by Demand Draft/M.O. payable to "Publications and Information Directorate". The titles already published will be sent to you as soon as the payment is received and the forthcoming titles will be sent by post as soon as they are published, one every month. With every order you will receive a free gift.

For further information write to:
Sales and Distribution Officer
Publications and Information Directorate
(CSIR)
Dr. K S Krishnan Marg, New Delhi 110 012

INDIAN JOURNAL OF CHEMISTRY

Section A: Inorganic, Bio-inorganic, Physical, Theoretical & Analytical Chemistry

Editorial Board

Prof. R C Mehrotra
Vice-Chancellor
Allahabad University
Allahabad 211 002

Prof. D V S Jain
Chemistry Department
Panjab University
Chandigarh 160 014

Prof. A Chakravorty
Department of Inorganic Chemistry
Indian Association for the
Cultivation of Science
Calcutta 700 032

Prof. V Krishnan
Department of Inorganic
& Physical Chemistry
Indian Institute of Science
Bangalore 560 012

Prof. K K Rohatgi Mukherjee
Department of Chemistry
Jadavpur University
Calcutta 700 032

Dr J P Mittal
Chemistry Division
Bhabha Atomic Research Centre
Bombay 400 085

Prof. S K Rangarajan
Director
Central Electrochemical Research Institute
Karaikudi 623 006

Prof. R C Srivastava
Department of Chemistry
Banaras Hindu University
Varanasi 221 005

Prof. E D Jemmis
Department of Chemistry
University of Hyderabad
Hyderabad 500 134

Dr S K Date
Physical Chemistry Division
National Chemical Laboratory
Pune 411 008

Prof. I Gutman
Faculty of Science
Yu. 34000, Kragujevac
Radoja Domanovica
Yugoslavia

Prof. A B Sannigrahi
Department of Chemistry
IIT, Kharagpur 721 302

Dr D Papousek
J. Heyrovsky Institute
of Physical Chemistry
Prague
Czechoslovakia

Prof. P P Singh
Department of Chemistry
M.D. University
Rohtak 124 001

Dr Pradip K Mascharak
Department of Chemistry
University of California
Santa Cruz
California 65064
USA

Dr G P Phondke Director, PID

Editors : Dr B.C. Sharma, Dr S. Sivakamasundari and Dr S.K. Bhasin
Sr. Scientific Assistant : Geeta Mahadevan

Published by the Publications & Information Directorate (CSIR), Hillside Road, New Delhi 110 012
Director: Dr G P Phondke

Copyright, 1992, by the Council of Scientific & Industrial Research, New Delhi 110 012

The Indian Journal of Chemistry is issued monthly in two sections: A and B. Communications regarding contributions for publication in the journal should be addressed to the Editor, Indian Journal of Chemistry, Publications & Information Directorate, Hillside Road, New Delhi 110 012.

Correspondence regarding subscriptions and advertisements should be addressed to the Sales & Distribution Officer, Publications & Information Directorate, Hillside Road, New Delhi 110 012.

The Publications & Information Directorate (CSIR) assumes no responsibility for the statements and opinions advanced by contributors. The Editorial Board in its work of examining papers received for publication is assisted, in an honorary capacity by a large number of distinguished scientists, working in various parts of India.

Annual Subscription: Rs. 400.00 £ 100.00 $ 150.00; 50% discount admissible to research workers and students and 25% discount to non-research individuals on annual subscription.

Single Copy: Rs. 40.00 £ 10.00 $ 15.00

Payments in respect of subscriptions and advertisements may be sent by cheque, bank draft, money order or postal order marked payable to Publications & Information Directorate, Hillside Road, New Delhi 110 012.

Claims for missing numbers of the journal will be allowed only if received within 3 months of the date of issue of the journal plus the time normally required for postal delivery of the journals and the claim.

AUTHOR INDEX

Aggarwal Sadhana 398
Akhtar Naheed 439
Ansari Mohd Ayub 439
Atamjyot 480

Balaji Rao S B 463
Boricha A B 457
Buigues J Mari 423
Bussiére P 482

Chakravarty Akhil R 408
Chaudhuri Mihir K 466
Chauhan Ashok K S 475

Das Birinchi K 408
Dash Anadi C 412
Domenech R Garcia 423

Ghosh T K 478

Hua Yang 449

Jain Mamta 452
Jaky M 417

Kanta Rao P 436
Khaja Masthan S 436
Krishna Pillay M 427
Kunjappu Joy T 432
Kushwah R S 439

Limaye S N 403
Lin-Wei Li 443
Li-Zhuang Zou 443
Lobana Tarlok S 460

Malik Ashok Kumar 480
Mcwhinnie William R 460
Mehrotra K N 452
Mishra L 393
Mohammed Sk Sazid 412
Mukherjee G N 478
Muthulakshmi B 427

Nair C K K 432
Naixiang Wei 449
Nanje Gowda N M 463

Pastor M Pascual 423
Paul Pradip C 466

Quan Wei 449

Rai A K 469
Ramachandriah G 457
Rama Rao K S 436
Rao A L J 480
Rongshengh Li 449

Sai Prasad P S 436
Saxena A K 469
Saxena M C 403
Saxena S 469
Sharma Rita 475
Sharma S P 398
Sharma V K 398
Shukla S N 472
Singh H 472
Singh P 439
Srivastava R C 393
Srivastava Ramesh C 475
Srivastava V K 472
Szammer J 417

Taqui Khan M M 457

Upadhyay S 393
Upadhyaya M K 472

Vinuesa J Manes 423

Wuyang Zhang 449

Xiao-Ling Wang 443

C.S.I.R. R.L. REGIONAL CENTRE
LUDHIANA-141 000

Indian Journal of Chemistry

Sect. A: Inorganic, Bio-inorganic, Physical, Theoretical & Analytical

VOLUME 31A NUMBER 7 JULY 1992

CONTENTS

Carrier mediated transport through liquid membranes—Studies on transport of nickel ions using tetradentate thioiminato schiff base ligands as carriers 393
L Mishra, S Upadhyay & R C Srivastava*

Thermodynamics of binary mixtures of non-electrolytes: Molar excess Gibbs free energy of mixing 398
V K Sharma*, S P Sharma & Sadhana Aggarwal

An indirect determination of changes in the inter-electronic repulsion (Racah) parameters and magnitude of 'extrastabilisation' in lanthanides 403
S N Limaye & M C Saxena*

Reactivity of PPh_3 toward $Ru_2Cl(O_2CMe)_4$: Synthesis and X-ray crystal structure of $[Ru(O_2CMe)(MeCN)_2(PPh_3)_2](ClO_4)$ 408
Birinchi K Das & Akhil R Chakravarty*

Reactions in micellar solutions: Part 13[1]—Kinetics and mechanism of the reversible complexation of iron(III) by ($\alpha\beta$S) (tetraethylenepentamine) (salicylato)cobalt(III) and *cis*-(ammine)bis(ethylenediamine) (salicylato)cobalt(III) ions in aqueous anionic micellar medium 412
Anadi C Dash* & Sk Sazid Mohammed

Oxidations with permanganate in a strong alkaline medium: Calculation of deprotonation constant 417
J Szammer* & M Jaky

Kinetics of the reaction of hydrazine with 2-hydroxy-1-naphthaldehyde 423
R Garcia Domenech*, J Manes Vinuesa, M Pascual Pastor & J Mari Buigues

Kinetics of reaction of triethylammonium carboxylates with α-halogeno carbonyl compounds in organic solvents: Part 3—Effect of solvents on the reaction of phenacyl bromide with triethylammonium acetate 427
M Krishna Pillay* & B Muthulakshmi

Notes

Binding of surfactants onto DNA and solubilization of DNA/surfactant complex in micelles 432
Joy T Kunjappu & C K K Nair*

Structure sensitive nitrogen chemisorption on supported ruthenium catalysts . . . 436
S Khaja Masthan*, K S Rama Rao, P S Sai Prasad & P Kanta Rao

Studies of inorganic precipitate membrane: Evaluation of membrane selectivity from bi-ionic potential and conductivity measurements 439
R S Kushwah*, Mohd Ayub Ansari, Naheed Akhtar & P Singh

Contd

Study on thermodynamics of aqueous solution of sodium tetraphenylborate . . . 443
Zou Li-Zhuang*, Li Lin-Wei & Wang Xiao-Ling

A new catalyst for the preparation of oleate of glycerin. 449
Li Rongsheng*, Yang Hua, Zhang Wuyang, Wei Quan & Wei Naixiang

Conductivity, viscosity and ultrasonic studies of rubidium caprylate 452
K N Mehrotra* & Mamta Jain

Voltammetry of [Ru(Hedta)(OH_2)] at HMDE 457
M M Taqui Khan*, G Ramachandriah & A B Boricha

Synthesis & multinuclear NMR studies of some 2-(2′-pyridyl)phenyl substituted organotellurium(IV)/mercury(II) compounds 460
Tarlok S Lobana* & William R Mcwhinnie

Synthesis and characterization of Co(II) and Ni(II) complexes of 2-substituted benzimidazoles 463
S B Balaji Rao & N M Nanje Gowda*

Complex peroxovanadates(V) containing chelated cysteinate as the co-ligand: Synthesis and spectroscopic studies 466
Mihir K Chaudhuri* & Pradip C Paul

Seven coordinated organotin(IV) complexes of 1,3-dihydro-1,3-dioxo-α-(substituted)-2H-isoindole-2-acetic acids 469
A K Saxena, S Saxena & A K Rai*

Synthesis, characterization and fungitoxicity of Cu(II), Ni(II), Zn(II), Co(II), Fe(III) and Mn(III) chelates with (5-phenyl-1,3,4-oxadiazol-2-yl)-N-benzoyl dithiocarbamate. 472
H Singh*, V K Srivastava, S N Shukla & M K Upadhyaya

Reactions of triarylantimony with some carboxylic acids 475
Ashok K S Chauhan*, Rita Sharma & Ramesh C Srivastava*

Mixed ligand complex formation of Cu^{2+} ion with 6-aminopenicillanic acid in the presence of bipyridine, glycine and adenine 478
G N Mukherjee* & T K Ghosh

Spectrophotometric determination of molybdenum in steel. 480
Atamjyot, Ashok Kumar Malik & A L J Rao*

Letter to Editor 482
P Bussiére

Authors for correspondence are indicated by (*)

Indian Journal of Chemistry
Vol. 31A, July 1992, pp. 393-397

Carrier mediated transport through liquid membranes – Studies on transport of nickel ions using tetradentate thioiminato schiff base ligands as carriers

L Mishra, S Upadhyay & R C Srivastava*
Chemistry Department, Banaras Hindu University, Varanasi-221 005, India

Received 13 December 1991; accepted 10 March 1992

Experiments have been carried out on the transport of nickel ions through chloroform liquid membrane, containing two new tetradentate thioiminato schiff bases as carriers. Variation of the rate of transport of nickel ion with concentration in the source phase and with the accompanying anion has been studied. The transport rates have been shown to correlate with the Gibb's free energy of hydration of the anion.

Carrier-mediated transport through liquid membranes has been utilized in several cases for separation of ions[1-4]. In the context of these studies liquid membrane is the name given to an organic phase immiscible with two aqueous phases, one containing the metal ion to be transported (source phase) and the other being the receiver phase. The carrier molecule though more or less insoluble in aqueous phase has finite solubility in the organic phase. This technique of carrier mediated transport for separation process draws inspiration from facilitated transport in biology, e.g., oxygen transport through haemoglobin[5].

In the present paper, we report studies on two new tetradentate thioiminato schiff bases as carriers for the transport of nickel ions through chloroform liquid membranes. Since nickel is also a toxic ion the present study appears relevant to pollution abatement in addition to being relevant to separation processes.

Materials and Methods

All the chemicals used in the synthesis of the ligands were of Analar grade. The two ligands, N, N′ hexamethylene-bis (monothioacetylacetonimine) (L_1) and N,N′-octamethylene-bis(monothioacetylacetonimine) (L_2) were synthesized using the method described by Gerlach and Holm[6]. For the synthesis of ligand (L_1), to a 0.05 *M* solution of β-ketoimine (prepared by the condensation of 1.0 mol of hexamethylenediamine and 2.0 mol of acetylacetone) in ethylenediamine and 2.0 mol of acetylacetone) in 100 mL of dichloromethane, 20.0 g (0.1 mol) of triethyloxonium tetrafluoroborate $(Et_3O)^+(BF_4)^-$ in 50 mL dichloromethane was added with stirring under dry nitrogen atmosphere. After stirring for 45 min at room temperature a fine suspension of 10 g (0.16 mol) of sodium hydrogen sulfide prepared in 100 mL of absolute ethanol was slowly added over a period of 1 hr. After filtration, the filtrate was concentrated to dryness *in vacuo* at room temperature. The yellowish crude product thus obtained was crystallized twice from its solution in acetone-water mixture. Similarly, for the synthesis of ligand (L_2) octamethylenediamine was used instead of hexamethylenediamine. Yield of both ligands was about 70%. Analytical data (C, H, N) of the two ligands were found to be satisfactory. IR(KBr pellet) of both the ligands showed bands in the region 1600-1500 cm^{-1} due to $\nu(C=C)$ and $\nu(C=N)$ while $\nu(C-S)+\nu(C-CH_3)$ appeared at 1300 and 840-780 cm^{-1}. NMR spectra of the ligands (in $CDCl_3$) showed signals at δ 2.1 and 2.5 ppm due to protons of CH_3 groups adjacent to nitrogens and sulphurs respectively. A triplet at δ 3.4 ppm corresponding to CH_2 protons arose due to $HN-CH_2$ spin coupling; a singlet due to CH protons appeared at δ 6.2 ppm and a broad signal appeared at δ 14.3 ppm which is assigned to SH protons.

The analytical and spectral data are consistent with the structures of the ligands shown in Fig. 1.

Apparatus and procedure

The all-glass transport cell used in the present studies was quite similar to the one used by Lamb

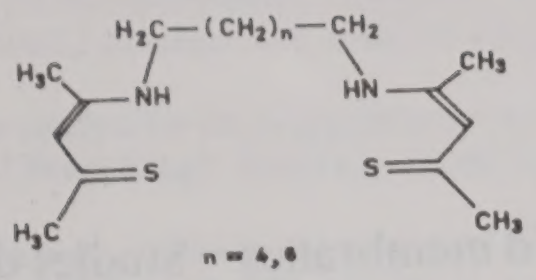

Fig. 1 – Structures of carrier ligands (for ligand L_1, n = 4, for ligand L_2, n = 6)

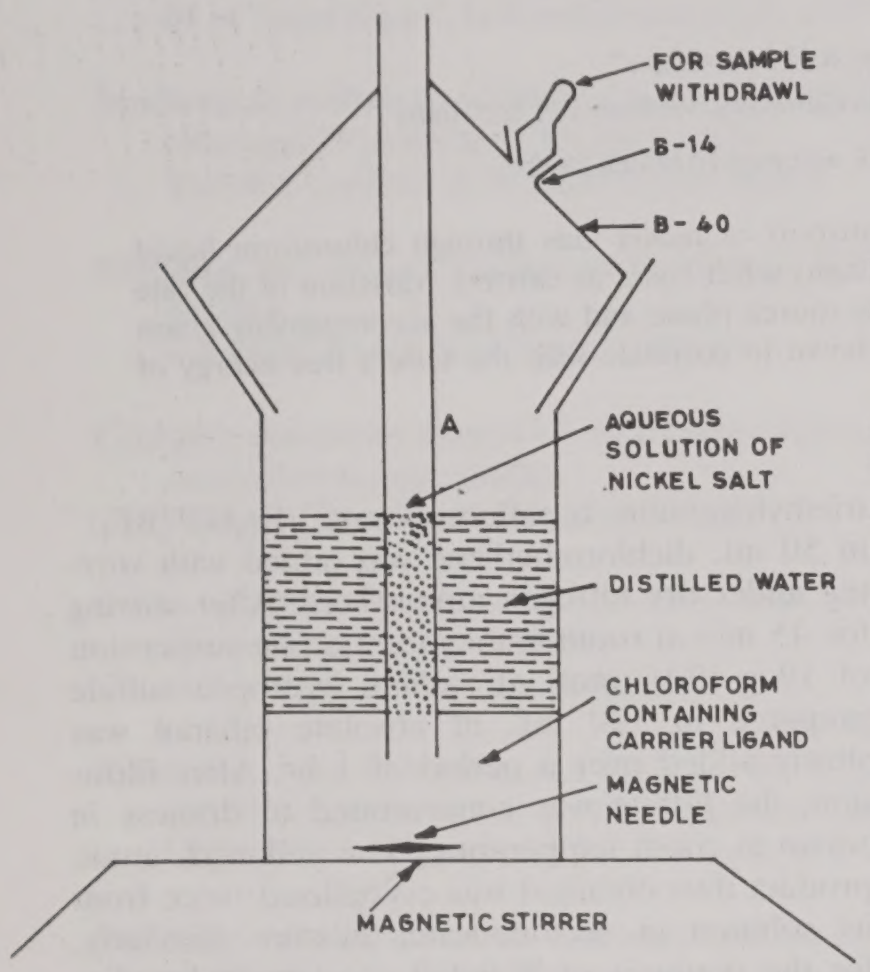

Fig. 2 – Transport cell

et al.[2] and is depicted in Fig. 2. A chloroform solution (20 ml) containing 10^{-3} *M* ligand was placed at the bottom of the cell. The aqueous solution of nickel salt of desired concentration was placed over the chloroform solution in the middle tube (A) of the transport cell. Distilled water was filled in the rest of the portion of the transport cell such that its level was same as that of the aqueous solution in tube (A). The chloroform solution, the aqueous salt solution in tube (A) and the distilled water outside the tube (A) will be referred to as liquid membrane phase, the source phase and the receiver phase respectively in the text of this paper. The liquid membrane phase was well stirred using a magnetic stirrer.

The experimental procedure was simple. Known volumes (1 mL) were withdrawn from the receiver phase at known intervals of time and analysed for the metal ion using atomic absorption

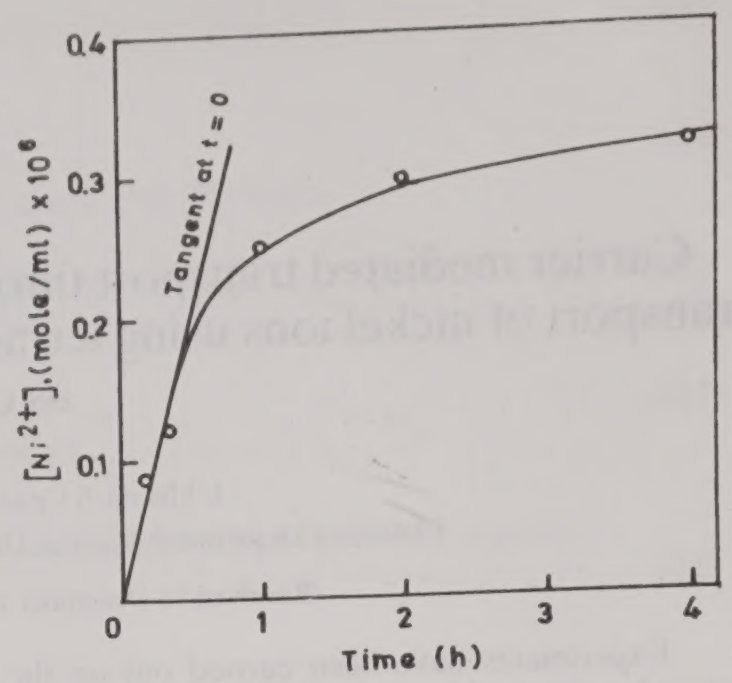

Fig. 3 – A typical plot showing variation in the concentration of Ni^{2+} in the receiver phase with time in the case of nickel chloride, (source phase concentration = 0.1 *M*)

spectrophotometer (Perkin Elmer-373). In order to study the effect of anions on transport, nickel salts (all Analar grade) with different anions were experimented with. For each metal salt control experiments were also performed in which everything was the same except that no carriers were taken. All experiments were carried out at constant temperature (30°C) obtained using a thermostat.

Results and Discussion

The initial rate of transport of the metal ion was very fast – within a few minutes one could see the change in colour of the receiver phase. As the time elapsed the rate of transport slowed down. This trend (shown in Fig. 3) can be understood in terms of the postulated mechanism[2] of the carrier mediated transport. The whole process is visualised to consist of four steps[2]: (i) cation in the source phase moves into the membrane phase accompanied by the anion and is complexed by the carrier ligand; (ii) complex-anion pair moves across the membrane; (iii) decomplexation takes place at the receiver phase/membrane phase interface and the cation and anion are released to the receiver phase and (iv) carrier ligand returns to repeat the cycle. From this postulated mechanism it is apparent that as the concentration of the metal ion in the receiver phase increases, the transport of the metal in the reverse direction also sets in, diminishing the net rate of transport of the metal ion from the source phase to the receiver phase. In the present study, therefore, transport data have been discussed in terms of initial rates of transport (J_c) which were determined from the

Table 1 – Variation of nickel ion transport rate with salt concentration

Sample	Initial conc. in source phase, C (M)	J_c (mol/h) $\times 10^6$
	With carrier ligand L	
$Ni(NO_3)_2$	2.0	6.720
	1.0	4.560
	0.5	3.172
$NiCl_2$	2.0	5.380
	1.0	3.973
	0.5	0.600
$NiSO_4$	2.0	2.044
	1.0	1.433
	0.5	0.191
	With carrier ligand L_2	
$Ni(NO_3)_2$	2.0	74.151
	1.0	24.336
	0.5	6.032
	0.1	0.329
	0.01	0.038
$NiCl_2$	2.0	23.477
	1.0	11.860
	0.5	4.540
	0.1	0.320
	0.01	0.016
$NiSO_4$	2.0	11.380
	1.0	4.241
	0.5	3.859
	0.1	0.167
	0.01	0.015

tangent at time $t=0$ in the plots of concentration (in the receiver phase) versus time (t) (Fig. 3).

The initial transport rates J_c of nickel ion from the source phase to the receiver phase through the liquid membrane phase at various source phase concentrations for both carriers are recorded in Table 1. In the control experiments no detectable transport of the metal ion was observed whereas in the presence of carriers, the transport was substantial (Table 1). A scrutiny of the values of J_c for the same anion and the same concentration in the source phase reveals that the carrier L_2 transports the nickel ions faster in the comparison to carrier L_1.

In view of the postulated mechanism[2] the rate of transport, J_c should depend on (i) the ease of

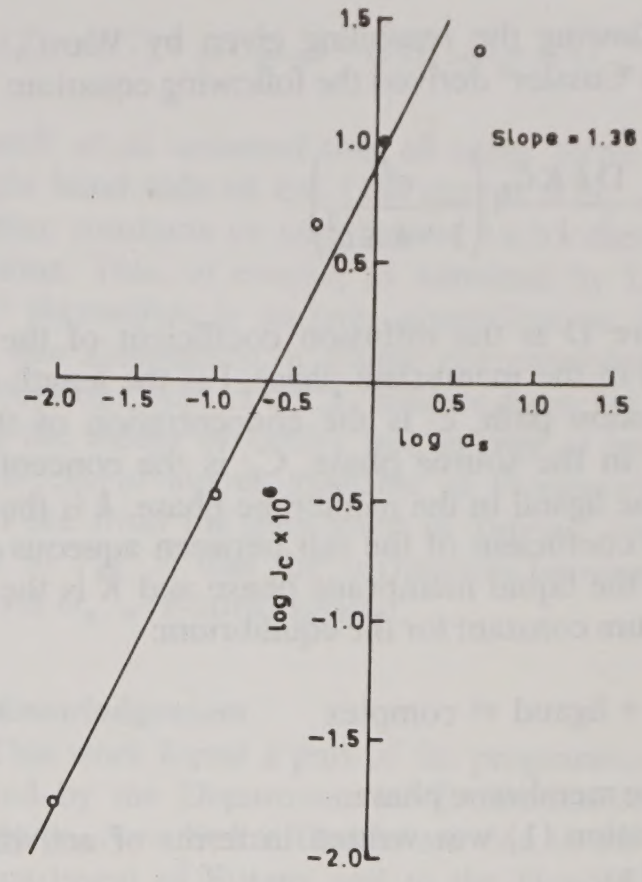

Fig. 4 – Variation of $\log J_c$ with $\log a_s$ for nickel chloride using carrier ligand L_2 (10^{-3} M) in the membrane phase. The activity coefficients values were taken from reference 11.

complexation (determined by the rates) of the metal ion with the carrier ligand, (ii) the rate of transport of the carrier-metal complex from the source phase boundary to the receiver phase boundary and (iii) the rate of decomplexation at the receiver phase boundary. Since the two binding sites between which the metal ion is to be held are more far apart in carrier L_2 than in carrier L_1 and also because carrier L_2 is heavier than carrier L_1, the factors (i) and (ii) are less favourable for carrier L_2. However, the factor (iii) appears to be more in favour of carrier L_2. Thus, it is the decomplexation factor which, at least in the present case, appears to determine the rate at which a carrier would transport the metal ion.

The transport rate J_c in case of both the carriers was found to be a function of salt concentration in the source phase (Table 1). The plots of $\log J_c$ versus $\log a_s$, a_s being the activity of the salt in source phase, were found to be straight lines.

A typical straight line plot of $\log J_c$ versus $\log a_s$ is shown in Fig. 4. There is one major point of difference between these plots (Fig. 4) and the corresponding plots obtained by Lamb *et al.*[2]: the slope in the former case is less than 2 which is equal to 2 in the latter case. The value of the slope equal to 2 was rationalized by Lamb *et al.*[2] using the theoretical treatment given by Ward[7] and Reusch and Cussler[8].

Following the reasoning given by Ward[7], Reusch & Cussler[8] derived the following equation:

$$J_c = \frac{DkKC_L}{l}\left(\frac{c_s^2}{1+kKc_s^2}\right) \quad \ldots (1)$$

where D is the diffusion coefficient of the complex in the membrane phase, l is the length of the diffusion path, c_s is the concentration of the cation in the source phase, C_L is the concentration of the ligand in the membrane phase, k is the partition coefficient of the salt between aqueous phase and the liquid membrane phase and K is the equilibrium constant for the equilibrium:

Salt + ligand ⇌ complex

in the membrane phase.
Equation (1) was written in terms of activities to read as,

$$J_c = \frac{DkKC_L}{l}\left(\frac{a_s^2}{1+kKa_s^2}\right) \quad \ldots (2)$$

If kKa_s^2 or $kKc_s^2 << 1$ ... (3)

Eqs (1) and)2) reduce to

$$J_c = \frac{DkKC_L}{l}c_s^2 \quad \ldots (4)$$

and $$J_c = \frac{DkKC_L}{l}a_s^2 \quad \ldots (5)$$

respectively. Thus plot of $\log J_c$ against $\log a_s$ should be a straight line of slope equal to 2.

Neither in the present experiments nor in the experiments of Lamb *et al.*[2] the movement of the ligand and of the complex from the source phase/membrane phase interface to the receiver phase/membrane phase interface and in the reverse direction could be diffusion controlled because the liquid membrane phase was well stirred. Since we chose higher concentration ranges than that in the experiments of Lamb *et al.*[2] the condition (3) in our case may not be valid. Further, the theoretical treatment of Reusch and Cussler[8] is restricted to uni-univalent electrolytes only which was not the case in the present study. The value of less than 2 of the slope of $\log J_c$ versus $\log a_s$ plots obtained in the present study could possibly be because of these reasons.

Table 2 – Data showing the variation of J_c with anion types and their free energies of hydration ($\Delta G_{g\to w^A}$)

Carrier ligand	Anion type	Conc. in source phase (M)	$-\Delta G_{g\to w^A}$* (kcal/mol)	$(\log J_c)\times 10^6$
L_1	NO_3^-	1.0	69.5	0.65
	Cl^-	1.0	75.8	0.59
	SO_4^{2-}	1.0	238.7	0.15
L_2	NO_3^-	1.0	69.5	1.38
	Cl^-	1.0	75.8	1.07
	SO_4^{2-}	1.0	238.7	0.62

*Refs. 9 and 10.

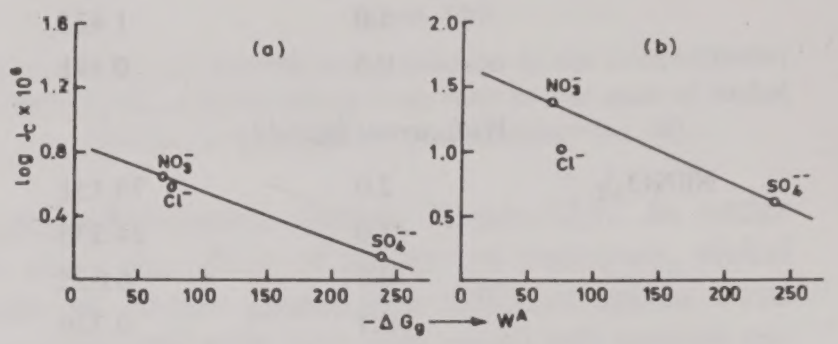

Fig. 5 – Plot of $\log J_c$ against ($-\Delta G_{g\to w^A}$). Curve a is for ligand L_1 (1.0 M) and curve b is for ligand L_2 (1.0 M).

Carrier ligands as well as the metal complexes with them have both hydrophobic and hydrophilic domains in their structures. Ligands, therefore, are expected to be present at the liquid membrane phase/aqueous phase interface in such an orientation that hydrophilic moieties are in the aqueous phase and the hydrophobic parts of the structure are present in the liquid membrane phase. The question that now arises is how does the carrier ligand-metal complex, which has both hydrophilic and hydrophobic domains in its structure, moves through the bulk of the liquid membrane phase from the source phase boundary to the receiver phase boundary. One possibility is that the transport takes place along the aqueous/nonaqueous interface such that the hydrophilic domains remain in the aqueous phase and the hydrophobic ones remain in the nonaqueous phase. This possibility, however, appears remote. The other possibility is that the complex moves through the bulk of the liquid membrane phase. If this happens the hydrophilic moieties of the complex have to be concealed from the hydrophobic environment of the liquid membrane phase. But what is the mechanism of concealment of hydrophilic moieties? Are some reversed micelle kind

of structures formed? We have no definite answer to these questions at this stage. Carrier L_2 which transports the metal ion faster is definitely more hydrophobic and more surface active than carrier L_1. What role this hydrophobicity factor plays in the efficiency of the carrier in transporting the ion is the other question which merits attention.

Effect of anions

As noted previously[1,2] anions affect the metal ion transport appreciably. For the three anions chosen in the present study the transport rates of the nickel ion were in the following order: $NO_3^- > Cl^- > SO_4^{2-}$. This trend can be rationalized using thermodynamic argument given by Lamb *et al.*[2]. Assuming that J_c is proportional to the partition coefficient k, which is related to the Gibb's free energy of partitioning between water and the membrane phase, ΔG_p, according to the equation,

$$\Delta G_p = -RT\ln k \quad \ldots (6)$$

One can write,

$$J_c = B\exp\left(-\frac{\Delta G_p}{RT}\right) \quad \ldots (7)$$

where B is a constant. The free energy of partitioning (ΔG_p) can be visualized as composed of three terms as given by the equation,

$$\Delta G_p = \Delta G_p^c + \Delta G_p^A + \Delta G^{cA} \quad \ldots (8)$$

where the superscript c, A and cA respectively indicate that the terms are for cation, anion and for interaction of cation with anion in the membrane phase. If $\Delta G_{g\to M^A}$ represents the free energy of transfer of the anion from the gas phase to the membrane phase and $\Delta G_{g\to W^A}$ that from the gas phase to water, one can write

$$\Delta G_p^A = \Delta G_{g\to M^A} - \Delta G_{g\to W^A} \quad \ldots (9)$$

Therefore,

$$\Delta G_p = \Delta G_p^c + \Delta G_{g\to M^A} - \Delta G_{g\to W^A} + \Delta G^{cA} \quad \ldots (10)$$

Lamb *et al.* assumed that all other terms on the right hand side of Eq. (10) except $\Delta G_{g\to W^A}$ were either constants or compensate each other for all anions. This, of course, as admitted by Lamb *et al.*[2] themselves is an over simplification. In view of this assumption, a simple correspondence between $\log J_c$ and $\Delta G_{g\to W^A}$ follows from Eq. 7. Using the values of Gibb's free energy of hydration ($\Delta G_{g\to W^A}$) of anions available in literature[9,10], one can see from the data given in Table 2 and plotted in Fig. 5, that the correlation between $\log J_c$ and $\Delta G_{g\to W^A}$ is corroborated.

Acknowledgement

This work forms a part of the programme sponsored by the Department of Environment, Govt. of India, New Delhi. Thanks are due to the Head, Department of Botany and to the Head, Department of Metallurgical Engineering of this University for permission to use their atomic absorption spectrophotometer facility.

References

1 Christensen J J, Lamb J D, Izatt S R, Starr S E, Weed G C, Astin M S, Slitt B D & Izatt R M, *J Am chem Soc*, 100 (1978) 3219.
2 Lamb J D, Christensen J J, Izatt S R, Bedke K, Astin M S & Izatt R M, *J Am chem Soc*, 102 (1980) 3399.
3 Izatt R M, Roper D K, Bruening R L & Lamb J D, *J membr Sci*, 45 (1989) 73.
4 Kim Jong-Inn & Stroeve Pieter, *J membr Sci*, 49 (1990) 37.
5 Scholander P F, *Science*, 131 (1960) 585.
6 Gerlach D H & Holm R H, *J Am chem Soc*, 91 (1969) 3457.
7 Ward W J, *AIChE J*, 16 (1970) 405.
8 Reusch C G & Cussler E L, *AIChE J*, 19 (1973) 736.
9 Friedman H L, Krishnan C V, in "*Water: A comprehensive treatise*, Vol. 3, edited by F Francks (Plenum Press, New York) 1973, pp. 55-58.
10 Smith D W, *J chem Educ*, 54 (1977) 540.
11 Harned H S & Owen B B, *The physical chemistry of electrolytic solutions*, 2nd Edn (Reinhold, New York) 1950, p. 561.

Indian Journal of Chemistry
Vol. 31A, July 1992, pp. 398-402

Thermodynamics of binary mixtures of non-electrolytes: Molar excess Gibbs free energy of mixing

V K Sharma*, S P Sharma & Sadhana Aggarwal

Department of Chemistry, Maharshi Dayanand University, Rohtak 124 001, India

Received 22 November 1991; revised and accepted 17 February 1992

Vapour liquid equilibrium data have been measured at 308.15 K for 1,2-dichloroethane (i) + pyridine (j), + α-picoline (j), + *n*-heptane (j) and *n*-heptane (i) + α-picoline (j) mixtures and the same have been utilized to calculate excess Gibbs free energy of mixing G^E. The G^E data have been analysed in terms of (i) Flory's theory (ii) Sanchez and Lacombe approach and (iii) Graph theoretical approach [using previously reported molar excess enthalpy H^E (T, X = 0.4 and 0.5) data alone] and it has been observed that the G^E data evaluated from graph-theoretical approach express the experimental G^E data better than the data evaluated from the other two approaches.

According to Wilhelm *et al.*[1] 1,2-dichloroethane exists as an equilibrium mixture of *trans* and *gauche* forms and the addition of such entities as benzene causes hindrance to its molecular rotation. Since pyridine acts as both N and π electron donor, the addition of pyridine and its homologues, like α-picoline, or even aliphatic hydrocarbon, like *n*-heptane, to 1,2-dichloroethane should influence, the rotation of 1,2-dichloroethane in a characteristic manner and this must be reflected in their excess functions. Further a number of approaches[2-6] have been put forward to explain excess thermodynamic data of mixtures of non-electrolytes and as the G^E data of [1,2-dichloroethane (i) + pyridine (j), + α-picoline (j), + *n*-heptane (j) and *n*-heptane (i) + α-picoline (j)] mixtures are not available in the literature, it was felt that G^E data of these mixtures would provide a very stringent test to check the conclusions of these approaches[2-6].

Materials and Methods

1,2-Dichloroethane, pyridine, α-picoline, *n*-heptane (A R Grade) were purified by standard methods[7,8] and their purities checked by measuring their density at 298.15 K ± 0.01 K and these values agreed to within $\pm 5 \times 10^{-5}$ gm cm^{-3} with their corresponding literature values[9].

Total vapour pressure of the present (i + j) mixtures were measured as a function of liquid-phase mole fraction of (i) at 308.15 ± 0.01 K by a static method[10] in the manner described earlier[11]. The heights of the mercury in the manometer were corrected to 273.15 K and at standard gravity. The composition of the liquid phase was determined using a Carl Zeiss interferometer in the manner described earlier[12]. The measured vapour pressures were reproducible to ± 0.18 Torr while the uncertainties in the liquid phase composition were about 0.01 mol %. The errors in the vapour pressure determination were estimated to be better than ± 0.3 Torr.

Results and Discussion

Our measured vapour pressures (Table 1) at 308.15 K for 1,2-dichloroethane, pyridine, α-picoline and *n*-heptane compare well within the experimental uncertainties with their corresponding literautre[13(a)-(d)] values.

Total vapour pressure for 1,2-dichloroethane (i) + pyridine (j), + α-picoline (j), + *n*-heptane (j) and *n*-heptane (i) + α-picoline (j) mixture are recorded in Table 1. G^E value for these systems were obtained by fitting vapour pressure (P) data to the expression

$$P = \gamma_i P_i' + \gamma_j P_j' \quad \ldots (1)$$

where P_i' and P_j' are the partial pressures and γ_i and γ_i are the activity coefficients of the compounds i and j and are related to the liquid composition x_i and x_i by

$$P_i' = x_i P_i \exp \cdot (V_i - \beta_{ii})(P - P_i)/RT - P\,\delta_{ij}\gamma_i^2/RT \quad \ldots [2]$$

$$P_i' = x_j P_i \exp \cdot (V_j - \beta_{ij})(P - P_i)/RT - P\,\delta_{ij}\gamma_i^2/RT \quad [3]$$

P_i, V_i and β_{ii} are the vapour pressure, molar volume and the second virial coefficient respectively of the pure component i and the cross second virial coefficient δ_{ij} is defined[11] by

$$\delta_{ij} = 2\beta_{ij} - \beta_{ii} - \beta_{jj} \quad \ldots (4)$$

where β_{ij} is the second virial coefficient of (i+j) mixture. It has been assumed that mixture virial coefficient is the arithmatic mean of β_{ii} and β_{jj} so that β_{ij} is zero and R and T have usual meanings. Since G^E is related to the activity coefficients γ_i, γ_j, by

$$G^E/RT = x_i\mu_i^E + x_j\mu_j^E = RT\Sigma x_i \ln \gamma_i \quad \ldots (5)$$

and if G^E is expressible as

$$G^E = x_i x_j[G_0 + G_1(x_i - x_j) + G_2(x_i - x_j)^2] \quad \ldots (6)$$

then Barker's[14] method was employed to evaluate G_0, G_1, G_2 by process of successive approximations. These constants and the corresponding G^E data are recorded in Table 1.

We are unaware of any G^E data at 308.15 K for the present (i+j) mixtures with which to compare our results. However, while the G^E data for 1,2-dichloroethane (i)+pyridine (j) mixture are negative, those of 1,2-dichloroethane (i)+ α-picoline (j) or *n*-heptane (i)+ α-picoline (j) and *n*-heptane (i)+ α-picoline (j) mixture are positive over the entire range of composition. At the simplest qualitative level if it be assumed that the 1,2-dichloroethane (i)+pyridine (j) mixture is characterized by the donor-acceptor type interactions between the empty 3*d* level of the Cl atoms of 1,2-dichloroethane (electron acceptor) and the lone pair of electrons on the N atom of pyridine ($\gamma_i < 1$, $\gamma_j > 1$; $0 < x_i < 0.67$ and $\gamma_i > 1$, $\gamma_j < 1$; $0.7 < x_i > 1.0$) then the introduction of $-CH_3$ substituent at position 2 in pyridine, as in α-picoline, would though render the lone pair of electrons on the N atom of pyridine to be more labile yet the bulky $-CH_3$ group of α-picoline would hinder considerably the approach of the Cl atoms of 1,2-dichloroethane to α-picoline. Consequently if the contribution due to repulsion factor outweighs the contribution due to interaction factor (i.e. γ_i, $\gamma_j > 1$; $0 < x_i < 1$) then G^E data for 1,2-dichloroethane (i)+ α-picoline (j) mixtures should be more positive than that of 1,2-dichloroethane (i)+pyridine (j) mixtures. The experimental G^E data for these mixtures lend credence to this view point. Such a scheme of molecular interactions would then require that the G^E values for 1,2-dichloroethane (i)+ *n*-heptane (j) and *n*-heptane (i)+ α-picoline (j) mixtures should be still more positive than those of the 1,2-dichloroethane (i)+ α-picoline (j) mixtures. The experimental data of these mixtures support it.

The G^E data of these binary mixtures were then analysed in terms of Flory's theory and Sanchez and Lacombe theory of fluid mixtures. G^E (T, x_i) according to Flory's theory[2,3] is given by

$$G^E(T,x_i) = 3T\left[x_i(P_i^*v_i^*/T_i^*)\ln(\tilde{v}_i^{1/3} - 1)/(\tilde{v}_{cal} - 1) + x_j(P_j^*v_j^*/T_j^*)\ln\frac{(\tilde{v}_j^{1/3} - 1)}{(\tilde{v}_{cal} - 1)}\right] + H^E \text{ (Flory's theory)} \quad \ldots (7)$$

where $\tilde{v}_{cal}^E$ (calculated excess reduced volume) is given by

$$\tilde{v}_{cal}^E = \tilde{v}_0^{7/3}[(4/3) - (\tilde{v}_0)^{1/3}]^{-1}(\tilde{T} - \tilde{T}_0) \quad \ldots (8)$$

and $$\tilde{v}_{cal} = \tilde{v}_0 + \tilde{v}_{cal}^E \quad \ldots (9)$$

where $\tilde{v}_0$, $\tilde{T}$ and $\tilde{T}_0$ are ideal reduced volume, reduced temperature and ideal reduced temperature of the mixture defined by Eqs (10-14).

$$\tilde{v}_0 = \phi_i\tilde{v}_i + \phi_j\tilde{v}_j \quad \ldots (10)$$

$$\tilde{T}_0 = (\tilde{v}_0^{1/3} - 1)/\tilde{v}_0^{4/3} \quad \ldots (11)$$

$$v_i = \{1 + [\alpha_i(T/3)/(1 + \alpha T)]\}^3 \quad \ldots (12)$$

$$v^* = v_i/\tilde{v}_j \quad \ldots (13)$$

$$\phi_i = 1 - \phi_j = N_i v_i^*/(N_i v_i^* + N_j v_j^*) \quad \ldots (14)$$

where x_i and v^* etc. denote respectively the mole fraction and the characteristic volume of the component (i) of the (i+j) binary mixture and all the quantities have their usual significance[2,3]. On the other hand $G^E(T, x_i)$ according to Sanchez and Lacombe theory[4,5] of fluid mixtures is given by

$$G^E(T, x_i) = H^E - KT\{\Sigma x_i \ln \phi_i + r(\tilde{v} - 1)\ln(1 - \tilde{\rho}) + \ln \tilde{\rho} - \Sigma x_i[r_i^0(\tilde{v} - 1)\ln(1 - \tilde{\rho}) + \ln \tilde{\rho}]\} \quad \ldots (15)$$

where

$$\phi_i = m_i(\rho_i^*)\cdot[\Sigma(m_i/\rho_i^*)^{-1}] \quad \ldots (16)$$

$$m_i = x_i M_i(\Sigma x_i M_i)^{-1} \quad \ldots (17)$$

$$r = \Sigma x_i r_i \quad \ldots (18)$$

$$r_i = r_i^0[v_i^*(v_{mix}^*)^{-1}] \quad \ldots (19)$$

Table 1—Measured vapour pressure P and derived activity coefficients γ_i and γ_j at 308.15 K for the various (i + j) mixtures as functions of the mole fraction of component (i)

x_i	P (Torr)	γ_i	γ_j
1,2-Dichloroethane (i) + pyridine (j)			
0.0000	35.1	—	—
0.1002	39.9	0.8378	1.0056
0.1298	41.9	0.8291	1.0079
0.1800	45.6	0.8185	1.0106
0.2811	53.7	0.8354	1.0062
0.3588	62.2	0.8665	0.9905
0.5092	74.2	0.9401	0.9313
0.6112	84.8	0.9814	0.8807
0.6689	91.5	0.9974	0.8542
0.7301	98.5	1.0075	0.8320
0.8510	112.4	1.0092	0.8216
0.8900	116.1	1.0064	0.8331
0.9395	119.7	1.0025	0.8632
1.0000	123.1	—	—

$G_0 = 721.73$ J mol^{-1}, $G_1 = 40.99$ J mol^{-1}, $G_2 = 581.59$ J mol^{-1}

x_i	P (Torr)	γ_i	γ_j
1,2-Dichloroethane (i) + *n*-heptane (j)			
0.0000	75.1	—	—
0.1006	101.2	1.9484	1.0137
0.1552	109.7	1.9115	1.0336
0.1994	116.5	1.8617	1.0565
0.2504	122.9	1.7907	1.0900
0.3004	128.4	1.7107	1.1308
0.3994	136.7	1.5389	1.2378
0.5205	143.8	1.3453	1.4077
0.5389	145.4	1.3187	1.4371
0.6711	140.6	1.1583	1.5415
0.7002	145.6	1.1308	1.7107
0.7902	142.5	1.0624	1.8490
0.9008	134.9	1.0137	1.9484
1.0000	123.1	—	—

$G_0 = 2594.08$ J mol^{-1}, $G_1 = 676.64$ J mol^{-1}, $G_2 = -244.16$ J mol^{-1}

1,2-Dichloroethane (i) + α-picoline (j)			
0.0000	19.8	—	—
0.0981	33.1	1.2022	1.0161
0.1724	42.1	1.1563	1.0419
0.2689	53.5	1.1357	1.0799
0.3521	63.2	1.1347	1.1083
0.4498	74.5	1.1366	1.1296
0.5014	80.2	1.1347	1.1349
0.5692	87.2	1.1266	1.1356
0.6328	93.1	1.1125	1.1351
0.7281	101.0	1.0811	1.1355
0.8009	106.3	1.0524	1.1473
0.8842	112.2	1.0216	1.1879
0.9221	114.9	1.0106	1.2217
1.0000	123.1	—	—

$G_0 = 731.47$ J mol^{-1}, $G_1 = 564.42$ J mol^{-1}, $G_2 = 579.28$ J mol^{-1}

n-Heptane (i) + α-picoline (j)			
0.0000	19.8	—	—
0.0952	46.8	3.2077	1.0062
0.1348	54.1	3.0719	1.0151
0.2750	76.2	2.4108	1.1000
0.2956	77.6	2.3103	1.1518
0.3996	81.9	1.8496	1.2762
0.4794	83.5	1.5626	1.4553
0.5450	84.6	1.3929	1.6505
0.7008	86.1	1.1260	2.2891
0.7989	87.4	1.0430	2.7820
0.9011	88.6	1.0070	3.1930
1.0000	75.1	—	—

$G_0 = 4040.36$ J mol^{-1}, $G_1 = 194.72$ J mol^{-1}, $G_2 = -783.99$ J mol^{-1}

$$v^*_{mix} = \phi_i v_i^* \quad \ldots (20)$$

$$\phi_i^0 = m_i(\rho_i^* v_i^*)^{-1}/(\sum_i m_i/\rho_i^* v_i^*) \quad \ldots (21)$$

$$\tilde{v}_{mix} = 1/\tilde{\rho}_{mix} \quad \ldots (22)$$

and all the terms have their usual significance[4,5]

Evaluation of G^E (T, x_i) according to Flory's theory[2,3] depends upon the knowledge of the reduced temperature $\tilde{T}$ defined by

$$\tilde{T} = [(\phi_i P_i^* \tilde{T}_i + \phi_j P_j^* \tilde{T}_j)/(\phi_i P_i^* + \phi_j P_j^*)] \times [1 - (\phi_i \theta_j x_{ij})/(\phi_i P_i^* + \phi_j P_j^*)] \quad \ldots (23)$$

where P_i^* is the characteristic pressure defined by

$$P_i^* = [\alpha_i/(K_T)_i]\, T\tilde{v}_i^2 \qquad \ldots (24)$$

$(K_T)_i$ is the isothermal compressibility of the component i and $\varkappa_{ij}$ is a pair potential term and hence depends on the adjustable parameters $\theta_j \varkappa_{ij}$. These parameters for a particular binary mixture were evaluated from the H^E (T, x = 0.5) datum[15] via Eq. (25)

$$\begin{aligned} H^E\ (T, x_i) = {} & x_i P_i^* v_i^* (\tilde{v}_i^{-1} - \tilde{v}_{calc}^{-1}) \\ & + x_j P_j^* v_j^* (\tilde{v}_j^{-1} - \tilde{v}_{calc}^{-1}) \\ & + x_i v_i^* \theta_j \varkappa_{ij} \tilde{v}_{cal}^{-1} \end{aligned} \qquad \ldots (25)$$

and were subsequently employed to predict G^E (T, x_i) data at various x_i for (i + j) mixture. Such G^E (T, x_i) data for the various (i + j) mixtures are recorded in Table 2 and are also compared with corresponding experimental values. (The coefficient of volume expansion, α, for the various components were evaluated from the molar volumes of components at different temperatures while $(K_T)_i$ values are calculated from the relationship[16]

$$(K_T)_i = \alpha_i T/\delta_i^2 \qquad \ldots (26)$$

where δ_i is the solubility parameter of component (i). The solubility parameters of the pure components were taken from literature[17]; those of α-picoline and pyridine were evaluated as suggested by Hildebrand and Scott[17].

Evaluation of G^E (T, x_i) by Sanchez and Lacombe theory[4,5] on the other hand requires a knowledge of the reduced density, $\tilde{\rho}_{mix}$, of the mixture which in principle can be evaluated from the equation of state of the mixture i.e.

$$\tilde{\rho}_{mix}^2 + \frac{RT}{\varepsilon^*_{mix}}[\tilde{\rho}_{mix}(1 - r_{mix}^{-1}) + \ln(1 - \tilde{\rho}_{mix})] + \tilde{p} = 0 \qquad \ldots (27)$$

Since the present (i + j) mixtures are not expected to satisfy this equation, a departure was made to evaluated, $\tilde{\rho}_{mix}$, data for them. For the present investigations we utilized[9,15] V^E (T, $x_i = 0.5$) and H^E (T, $x_i = 0.5$) data at 308.15 K to evaluate ε^*_{mix} and $\tilde{\rho}_{mix}$ data for the binary mixture. These $\tilde{\rho}_{mix}$ and ε^*_{mix} values were next utilized to see as to how far this particular mixture satisfied Eq. (27). Once the equation of state for the mixture was so established, it was then solved by numerical techniques to yield $\tilde{\rho}_{mix}$ and hence G^E for the mixture

Table 2—Comparison of theoretical G^E values at 308.15 K with the corresponding experimental values for the various (i + j) mixtures

System	x_i	G^E (J mol^{-1})			
		Sanchez & Lacombe theory	Graph theory	Exptl.	Flory's theory
1,2-dichloroethane (i) + pyridine (j)	0.1	−481.1	−14.3	−34.4	36.6
	0.3	−711.4	−45.5	−135.5	49.4
	0.7	−1004.5	−60.7	−128.6	55.6
	0.9	−920.3	−36.3	−28.5	48.8
1,2-dichloroethane (i) + α-picoline (j)	0.1	459.2	−123.2	58.6	−47.7
	0.3	1095.3	−242.9	125.7	−142.1
	0.7	1566.1	−225.6	220.0	−323.1
	0.9	1441.2	−112.0	139.8	−351.1
1,2-dichloroethane (i) + *n*-heptane (j)	0.1	−1852.1	475.5	170.7	184.5
	0.3	1146.3	1042.0	479.7	553.3
	0.7	1412.2	1093.0	593.4	1291.0
	0.9	1913.1	576.1	268.1	1659.9
n-heptane (i) + α-picoline (j)	0.1	499.8	357.9	304.5	230.9
	0.3	1380.9	811.6	805.8	612.1
	0.7	512.1	1026.7	838.5	1111.5
	0.9	−1081.4	617.2	332.5	1556.1

at any x_i. Such G^E data for the various (i+j) mixtures are recorded in Table 2 and are also compared with their corresponding experimental values.

G^E data were also analysed interms of graph-theoretical approach[6]. According to this approach G^E, γ_i, γ_j for an (i+j) mixture are given by

$$G^E(T, x_i) = RT \sum_{G_{i+j}} x_i \ln \gamma_i \quad \ldots (28)$$

where

$$\ln \gamma_i = \frac{x_j(\bar{x}_{ij}/RT)\, k_{ij}({}^3\xi_i/{}^3\xi_j)}{x_i + x_j\, k_{ij}({}^3\xi_i/{}^3\xi_j)} \quad \ldots (29)$$

$$\ln \gamma_j = \frac{\bar{x}_{ij}}{RT} k_{ij}({}^3\xi_i/{}^3\xi_j) \left[\ln \left\{ \frac{x_i + x_j k_{ij}({}^3\xi_i/{}^3\xi_j)}{x_j\, k_{ij}({}^3\xi_i/{}^3\xi_j)} \right. \right.$$

$$\left. \left. - \frac{x_i}{x_i + x_j\, k_{ij}({}^3\xi_i/{}^3\xi_j)} \right\} \right] \quad \ldots (30)$$

where

$${}^3\xi_i = (\delta_l\, \delta_m\, \delta_n\, \delta_o)^{-0.5} \quad \ldots (31)$$

and δ_l etc. denote the degree of the vertices of the molecular graph of component i. All other terms have their usual meaning[6].

γ_i, γ_j, G^E data for the present binary (i+j) mixtures were next evaluated from Eqs (28)-(31) using H^E (T = 308.15 K, x_i = 0.4 and 0.5) alone[15] in the manner described earlier[12]. Such G^E data are recorded in Table 2 and are also compared with their corresponding experimental values.

Examination of data in Table 2 has revealed that while the G^E (T, x_i) values evaluated for 1,2-dichloroethane (i) + pyridine (j) mixture from Flory's and Sanchez theory make very poor agreement (Flory's theory even fails to predict the correct sign) with the corresponding experimental values, G^E values calculated from graph theoretical approach correctly predicts the sign of G^E data, although the quantitative agreement between the theoretical and experimental values is not very good. Further G^E (T, x_i) values evaluated for 1,2-dichloroethane (i) + *n*-heptane (j) and *n*-heptane (i) + α-picoline (j) by graph theoretical approach are closer to the experimental values than the values evaluated by Flory's and Sanchez theory's, although the quantitative agreement is not good. The disagreement between the experimental and theoretical values for the various mixtures may be due either to the uncertainties in the evaluation of the characteristic parameters or due to limitations with the theories.

Acknowledgement

The authors express their thanks to the Head of the Chemistry Department and the authorities of Maharshi Dayanand University, Rohtak for providing research facilities. Authors are grateful to Dr. P.P. Singh, Professor, Department of Chemistry, Maharshi Dayanand University, Rohtak, for his valuable suggestions.

References

1 Wilhelm E, Schana R, Becker G, Findenegg & Koheer F, *Trans Faraday Soc*, 65 (1969) 1433.
2 Flory P J, *J Am chem Soc*, 87 (1965) 1833.
3 Flory P J & Abe A, *J Am chem Soc*, 87 (1965) 1838.
4 Lacombe R H & Sanchez I C, *J phys chem*, 80 (1976) 2352.
5 Sanchez I C & Lacombe R H, *J phys chem*, 80 (1976) 2568.
6 Singh P P, Dahiya H P & Dangar S, *Z phys chem*, (*Leipzig*), 4 (1988) 269.
7 Vogel A I, *A text book of practical organic chemistry* (ELBS/Longmans, London) 1978, p 266.
8 Giaqul W F, Hornubg E W, Kunzler J E & Rubin T R, *J Am chem Soc*, 80 (1960) 62.
9 Nigam R K, Singh P P, Aggarwal S & Sharma S P, *Fluid phase Equilibria*, 16 (1984) 25.
10 Taha A A, Grigsby R D, Johnson J R, Christian S D & Affsprung, *J chem Edu*, 43 (1966) 432.
11 Khosla M P, Mahl B S, Chopra S L & Singh P P, *Z phys Chem*, (*Leipzig*), 25 (1972) 129.
12 Dahiya H P, Singh P P & Dagar S, *Fluid phase Equilibria*, 33 (1987) 191.
13 *CRC handbook of physics and chemistry*, 59th Edn, edited by R C Weast (CRC press in C Florida), 1970, p (a) D-242 (b) D-245 (c) D-246 (d) D-248.
14 Barber J A, *Aust J Chem*, 6 (1953) 207.
15 Nigam R K & Aggarwal S, *Fluid phase Equilibria*, 26 (1986) 181.
16 Hilderbrand J H & Scott R L, *The solubility of non-electrolytes*, Vol. 4 (Dover Publications, INC New York), 1964, 429.
17 Hilderbrand J H & Scott R L, *The solubility of non-electrolytes*, Vol. 4 (Dover Publications, INC New York), 1964, 430.

Indian Journal of Chemistry
Vol. 31A, July 1992, pp. 403-407

An indirect determination of changes in the inter-electronic repulsion (Racah) parameters and magnitude of 'extrastabilisation' in lanthanides

S N Limaye & M C Saxena*
Department of Chemistry, Dr Harisingh Gour University, Sagar (MP) 470 003, India

Received 17 June 1991; revised and accepted 13 January 1992

Following the argument that 'extrastabilisation' of specific *f*-configurations is a consequence of 'nephelauxetic effect' a five parameter semi-empirical equation expressed in terms of 'inter-electronic repulsion (Racah) parameters' (IERP) has been used to determine the 'extrastabilisation' in the free energy of complexation for trivalent lanthanides. The extrastabilisation has been expressed in terms of δE^k-the changes in IERP. The calculated values of δE^k are in good agreement with the reported range of δE^1 and δE^3, ~ 1% of E^1 or E^3 and $-0.195 < \delta E^3/\delta E^1 < 0.214$. The magnitude of extrastabilisation, δE_{st}, has been studied in context of ligand and/or donor atom characteristics, which shows an interesting dependence. The sequence of δE_{st} with respect to f^q-configurations is $4f^7 \gg 4f^3 - 4f^4 \approx 4f^{10} - 4f^{11}$.

The '*f*-effect' of Nyholm[1] (also called gadolinium break[2]) has emerged as a 'general periodicity' in the series of *f*-elements. The 'tetrad-effect'[3] or 'double-double effect'[4] has now been interpreted as 'extrastabilisation' of specific *f*-configurations as a result of 'nephelauxetic effect'[5], the micro-components of which are the phenomenological changes in the 'inter-electronic repulsion parameters' (Racah parameters[6]) (IERP-Racah henceforth used in text). Based on these arguments, theoretical estimations of 'extrastabilisation' and its correlation with periodicities have been attempted and discussed by Spitsyn[7]. Linear interpolation method[8] of Siekierski, 'inclined W[≷] systematics of Sinha[9] and the differential plot method of Saxena[10] are some of the several qualitative attempts, that have been made to demonstrate the mode of this periodicity.

Besides these studies, no attempt seems to have been made so far to estimate the variation in 'extrastabilisation' (δE_{st}) or IERP-Racah (δE^k) values and a study of its dependence on the changes in the metal-ion environment. In the present study, we have made an effort to indirectly estimate the changes in δE^k values and magnitude of δE_{st} using the formation constant values of complexes formed by several organic ligands and examine the possibility of any relationship between the δE_{st} and ligand donor group/atom characteristics.

Method of calculation

The 'extrastabilisation' δE_{st} has been calculated with the help of a five-parameter semi-empirical equation suggested by Spitsyn[7]. The reduced form of the equation may be expressed as,

$$-\Delta G_{complex} = E_B + \delta E_{st} \quad \ldots (1)$$

where $\Delta G_{complex}$ = free energy of complexation, E_B = energy of the baricentre of the f^q-configuration, δE_{st} = energy of 'extrastabilisation'.

The parameters E_B and δE_{st} are given by,

$$E_B = C + qV + q(q-1)/2.\, E^0 \quad \ldots 1(a)$$

and

$$\delta E_{st} = K_1 \cdot \delta E^1 + K_3 \cdot \delta E^3 \quad \ldots 1(b)$$

where, C and V are constants, q = number of *f*-electrons, E^0, E^1, E^3 are inter-electronic repulsion-Racah† parameters (IERP-Racah), and K_1, K_3 are S- and L-dependent coefficients given by Eqs (2) and (3)

$$K_1 = 18/13.\, S(1/2 - S) \quad \ldots (2)$$

$$K_3 = L/180.\, [L(222 - 48L) - 234] \quad \ldots (3)$$

A matrix based software was devised (G5215AP with PL-1) to calculate the values of various parameters of Eq. 1 (1a, 1b) using the formation constant values for all the members of Ln-series. The values of δE_{st} ($= K_1 \cdot \delta E^1 + K_3 \cdot \delta E^3$) and δE^1, δE^3 and $\delta E^3/\delta E^1$ values for some representative cases are given in Table 1.

†The advantages in the use of Racah notations[7] are (i) the dependence of ground energy term on S and L is separated in different coefficients of K_n, and, (ii) $K_2 = 0$ according to the values of S, q/2 or 14 − q/2.

Table 1—Values of extrastabilisation, ∂E_{si} (for f^q-configuration; q = 3,4; 7; 10,11) and $\partial E^3/\partial E^1$-nephelauxetic ratio for various ligand environments

	Ligand/Geometry	δE_{si} q = 3,10	4,11	7	$\partial E^3/\partial E^1$
	A. Ligand				
1.	Formate	7	24	217	−0.119
2.	Acetate	9	9	25	0.116
3.	Hydroxyacetate	56	108	350	0.012
4.	Thioacetate	9	22	22	0.062
5.	Chloroacetate	4	19	23	−0.210
6.	Methoxyacetate	5	11	50	−0.254
7.	Iodoacetate	140	178	250	0.275
8.	Dihydroxymethylpropionate	42	111	386	0.099
9.	Propionate	67	79	85	0.442
10.	Isobutyrate	24	35	75	0.124
11.	Hydroxyisobutyrate	263	322	420	0.333
12.	Hydroxybutyrate	160	212	368	0.201
13.	Thioglycolate	21	21	56	0.181
14.	Diglycolate	112	137	174	0.346
15.	Lactate	113	168	388	0.125
16.	Malate	45	160	380	−0.092
17.	Salicylate	376	475	692	0.277
18.	Sulphosalicylate	74	100	141	0.077
19.	Phthalate	243	243	577	0.060
20.	Mandelate	47	47	338	−0.101
21.	Anthranilate	34	34	87	0.063
22.	Oxalate	51	214	1139	−0.067
23.	Oxydiacetate	118	153	246	0.232
24.	Acetylacetonate	138	144	653	0.355
25.	Benzylacetonate	214	311	577	0.119
26.	Isonitroacetonate	191	230	282	0.369
27.	Dihydroxyacetophenone	364	510	1028	0.146
28.	Dihydroxybenzaldehyde	230	450	900	0.154
29.	Catecholate	143	355	690	0.258
30.	Methyltropolonate	98	140	208	0.134
31.	Citrate	118	174	397	0.106
32.	Tartrate	139	129	207	0.122
33.	Glycinate	388	502	799	0.236
34.	Valinate	97	178	572	0.019
35.	Picolinate	57	134	375	0.246
36.	Dipicolinate	6	40	231	0.081
37.	Iminodiacetate [IMDA]	150	378	840	0.195
38.	Ethylenediaminediacetate [EDDA]	215	313	687	0.117
39.	Ethylenediaminedimalonate	89	179	625	0.237
40.	Ethylenediaminedisuccinate	409	620	824	0.318
41.	Ethylenediaminediglutarate	261	382	852	0.112
42.	Hydroxyethylethylenediaminetriacetate [HEDTA]	148	369	755	0.239

—*Contd*

Table 1—Values of extrastabilisation, ∂E_{st} (for f^q-configuration; q = 3,4; 7; 10,11) and $\partial E^3/\partial E^1$-nephelauxetic ratio for various ligand environments —*Contd*

	Ligand/Geometry	δE_{st} q = 3,10	4,11	7	$\partial E^3/\partial E^1$
43.	Nitrilotriacetate [NTA]	61	160	561	0.098
44.	Methylnitrilotriacetate [HC_3-NTA]	239	324	594	0.179
45.	Ethylnitrilotriacetate [H_5C_2-NTA]	292	386	658	0.208
46.	Propylnitrilotriacetate [H_7C_3-NTA]	133	213	556	0.066
47.	Isopropylnitrilotriacetate [$(H_3C)_2$-CH-NTA]	109	179	625	0.237
48.	Oxy-bis(ethylenenitrilo)tetraacetate [EEDTA]	105	231	489	0.228
49.	Ethylenebis(oxyethylenenitrilo)tetraacetate [EGTA]	253	288	297	0.061
50.	Cyclohexanediamintetraacetate [CDTA]	135	343	868	0.174
51.	Propylenediaminetetraacetate [PDTA]	83	218	781	0.094
52.	Ethylenediaminetetraacetate [EDTA]	169	430	1169	0.155
53.	Diethylenetriaminepentaacetate [DTPA]	58	152	525	0.101
54.	Triethylenetriaminehexaacetate [TTHA]	38	123	591	−0.054
55.	Quinolinecarboxylate	2	16	96	0.082
56.	8-Hydroxyquinolinate	106	145	272	0.172
57.	5,7-Dinitro, 8-hydroxyquinolinate	244	311	469	0.260
58.	5,7-Dichloro, 8-hydroxyquinolinate	168	223	389	0.199
59.	5,7-Diiodo, 8-hydroxyquinolinate	200	273	479	0.204
60.	5,7-Dibromo, 8-hydroxyquinolinate	189	243	479	0.204
61.	5-Sulpho, 8-hydroxyquinolinate	223	314	640	0.123
62.	Ferron	238	355	818	0.102
63.	Xylenol orange	26	57	177	0.145
64.	4(2-Pyridylazo)naphthol [PAN]	222	290	479	0.222
65.	1(2-Pyridylazo)resorcinol [PAR]	12	40	189	−0.054
66.	Dimethylglyoximate [DMG]	106	267	716	0.159
67.	8-Hydroxyquinolene-N-oxide	100	141	284	0.145
68.	Chloride (Cl^-)	122	137	103	0.072
69.	Phosphate (PO_4^{3-})	47	93	328	−0.005
70.	Methylphosphate ($CH_3PO_4^{2-}$)	14	21	48	0.099
71.	Carbonate (CO_3^{2-})	81	220	968	−0.041
72.	Hydroxy (OH^-)	128	204	534	0.067
	B. Geometry				
1.	Hydroxy-trigonaltriprism*	85	199	797	−0.025
2.	Hydroxy-squareantiprism*	114	221	742	0.005
3.	Hydroxy-dodecahedron*	84	168	591	−0.001
4.	Hydroxy-cube*	14	21	49	−0.041

Values in calories
*From "Coordination bond energy values", Kobayashi H *et al.*, *J chem Soc, Faraday Trans I*,84(5)(1988) 1517.

In the process of complexation the aqua ions in the lanthanide aquo complex are replaced by the ligand (L) donor atoms/groups causing a change in the metal-ion environment, thus causing a change in the IERP (δE^k) values. In lanthanides (Ln), the 4f-orbitals being strongly shielded by the outer-lying (5*s* or 6*s*) orbitals, are less available for bonding and the Ln-L interaction is predominantly ionic. Under the negligible effect of spin-orbit coupling the susceptibility of f^q-configuration to the ligand donor group/atom, (the environment as a whole) may be observed from the changes in the δE^k and δE_{st} va-

lues. Thus, a plausible role of the ligand (including aqua ion when compared to that of the gaseous ion) in this 'extrastabilisation' may be attributed to (i) change in the ratio $\delta E^3/\delta E^1$, i.e., nephelauxetic ratio as a result of complexation (replacement of aqua ion by ligand) and (ii) involvement of the metal ion in (probable/partial) covalent bonding‡.

On the basis of these arguments some kind of dependence of 'extrastabilisation' (magnitude) on the nature of ligand groups/atoms is expected. Such dependence has been examined for the present series of complexes (representative cases, Table 1). The variation in δE_{st} (for f^1-configuration only) with respect to ligand is observed to be as follows:

1. Formate ⋙ Acetate ≈ HS-Gly ⋘ Gly < Glycn
2. HO-Acetate < Lactate < Mal < Sal
3. Di-Pic < Pic < Glycn < IMDA
4. NTA < EDDA < HEDTA < IMDA
5. HEDTA < NTA < PDTA < CDTA < EDTA ≈ OXAL > DTPA ≈ TTHA
6. Tri-Tri-Prism < SAP < Dodecahedron < Cube
7. $Cl^- < PO_4^{3-} < OH^- < CO_3^{2-}$

The observed sequence of ligands is an approximate sequence of their basic strengths. For a finer analysis the difference between the polarizing power of aqua (as a ligand in aquo complex) and the ligand (displacing aqua ion) is under study.

The values of δE_{st} observed for the present series of ligands, with respect to the f^q-configuration, follow the sequence: $f^7 \gg f^3 - f^4 \approx f^{10} - f^{11}$, which is in agreement with the inter-electronic repulsion theory[6], whereas the values of δE^k are in agreement with the stated range[6] of δE^1 or $\delta E^3 \sim 1\%$ of E^1 and E^3 and the ratio[7] of $\delta E^3/\delta E^1$ as $-0.194 < \delta E^3/\delta E^1 < 0.214$. These results support the validity of the proposed hypothesis. The plots of δE_{st} vs $4f^q$ (figures not shown) exhibit a general 'inverted organpipe' for $K_1 \cdot \delta E^1$ and 'inverted tulip' with $K_3\, \delta E^3$.

Conclusion

It may be stated that the present report is a first attempt to (i) determine δE^k values with the help of semi-empirical data and (ii) seek a relationship between δE_{st} and ligand (donor group/atom) characteristics for lanthanides. The observed values of δE^k and the relationship for extra-stabilisation of certain f^q-configurations, though tentative, are significant and provocative. A detailed analysis of the hypothesis is under study.

It is, however, necessary to note that though the indirect determination of δE^k parameters may appear to be simple, the exact explanation of this phenomenon lies hidden in the theory of 'nephelauxetic effect' for which any quantitative explanation is yet to be found. One can believe that the explanation can be found through a correlation with ligand polarizability and more generally with the dielectric properties of the medium[11], but for conclusive comments it is difficult to correlate the crystal field parameters and 'nephelauxetic effect'. To seek a quantitative explanation for the 'nephelauxetic effect' it is necessary to make a theoretical approach similar to the one for crystal field parameters. The phenomenon does not seem to be directly linked to chemical bonding, at least in the frame-work of LCAO-theory. Structure as well as nature of ligand are important. The solution is probably under the influence of dielectric conditions at the ion-site on the configuration mixing between $4f^n$ and excited configuration[12]. The picture is yet 'blurred' and needs greater attention for a refined projection.

‡There is no convincing proof of the direct involvement of f-orbitals in covalent bonding; however, the possibility of covalency in Ln(III) (and actinide) complexes cannot be ruled out[5].

Acknowledgement

One of the authors (SNL) is thankful to the Department of Education, Ministry of Human Resource Development, New Delhi, for the award of a Post-doctoral fellowship. He also expresses his deep sense of gratitude to Prof. K B Yatsimirskii, Ukr. Acad. Sci., Kiev, Prof. (Mrs) G V Ionova and Dr V G Vokhmin of the Laboratory of Quantum Chemistry, Institute of Physical Chemistry, Acad. Sci. SSR, Moscow, for their interest and valuable suggestions.

References

1 Nyholm R S, *Progress in Chemistry*, 32(3) (1963) 351, (From Chemistry of complexes of rare earth elements, edited by K B Yatsimirskii, Ref. No. 282, p. 39 (M. Nauka, Moscow) (Russ.).
2 Gut R & Schwarzenbach G, *Helv chim Acta*, 39 (1956) 1589.
3 Peppard D F, Mason G W & Lewey S, *J inorg nucl Chem*, 31 (1969) 2271.
4 Fidelis I & Siekierski S, *J inorg nucl Chem* (a) 33 (1971) 319; (b) 377; (c) 32 (1970) 519.
5 Jorgensen C K, (a) *J inorg nucl Chem*, 32 (1970) 3127; (b) *Handbook on the physics and chemistry of rare earth elements*, edited by K A Gschneidner, Vol. 4 (1979) 111.
6 Nugent L J, *J inorg nucl Chem*, 32 (1970) 3485.
7 Spitsyn V I, Vokhmin V G & Ionova G V, (a) *Int rev phys Chem*, 4(1) (1984) 57; (b) *Regularities in the properties of Ln(s) and An(s)*, edited by B I Tananev (M Nauka, SSSR) (1990) (Russ.).
8 Siekierski S, *J inorg nucl Chem*, 43 (1981) 3381.

9 Sinha S P, (a) *Systematics and the properties of lanthanides*, (D Reidel Publ Co) NATO-ASI, C-109 (1983) 71; (b) *Helv chim Acta*, 58 (1975) 1978; (c) *Struct and Bond*, 25 (1976) 35.

10 Verma S & Saxena M C, (a) *Ind Acad Sci (Chem. Sci)*, 99 (1987) 217; (b) Limaye S N & Saxena M C, *Nat Acad Sci Lett*, 12(4) (1989) 115.

11 (a) Limaye S N, Kopyrin A A & Saxena M C, *Proc Int Conf on f-Elem*, Leuven K U, *Belgium*, *PS*-2.39 (1990); (b) Limaye S N, Shilov S M, Batyaev I M & Saxena M C, *Rare earth elements Workshop*, Venice, Italy (1991).

12 Fidancev E A, Blaise M L & Caro P, *New J Chem*, 6(11) (1987) 467.

Indian Journal of Chemistry
Vol. 31A, July 1992, pp. 408-411

Reactivity of PPh_3 toward $Ru_2Cl(O_2CMe)_4$: Synthesis and X-ray crystal structure of $[Ru(O_2CMe)(MeCN)_2(PPh_3)_2](ClO_4)$

Birinchi K Das & Akhil R Chakravarty*
Department of Inorganic and Physical Chemistry, Indian Institute of Science, Bangalore 560 012

Received 23 September 1991; revised and accepted 24 January 1992

A new ruthenium(II) complex of the type $[Ru(O_2CMe)(MeCN)_2(PPh_3)_2](ClO_4)$ (**1**) has been isolated from a reaction between $Ru_2Cl(O_2CMe)_4$ and PPh_3 in MeCN followed by the addition of $NaClO_4$. The structure of **1** is determined by single crystal X-ray studies. The crystal belongs to the monoclinic space group C2/m with the following unit cell dimensions for the $C_{42}H_{39}N_2O_6P_2ClRu$ (M = 866.15): a = 23.295(1)Å, b = 23.080(1)Å, c = 9.159(1)Å, β = 107.32(1)°, V = 4701(1)Å^3, Z = 4, D_c = 1.224 gcm^{-3}. λ(Mo − K_α) = 0.7107Å, μ(Mo − K_α) = 4.09 cm^{-1}, T = 293K, R = 0.081 (R_w = 0.094) for 2860 reflections with $I \geq 3\sigma(I)$ and g = 0.015853. In the complex cation, the symmetry about the metal centre is essentially octahedral showing the presence of a chelating acetato, two *cis*-oriented MeCN and two *trans*-disposed PPh_3 ligands. The mechanistic aspects of the core cleavage reaction are discussed.

Among the dimetallic tetracarboxylates with a metal-metal multiple bond, the diruthenium(II, III) complexes with a spin-quartet ground state display[1-3] unusual reactivity towards tertiary phosphine ligands. Earlier studies have shown[4,5] that instead of forming stable diaxial adducts, PPh_3 reacts with $Ru_2Cl(O_2CMe)_4$ in MeOH to form a μ-oxodiruthenium(III) complex, $Ru_2O(O_2CMe)_4(PPh_3)_2$. In presence of excess PPh_3, a similar reaction leads[6] to the formation of two monomeric ruthenium(II)carbonyl complexes. In MeCN medium, the reaction proceeds to form an intermediate μ-aquadiruthenium(II, III) complex which disproportionates to a μ-aquadiruthenium(II) and μ-oxodiruthenium(III) complexes[7,8]. Herein we report the isolation of a new monomeric ruthenium(II) complex, $[Ru(O_2CMe)(MeCN)_2(PPh_3)_2](ClO_4)$ (**1**), from a reaction of $Ru_2Cl(O_2CMe)_4$ with PPh_3 in MeCN. Complex **1** is structurally characterized by X-ray studies.

Materials and Methods

$Ru_2Cl(O_2CMe)_4$ was prepared using a literature procedure[4]. Elemental analysis was obtained from a Heraeus CHN − O Rapid instrument.

*Synthesis of $[Ru(O_2CMe)(MeCN)_2(PPh_3)_2](ClO_4)$ (**1**)*

$Ru_2Cl(O_2CMe)_4$ (400 mg, 0.85 mmol) in MeCN (15 cm^3) was reacted with PPh_3 (450 mg, 1.7 mmol) under stirring condition at 25°C for 24 h. The purple precipitate of $Ru_2O(O_2CMe)_4(PPh_3)_2$[4,5], formed as a major product (yield ~80%), was removed by filtration. A saturated aqueous solution of $NaClO_4$ was added to the filtrate. The resulting precipitate was washed with cold $CHCl_3$ to obtain a brownish-yellow solid (**1**) (yield ~115 mg). Single crystals of this complex, suitable for X-ray studies, were obtained on slow evaporation of a solution of **1** in an acetone-*n*-hexane mixture. [Found: C, 57.4; H, 4.0; N, 3.7. Calc. for $C_{42}H_{39}N_2O_6P_2ClRu$: C, 58.2; H, 4.5; N, 3.2%]. The complex shows poor solubility in common organic solvents.

X-ray crystallographic procedures

A brownish-yellow crystal (approximate dimension: 0.3 × 0.3 × 0.2 mm) was mounted on a glass fibre with epoxy cement. The initial cell parameters were obtained from oscillation and Weissenberg photographs. The final C-centered monoclinic unit cell parameters were obtained by indexing 25 reflections in the range of $14° < 2\theta < 28°$, using an automated four-circle Enraf-Nonius CAD-4 diffractometer equipped with a graphite-monochromated Mo − K_α radiation (λ = 0.7107Å). Data collection was done by ω-2θ scan technique in the limit of $4° \leq 2\theta \leq 50°$ ($-27 \leq h \leq 27$, $0 \leq k \leq 27$, $0 \leq l \leq 10$). There were 4236 unique reflections with 2860 having $I \geq 3\sigma$ (I). Three intensity standards, checked every hour of exposure time, show no significant decay of the crystal during data collection. Out of three possible space groups, C2, Cm and C2/m, the statistics and successful refinement

of the structure indicated C2/m as the correct choice. The data were corrected for Lorentz and polarization effects. The structure was solved by the Patterson method using SHELXS-86[9] and refined by Fourier technique using SHELX-76[10] programs. Scattering factors of the atoms were taken from the *International Tables for X-ray Crystallography*[11]. On getting the final model, an empirical absorption correction[12] was applied on the data. The transmission coefficients were in the range of 0.82-1.00. Final refinement gave $R = 0.081$ and $R_w = 0.094$, with a weighting scheme $w = k/[\sigma^2(F_0) + gF_0^2]$, $g = 0.015853$, $R = \Sigma ||F_0| - |F_c||/\Sigma |F_0|$, $R_w = [\Sigma w(|F_0| - |F_c|)^2/\Sigma w|F_0|^2]^{1/2}$. The number of parameters in the final refinement was 257. The highest shift/esd was 0.07. The ClO_4^- anion was found to be in a highly disordered state. Two oxygen atoms corresponding to one-half of the ClO_4^- group were modelled by eight low electron density peaks. The Cl atom, however, refined well. The higher residual values could be related to the disorderness in the anion. All the atoms other than the oxygen atoms belonging to the disordered ClO_4^- anion were refined anisotropically. The positional parameters along with equivalent isotropic thermal parameters and the site occupancy factors of the oxygen atoms belonging to the ClO_4^- anion are given in Table 1. The anisotropic thermal parameters and the structure factor tables are available with the authors on request.

Crystal data

The cell constants and crystallographic data are: mol. formula, $C_{42}H_{39}N_2O_6P_2ClRu$; mol. wt., 866.15; monoclinic C2/m; $a = 23.295(1)$Å, $b = 23.080(1)$Å, $c = 9.159(1)$Å, $\beta = 107.32(1)°$; $V = 4701(1)$Å^3, $Z = 4$; $D_c = 1.224$ gcm^{-3}; μ(Mo-K_α) = 4.09 cm^{-1}; $\lambda = 0.7107$Å, T = 293K; transmission coeff.: 0.82-1.00.

Results and Discussion

The reaction of $Ru_2Cl(O_2CMe)_4$ with PPh_3 in MeCN leads to the formation of a monomeric ruthenium(II) complex as a minor product and a μ-oxodiruthenium(III) species as a major product as shown by Eq. (1),

$$Ru_2Cl(O_2CMe)_4 + PPh_3 \xrightarrow{MeCN} Ru_2O(O_2CMe)_4(PPh_3)_2 + [Ru(O_2CMe)(MeCN)_2(PPh_3)_2]^+ \quad \ldots (1)$$

The source of oxo-ligand could be the MeCN solvent containing H_2O as an impurity. The cationic complex is isolated as a perchlorate salt and is structurally characterized by X-ray crystallographic studies.

Table 1—Fractional atomic coordinates and isotropic thermal parameters* ($\times 10^3$) for $[Ru(O_2CMe)(MeCN)_2(PPh_3)_2](ClO_4)$ (**1**)

Atom	x	y	z	U_{iso} (Å^2)
Ru	0	0.2494(1)	0	34(0.4)
P	0.1030(1)	0.2501(1)	0.0043(2)	37(0.8)
N	0.0143(3)	0.1859(3)	0.1558(7)	42(2)
C10	0.0254(4)	0.1494(4)	0.2421(11)	57(3)
C20	0.0403(6)	0.1003(5)	0.3520(15)	112(6)
O1	0.0071(3)	0.3290(2)	0.1239(8)	57(2)
C1	0	0.3571(5)	0	69(6)
C2	0	0.4239(7)	0	113(10)
C11	0.1502(3)	0.1935(3)	0.1190(9)	41(3)
C12	0.2040(4)	0.2050(4)	0.2324(10)	59(4)
C13	0.2372(4)	0.1611(5)	0.3218(12)	71(4)
C14	0.2184(5)	0.1043(5)	0.2953(13)	77(5)
C15	0.1652(5)	0.0925(4)	0.1744(13)	76(4)
C16	0.1325(4)	0.1359(4)	0.0922(10)	50(3)
C21	0.1130(4)	0.2403(3)	−0.1852(9)	45(3)
C22	0.1527(4)	0.2025(4)	−0.2165(10)	61(4)
C23	0.1617(5)	0.1969(4)	−0.3566(11)	66(4)
C24	0.1246(5)	0.2304(6)	−0.4754(13)	75(4)
C25	0.0845(5)	0.2670(6)	−0.4511(11)	79(4)
C26	0.0771(4)	0.2750(6)	−0.3063(11)	73(4)
C31	0.1450(3)	0.3170(3)	0.0759(9)	43(2)
C32	0.1813(4)	0.3431(4)	0.0012(12)	61(4)
C33	0.2136(5)	0.3930(5)	0.0603(18)	97(6)
C34	0.2107(5)	0.4145(5)	0.1986(17)	96(6)
C35	0.1741(5)	0.3892(5)	0.2804(14)	79(4)
C36	0.1395(4)	0.3381(4)	0.2111(11)	63(4)
C1	0.1203(1)	0	0.7413(4)	65(1)
O11	0.0612(4)	0	0.6002(11)	38(2)[a]
O12	0.1806(4)	0	0.8832(12)	44(2)[a]
O13	0.1165(6)	0.0681(5)	0.7552(15)	35(3)[a]
O14	0.1622(8)	0	0.6315(22)	44(4)[a]
O15	0.0839(8)	0	0.8663(23)	36(4)[a]
O16	0.1338(9)	0.0667(8)	0.7128(24)	18(4)[a]
O17	0.0812(14)	0.0248(14)	0.8386(35)	29(6)[a]
O18	0.1580(14)	0.0325(13)	0.6356(36)	36(7)[a]

*The anisotropically refined atom have been given an equivalent isotropic thermal parameter defined as

$$U_{iso}(eq) = 1/3\,[\Sigma_i \Sigma_j U_{ij} a_i^* a_j^* \mathbf{a}_i \cdot \mathbf{a}_j]$$

[a]Isotropically refined atoms; site occupancy factors are: O11, O12(0.35); O13(0.40); O14, O15, O16(0.20); O17, O18(0.15).

An ORTEP[13] view of the complex cation is shown in Fig. 1. Table 2 lists the bond distances and angles in complex (**1**). In complex (**1**), the geometry around the metal centre is essentially octahedral. The coor-

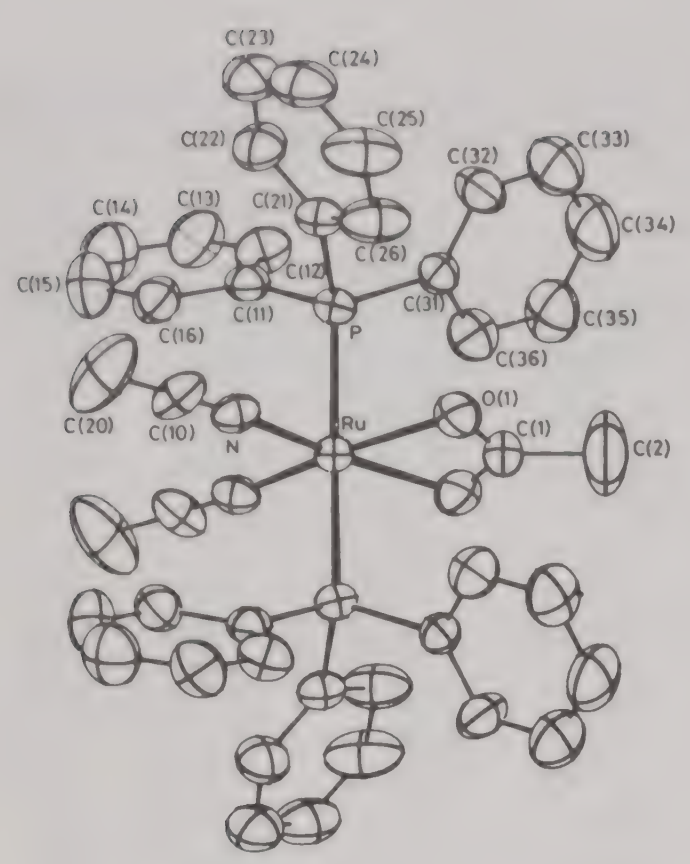

Fig. 1—An ORTEP view of $[Ru(O_2CMe)(MeCN)_2(PPh_3)_2]^+$ cation along with atom numbering scheme.

Table 2—Bond distances (Å) and angles(deg) for $[Ru(O_2CMe)(MeCN)_2(PPh_3)_2](ClO_4)$ (**1**)

Bond distances (Å)

Ru-P	2.388(2)	Ru-N	2.002(7)
Ru-O1	2.140(6)	P-C11	1.826(8)
P-C21	1.833(9)	P-C31	1.841(7)
N-C10	1.131(11)	C10-C20	1.487(13)
O1-C1	1.275(8)	C1-C2	1.542(18)
C11-C12	1.395(10)	C11-C16	1.392(11)
C12-C13	1.385(13)	C13-C14	1.381(16)
C14-C15	1.421(14)	C15-C16	1.345(13)
C21-C22	1.362(13)	C21-C26	1.421(13)
C22-C23	1.366(15)	C23-C24	1.403(15)
C24-C25	1.326(19)	C25-C26	1.400(15)
C31-C32	1.375(14)	C31-C36	1.372(13)
C32-C33	1.394(14)	C33-C34	1.381(23)
C34-C35	1.418(20)	C35-C36	1.462(14)
Cl-O11	1.583(8)	Cl-O12	1.605(9)
Cl-O13	1.582(12)	Cl-O14	1.596(22)
Cl-O15	1.615(23)	Cl-O16	1.608(19)
Cl-O17	1.560(36)	Cl-O18	1.667(36)

Bond angles (deg)

O1-Ru-O1′	61.7(2)	O1-Ru-N′	167.5(2)
O1-Ru-P′	85.5(2)	N-Ru-O1′	167.5(2)
N-Ru-N′	85.9(3)	N-Ru-P′	88.3(2)
N-Ru-O1	106.3(3)	P-Ru-O1′	85.5(2)
P-Ru-N′	88.3(2)	P-Ru-P′	179.2(1)

contd

Table 2—Bond distances (Å) and angles(deg) for $[Ru(O_2CMe)(MeCN)_2(PPh_3)_2](ClO_4)$ (**1**)—*Contd.*

P-Ru-O1	93.8(2)	P-Ru-N	92.3(2)
Ru-P-C31	115.9(2)	Ru-P-C21	113.2(3)
Ru-P-C11	115.8(2)	C21-P-C31	103.7(3)
C11-P-C31	103.3(3)	C11-P-C21	103.4(4)
Ru-N-C10	176.0(7)	N-C10-C20	178.3(10)
Ru-O1-C1	89.8(3)	O1-C1-O1′	118.8(3)
O1-C1-C2	120.6(2)	P-C11-C16	119.1(6)
P-C11-C12	123.1(6)	C12-C11-C16	117.8(8)
C11-C12-C13	121.4(9)	C12-C13-C14	119.9(10)
C13-C14-C15	118.4(10)	C14-C15-C16	120.7(10)
C11-C16-C15	121.6(9)	P-C21-C26	117.3(7)
P-C21-C22	124.3(6)	C22-C21-C26	118.4(8)
C21-C22-C23	124.2(9)	C22-C23-C24	116.4(10)
C23-C24-C25	121.5(10)	C24-C25-C26	122.3(11)
C21-C26-C25	117.1(10)	P-C31-C36	115.9(6)
P-C31-C32	122.0(6)	C32-C31-C36	122.0(8)
C31-C32-C33	120.6(10)	C32-C33-C34	119.0(11)
C33-C34-C35	122.6(12)	C34-C35-C36	116.3(10)
C31-C36-C35	119.4(9)	O17-Cl-O18	131.7(16)
O16-Cl-O18	46.6(13)	O16-Cl-O17	85.2(14)
O15-Cl-O18	152.9(10)	O15-Cl-O17	22.5(12)
O15-Cl-O16	106.5(9)	O14-Cl-O18	26.8(11)
O14-Cl-O17	158.4(12)	O14-Cl-O16	73.3(7)
O14-Cl-O15	174.4(10)	O13-Cl-O18	69.6(12)
O13-Cl-O17	62.2(13)	O13-Cl-O16	23.1(8)
O13-Cl-O15	83.6(5)	O13-Cl-O14	96.3(5)
O12-Cl-O18	89.1(12)	O12-Cl-O17	93.2(11)
O12-Cl-O16	88.0(7)	O12-Cl-O15	86.8(8)
O12-Cl-O14	87.6(8)	O12-Cl-O13	89.5(5)
O11-Cl-O18	90.4(11)	O11-Cl-O17	87.3(12)
O11-Cl-O16	91.8(7)	O11-Cl-O15	93.8(8)
O11-Cl-O14	91.8(8)	O11-Cl-O13	90.6(5)
O11-Cl-O12	179.4(5)		

dination sphere consists of a chelating acetato, two *cis*-oriented MeCN and two *trans*-disposed PPh_3 ligands. The complex has a mirror plane which coincides with the ac plane of the crystal lattice and passes through the ruthenium atom as well as the carbon atoms of the acetato ligand. The observed long Ru-O distance of 2.140(6)Å could be due to the *trans*-influence of the MeCN ligands which show a relatively shorter Ru-N distance of 2.003(7)Å. The *trans*-arrangement of the PPh_3 ligands in complex (**1**) could be due to steric reasons.

The mechanistic aspects of the core cleavage reaction are of importance. Complex (**1**) has a structural similarity with the carbonyl complexes,

$RuH(CO)(O_2CR)(PPh_3)_2$ and $RuCl(CO)(O_2CR)(PPh_3)_2$, obtained from a reaction of $Ru_2Cl(O_2CR)_4$ with PPh_3 in RCH_2OH. This indicates the involvement of a structurally analogous diruthenium intermediate in these reactions. Recent reports[6,7,14] from our laboratory have shown that a μ-aquadiruthenium(II, III) complex, $Ru_2(OH_2)Cl(MeCN)(O_2CR)_4(PPh_3)_2$, belonging to the Class II type of mixed-valence systems[15], is an active intermediate in the reaction in MeCN. This unstable complex converts[14] readily to the μ-oxodiruthenium(III) complexes, $Ru_2O(O_2CR)_4(PPh_3)_2^2$ and $Ru_2O(MeCN)_4(O_2CR)_2(PPh_3)_2^{2+}$. It is likely that the intermediate, on further reaction with PPh_3, undergoes a core cleavage reaction to form the monomeric ruthenium(II) complex (**1**). The experimentally observed poor yield of the monomeric species suggests that the intramolecular chelate ring formation is a facile process than the cleavage of the triply bridged dimeric core of the μ-aqua intermediate species.

Acknowledgement

We are grateful to the Department of Science and Technology, Govt of India, for financial support.

References

1 Cotton F A & Walton R A, *Multiple bonds between metal atoms* (Wiley Interscience, New York) 1982; Cotton F A & Walton R A, *Structure and Bonding* (*Berlin*), 62 (1985) 1.
2 Stephenson T A & Wilkinson G, *J inorg nucl Chem*, 28 (1966) 2285.
3 Norman J G Jr, Renzoni G E & Case D A, *J Am chem Soc*, 101 (1979) 5256.
4 Mitchell R W, Spencer A & Wilkinson G, *J chem soc, Dalton Trans*, (1973) 846.
5 Barral M C, Jiménez-Aparicio R, Royer E C, Urbanos F A, Monge A & Ruiz-Valero C, *Polyhedron*, 10 (1991) 113.
6 Mandal S K & Chakravarty A R, *Inorg chim Acta*. 132 (1987) 157.
7 Das B K & Chakravarty A R, *Inorg Chem*, 29 (1990) 1783.
8 Das B K & Chakravarty A R, *Inorg Chem*, 29 (1990) 2078.
9 Sheldrick G M, *SHELXS*-86, *A computer program for automatic solution of crystal structures* (Universität Göttingen) 1986.
10 Sheldrick G M, *SHELX*-76, *A program for crystal structure determination* (University of Cambridge, England) 1976.
11 *International tables for X-ray crystallography*, Vol 4 (Kynoch Press, Birmingham) 1974.
12 North A C T, Phillips D C & Mathews F S, *Acta Crystallogr*, A24 (1968) 351.
13 Johnson C K, *ORTEP*, Report *ORNL*-3794, (Oak Ridge National Laboratory, Tennessee) 1971.
14 Das B K & Chakravarty A R, *Inorg Chem*, 30 (1991) 4978.
15 Robin M B & Day P, *Adv Inorg Chem Radiochem*, 10 (1967) 247.

Indian Journal of Chemistry
Vol. 31A, July 1992, pp. 412-416

Reactions in micellar solutions: Part 13[1]—Kinetics and mechanism of the reversible complexation of iron(III) by ($\alpha\beta$S)(tetraethylenepentamine)(salicylato)cobalt(III) and *cis*-(ammine)bis(ethylenediamine)(salicylato)cobalt(III) ions in aqueous anionic micellar medium

Anadi C Dash* & Sk Sazid Mohammed

Department of Chemistry, Utkal University, Bhubaneswar 751 004, India

Received 11 November 1991; accepted 23 January 1992

The kinetics of the reversible complexation of iron(III) with *cis*-(ammine)bis(ethylenediamine)(salicylato)cobalt(III) and ($\alpha\beta$S)(tetraethylenepentamine)(salicylato)cobalt(III) ions have been investigated at 25.0°C in the aqueous anionic micellar medium of sodium dodecyl sulphate. The kinetic findings indicate that the reactants are strongly bound to the micelle surface and the reaction occurs in the water rich zone of the micelle-bulk aqueous interface. The reaction of $FeOH^{2+}$ with $N_5CoO_2CC_6H_4OH^{2+}$ contributes to the formation of the binuclear species, $N_5CoO_2CC_6H_4OFe^{4+}$, the dissociation of which is not catalysed by H^+ in the micellar pseudo-phase unlike that for the aqueous medium reported earlier. The micellar retardation of the formation and dissociation of the binuclear species are governed by coluombic and hydrophobic interaction effects.

In an earlier paper[1] we have reported the kinetics of complexing of oxalatopentaamminecobalt(III) with Ni^{2+} and Fe^{3+} in the presence of the anionic micelles of sodium dodecyl sulphate (SDS). The observed rate enhancement was accounted for by the electrostatic enrichment of these hydrophilic cationic reactants in the micellar pseudo-phase. However, the micellar pseudo-phase also provides a medium with some degree of hydrophobicity due to the partial exposure of the hydrocarbon tail of the surfactant molecule to the aqueous environment[2]. Our earlier studies of the complexation equilibria of salicylatopentaminecobalt(III) ions ($N_5CoSalH^{2+}$; $N_5 = (en)_2(NH_3)$, $(trien)(NH_3)$, tetren)[3] with Fe^{3+}, and the acid and base hydrolysis of acidoamine cobalt(III) complexes possessing nonlabile amine ligands of varying degree of hydrophobicity[4,5] indicated that both hydrophobic and electrostatic effects contribute to the micellar mediation of such reactions.

These studies encouraged us to examine to what extent the anionic micelles can mediate the kinetics of complexing of $Fe(OH_2)_6^{3+}$ and $Fe(OH_2)_5OH^{2+}$ with the salicylatopentaminecobalt(III) ions of similar charge type and of varying degree of hydrophobicity. The kinetics and mechanism of the binuclear complexation of Fe^{3+} with the salicylatopentaminecobalt(III) ions in aqueous medium in absence of micelles has been reported earlier[6] which would serve as the basis for comparison.

Materials and Methods

The *cis*-(ammine)bis(ethylenediamine)(salicylato)cobalt(III) perchlorate and ($\alpha\beta$S)-(tetren)(salicylato) cobalt(III) perchlorate were prepared and characterized by analytical and UV-visible spectral data as described earlier[6,7]. Fe(III) perchlorate solution was prepared and estimated for Fe(III) and free $HClO_4$ contents as described earlier[8]. Sodium dodecyl sulphate (E. Merck, G R, purity 99%) was used without further purification. All solutions were prepared in doubly distilled water. The solution of the surfactant was filtered quantitatively before use to get optical clarity. Standard $NaClO_4$ and $HClO_4$ were used to adjust *p*H and ionic strength of the reaction mixtures wherever necessary.

Procedure and instrumentation

The spectral measurements were made with a JASCO UV-visible recording spectrophotometer model 7800. The *p*H measurements were made with ELICO digital *p*H meter model LI 120 equipped with a combined glass-Ag/AgCl, NaCl (2 mol dm^{-3}) electrode C151. Standard buffers of *p*H 1.68 (potassium tetroxalate) and 4.01 (potassium phthalate) were used to calibrate the *p*H meter. The $[H_w^+]$ values in the aqueous pseudo-phase of the micellar solutions were calculated from the measured *p*H values using a calibration curve drawn for the aqueous $HClO_4$ solutions (pH_{obsd} versus $p[H_w^+]$

plots) of varying concentrations in the range pH = 1-2.

Kinetic measurements were performed at 25.0 ± 0.1°C. using a fully automated HITECH (U K) SF 51 stopped flow spectrophotometer. The reactants (Fe(III) and salicylatocobalt(III) substrates) loaded separately in two syringes under identical composition of the reaction medium, were rapidly mixed using pneumatic drive and the progress of the reaction was monitored at 540 nm at which $N_5CoSalFe^{4+}$ was the significantly absorbing species {$\varepsilon_{540\,nm} = 1040$ dm^{3}mol^{-1}cm^{-1} for (tetren) $CoSalH^{2+}$ in aqueous medium}[3]. The concentrations of the cobalt(III) substrates were (3.0-3.4) × 10^{-4} mol dm^{-3} and $[Fe^{3+}]_T$ had to be varied in a narrow range (= 0.001-0.005 mol dm^{-3}) due to severe solubility limitations in the presence of SDS. However, the extent of depletion of Fe(III) due to complexation was too small to affect the pseudo-first order kinetics.

The absorbance-time data (in terms of voltage output) displayed on the monitor of the online APPLE IIGS PC were fitted to a single exponential equation applicable to first order kinetics by the help of ADS_2 software from M/s HITECH. At least seven replicate measurements were made for any run.

Results and Discussion

The rate data for the complexation of *cis*-

Table 1—Rate data for complexation of *cis*-$[Co(en)_2(NH_3)SalH]^{2+}$ with Fe^{3+} at 25.0 ± 0.1°C

$10^3[Fe^{3+}]_T$ (mol dm^{-3})	$[HClO_4]_T$ (mol dm^{-3})	$[SDS]_T$ (mol dm^{-3})	k_{obs} (s^{-1})	$k_f^M/\bar{V}^{(a)}$ (s^{-1})	$k_r^{M(a)}$ (s^{-1})
1.00	0.025	0.040	0.17 ± 0.01	1.65 ± 0.12	0.121 ± 0.009
2.00	0.025	0.040	0.21 ± 0.02		
3.00	0.025	0.040	0.25 ± 0.02	($p[H_w^+]$ = 1.86 ± 0.01)	
4.00	0.025	0.040	0.32 ± 0.02		
1.00	0.025	0.060	0.20 ± 0.01	2.03 ± 0.10	0.165 ± 0.005
2.00	0.025	0.060	0.24 ± 0.01		
3.00	0.025	0.060	0.28 ± 0.01	($p[H_w^+]$ = 2.01 ± 0.01)	
4.00	0.025	0.060	0.31 ± 0.01		
1.00	0.025	0.080	0.18 ± 0.01	2.17 ± 0.07	0.155 ± 0.007
2.00	0.025	0.080	0.22 ± 0.01		
3.00	0.025	0.080	0.24 ± 0.01	($p[H_w^+]$ = 2.08 ± 0.02)	
4.00	0.025	0.080	0.27 ± 0.01		
1.00	0.050	0.040	0.18 ± 0.02	1.40 ± 0.10	0.140 ± 0.001
2.00	0.050	0.040	0.22 ± 0.010		
3.00	0.050	0.040	0.26 ± 0.010	($p[H_w^+]$ = 1.37 ± 0.01)	
4.00	0.050	0.040	0.30 ± 0.01		
1.00	0.100	0.040	0.16 ± 0.01	1.08 ± 0.08	0.128 ± 0.003
2.00	0.100	0.040	0.19 ± 0.01		
3.00	0.100	0.040	0.22 ± 0.01	($p[H_w^+]$ = 1.11 ± 0.01)	
4.00	0.100	0.040	0.25 ± 0.01		
5.00	0.100	0.040	0.29 ± 0.02		
1.00	0.025	0.100	0.17 ± 0.01	2.84 ± 0.08	0.146 ± 0.007
2.00	0.025	0.100	0.21 ± 0.01		
3.00	0.025	0.100	0.24 ± 0.01	($p[H_w^+]$ = 2.15 ± 0.02)	
4.00	0.025	0.100	0.27 ± 0.01		
5.00	0.025	0.100	0.29 ± 0.01		
1.00	0.100		0.35 ± 0.01[(b)]		
2.00	0.100		0.36 ± 0.01		
3.00	0.100		0.38 ± 0.01		
4.00	0.100		0.42 ± 0.01		
5.00	0.100		0.45 ± 0.03		

(a) mean values of $k_f^M/\bar{V}$ and k_r^M quoted are for cmc = 0.002, 0.004, 0.006 and 0.008 mol dm^{-3}.
(b) No SDS.

$[Co(en)_2(NH_3)SalH]^{2+}$ and $[Co(tetren)SalH]^{2+}$ are collected in Tables 1 and 2 respectively. At fixed $[SDS]_T$ and $[H^+]_T$, k_{obs} increases with increasing $[Fe^{3+}]_T$] and k_{obs} versus $[Fe^{3+}]_T$ plots are satisfactorily linear with positive gradients and intercepts. The rate measurements were made at $[SDS]_T \gg$ cmc and the cmc of SDS under the experimental condition is likely to be much less than its reported value ($=0.008$ mol dm^{-3}) in the absence of any additives[9]. Further it is known that highly charged cations are strongly bound to the anionic micelles of SDS[4,5,10]. Hence it is reasonable to assume that the complexation reaction occurs exclusively in the anionic micellar pseudo-phase. A comparison of the values of k_{obs} at $[H^+]=0.10$, $[Fe^{3+}]_T=0.0010$-0.0050, $[SDS]_T=0$ and 0.040 mol dm^{-3} (see Tables 1 and 2) clearly reveals the rate retarding influence of the SDS micelles in contrast to what is expected from the apparent enhancement of the concentrations of the ionic reactants due to their selective partitioning in to the anionic micellar pseudo-phase. This contrasting behaviour is accounted for if it is assumed that both $Fe(OH_2)_5OH^{2+}$ and $Fe(OH_2)_6^{3+}$, the concentrations of which are controlled by the acidity of the micellar pseudo-phase, take part in the complexation kinetics. The cobalt(III) substrates, however, will exist exclusively in the phenol form ($pK_{OH} > 10$)[7] under the experimental condition. A reasonable reaction mechanism is shown in Scheme1. In Scheme 1, the superscript/subscript 'M' denote the micellar pseudo-phase; the number of water molecules in the primary coordination spheres of both the product and the reactant Fe(III) species to satisfy the octahedral coordination are dropped for

Table 2— Rate data for complexation of ($\alpha\beta$S)(tetren)CoSalH^{2+} with Fe^{3+} at 25.0 ± 0.1°C

$[Fe^{3+}]_T$ 10^3(mol dm^{-3})	$[HClO_4]_T$ (mol dm^{-3})	$[SDS]_T$ (mol dm^{-3})	k_{obs} (s^{-1})	$k_f^M/\bar{V}$[a] (s^{-1})	k_r^M[a] (s^{-1})
1.00	0.025	0.040	0.46 ± 0.01	2.73 ± 0.20	0.39 ± 0.01
2.00	0.025	0.040	0.55 ± 0.01		
3.00	0.025	0.040	0.62 ± 0.02	($p[H_w^+]=1.85\pm0.01$)	
4.00	0.025	0.040	0.69 ± 0.02		
1.00	0.025	0.080	0.44 ± 0.02	4.25 ± 0.14	0.38 ± 0.014
2.00	0.025	0.080	0.49 ± 0.01		
3.00	0.025	0.080	0.57 ± 0.03	($p[H_w^+]=2.04\pm0.02$)	
4.00	0.025	0.080	0.60 ± 0.03		
2.00	0.025	0.100	0.47 ± 0.02	4.55 ± 0.12	0.38 ± 0.02
3.00	0.025	0.100	0.52 ± 0.03	($p[H_w^+]=2.15\pm0.02$)	
4.00	0.025	0.100	0.58 ± 0.02		
5.00	0.025	0.100	0.61 ± 0.02		
1.00	0.050	0.040	0.48 ± 0.02	2.16 ± 0.16	0.44 ± 0.03
2.00	0.050	0.040	0.58 ± 0.02		
3.00	0.050	0.040	0.64 ± 0.02	($p[H_w^+]=1.42\pm0.02$)	
4.00	0.050	0.040	0.68 ± 0.01		
1.00	0.100	0.040	0.43 ± 0.04	1.54 ± 0.11	0.37 ± 0.01
2.00	0.100	0.040	0.46 ± 0.02		
3.00	0.100	0.040	0.51 ± 0.05	($p[H_w^+]=1.11\pm0.01$)	
4.00	0.100	0.040	0.55 ± 0.04		
5.00	0.100	0.040	0.60 ± 0.04		
2.00	0.100	0.080	0.42 ± 0.02	5.89 ± 0.20	0.26 ± 0.014
3.00	0.100	0.080	0.51 ± 0.03	($p[H_w^+]=1.13\pm0.01$)	
4.00	0.100	0.080	0.57 ± 0.02		
5.00	0.100	0.080	0.66 ± 0.02		
2.00	0.100		0.63 ± 0.06[b]		
3.00	0.100		0.77 ± 0.05		
4.00	0.100		0.82 ± 0.06		
5.00	0.100		0.90 ± 0.07		

(a) mean values of $k_f^M/\bar{V}$ and k_r^M quoted are for cmc = 0.002, 0.004, 0.006, and 0.008 mol dm^{-3}.
(b) No SDS.

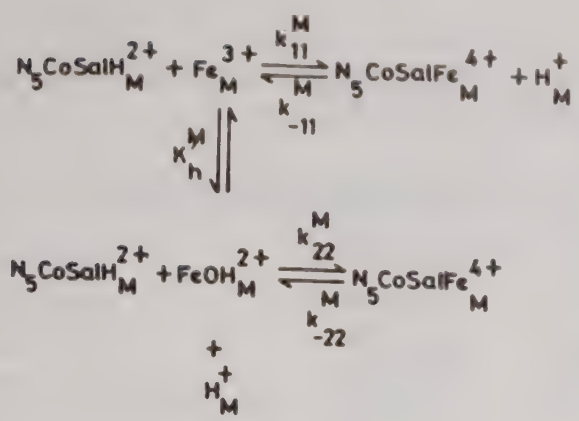

Scheme 1

convenience. We have earlier pointed out that the binuclear species are chelates in which Fe(III) is chelated by the phenol group (with deprotonation) and the carboxylate group bound to the cobalt(III) centre[6–8]. In accord with Scheme 1, k_{obs} takes the form given in Eq. (1).

$$k_{obs} = k_f^M m_{Fe}^s/\bar{V} + k_r^M \quad \ldots(1)$$

where

$$k_f^M = \frac{k_{11}^M + k_{22}^M K_h^M/(m_H^s/\bar{V})}{1 + K_h^M/(m_H^s/\bar{V})} \quad \ldots(2)$$

$$k_r^M = k_{-11}^M (m_H^s/\bar{V}) + k_{-22}^M \quad \ldots(3),$$

k_{ii}^M (ii = ±11, ±22) and K_h^M stand for the rate constants for various steps and hydrolysis constant of Fe^{3+} in the micellar pseudo-phase respectively; $m_{Fe}^s = [Fe^{3+}]_T/[Dn]$, $m_H^s = ([H^+]_T - [H_w^+])/[Dn]$, $[Dn] = [SDS]_T - cmc$, and $\bar{V}$ denotes the molar volume of the micellar pseudo-phase which is the residence site of the reactants.

It is assumed in Eq. (3) for the reverse reaction that appreciable protonation of the binuclear species did not occur in the micellar pseudo-phase. The values of $k_f^M/\bar{V}$ and k_r^M at each $p[H_w^+]$ and $[SDS]_T$ were calculated by fitting $k_{obs} - m_{Fe}^s$ data to Eq. (1); k_{obs} was weighted inversely as its variance and cmc was used as an adjustable parameter in the range 0.002-0.008 mol dm^{-3}. The calculated values of the parameters are given in Tables 1 and 2 which further indicate that these are insensitive to the chosen values of cmc.

The values of k_r^M for both the cobalt(III) substrates turned out to be independent of m_H^s (calcd. m_H^s varied from 0.187 to 0.621 for cmc = 0.004 mol dm^{-3}). This further indicated that the dissociation of the binuclear species occurred exclusively via the acid independent path and k_r^M is reconciled with k_{-22}^M (i.e. $k_{-11} m_H^s/\bar{V} \ll k_{-22}^M$) (see Eq. 3). This is in contrast with the observed acid catalysis in the dissociation of the binuclear species in fully aqueous medium reported earlier[6]. Evidently the protonation of the highly charged binuclear species, $N_5CoSalFe^{4+}$, is not favourable despite the negative charge of the micellar head group.

The calculated values of $(k_f^M/\bar{V})m_H^s$ also turned out to be constant under the experimental conditions for both the substrates for any chosen value of cmc in the range 0.002 to 0.008 mol dm^{-3}. This further indicated that Eq. (2) essentially reduced to Eq. (4),

$$k_f^M/\bar{V} = k_{22}^M K_h^M/m_H^s \quad \ldots(4)$$

under the experimental conditions. Hence the formation of the binuclear species occurred exclusively via the reaction of $FeOH^{2+}$ with the phenol form of the cobalt(III) substrates in the micellar pseudo-phase. This is in contrast with the involvement of both Fe^{3+} and $FeOH^{2+}$ in the aqueous medium reported earlier[6]. Similar observations were also made in the study of the kinetics of complexation of Fe^{3+} with $(NH_3)_5CoO_4C_2H^{2+}$ in the presence of micelles[1]. Cavasino *et al.*[11] also reported recently that the complexation between iron(III) and 4[(alkyl carbonyl)amino]-2 hydroxy benzoic acid in the non-ionic micellar media of Brij 35 involved $FeOH^{2+}$ and not Fe^{3+}. This trend is rather surprising as the columbic repulsion between the like charged species (i.e. Fe^{3+} and $N_5CoSalH^{2+}$) is expected to be favourably mediated by the anionic micelles. That it is not so, clearly reveals the importance of the low polarity of the microenvironment of the reactants in the micellar pseudo-phase[9]. Also binding of the reactants to the anionic head groups acts against the formation of the highly charged encounter complex, $\{N_5CoSalH^{2+}, Fe^{3+}\}$, the precursor for the associative interchange mode of the ligand substitution valid for $Fe(OH_2)_6^{3+}$ (ref. 12).

The values of $k_{22}^M K_h^M$ ($= (k_f^M/\bar{V})m_H^s$) turned out insensitive to the chosen values of cmc in the range 0.002 to 0.008 mol dm^{-3}. The mean values of this parameter along with other relevant rate data are summarised in Table 3 for comparison.

The values of k_{-22} (see Table 3) indicate that the anionic micelles exert retarding effect on the dissociation rates of the binuclear species. The values of the relative rate constants, $k_{-22}^W/k_{-22}^M = 2.1$ and 1.9 for $(en)_2(NH_3)coSalFe^{4+}$ and $(tetren)CoSalFe^{4+}$ species respectively, may be compared with that for $(NH_3)_5CoC_2O_4Fe^{4+}$ ($k_{-22}^W/k_{-22}^M = 3.8$ at 25°C)[1]. The retardation of the dissociation of the binuclear complex, $(NH_3)_5CoC_2O_4Ni^{3+}$ exerted by SDS micelles relative to the aqueous medium was, however, less ($k^{W22}/k_{-22}^M = 1.2$ at 25°C)[1]. In contrast to this we also observed that the dissociation rate of $(NH_3)_5CoC_2O_4Ni^{3+}$ increased with decreasing die-

Table 3—Comparison of the rate parameters for the formation and dissociation of the binuclear species, $RCoSalFe^{4+}$, in aqueous phase and anionic micellar pseudo-phase of SDS at 25.0 ± 0.1°C

R	Medium	k_{11} ($dm^3mol^{-1}s^{-1}$)	$k_{22}K_h$ (s^{-1})	k_{22} ($dm^3mol^{-1}s^{-1}$)	k_{-22} (s^{-1})
$(en)_2(NH_3)$	aqueous[a]	5.1 ± 2.8	1.29 ± 0.11	766 ± 67	0.30 ± 0.01
	SDS micelles[b]	not observed	0.56 ± 0.08	331 ± 47[c]	0.14 ± 0.02
(tetren)	aqueous[a]	5.6 ± 0.4	1.12 ± 0.02	663 ± 11	0.72 ± 0.02
	SDS micelles[b]	not observed	0.87 ± 0.08	513 ± 52[c]	0.37 ± 0.06

(a) Values of the parameters refer to $I = 1.0$ mol dm^{-3} (ref. 6)

(b) Values of the parameters for the reaction in the micellar pseudo-phase.

(c) Based on $K_h^M(Fe^{3+}) = K_h^W(Fe^{3+}) = 1.69 \times 10^{-3}$ mol dm^{-3} (25°C, $I = 1.0$ mol dm^{-3} (ref. 14).

lectric constant of MeOH-water media[13]. These facts reflect that the expected rate enhancing effect of the micellar medium due to its lower polarity (dielectric constant = 40)[9] is more than off set by the stabilizing effect of the micelles on the dissociation rates of these highly charged binuclear species. Increasing hydrophobicity of the binuclear species of the same charge type for the same complexing metal ion appears to reduce the micellar retardation as evident from the values of k_{-22}^W/k_{-22}^M for the binuclear complexes of Fe^{3+} with oxalatopentaamminecobalt(III)[1] and salicylatopentaminecobalt(III) ions. The relative values ofthe dissociation rate constants of $N_5CoO_2CC_6H_4OFe^{4+}$, $\{k_{-22}(\text{tetren})/k_{-22}[(en)_2(NH_3)] = 2.6$ and 2.4 in SDS micelles and water respectively$\}$ stands in good support of the fact that the reactions occurred in the water rich region of the micelle-bulk aqueous interface.

The values of the formation rate constant (k_{22}^M) given in Table 3 are based on $K_h^M = K_h^W$. This assumption leads to the micellar retardation for the complexation reaction $\{k_{22}^W/k_{22}^M = 2.3$ and 1.3 for $(en)_2(NH_3)$ and (tetren) substrates respectively$\}$ of both the substrates, the effect being relatively less for the tetren complex. Also it is worth noting that there exists a differentiating action of the micelles, probably of hydrophobic origin, when we compare the values of $(k_{22})(\text{tetren})/k_{22}[(en)_2(NH_3)]$ $\{= k_{22}K_h(\text{tetren})/k_{22}K_h[(en)_2(NH_3)]\}$ which are 1.5 ± 0.2 for SDS micelles and 0.86 ± 0.11 for water.

Acknowledgement

This work was supported by a research grant to A C D from the Department of Atomic Energy, Government of India. Sk S M is thankful to D A E for a junior research fellowship and to Miss J Pradhan for her ungrudging assistance during the experimental work and preparation of the manuscript.

References

1 Part 12: Dash A C & Mohammed Sk Sazid, *Indian J Chem*, 31A (1992) 166.

2 Menger F M, in *Surfactants in solution*, vol. 1, edited by K L Mittal & B Lindman (Plenum, New York) 1984, p. 347.

3 Dash A C & Mohanty A K, *Indian J Chem*, 28A (1989) 868.

4 Dash A C & Nayak R C, *Inorg Chem*, 25 (1986) 2237; Dash A C & Nayak R C, *J chem Soc Faraday Trans* 1, 83 (1987) 1307; Dash A C & Mohanty A K, *Indian J Chem*, 28A (1989) 989.

5 Dash A C, Prusti J, Pradhan J & Das P K, *J chem Soc Faraday Trans* 1, 86 (1990) 507; Tachiyashiki S & Yamatera H, *Inorg Chem*, 25 (1986) 3043.

6 Dash A C & Harris G M, *Inorg Chem*, 21 (1982) 2336.

7 Dash M S & Dash A C, *J inorg nucl chem*, 38 (1976) 571.

8 Dash A C & Nanda R K, *Inorg Chem*, 12 (1973) 2024.

9 Cordes E H & Gitler C in *Progress in bioorganic chemistry*, edited by E T Kaiser & F J Kezdy (Wiley, New York) (1973) vol. 1, p. 1.

10 Stilbs P, Jermer J & Lindman B, *J Colloid interface Sci*, 60 (1977) 232; Fletcher P D I & Robinson B H, *J chem soc Faraday Trans* 1, 80 (1984) 2417.

11 Cavasino F P, Sbrizillo C, Pelizzetti E & Pramauro E, *J phys Chem*, 93 (1989) 469.

12 Grant M & Jordan R B, *Inorg Chem*, 20 (1981) 55; Funahasi S, Ishihara K & Tanaka M, *Inorg Chem*, 22 (1983) 2070; Dash A C & Mohammed Sk Sazid, *Indian J Chem*, 29A (1990) 740.

13 Dash A C & Pradhan J, *Int J chem Kinetics*, (in the press).

14 Milburn R M, *J Am chem Soc*, 79 (1957) 537.

Indian Journal of Chemistry
Vol. 31A, July 1992, pp. 417-422

Oxidations with permanganate in a strong alkaline medium: Calculation of deprotonation constant

J Szammer* & M Jáky

Central Research Institute for Chemistry, Hungarian Academy of Sciences, H-1525 Budapest, P.O. Box 17, Hungary

Received 25 June 1991, revised and accepted 25 December 1991

The process $2MnO_4^- + substrate \rightarrow 2MnO_4^{2-} + product$, has been studied employing the substrates methanol, ethanol, *n*-butanol and formaldehyde in aqueous solutions of [alkali] in the region of 0.1-2.0 mol dm^{-3}. The reactive species is the alkoxy anion and the deprotonation constant (K_B) of these substrates can be calculated from the kinetic data, which are in good agreement with literature data obtained by other methods. The procedure seems to be applicable for the determination of the deprotonation constant of other organic substrates containing a hydroxyl group. A mechanism based on electron abstraction from the alkoxy anion and simultaneous nucleophilic attack by OH^- has been proposed.

It has been known[1-4] for a long time that permanganate ion in alkaline medium oxidises numerous organic compounds, which are not or only very slowly oxidised by this compound in acidic or neutral media. If $[OH] \geq 1$ mol dm^{-3}, pemanganate is reduced only to manganate in the majority of cases, and this undergoes further reaction at a much slower rate, owing to its considerably lower reactivity[3-6].

Thus the process, Mn(VII) → Mn(IV), consisting of several steps can be divided into partial steps and each can individually be studied. Manganese dioxide appears almost at the end when permanganate has been totally consumed in the reaction and, hence, the reaction can be followed spectrophotometrically. Nevertheless, the mechanisms of the reactions are not yet clear, and in some cases the doubt persists whether direct oxidation or oxidation induced by hydroxyl radical takes place. Permanganate is, mainly, reduced spontaneously to manganate in alkaline medium with the evolution of O_2, and as the first step of the complex mechanism, hydroxyl radical is formed[7] (see Eq. 1).

$$MnO_4^- + OH^- \underset{k_{-1}}{\overset{k_1}{\rightleftharpoons}} MnO_4^{2-} + HO^{\cdot} \qquad \ldots(1)$$

which undergoes further reaction represented by Eq. (2),

$$RH + {}^{\cdot}OH \xrightarrow{k_2} R^{\cdot} + H_2O \qquad \ldots(2)$$

This mechanism is supported by experiments carried out with labelled ^{18}O and the results indicate that the oxygen atom is always generated from water and O_2 evolution observed in the absence of substrate is suppressed when substrate is present, and racemic products are always obtained[7-10]. Symons found that reaction (1) was the rate-determining step and he could estimate the value of k_1 as 3×10^{-3} $mol^{-1} dm^{-3} s^{-1}$ at $[OH^-] = 1.0$ mol dm^{-3}. The earlier assumption of Wiberg[11] that the oxidation of substituted benzene derivatives also occurs by this mechanism does not appear to be logical because the rate constants measured by him were greater by several orders of magnitude. At the same time, it is likely that the C – H bond of the tertiary carbon atom is oxidized by this radical pathway[12,13], even the primary carbon atom is oxidised in this way but this oxidation is slower by two orders of magnitude than that found by Zielinski in the case of acetic acid[14]. These facts lead to the conclusion that the oxidation of alcohols and carbonyl compounds cannot take place by the intervention of hydroxyl radical due to the high reaction rate, and only a direct oxidation can be assumed. Nevertheless, since the process,

$$MnO_4^- + MnO_4^{3-} \rightarrow 2MnO_4^{2-} \qquad \ldots(3)$$

is very fast[2,5,6], it is difficult to decide if permanganate is reduced in one-electron steps (Scheme 1),

$$Mn(VII) + S \xrightarrow{k_1} Mn(VI) + S^{\cdot}$$

$$Mn(VII) + \overline{S^{\cdot}} \xrightarrow{k_2} Mn(VI) + Product$$

$$k_2 \gg k_1$$

Scheme 1

or hypomanganate is formed previously in a two-electron step, followed by a fast reaction (3) (Scheme 2).

$$Mn(VII) + S \xrightarrow{k_1} Mn(V) + Product$$

$$Mn(VII) + Mn(V) \xrightarrow{k_2} 2Mn(VI)$$

$$k_2 \gg k_1$$

Scheme 2

Permanganate oxidation of primary alcohols also proceeds in acid medium[16-21], but this reaction is not as fast as in alkaline medium[15]. The reaction rate in alkaline medium increases with increase in $[OH^-]$, indicating considerably higher reactivity of the alcoholate anion than that of the undissociated alcohol molecule. A mechanism based on hydride (H^-) ion abstraction was proposed by Stewart[22,23] in the case of substituted benzhydrols and by Freemann[24] in the case of mandelic acid based on extremely high kinetic isotope effect and on the observation that according to the investigations carried out with ^{18}O, no oxygen atom is transferred into the product. At the same time, they admitted that the above observations are not in harmony with the very little substituent effect; therefore, the one-electron oxidation mechanism with H^+ abstraction or with H atom elimination can not be excluded either.

In the case of aldehydes, a few investigations were carried out mainly in acidic medium[25-27], in alkaline medium, a mechanism based on H^- abstraction from the hydrate form, similar to that for alcohols was proposed in the oxidation of fluoral[28] and furfural[29].

Concerning the substrates studied by us in the present paper, methanol is quantitatively oxidized to carbon dioxide[1] while ethanol yields 10-20 mol% oxalic acid[1,30,31] also. As for the kinetics, in alkaline medium rate constants higher by three orders of magnitude have been measured[32] at $[OH^-] = 0.2$ mol dm^{-3} compared to those in neutral and acidic media[17,18,21]. It has been known for a long time that formaldehyde, being almost completely hydrated[33], behaves as a geminal glycol rather than as a carbonyl compound. The hydration of acetaldehyde and *n*-butyraldehyde is not complete, presumably due to enolization. Therefore, the substrate choice is restricted and such substrates have not been pictured within present investigation. Formic acid is a typical example of how complicated the oxidation of such a simple substrate leading to a consistent end-product can be, because in spite of numerous thorough investigations, several mechanisms are assumed[34-38].

Materials and Methods

The reagents $KMnO_4$, $NaClO_4$ and NaOH were of AR (Merck) grade. The substrates were extra pure reagent from Fluka.

Stoichiometry

Substrate (2.0×10^{-4} mol) was added to permanganate (6.0×10^{-4}-16.0×10^{-4} mol) after previous adjustment of appropriate [alkali] in both solutions. After the reaction time, solid KI was added, followed by 10% H_2SO_4. Excess permanganate at the end of the reaction was titrated against thiosulfate solution. If the reaction time exceeded 15 min, the oxidation equivalent did not change at any [alkali].

Products

After adjustment of appropriate [alkali], permanganate solution exceeding the determined stoichiometric ratio was added to ethanol or acetaldehyde (1.0×10^{-3} mol). After a reaction period of 15 min, the excess permanganate and manganate were reduced by hydrazine hydrate solution to manganese dioxide. After filtration, the solution was neutralized, acidified with acetic acid and finally calcium oxalate was precipitated by a standard method. Oxalic acid was qualitatively identified by the diphenylamine test, and determined quantitatively by weight measurement. The reaction was carried out as described above and after filtering the MnO_2 formed, phosphoric acid (50 ml, 85%) was added to the solution which was distilled till no more distillate was obtained. After the addition of water (2×50 ml) distillation was continued. The acetic acid content of the distillate was determined by titration with alkali.

Kinetics

Kinetic measurements were performed on a Shimadzu recording spectrophotometer (model UV 300) equipped with a rapid mixing attachment (model RMA-1A) and on a Hewlett-Packard (8452A) spectrophotometer connected to a rapid kinetics accessory (HI-TECH-SFA-11). Each k_{obs} and k_0 value represents a mean value of 3 to 5 individual measurements. For the calculation of initial slopes and for curve fittings a Hewlett-Packard 9000-300 type computer, directly coupled to the spectrophotometer, was used.

Results

Stoichiometry

The oxidation equivalents required for the oxida-

tion of substrates to end products were determined by iodometric titration of the excess of permanganate at the end of reaction. The oxidation equivalent values per mole obtained at each [alkali] were: 6.0 ± 0.2 for methanol; 4.0 ± 0.2 for formaldehyde, ethanol and *n*-butanol; and 2.0 ± 0.1 for formic acid.

Products

Excess permanganate was added to ethanol. After the oxidation was over, the unreacted permanganate and manganate were removed as manganese dioxide. No calcium oxalate could be precipitated from the reaction mixture but, after acidifying by conc. phosphoric acid, 100 ± 4 mol % acetic acid could be distilled. When the same experiment was carrried out with previously basified acetaldehyde, the reaction mixture contained only about 70 mol % acetic acid; oxalic acid was also present.

Kinetic measurements

Kinetic measurements were carried out under pseudo-first order conditions (at least 10-fold excess of substrate). Decay of permanganate was followed spectrophotometrically at 524 nm. The $[OH^-]$ was adjusted by adding NaOH while the ionic strength was maintained constant by adding $NaClO_4$. The temperature was uniformly maintained at 25°C. During reaction, colour of the reaction mixture changed from violet to blue and finally to green. The spectrum of the green solution was identical to that of MnO_4^{2-}. The spectrophotometer could record the total spectrum every 0.5 second. This enabled us to observe that the blue colour originated from violet of permanganate and the green from manganate, excluding the accumulation of hypomanganate.

The $\log(A - A_\infty)$ versus time plots (A = the absorbance measured at 524 nm), except for methanol, were good linear at least up to 75% consumption of permanganate, indicating first order in [permanganate]. The k_{obs} values calculated from the slopes of the linear plots are listed in Table 1. For methanol, the k value calculated from the slope extrapolated to zero by numerical method was taken as k_{obs} value. The value obtained did not change by decreasing the initial [permanganate] to its half value, indicating that the first order in [permanganate] is valid for methanol as well. At the same time, k_{obs} versus $[S]_0$ plots were linear passing through the origin in all cases, verifying that the reaction is first order in [substrate] at a given $[OH^-]$ leading to the rate law (4).

$$-\frac{d[MnO_4^-]}{dt} = k_{obs}[MnO_4^-] = k_0[S]_0[MnO_4^-] \quad \ldots(4)$$

The k_0 values measured at diverse $[OH^-]$ are listed in Table 2, together with k_0 values measured at *p*H 4.6 and, in the case of formic acid at $[H^+] = 1.0$ mol dm^{-3}. For assessing the role of manganate some measurements were performed also with manganate ion. The aim was to determine the inaccuracy caused by the consumption of manganate in the value of A_∞. The k_0 values obtained in the presence of manganate by the method of initial fitting (these are also listed in Table 2) are by orders of magnitude smaller than those of permanganate, thus the interference due to manganate can be neglected.

The kinetic stoichiometric factor of the reactions relates to the number of fast steps following the rate determining step. For the determination of this, the following relatively sensitive method was applied. The reagents were reacted with each other in the ratio of the assumed $[MnO_4^-]_0 = \nu[S]_0$ initial concentration ratio, and if this ratio was correct, then the integrated kinetic Eq. (5) must hold.

$$\frac{1}{[MnO_4^-]} - \frac{1}{[MnO_4^-]_0} = kt \quad \ldots(5)$$

The $1/[MnO_4^-]$ versus time plot were linear at initial concentrations $\nu = 4$ for ethanol and butanol

Table 1—Pseudo-first order rate constants at varying [substrate]

$[MnO_4^-] = 1.0 \times 10^{-3}$ mol dm^{-3}; $[NaOH] = 0.50$ mol dm^{-3}; $I = 2.0$ mol dm^{-3}; temp. = 25°C

$10^2 \times [Substrate]_0$ (mol dm^{-3})	$10^2 \times k_{obs}$ (s^{-1})				
	Methanol	Formaldehyde hydrate	Formic acid	Ethanol	*n*-Butanol
1.0	0.82	121	9.3	3.27	7.39
2.0	1.58	249	17.7	6.62	14.3
3.0	2.46	353	28.4	9.71	21.7
4.0	3.24	491	38.0	13.2	30.1
5.0	4.18	602	45.9	16.1	37.3

Table 2—Dependence of rate constants (k_0, $dm^3 mol^{-1} s^{-1}$) on $[OH^-]$
$[Substrate]_0 = 1.00 \times 10^{-2}$ mol dm^{-3}; $[MnO_4^-]_0 = 1.0 \times 10^{-3}$ mol dm^{-3}; (or $[MnO_4^{2-}]_0 = 1.0 \times 10^{-3}$)[d];
$I = 2.0$ mol dm^{-3}; temp. = 25°C.

$[OH^-]$ (mol dm^{-3})	Methanol	Formaldehyde hydrate	Formic acid	Ethanol	*n*-Butanol
0.10	0.18	47.4	9.1	0.66	1.49
0.25	0.43	79.3	9.4	1.65	3.72
0.50	0.82	121	9.3	3.27	7.39
0.75	1.17	160	9.2	4.85	11.04
1.00	1.48	196	9.5	6.41	14.6
1.50	2.03	264	9.2	9.35	21.5
2.00	2.49	327	9.4	12.3	28.5
0.10[a]	0.079	24.2	5.1	0.34	0.92
*p*H 4.6[b]	~0	9×10^{-2}	—	~0	~0
$[H^+] = 1.0$[c]	—	—	1.5×10^{-3}	—	—
0.25[d]	4.3×10^{-3}	13.5	59×10^{-3}	6.9×10^{-3}	14.2×10^{-3}
2.00[d]	14.0×10^{-3}	5.6	62×10^{-3}	26.8×10^{-3}	37.4×10^{-3}

[a]Ionic strength = 0.10 mol dm^{-3}
[b]Adjusted by adding succinic acid buffer
[c]$[HClO_4] = 1.0$ mol dm^{-3}
[d]Oxidation by manganate (MnO_4^{2-})

and at $\nu = 2$ for formaldehyde and formic acid. The k values obtained from the slopes were identical to those obtained under pseudo-first order conditions. Thus, the consumption ratio $\Delta[MnO_4^-]/\Delta[S]$ in the process measured kinetically is 4 and 2, respectively. For methanol, no consistent ν value could be obtained.

Discussion

It should be noted that the problem has been partially treated in an earlier publication[15] (at an ionic strength of 1.5 mol dm^{-3}), but the kinetic data have not been used there for the determination of K_B value. On the other hand, earlier we had considered other assumptions concerning the mechanism as well.

The results of stoichiometric measurements indicate that the oxidation equivalents consumed decrease by two in the series: methanol-formaldehyde-formic acid, suggesting that these substrates are transformed into each other in the same sequence, each of them being oxidized finally to carbon dioxide. Ethanol and butanol are converted, via the corresponding aldehydes, into acetic acid and butyric acid, respectively, although their oxidation is very slow; therefore, their consumption need not be taken into account. Oxidation of ethanol yielded acetic acid quantitatively. The oxidation must proceed via acetaldehyde in spite of the fact that in the oxidation of acetaldehyde some oxalic acid is also formed, which could not be found in the case of oxidation of ethanol. This is presumably due to the formation of geminal glycol in the direct oxidation step; its enolization followed by elimination of water is slower than its direct oxidation. Oxidation studies on acetaldehyde and butyraldehyde indicate that both these aldehydes react with at least 150 times higher rate constant in the whole [alkali] range than the corresponding alcohol. Thus the oxidation of aldehydes can be considered with a factor of two, which is supported by the measured $\nu = 4$ value. Oxidation kinetics of formaldehyde, estimated from the calculations of Benson[39], is not disturbed by formic acid reacting slower. In the case of methanol, the situation is somewhat different. The intermediate product, formaldehyde, always reacts at a rate more than 130 times higher than methanol. This can be taken into account theoretically by a factor of two, while formic acid formed from formaldehyde reacts further at a rate of only 4-55 times higher than methanol. Consequently, the k_0 values for methanol had to be determined by numerical extrapolation to zero in which no intermediate products are yet present.

The value of k_0, except for formic acid, increases with increase in $[OH^-]$, indicating that the alcoholate anion is the reactive form.

Assuming

$$AOH + OH^- \overset{K_B}{\rightleftharpoons} AO^- + H_2O \qquad \ldots(6)$$

we get,

$$K_B = \frac{[AO^-]}{[AOH][OH^-]} \quad \ldots(7)$$

(Owing to the ionic strength of 2.0 mol dm^{-3}, K_B is of course not a thermodynamic constant.)

Considering that

$$[S]_0 = [AOH] + [AO^-] \quad \ldots(8)$$

we get,

$$[AO^-] = \frac{K_B[OH]}{1 + K_B[OH^-]}[S]_0 \quad \ldots(9)$$

At *p*H 4.6 only the undissociated form can be present and, according to the k_0 values measured here, this form reacts at a rate constant several orders of magnitude smaller than the deprotonated form. This indicates that the permanganate consumption of the undissociated form is within the limits of error of the measurement; thus its role can be neglected in the kinetic equation.

Consequently, the rate law assumes the form (10)

$$-\frac{d[MnO_4^-]}{dt} = k' \frac{K_B[OH^-]}{1 + K_B[OH^-]}[S]_0[MnO_4^-] \quad \ldots(10)$$

Equations (10) and (4) lead to:

$$k_0 = k' \frac{K_B[OH^-]}{1 + K_B[OH^-]} \quad \ldots(11)$$

The value of k_0 varies parallel to the ionic strength, indicating again that two reactants with equal charge, i.e., negatively charged MnO_4^- and negatively charged species, react in the rate determining step.

In the case of formic acid, the dissociation is suppressed only at high acidity ($pK_a = 3.75$) and the low rate constant measured at $[H^+] = 1.0$ mol dm^{-3} indicates considerably lower reactivity of the undeprotonated species. In the measuring region $[OH^-] = 0.10\text{-}2.0$ mol dm^{-3}, already the anion is present, and consequently k_0 does not change.

Equation (11) can be linearized by reciprocal formation and the plots $1/k_0$ versus $1/[OH^-]$ were linear except for formaldehyde. The k' and K_B values obtained from the slopes and intercepts of these linear plots, as well as those by direct simulation of Eq. (11) are listed in Table 3. In our opinion it is just the form of $k_0 \sim [OH^-]$ function following the deprotonation curve that verifies completely the participation of alkoxy anion in the oxidation.

The kinetic results obtained for formaldehyde could not be fitted by Eq. (11). It had to be assumed that the deprotonation of other hydroxyl groups of formaldehyde hydrate also occurs simultaneously. The corresponding four-parameter fitting according to Eq. (12)

$$k_0 = \frac{k_1' K_{B1}[OH^-] + k_2' K_{B1} K_{B2}[OH^-]^2}{1 + K_{B1}[OH^-] + K_{B1} K_{B2}[OH^-]^2} \quad \ldots(12)$$

was already found satisfactory. (In Eq. (12) k_1' denotes the rate constant of formaldehyde monoanion

Table 3—Kinetically determined equilibrium and rate constants at 25°C
(Ionic strength = 2.0 mol dm^{-3})

	Methanol	Formaldehyde hydrate	Formic acid	Ethanol	*n*-Butanol
K_B ($dm^3 mol^{-1}$)	0.234 ± 0.01	19 ± 2 (0.080 ± 0.03)[a]	—	4.3(±0.2) × 10^{-2}	2.6(±0.1) × 10^{-2}
k' ($dm^3 mol^{-1} s^{-1}$)	7.8 ± 0.4	56 ± 6 (2070 ± 800)[a]	9.4 ± 0.4	157 ± 7	570 ± 60
ν	2	2	2	4	4
k ($dm^3 mol^{-1} s^{-1}$)	3.9	28 (1035)[a]	4.7	39.2	142
pK_a	14.63	12.72 (15.1)[a]	—	15.37	15.58
pK_a[b]	15.5[40] 15.09[41] 15.07[42] —	13.27[44]	3.75	15.9[40] 15.93[41] 15.83[42] 15.14[43]	— 16.1[41] 15.87[42]

[a]For dianion
[b]Literature data

while k'_2 that of the dianion.) Owing to the relatively narrow range of $[OH^-]$ of the measurements, the rate constants of formaldehyde could be calculated within broad limits of error. Consequently, these constants are informative only.

The constants k relating to the rate determining step are listed in Table 3 as well. The reaction proceeds either by Scheme 1 or by Scheme 2; the quick second reaction involves the appearance of a factor of 2. If the intermediate product reacts more than 150 times faster, this requires another multiplying factor of two. Thus, $k = k'/\nu$. Table 3 also contains literature pK values which are in accord with the values measured by us presently with the observation that acidity decreases in the sequence methanol-ethanol-butanol. Compared to the thermodynamic values, we have measured pK_a values lower by about half a unit, but it can be explained by the high ionic strength.

Now coming to the mechanism, we do not accept the assumptions based on H^- or H abstraction. The C – H bond does not seem more loosened in the alcoholate anion than in the neutral molecule. Therefore, the abstraction of either H^- or H atom from the non-dissociated species might just as well or even more readily take place. Electron abstraction from the oxygen atom of the anion and simultaneous proton elimination seem more probable. This is the two-electron step corresponding to that shown in Scheme 2. The positively polarized C-atom is *ab ovo* surrounded by OH^- ions in the concentrated alkaline solution, and the nucleophilic attack of OH^- on the carbon atom can take place simultaneously with the electron abstraction. The transition state in such a mechanism can be represented by structure (I).

The reactivity sequence in terms of constants k is in harmony with the inductive effect in the case of alcohols. By the increasing length of the electron donating alkyl chain, the electron can more easily be abstracted from the alkoxy O-atom of ethanol and butanol than from methanol. Likewise, in the case of formaldehyde the C – H bond in the dianion is hardly more fragile than in the monoanion. Therefore, the difference of about one and a half order of magnitude between k_1 and k_2 supports the mechanism based on electron abstraction as well; the electron abstraction from the dianion with higher electron density is more favoured.

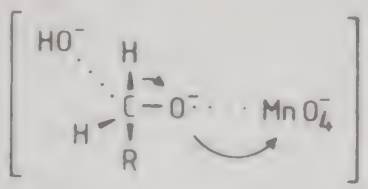

I

R = H, CH_3, C_3H_7

References

1 Drummond A Y & Waters W A, *J chem Soc*, (1953) 453.
2 Pode J F S & Waters W A, *J chem Soc*, (1956) 717.
3 Ladburry J W & Cullis C F, *Chem Rev*, 58 (1958) 403.
4 Waters W A, *Quart Rev*, 12 (1958) 277.
5 Carrington A & Symons M C R, *Chem Rev*, 63 (1963) 443.
6 Stewart R, *Oxidation in organic chemistry Part A*, edited by Wiberg K B, (Academic Press, New York) 1965.
7 Symons M C R, *J chem Soc*, (1954) 3676.
8 Lott K A K & Symons M C R, *Disc Faraday Soc*, 29 (1960) 205.
9 Kenyon J & Symons M C R, *J chem Soc*, (1953) 2129.
10 Kenyon J & Symons M C R, *J chem Soc*, (1953) 3580.
11 Wiberg K B & Stewart R, *J Am chem Soc*, 77 (1955) 1786.
12 Heckner K H, Landsberg R & Dalchau S, *Berichte der bunsenges für phys Chem*, 72 (1968) 649.
13 Heckner K H, Dalchau S & Landsberg R, *Z praktische Chem*, 313 (1971) 153.
14 Zielinski M, *J radioanal Chem*, 80 (1983) 237.
15 Jáky M & Simándy L I, *React Kinet Catal Lett*, 18 (1981) 485.
16 Fatiadi A J, *Synthesis*, (1987) 85.
17 Barter R M & Littler J S, *J chem Soc B*, (1967) 205.
18 Banerji K K, *Bull chem Soc Japan*, 46 (1973) 3623.
19 Banerji K K, *J chem Soc, Perkin Trans* 2, (1973) 435.
20 Bhatia I & Banerji K K, *J chem Soc, Perkin Trans* 2, (1983) 1577.
21 Gupta K K S, Adhikari M & Gupta S S, *React Kinet Catal Lett*, 38 (1989) 313.
22 Stewart R, *J Am chem Soc*, 79 (1957) 3057.
23 Stewart R & Van der Linden R, *Disc Faraday Soc*, 29 (1960) 211.
24 Freeman F & Scott M A H, *J org Chem*, 35 (1970) 2989.
25 Banerji K K, *Z Naturforsch*, 27B (1972) 772.
26 Banerji K K, *Indian J Chem*, 11 (1973) 242.
27 Freeman F, Liu D K & Moore G R, *J org Chem*, 47 (1982) 56.
28 Stewart R & Mocek M M, *Can J Chem*, 41 (1963) 1160.
29 Freeman F, Brant J B, Hester N B, Kamego A A, Kasner M L, McLaughlin T G & Paull E W, *J org Chem*, 35 (1970) 982.
30 Denis J, *Am chem J*, 38 (1910) 564.
31 Evans W L & Day J E, *J Am chem Soc*, 38 (1916) 375.
32 Kreingold S U, Khefilyan L I & Antonov V N, *Zh anal Khim*, 32 (1977) 2424.
33 Holluta J & Mutschin A, *Z phys Chem*, 150 (1930) 381.
34 Wiberg K B & Stewart R, *J Am chem Soc*, 78 (1956) 1214.
35 Halpern J & Taylor S M, *Disc Faraday Soc*, 29 (1960) 174.
36 Candlin J P & Halpern J, *J Am chem Soc*, 85 (1963) 2518.
37 Bell R P & Onwood D P, *J chem Soc B*, (1967) 150.
38 Perez-Benito J F, Arias C & Brillas E, *Int J chem Kinet*, 22 (1990) 261.
39 Benson S W, *J chem Phys*, 20 (1952) 1605.
40 Ballinger P & Long F A, *J Am chem Soc*, 82 (1960) 795.
41 Murto J, *Acta Chem Scand*, 18 (1964) 1043.
42 Takahashi S, Cohen L A, Miller H K & Peake E G, *J org Chem*, 36 (1971) 1205.
43 Jandik P, Meltes L & Zuman P, *J phys Chem*, 87 (1983) 238.
44 Bell R P & Onwood D P, *Trans Faraday Soc*, 58 (1962) 1557.

Indian Journal of Chemistry
Vol. 31A, July 1992, pp. 423-426

Kinetics of the reaction of hydrazine with 2-hydroxy-1-naphthaldehyde

R Garcia Domenech*, J Mañes Vinuesa, M Pascual Pastor & J Mari Buigues
Department of Chemical Physics, Faculty of Pharmacy, University of Valencia, Avda Blasco Ibañez, 13. 46010-Valencia, Spain

Received 22 October 1991; revised and accepted 29 January 1992

Hydrazine in aqueous solution reacts with 2-hydroxy-1-naphthaldehyde in ethanol leading slowly to highly insoluble yellow reaction product. Based on UV-Vis, IR and mass spectrophotometric studies, the compound is characterized as an aldazine, 2,2′-dihydroxy-1-naphthaldazine. Kinetics of the reaction has been followed by spectrophotometric measurements of the absorbance of the reaction product as a function of time. Under excess [2-hydroxy-1-naphthaldehyde] the reaction follows a pseudo-first order kinetics. Under excess [hydrazine], also the reaction follows a pseudo-first order kinetics. Yet important kinetic differences have been found between both the processes. Under excess of 2-hydroxy-1-naphthaldehyde, the reaction is controlled thermally, under excess of hydrazine, the rate constant is temperature independent. According to these results the process takes place in two steps with the formation of an intermediate product. The mathematical treatment of the kinetic results is consistent with the proposed mechanism.

Hydrazine ($NH_2 - NH_2$) is widely used as a strong reducing agent for corrosion control in boilers and hot-water heating systems; also for metal plating, and for reducing noble-metal catalysts and unsaturated bonds in organic compounds[1]. It is the starting material for many derivatives like antioxidants, polymers, plant-growth regulators and pesticides[2]. Besides this, hydrazine is used in the synthesis of pharmaceuticals, such as hydralazine, hydrocarbazine, mebanazine, isoniazide, etc. Since hydrazine is a highly toxic compound[3,4] (at high doses it may cause hepatic damage and depression of the nervous system[5] as well as mutagenic[6,7] and carcinogenic effects) it becomes necessary to determine its existing levels in drugs[8-10].

The aim of this work is to complete recent studies dealing with the determination of hydrazine based on its reaction with 2-hydroxy-1-naphthaldehyde and subsequent extraction of the reaction product with chloroform[11]. The present study deals with two basic aspects, the structural characterization of the reaction product and the evaluation of the stoichiometry of the process: hydrazine + 2-hydroxy-1-naphthaldehyde → product and the study of the reaction mechanism. Thin layer chromatography (TLC) and spectroscopic techniques, such as UV, IR and mass spectrophotometric are used in this study.

Materials and Methods

Hydrazine stock solution was prepared weekly from hydrazine sulphate (Panreac) in distilled water and standardized by bromate titration[11]. 2-Hydroxy-1-naphthaldehyde (Ega-Chemie), was prepared in ethanol. Both solutions were maintained with refrigeration while not in active use. All other chemicals used like acetic acid, sodium acetate, Na_2-EDTA and $CHCl_3$ were provided by Panreac.

Isolation of product

Hydrazine sulphate 0.01 *M* and 2-hydroxy-1-naphthaldehyde in ethanol 0.01 *M*, were added to distilled water (25 ml) in approximately stoichiometric proportions. The contents were mixed by gentle shaking, and kept at 100°C for 5 min. A yellow precipitate appeared, which was filtered off and washed with three portions of ethanol and dried at 80°C to constant weight.

Influence of pH

The effect of *p*H on the reaction has been studied within the *p*H range of 1.8-8.4. With a *p*H of less than 7.0, hydrazine condenses with 2-hydroxy-1-naphthaldehyde, and the corresponding yellow aldazine is formed. The absorbances are proportional to the concentration of the problem substance. The sensitivity of the reaction increases with *p*H and the optimum values in order to determine hydrazine in the area between 3.6 and 6.6 are to be found.

Spectroscopic studies

Absorbance measurements and spectra of 2-hydroxy-1-naphthaldehyde and of reaction product

were recorded using a Shimadzu UV-240 spectrophotometer equipped with 1 cm quartz cells. A Riber 10C spectrometer was used for the mass spectrum of reaction product. Accelerating voltage was 1800V. Ionization energy was 70 eV. Solid injector temperature was set at 180°C.

The infrared spectra were obtained using a Perkin-Elmer 843 infrared spectrophotometer, on solid samples prepared as potassium bromide discs.

Chromatographic determinations

TLC aluminium sheet silicagel 60, layer thickness 0.2 mm (Merck) was used as adsorbent for the separation of reaction product. Chloroform-ethanol-toluene-ammonia (14:11:80:0.5) was chosen as the developing solution. Reaction product spots on the chromatogram were detected by exposure to UV radiation and later evaporated off to allow the formation of crystals.

Linearity study

Stock solution of reaction product in $CHCl_3$ were prepared to contain 100 mg/ml. Aliquots of this solution, representing amounts of reaction product ranging from 20 to 0.3 mg was pipetted into individual volumetric flask (10 ml) and the absorbance of each solution was recorded at 412 nm.

Kinetics studies

Reactions of the hydrazine with 2-hydroxy-1-naphthaldehyde were studied at *p*H 4.5 and at temperatures of 20, 30, 40, 50 and 60°C. Two series were made, one under excess of 2-hydroxy-1-naphthaldehyde and another with excess hydrazine. Experimental conditions for each study were as follows:

Under excess of 2-hydroxy-1-naphthaldehyde, hydrazine solution (1 ml, 2×10^{-4} *M*) was pipetted into a series of glass-stoppered tubes and diluted to 5 ml with distilled water; added acetate buffer (1 ml), Na_2-EDTA (1 ml, 0.02 *M*) and 2-hydroxy-1-naphthaldehyde (1 ml, 0.01 *M*) were added all under thermal equilibrium and absorbance was recorded at 412 nm as a function of time. For pseudo-first order kinetic studies, the rate constants were calculated from the appropriate logarithmic relationship by linear least-square analysis. The rate constant was calculated using Eq. (1).

$$\ln\{(A_f - A_t)/(A_f - A_0)\} = -k_{obs} \cdot t \quad \ldots (1)$$

where A_0 = initial absorbance of the reaction product, A_f = final absorbance and k_{obs} = apparent rate constant.

Under excess of hydrazine, the same experimental conditions were used except that [hydrazine] was 0.01 *M*, and [2-hydroxy-1-naphthaldehyde solution] was 2×10^{-4} *M*.

Results and Discussion

Characterization of the reaction product

Hydrazine reacts in aqueous-ethanolic phase with 2-hydroxy-1-naphthaldehyde to form a water and alcohol insoluble yellow product. Purification of the reaction product was accomplished by TLC and the compound showed an R_f value of 0.90 while 2-hydroxy-1-naphthaldehyde had an R_f value less than 0.62.

The UV-visible spectrum of the product in chloroform, and of 2-hydroxy-1-naphthaldehyde in ethanol showed different absorption bands. It has a maximum at 412 nm, whereas 2-hydroxy-1-naphthaldehyde has no absorption around this wavelength hence studies were carried out at 412 nm.

The IR spectrum for the product shows bands at 3444, 2920, 1618, 1602 and 1576 cm^{-1} and is consistent with the absence of C=O stretching vibrations. The new band at 1618 cm^{-1} is assigned to $-CH=N-N=CH-$ stretching vibrations. The mass spectrum contains a molecular ion peak at m/z 340 and 40.92% relative abundance a value which coincides with molecular weight of the expected product. Based on these results, it was concluded that the reaction product is an aldazine, the 2,2′-dihydroxy-1-naphthaldazine (I), with a molecular weight of 340, in agreement with the studies reported by Manes *et al.*[12].

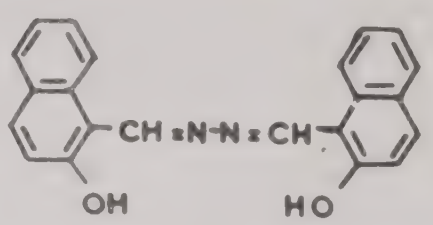

(I)

Structure (I) implies a stoichiometry 1:2 (hydrazine:aldehyde) for the process,

$$\text{hydrazine} + 2\ \text{aldehyde} \rightarrow \text{aldazine} \quad \ldots (2)$$

where aldehyde = 2-hydroxy-1-naphthaldehyde and aldazine = 2,2′-dihydroxy-1-naphthaldazine.

Linearity and reversibility studies

Linearity between aldazine absorbance, A_t (at 412 nm) and [aldazine] was observed. For [aldazine] lower than 6×10^{-5} mol/dm^3, ($A_t = 0.0039 + 28590$ [aldazine]; $r = 0.9997$, $n = 7$). Absorptivity coefficient at this wavelength was of 28590 $dm^3.mol^{-1}.cm^{-1}$. For the reversibility study of the process, the reaction was carried out under excess of aldehyde, in a water-bath at around boiling temperature dur-

ing the time needed to reach the maximum absorbance.

From the stoichiometry of the process and the relationship between [aldazine] obtained at equilibrium and the initially used [hydrazine], it can be concluded that the process should be taken as irreversible.

Kinetic study

Using the method of the integrated-rate equations, the best least-square values were obtained considering a pseudo-first order with respect to hydrazine (with [2-hydroxy-1-naphthaldehyde] excess) (at temps = 20, 30, 40, 50 and 60°C, n = 3 and r = 0.9959, 0.9966, 0.9944, 0.9922 and 0.9912 respectively). Under excess [hydrazine], the kinetic results obtained, showed a linear relationship between $\ln\{(A_f - A_t)/(A_f - A_0)\}$ and time, implying a pseudo-first order with respect to 2-hydroxy-1-naphthaldehyde (at temps = 20, 30, 40, 50 and 60°C, n = 3 and r = 0.9901, 0.9946, 0.9936, 0.9904 and 0.9913 respectively). Nevertheless, important kinetic differences were found between both processes. When the reaction was carried out under excess [aldehyde], it became thermally controlled (see Table 1). The rate constant k_{obs} increases with temperature. When the reaction was carried out under excess [hydrazine], the reaction seems to be temperature independent ($k'_{obs.}$ does not depend on temperature).

These observations lead us to assume that the process did not occur in a single step and that a probable mechanism for the reaction would be, as in Scheme 1.

$$\text{hydrazine} + \text{aldehyde} \underset{k_{-1}}{\overset{k_1}{\rightleftharpoons}} C_1 \qquad \ldots (3)$$

$$C_1 + \text{aldehyde} \xrightarrow{k_2} \text{aldazine} \qquad \ldots (4)$$

Scheme 1

where $k_1 \gg k_{-1}$

The reaction could take place in two steps with formation of an intermediate product C_1. The first step would be the rate-determining step of the reaction under excess [aldehyde], while the second step would be the rate-determining step under excess [hydrazine]. This is quite reasonable if we take into account the considerable size difference between hydrazine and the aldehyde and, hydrazine and C_1.

In order to verify our hypothesis the kinetic results must be consistent with our proposed mechanism,

$$v = d[\text{aldazine}]/dt = k_2[C_1][\text{aldehyde}] \qquad \ldots (5)$$

Table 1—Values of the rate constant $k_{obs.}$ for the hydrazine-2-hydroxy-1-naphthaldehyde reaction at different temperatures

T(K)	$10^5\, k_{obs.}\ (s^{-1})$ under excess of [2-hydroxy-1-naphthaldehyde]	$10^5\, k'_{obs.}\ (s^{-1})$ under excess of [hydrazine]
293	2.23	1.64
303	3.76	1.57
313	7.57	1.54
323	17.09	1.95
333	37.55	1.40

Equation (6) must be satisfied at all times:

$$[\text{aldehyde}]_0 = [\text{aldehyde}] + [C_1] + 2[\text{aldazine}] \qquad \ldots (6)$$

where $[\text{aldehyde}]_0$ = initial [2-hydroxy-1-naphthaldehyde]

$$v = k_2[C_1]\{[\text{aldehyde}]_0 - [C_1] - 2(\text{aldazine}]\} \qquad \ldots (7)$$

$$v = k_2[C_1]\{[\text{aldehyde}]_0 - [C_1]\} - 2k_2[C_1][\text{aldazine}] \qquad \ldots (8)$$

Under excess [aldehyde], if the first step is the rate-determining step, i.e. $k_1 \ll k_2$, $[C_1]$ may be assumed as approximately constant and very small.

Then

$$k_2[C_1]\{[\text{aldehyde}]_0 - [C_1]\} \approx \text{constant} = A \qquad \ldots (9)$$

$$2k_2[C_1] \approx \text{constant} = B \qquad \ldots (10)$$

and

$$v \approx A - B\,[\text{aldazine}] \qquad \ldots (11)$$

Plotting the rate of reaction versus [aldazine] for the runs carried out at different temperatures a linear dependence between them (Fig. 1) is obtained.

Quite different conclusions are reached under excess of [hydrazine]. If the rate determining step is the second one, $[C_1]$ will not be constant and consequently there will be no linear dependence between the rate of reaction and [aldazine]. (Fig. 2).

In fact, since

$[\text{aldehyde}]_0 = [\text{aldehyde}] + [C_1] + 2[\text{aldazine}]$ and

$[\text{hydrazine}]_0 = [\text{hydrazine}] + [C_1] + [\text{aldazine}]$, then

$$[\text{aldehyde}] = [\text{aldehyde}]_0 - [\text{hydrazine}]_0 + [\text{hydrazine}] - [\text{aldazine}] \text{ and}$$

$$[C_1] = [\text{hydrazine}]_0 - [\text{hydrazine}] - [\text{aldazine}]$$

and Eq. (7) becomes:

$$v = k_2\{[\text{hydrazine}]_0 - [\text{hydrazine}] - [\text{aldazine}]\}\{[\text{aldehyde}]_0 - [\text{hydrazine}]_0 + [\text{hydrazine}] - [\text{aldazine}]\} \qquad \ldots (12)$$

Under these conditions $[\text{hydrazine}] \approx [\text{hydrazine}]_0$, and

$$v = -k_2[\text{aldehyde}]_0\,[\text{aldazine}] + k_2[\text{aldazine}]^2 \qquad \ldots (13)$$

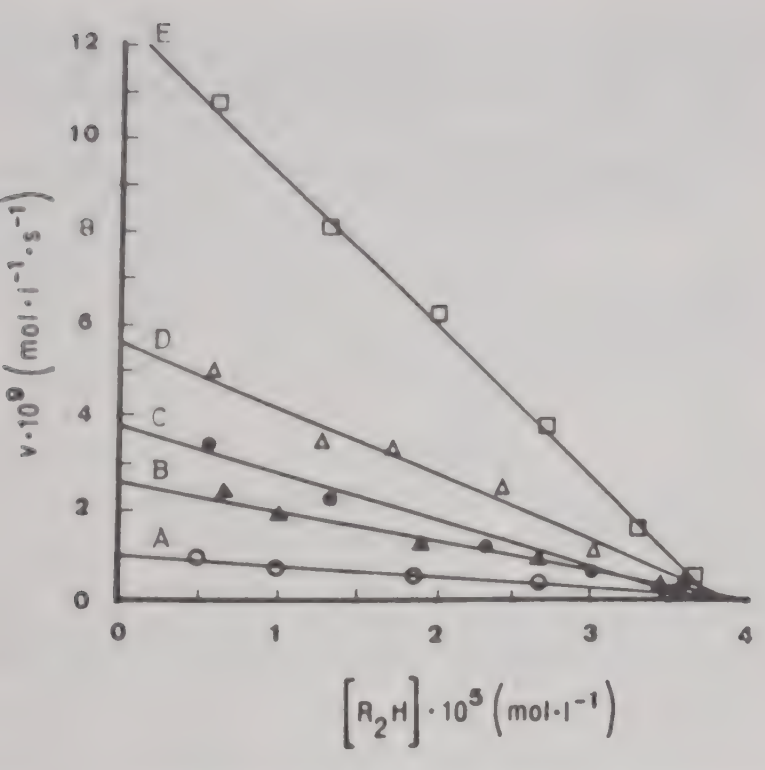

Fig. 1—Plots of the reaction rate versus [aldazine] under excess [2-hydroxy-1-naphthaldehyde], at different temperatures. (A – 20°; B – 30°, C – 40°, D – 50°, E – 60°C)

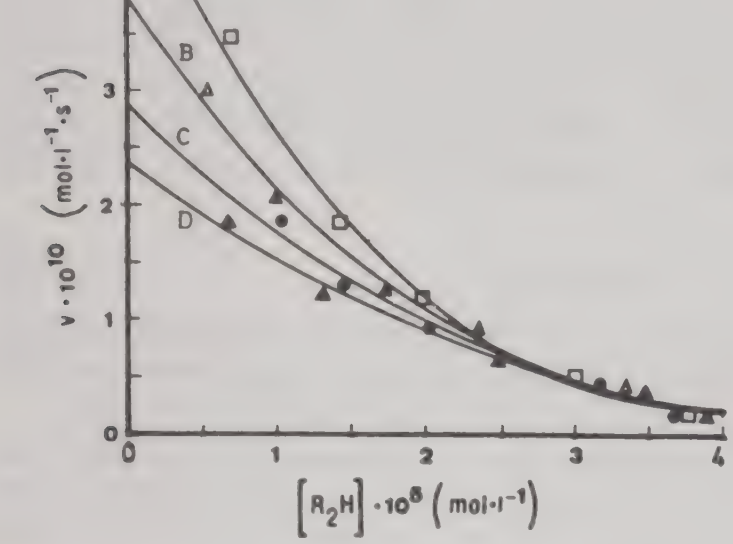

Fig. 2—Plots of the reaction rate (v) versus [aldazine] under excess [hydrazine], at different temperatures. (A – 20°, B – 30°, C – 40°, D – 60°C)

Table 2—Reactions under excess [hydrazine] at different temperatures. Values of the coefficients corresponding to Eq. (13). $v = -k_2[\text{aldehyde}]_0[\text{aldazine}] + k_2[\text{aldazine}]^2$

T(K)	[aldazine] coefficient $\times 10^5$ (s^{-1})	[aldazine]^2 coefficient ($dm^3.mol^{-1}\,s^{-1}$)	Correlation coefficient (r)
293	−7.1055	2.3045	0.993
303	−4.2277	1.4132	0.998
313	−3.4361	1.5235	0.991
333	−5.1388	1.9167	0.991

If the proposed mechanism is correct, there will be a quadratic relationship between v and [aldazine]. The coefficients for [aldazine] and [aldazine]^2 are shown in Table 2.

It should be noticed that the [aldazine] coefficients are always negative while the [aldazine]^2 coefficients are always positive as Eq. (17) shows. Also, there is no independent term, as expected from the mathematical analysis. The correlation coefficients found for a quadratic adjustment are in all the cases greater than 0.991, which again confirms the proposed mechanism.

Dependence between the rate constant and temperature using Arrhenius equation was also studied. For the process using an excess [aldehyde], $\Delta H^{\neq}$ was found to be 56.901 kJ.mol^{-1} and $\Delta S^{\neq} = -22.8$ J.mol^{-1}.K^{-1}. Under these conditions the reaction is thermically controlled. Under excess [hydrazine], $\Delta H^{\neq} = -2.320$ kJ.mol^{-1} and $\Delta S^{\neq} = -229.3$ J.mol^{-1}.K^{-1}. The negative $\Delta H^{\neq}$ value for the reaction using excess [hydrazine], is further evidence of a two step mechanism, i.e., that the observed rate constant is a product of the rate constant of the second step and the equilibrium constant of the initial step. Since equilibrium constants may increase or decrease with increase in temperature, the product of the rate constant and equilibrium constant may also increase or decrease with increase in temperature.

References

1 Snell F & Hilton C L, *Encyclopedia of industrial chemical analysis*, Vol. 14 (Interscience, New York), (1971) 232.

2 *Evaluation of some pesticide residues in food AGP*, 1976/M/14. Food and Agricultural organisation of the United Nations, Rome (1976) 377.

3 Smith F B & Clark D A, *Toxicol appl pharmacol*, 21 (1972) 186.

4 Frejaville J P & Bourdon R, *Toxicologie clinique et analytique. Flammarion Medecine-Sciences*, (1975) 596.

5 Lauwerys R, *Toxicologia industrielle et intoxications profesionelles* (Masson, Paris), (1982) 227.

6 Loomis T A, *Fundamentos de toxicologia*, (Ed Acribia) (1982) 247.

7 Vernot E H, MacEwen J D, Bruner R H, Haus C C & Kintread E R, *Fundam appl toxicol*, 5 (1985) 1050.

8 *Farmacopea Europea*, Vol. 1 Ed. Consejo General de Colegios de Farmacéuticos, (1969) 327.

9 *Farmacopea Internacional*, Vol. 2, Organización Mundial de la Salud, Ginebra, (1983) 175.

10 *Guia de Riesgos Químicos NIOSH/OSHA. Traduction of NIOSH/OSHA Pocket guide to chemical hazards*, Instituto Nacional de Seguridad e Higiene en el Trabajo, Barcelona (1982).

11 Mañes J, Campillos P, Font C, Martre H & Prognon P, *Analyst*, 112 (1987) 1183.

12 Mañes J, Gimeno M J, Molto J C & Font G, *J pharm biomed anal*, 6 (1988) 1023.

Indian Journal of Chemistry
Vol. 31A, July 1992, pp. 427-431

Kinetics of reaction of triethylammonium carboxylates with α-halogeno carbonyl compounds in organic solvents: Part 3—Effect of solvents on the reaction of phenacyl bromide with triethylammonium acetate

M Krishna Pillay* & B Muthulakshmi
Department of Chemistry, Bharathidasan University, Tiruchirapalli 620 024

Received 29 January 1991; revised 8 October 1991; rerevised and accepted 28 December 1991

Kinetics of the reaction of phenacyl bromide with acetic acid in the presence of triethylamine in aqueous acetone and in various solvents have been investigated. The rate constant of the reaction is 50 to 300 times higher in aprotic solvent than in protic solvents. The simple regression and multiple regression of $\log k_2$ with various solvent parameters have led to the conclusion that in addition to the solvent polarity, various other solvent properties simultaneously influence the reaction rate.

Organic acids readily form esters with compounds containing activated halogen in the presence of triethylamine in acetone medium[1]. Kinetics of the reaction of phenacyl bromide with benzoates[2], phenoxyacetates[2] and cinnamates[3] have been reported in acetone and in acetone-water medium containing different percentages of water. In the present work, kinetics of similar reactions of phenacyl bromide with acetic acid is studied in acetone, in aq. acetone and in other organic solvents with a view to find the nature of the active nucleophile.

Materials and Methods

Phenacyl bromide was prepared by following reported procedure[4]. All the solvents and acetic acid were purified by standard methods.

Thermally equilibrated (±0.01°) solutions of phenacyl bromide (25 ml, 0.05 mol dm^{-3}) and triethylamine (25 ml, 0.05 mol dm^{-3}) and acetic acid (0.05 mol dm^{-3}) in acetone were mixed. The reaction was followed by pipetting out 5 ml aliquots of the reaction mixture at regular time intervals, adding it to silver nitrate solution (10 ml, 0.025 mol dm^{-3}) in the presence of nitric acid (10 ml, 25%) to precipitate the silver bromide. The excess unused silver nitrate was estimated with standard ammonium thiocyanate (0.025 mol dm^{-3}) using ferric alum indicator. The rate constant k_2 was calculated by using the second order rate equation for equal concentrations of the reactants.

Results and Discussion

Kinetics of the reaction of phenacyl bromide with triethylammonium acetate at 35°C were carried out in acetone and in aq. acetone. In pure acetone, the triethylammonium acetate can exist as: (1) a tight-ion pair with complete proton transfer, (2) a symmetrical carboxylate which is involved in hydrogen bonding with triethylammonium ions, (3) an unsymmetrical structure in which triethylammonium ion is preferentially bonded to one of the oxygens, (4) case (3) in which the solvent molecule also is hydrogen-bonded to carboxylate[5].

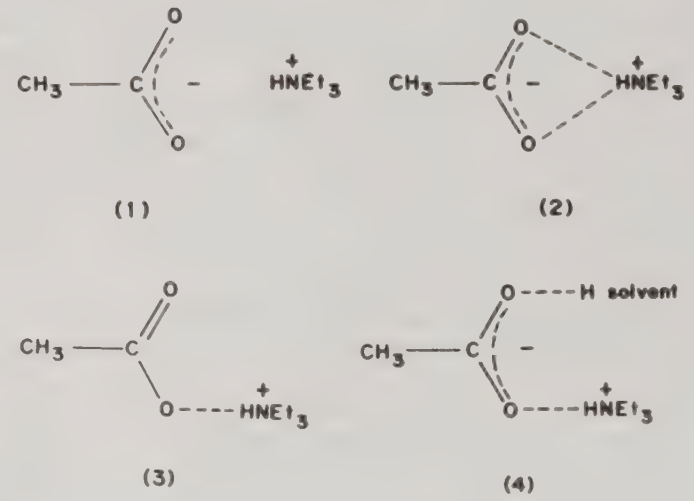

Carboxylic acids undergo esterification with phenacyl bromide readily in the presence of triethylamine in acetone. This acceleration in activity compared to that of sodium carboxylate in aqueous-acetone[2] can be attributed to the coordination of triethylammonium ion with carboxylate ion by hydrogen bonding[6]. Hydrogen bond-assisted organic reactions have been already realized[7]. The mechanism for the present reaction is assumed to be similar to that of triethylammonium benzoate-phenacyl bromide reaction (S_N2 type). Ion-pair is assumed to be the effective nucleophile[8]. It is represented as shown in Scheme 1.

Table 1—Relative reduction in rate constant by adding 5% water and pK_a values of triethylammonium carboxylate-phenacyl bromide reaction at 35°C

Carboxylate	pK_a of acid	$k_2 \times 10^2$ ($dm^3\ mol^{-1}\ s^{-1}$) 100% Acetone	$k_{2w} \times 10^2$ ($dm^3\ mol^{-1}\ s^{-1}$) 95 % Acetone + 5% water	$\frac{k_2}{k_{2w}}$
Acetate	4.76[a]	1.05	0.802	1.31
Cinnamate	4.4[b]	1.40	0.918	1.53
Benzoate*	4.72[b]	1.56	0.838	1.85
Phenylmercaptoacetate	3.88[b]	2.07	0.983	2.10
Phenoxyacetate*	3.17	1.95	0.620	3.14
Phenylsulphonylacetate	2.51	1.50	0.433	3.46

*At 30°C, ref. 2, [a]ref. 5, [b]ref. 7.

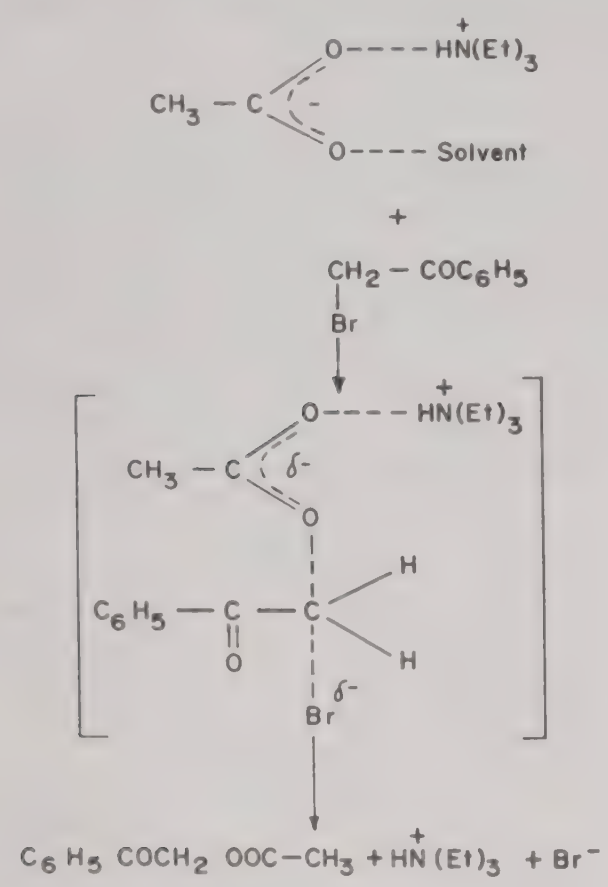

Scheme 1

The rate constant values for the reactions of phenacyl bromide with triethylammonium complex of some acids in acetone at 35°C are given in Table 1. The order of reactivity is found to be: acetate < cinnamate < benzoate < phenylmercaptoacetate < phenoxyacetate. This order is just the reverse of the basicity order of the anion as determined from the pK_a value of the corresponding acids. In aq. acetone reactivity order of sodium carboxylates corresponds to the basicity order[9].

Effect of addition of water

To study the effect of added water on the rate, the reaction between phenacyl bromide and triethylammonium acetate was carried out in acetone water mixtures of varying compositions. The results are presented in Table 2. The magnitude of change in second order rate constant for triethylammonium acetate-phenacyl bromide reaction is about 24% ($k_2 = 1.05$ to $0.802 \times 10^{-2}\ dm^3\ mol^{-1}\ s^{-1}$) when the reaction medium is changed from pure acetone to 5% aq. acetone. This magnitude is not that much high for subsequent addition of water. The change in rate with change in polarity of the solvent (change in concentration of water) is represented in the plot of k_2 versus solvent composition (Fig. 1).

Table 2—Effect of water on the rate of reaction of phenacyl bromide with triethylammonium acetate and y-values

% of acetone	mole fraction of water	$k_2 \times 10^3$ ($dm^3\ mol^{-1}\ s^{-1}$) at 35°C	log k_2	y-values
100	—	10.53	—	—
95	0.176	8.02	−2.0958	−2.760
90	0.312	6.50	−2.1877	−1.856
85	0.418	4.71	−2.3270	−1.308
80	0.505	3.51	−2.4547	−0.673
75	0.576	2.47	−2.6073	−0.308
70	0.636	2.12	−2.6737	+0.130
65	0.686	1.43	−2.8447	+0.385
60	0.731	1.14	−2.9431	+0.796

The log k_2 values are correlated with Grunwald-Winstein y-values to study the solvent effect on the system. To apply Grunwald-Winstein equation,

$$\log k = \log k^0 + my \quad \ldots (1)$$

the y-values of the solvent pairs are taken from the literature[10]. Some y-values are obtained by interpolation. The log k_2 values and the y-values used for computation are given in Table 2. The eight data points in Table 3 have been fitted to Eq. 1 by least squares analysis to yield the regression Eq. 2 with a

Table 3—Log k_2 values and solvent parameters*

Solvent	$Y=\frac{\varepsilon-1}{2\varepsilon+1}$	$P=\frac{n^2-1}{2n^2+1}$	E	B	$k_2\times10^3$ dm^3 mol^{-1} s^{-1} 35°C	log k_2
DMF	0.4798	0.2044	2.60	159	55.09	−1.2588
Acetone	0.4651	0.1803	2.13	116	10.53	−1.9855
Butanone	0.4605	0.1875	1.35	109	7.12	−2.1476
Dichloromethane	0.4217	0.2035	2.68	40	2.06	−2.6870
Dioxan	0.2231	0.2028	3.98	129	0.904	−3.0437
Chloroform	0.3586	0.2013	3.17	35	0.549	−3.2602
Ethanol	0.4701	0.1813	11.57	—	0.553	−3.2576
t-Butyl alcohol	0.4422	0.1898	5.15	—	0.492	−3.3078
Isopropyl alcohol	0.4623	0.1870	8.70	—	0.425	−3.3712
n-Propyl alcohol	0.4640	0.1901	10.58	—	0.303	−3.5191
n-Butyl alcohol	0.4584	0.1948	10.30	160	0.240	−3.6203
Methanol	0.4774	0.1689	14.94	—	0.221	−3.6536
Isoamyl alcohol	0.4507	0.1975	7.38	—	0.203	−3.6919

*Koppel I A & Palm V A in N B Chapman and J Shorter edited, *Advances in linear free energy relationships* (Plenum Press, London) 1972.

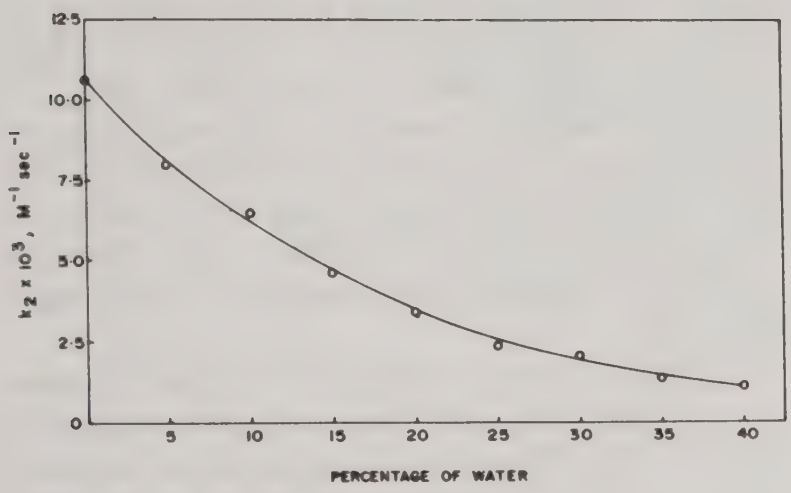

Fig. 1—Plot of k_2 versus solvent composition

correlation coefficient $r=0.980$ and the standard deviation of the estimate, $s=0.065$.

$$\log k_2 = -2.690 - 0.248y \quad \ldots (2)$$

The correlation is only satisfactory. The magnitude of the decrease in the rate constant is significant during the initial addition of water. The rate constants decrease systematically to about 20%. It may be due the decomposition of the hydrogen-bonded complex[2] (a reactive species) to a solvent separated ion-pair or to a hydrated carboxylate ion (less reactive) and triethylammonium ion. However, in pure plain acetone (aprotic solvent) the anions undergo desolvation making them more active nucleophile.

The decrease in rate constant for the addition of 5% water in acetone and k_2/k_{2W} values (k_2 rate constant in plain acetone and k_{2W} is the rate constant in acetone containing 5% water) for the reactions of triethylammonium carboxylates phenacyl bromide are given in the Table 1. The decrease in rate constant has the following order: acetate < cinnamate < benzoate < phenylsulphonylacetate < phenoxyacetate < phenylmercaptoacetate. Acetate has less decrease (1.3 times) compared to that of benzoate (1.8 times) in the reaction rate. Water molecules may coordinate with benzoate more efficiently compared to acetate due to the presence of π-electrons of benzene ring of benzoate[11-13] (i.e. hydrogen-bond between the hydrogen of the water and the electrons of the benzene ring). Phenoxyacetate has an additional oxygen atom while phenylsulphonylacetate has two oxygen atoms for water molecules to coordinate. This factor is responsible for the significant retardation (nearly 3 and 3.5 times) of the reaction rate. Phenylmercaptoacetate has lower decrease in the rate constant than phenoxyacetate due to the difference in the electronegative character of S and O atoms. The plot between log k_2/k_{2W} for reactions of some carboxylic acids with phenacyl bromide in the presence of triethylamine in acetone and 5% aq. acetone at 35°C and pK_a values of the corresponding acids presented in Table 1 is found to be linear ($r=0.995$, $s=0.125$) (Fig. 2).

The nature of the complex formed between amines and carboxylic acids and the extent of complex formation depend on the strength of the acids

Table 4—The data from the regression for the solvents used

Number of solvents	Solvent parameters	log k_2 from regressions	r(R)	s(S)
6[a]	Y	− 13.776 + 22.304 Y	0.900	0.100
6[a]	P	+ 1.751 − 27.596 P	0.992	0.026
6[a]	B	− 3.253 + 0.014 B	0.965	0.219
6[a]	E	—	0.426	—
5[b]	E and Y	− 11.043 + 18.024 Y + 0.376 E	0.972	0.245
5[c]	E and Y	− 14.000 + 28.00 Y − 0.024 E	0.927	0.071
5[b]	B and Y	− 5.607 + 5.751 Y − 0.009 B	0.982	0.193
6[b]	Y, σ^* and ^nH	− 15.596 + 25.122 Y − 3.833 σ^* + 0.011^n H	0.846	—

[a]Six aprotic solvents from Table 3
[b]Five aprotic solvents from Table 3
[c]Five hydroxylic solvents from Table 3
[d]Six hydroxylic solvents from Table 3

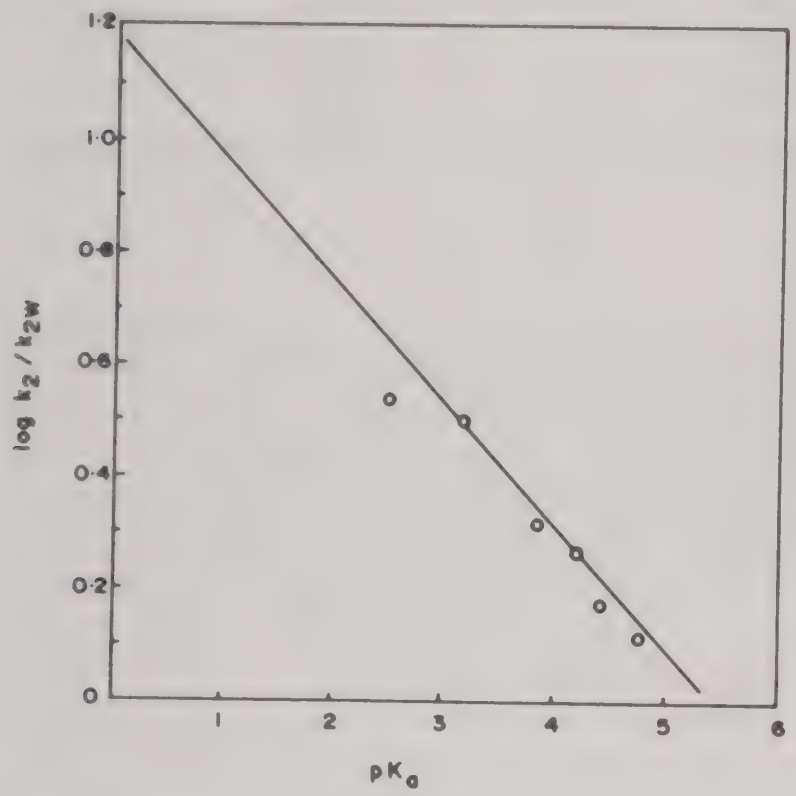

Fig. 2—Plot of log k_2/k_{2w} versus pK_a

and bases, the type of the solvent and temperature. From the extensive spectral studies it is inferred that the complexes exist as ion-pair in protic solvents[13−18]. In solvents of low dielectric constants such as CCl_4, cyclohexane, etc. acetic acid is present as a simple hydrogen-bonded complex with little ionisation[18]. In solvents like $CHCl_3$ or CH_3CN the complex does not show any identifiable NH^+ adsorption[13], but there is ionization of acetic acid[2]. But in DMSO there is clear evidence of the NH^+ absorption in IR for benzoic acid-amine complex[18]. It is clear from the above facts that nature of triethylammonium acetate complex is different in different solvents. The kinetic data in various solvents are presented in Table 3. The fact that the reaction does not take place with acetic acid even in the presence of triethylamine in benzene, CCl_4 and cyclohexane indicates that triethylamine has not caused the ionization of acetic acid. But the reaction does occur in dioxan, $CHCl_3$ and CH_2Cl_2, the solvents of intermediate polarity. The rates of the reaction in DMF is five times faster than that in acetone. In DMF the acid-amine complex can exist as a tight ion-pair in equilibrium with the dissociated ion-pair. The high reactivity in DMF is due to anion desolvation[19−20], the process which increases the nucleophilicity of the acetate anions. In dioxan the rate is faster than in $CHCl_3$ even though dioxan have lower dielectric constant (2.21) compared to $CHCl_3$ (4.7). This exceptional behaviour has been noted in other reactions as well.

It is evident from the data in Table 3 that the reaction is 50-300 times faster in aprotic solvents than in protic solvents. This is the consequence of two obvious effects operating in the solvent solute systems: (i) the anion desolvation[19,20] in aprotic solvents like DMF, which leads to net rate enhancement, (ii) solvation of anion in protic solvent through hydrogen bonding which leads to net rate-retardation. The nucleophile (CH_3COO^-) is made less potent by extensive solvation through hydrogen bonding by the hydroxylic solvent like ethanol. In aprotic solvents like acetone and chloroform the acid-amine complex has been found to exist as proton-transferred hydrogen-bonded complex 4.

Effect of solvents on the reaction in terms of solvent parameters

With a view to checking the linear correlation between the log k_2 values and solvent parameters, the log k_2 values are subjected to simple as well as multiple linear correlations. The results are presented in Table 4. An analysis of the results indicates that the

correlation is only fair. This may be due to the fact that the active species, triethylammonium acetate, may exist as different entities in different solvents as concluded from spectroscopic and other physical methods. It can also be inferred that in addition to the solvent polarity, various other solvent properties simultaneously influence the reaction rate.

References

1 Fieser L F & Fieser M, *Reagents for organic syntheses*, Vol. 1 (John Wiley, New York) (1967) p 1198.
2 Krishna Pillay M, Kannan K & Ramasubramanian, *Tetrahedron*, 39 (1983) 3899.
3 Krishna Pillay M & Balasubramanian, *J Indian chem Soc, LXIV* (1987) 24.
4 Cowper R W & Davidson L H, *Org synth*, Vol. II (1943) p 1480.
5 Hughes E D, *Trans Faraday Soc*, 37 (1941) 604; *Quart Rev*, 5 (1951) 5.
6 Ono N, Yamada T, Saito T, Tanka K & Kaji A, *Bull chem Soc, Japan*, 51 (1978) 2401.
7 Clark J H & Miller J, *J Am chem Soc*, 99 (1977) 498.
8 Mishra P, Nayak P L & Rout M K, *Indian J Chem*, 10 (1970) 252.
9 Ananthakrishna Nadar P & Kannan K, *Indian J Chem*, 16B (1979) 1129.
10 Hoefnagel A J & Wepoles B M, *J Am chem Soc*, 95 (1973) 5357.
11 Oki & Iwamura H, *Bull chem Soc, Japan*, 32 (1959) 1135.
12 Hanif Aslam M, Burden A G, Chapman N B & Shorter J, *J chem Soc, Perkin II*, (1981) 1500.
13 Detar D F & Novak R W, *J Am chem Soc*, 92 (1970) 1361.
14 Smith J W & Vitovia M C, *J chem Soc (A)* (1968) 2468.
15 Barrow G M, *J Am chem Soc*, 78 (1956) 5802.
16 Tasereskaya M N, Zh Obshck Khim, 48 (1978); *Chem Abstr*, 90 (1979) 86531.
17 Tasereskaya M N & Drupova V I, 46 (1972) 2808, *Chem Abstr*, 78 (1975) 157.
18 Odinokov S E, Mashbovsky A A, Dzizenko A K & Glagounov V P, *Spect Lett*, 8 (1975) 157.
19 Pamgrati G P & Sinha T K, *Indian J Chem*, 23B (1984) 57.
20 Parber A J, *Chem Rev*, 69 (1961).

Indian Journal of Chemistry
Vol. 31A, July 1992, pp. 432-435

Notes

Binding of surfactants onto DNA and solubilization of DNA/surfactant complex in micelles

Joy T Kunjappu
Chemistry Division
and
C K K Nair*
Radiation Biology and Biochemistry Division, Bhabha Atomic Research Centre, Trombay, Bomay 400 085

Received 1 November 1991; revised and accepted 20 January 1992

Interaction of cationic surfactant cetyl trimethyl ammonium bromide (CTAB) with calf-thymus deoxyribonucleic acid (DNA) proceeds mainly by an electrostatic binding mechanism. At a critical precipitation concentration, monitored by transmission measurements, the DNA-CTAB complex has been found to precipitate as an insoluble complex which shows a 1:1 correspondence between the charge equivalents of DNA and CTAB. The complex is found to be solubilized in sodium dodecyl sulfate micelles and still retains the bound structural integrity within the micelles.

Deoxyribonucleic acid (DNA)-surfactant interaction has been addressed only on a few occasions[1-3], eventhough a classical link exists between DNA and surfactants in the separation of DNA from membranes and proteinaceous materials of the cell[4]. Surfactant molecules may aggregate on the polymeric DNA backbone as they do on many organic polymeric materials. This may result in the uncoiling of the double stranded helical structure since the aggregates may act as tiny 'molecular weights' weakening the cohesive forces within the DNA structure. Such an uncoiling can have benign implications in genetic engineering. Another reason for studying DNA-surfactant interaction is the close proximity of bilayered fatty membranes functioning as cell boundaries. In such studies, one can look upon a wealth of literature pertaining to polymer-surfactant interactions[5-7]; the polymer could be of natural or synthetic origin. The interaction of proteins with surfactants has also been treated in literature in some detail[5,6,8].

The interaction of DNA with molecules belongs to the electrostatic, hydrophobic and intercalative types. These interactions affected the sequence specificity of molecules and the conformational features of the macromolecules in the bound state. As far as surfactants are concerned, the electrostatic and hydrophobic contributions would surpass the intercalative contribution. The former contribution operates in the case of interaction with charged surfactants whereas hydrophobic contribution arises from the interaction of hydrocarbon chain with the hydrophobic region of DNA, and operates no matter the surfactant is charged or not.

In the present paper we report the preliminary results on interaction of the cationic surfactant cetyl trimethyl ammonium bromide (CTAB) with calf-thymus DNA, their precipitation behaviour and the solubilization of the precipitated complex in micelles.

Experimental

Calf-thymus DNA (Sigma chemicals) was used as such in 0.05 mol dm^{-3} sodium phosphate buffer at a *p*H of 7. The DNA was dissolved under aseptic conditions with minimal shear. Cetyl trimethyl ammonium bromide (CTAB) and sodium dodecyl sulfate (SDS) were of > 99% purity (Sigma chemicals).

Transmission measurements on DNA and/or surfactant sample solutions were done with a Hitachi model-337 double beam UV/vis spectrophotometer at 420 or 600 nm. The compounds had negligible absorption of the analysing light at these wavelengths. Measurements on the DNA and surfactant solutions were performed within one hour of mixing.

Results and discussion

Figure 1 shows the transmission data for DNA solution at a concentration of 50 μg/ml as a function of [CTAB] at 600 nm on a semilogarithmic graph.

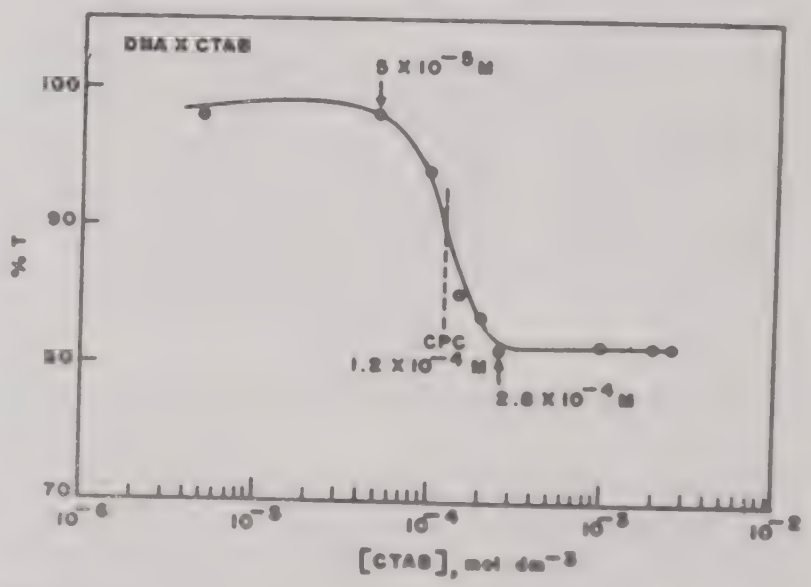

Fig. 1—Transmission of DNA (50 μg/ml) titrated with CTAB in phosphate buffer measured at 600 nm.

The DNA solution remains fully transparent until [CTAB] > 5×10^{-5} mol dm^{-3}. Then onwards, the transmission goes down and reaches a plateau around a [CTAB] = 2.8×10^{-4} mol dm^{-3} with the addition of CTAB. A concentration defined as critical precipitation concentration (CPC) may be observed in this case which corresponds to a maximum interaction between DNA and surfactant at a given [DNA]. In the present case the CPC is at [CTAB] ~ 1.2×10^{-4} mol dm^{-3}.

The significance of CPC in the present case may be appreciated by correlating the number equivalents of phosphate groups of DNA in solution with the molecular concentration of the surfactant. Using a molar extinction coefficient of 3×10^3 mol^{-1} dm^3 cm^{-1} at 260 nm, a 50 μg/ml solution with an absorbance of unity corresponds to a DNA-phosphate concentration of ~ 3×10^{-4} g.eq.dm^{-3}. This value is in close agreement with the CTAB concentration corresponding to maximum precipitation of DNA-CTAB complex. The complex has apparently got precipitated by the neutralization of charge on the phosphate group by the cationic surfactant. Such a condition induces a high degree of hydrophobicity in the DNA-CTAB complex bringing down the solubility of the complex. An argument of this kind obviates the electrostatic interaction between DNA and the surfactant. However, it may be mentioned that a possibility exists in which the DNA bound CTAB and free CTAB may be in equilibrium in solution. But, the amount of free CTAB in the equilibrium is considerably less in the present case as is seen from the precipitation phenomenon. These arguments are in line with the observation made by Chatterjee and Chattoraj[9] on similar systems made with equilibrium dialysis studies.

The absorbance of samples (~ 1.00) corresponding to points in Fig. 1 remains constant in the pre-precipitation region showing that the binding of the cationic surfactant molecules on to the phosphate groups of DNA does not weaken the H-bonded stabilization of base pairs. A weakening of H-bonding would have led to an increase in absorbance at 260 nm to the extent of ~ 40% in the temperature range of 60-70°C. That an effect comparable to the temperature induced hyperchromicity in DNA was not observed with increased surfactant binding shows the ineffectiveness of the bound surfactant molecules to affect the cohesive forces in DNA. The electrostatically bound surfactant molecules can interact with hydrophobic regions in DNA forming a complex. However, the intercalative mechanism may not be operative in this case.

Figure 2 shows the transmission curves for the DNA-CTAB complex formation for different amounts of added SDS. The complex corresponded to a composition of 50 μg/ml of DNA and 5×10^{-4} mol dm^{-3} of CTAB. The precipitated complex solubilizes in SDS above its CMC ($CMC_{SDS} = 8 \times 10^{-3}$ mol dm^{-3}). The transmission data are presented for two different wavelengths—420 and 600 nm. It may be seen from Fig. 2 that SDS does not bind to DNA either in premicellar or postmicellar regions. This observation indicates that complete charge neutralization on DNA is a necessary condition for the solubilization of DNA in SDS micelles. In the present case, such a situation is made possible by the complexation of DNA with CTAB. The enhanced hydrophobicity of the neutralized complex may also be an additional factor for the increased solubility of the complex.

Figure 3 shows the effect of adding CTAB solution to DNA (50 μg/ml) in the presence of SDS micelles ([SDS] = 2.5×10^{-2} mol dm^{-3}). The curve for pure DNA is also presented for the sake of compar-

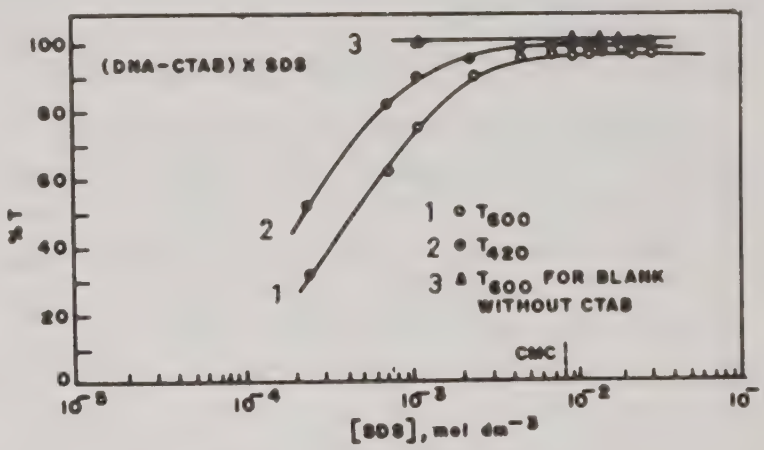

Fig. 2—Transmission of DNA-CTAB complex (50 μg/ml DNA + 5×10^{-4} mol dm^{-3} CTAB) in phosphate buffer titrated with SDS measured at 600 and 420 nm.

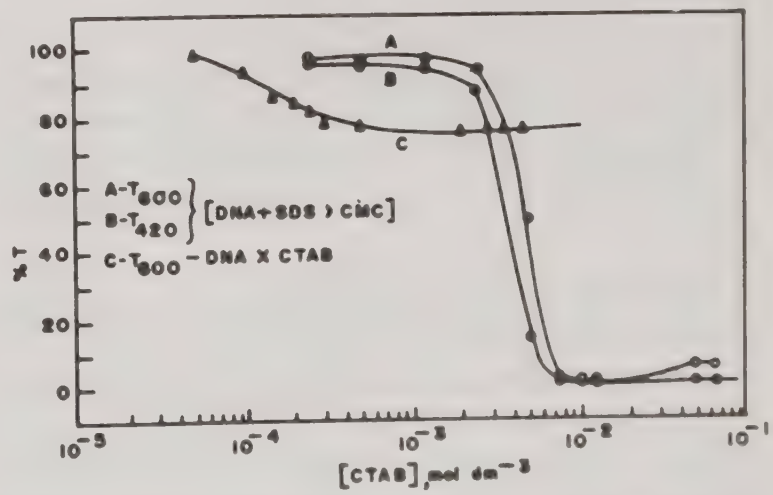

Fig. 3—Transmission of DNA (50 μg/ml) in phosphate buffer titrated with CTAB solution in presence of SDS (2.5×10^{-2} mol dm^{-3}) measured at 420 [B] and 600 [A] nm and transmission of DNA-CTAB complex [C] (50 μg/ml and 5×10^{-4} mol dm^{-3} CTAB) solubilized in SDS micelles (2.5×10^{-2} mol dm^{-3}) on titration with DNA solution

ison. The precipitated complex remains dissolved in SDS micelles. At [CTAB] $\sim 4 \times 10^{-3}$ mol dm^{-3}, the solution once again becomes turbid. Even after giving allowance for the number of molecules of CTAB consumed in binding onto DNA ($\sim 2 \times 10^{-4}$ mol dm^{-3}), the amount of CTAB left in solution far exceeds the CMC of the surfactant. Probably due to the interaction between micelles of opposite charges, the stability of the solution decreases resulting in reprecipitation of the complex. Another possibility is that the cationic surfactant molecules which might be partly serving as counter ions of SDS micelles in place of sodium ions, complex with the free SDS molecules present in solution in excess of the amount required for micellization, thus destabilizing the micelles. Curiously enough, the concentration of the free SDS molecules in solution, which is taken as the CMC of the SDS (8×10^{-3} mol dm^{-3}), coincides with the concentration of CTAB corresponding to the point of total precipitation. A third reason contributing to the instability may be the formation of mixed micelles of cationic and anionic surfactant molecules which imparts to the micelle an altogether different charge distribution[10,11].

An interesting question arises about the nature of the DNA-CTAB complex in the solubilized form in SDS micelles, i.e., whether the complex remains intact while solubilizing in micelles or whether the cationic surfactant detaches from the neutral complex and goes into the aqueous bulk region. To answer this, the precipitated complex dissolved in the micelles was titrated with fresh DNA solution. If CTAB dissociated from the DNA-CTAB complex were present as free molecules in solution, then fresh precipitation would have been observed at increasing DNA concentration. There is no such precipitation under the above conditions.

The samples corresponding to the points in the above figures also did not register any change in absorbance at 260 nm. This, again, indicates that the binding and vicinity of surfactant in the molecular or micellar state have not weakened the duplex pair in DNA.

Surfactant-sensitive single electrode potentiometric, surface tension and equilibrium dialysis techniques have been used earlier to bring out the thermodynamic aspects of surfactant binding onto DNA[2]. When no positive interaction was observed with an anionic surfactant like SDS, positive interaction implying co-operative effects was shown to take place in the case of cationic surfactants and fatty acids[3]. Even before registering sharp changes in the property measured, the binding curves exhibited continuous changes in the precipitation region indicating molecular interaction of surfactant molecules with DNA even from the very beginning of the binding isotherm. But, there is no compelling evidence to prove the positive interaction of individual surfactant molecules with DNA backbone in the preprecipitation region. Also, the site of electrostatic binding is to be confirmed. Admittedly, transmission measurements are sensitive only at the onset of precipitation of the complex.

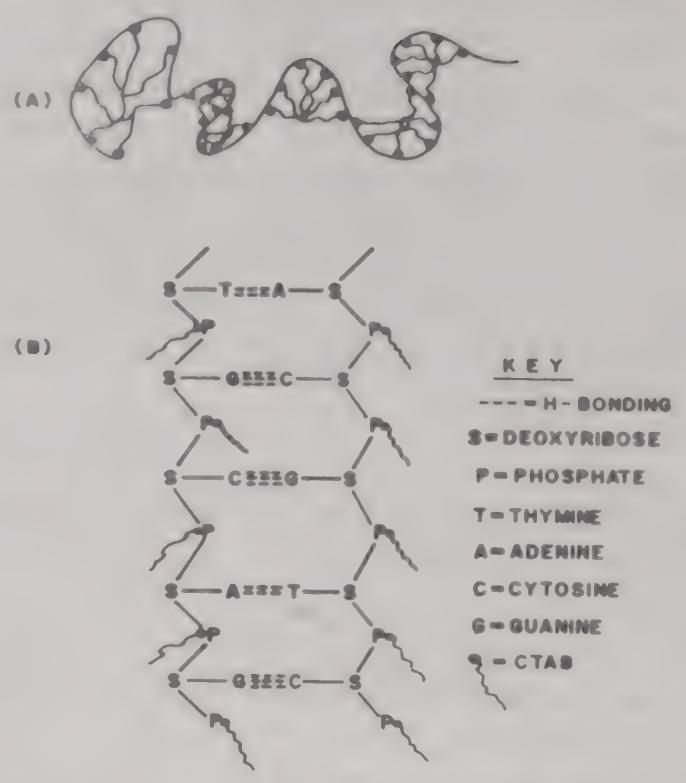

Fig. 4—Visualization of binding of a cationic surfactant (A): Cooperative effect among surfactant molecules results in the aggregation of surfactant molecules on the polymer backbone in PAA: (B): Representation of aggregation of surfactant molecules on DNA.

The DNA-cationic surfactant interaction has been treated theoretically by considering the electrostatic condensation of amphiphillic ions in the vicinity of DNA and by the co-operative binding on the available site of the polyion[1]. However, there is no clear cut evidence for the latter hypothesis although differences in the hydrophobic effect as understood from the binding parameter for C_{12}- and C_{14}- cationic surfactants suggest such a possibility. It is worth mentioning that this interaction has been treated as an entropy-controlled hydrophobic electrostatic effect rather than a pure electrostatic effect[9].

It may be noted that DNA-CTAB interaction does not result in the aggregation of surfactant molecules about a bound surfactant molecule. Such a situation prevails in the binding of CTAB to polymers like polyacrylic acid (PAA)[12]. In this case, the number of bound surfactant molecules is substantial and their proximity is quite favourable for co-operative binding among themselves. Such a possibility in the DNA case would have helped to solubilize the

complex by the agency of bound surfactant molecules. The two situations may be visualized as represented in Fig. 4.

Acknowledgements

The authors thank Drs R M Iyer and J P Mittal for their encouragement.

References

1 Delville A, *Chem Phys Letters*, 118 (1985) 617.
2 Hayakawa K, Santerre J P & Kwak J C T, *Biophys Chem*, 17 (1983) 175.
3 Chatterjee R, Mitra S P & Chattoraj D K, *Indian J Biochem Biophys*, 16 (1979) 22.
4 Marmur J, *J mol Biol*, 3 (1961) 208.
5 Goddard E D, *Colloids and Surfaces*, 19 (1986) 255.
6 Robbin I D, *Anionic surfactants in physical chemistry of surfactant action*, edited by E H Luccassen-Reynders (Marcel Dekker, New York) 1981.
7 Hayakawa K, Santerre J P & Kwak J C T, *Macromolecules*, 16 (1983) 1642.
8 Tsujii K & Tokiwa F, *J Am Oil chem Soc*, 54 (1977) 585.
9 Chatterjee R & Chattoraj D K, *Biopolymers*, 18 (1979) 147.
10 Shinoda K, *J phys Chem*, 58 (1954) 541.
11 Baglioni P, in *Surfactant in solution*, edited by K L Mittal & P Bothorel, (Plenum, New York), 1986, pp. 309-404.
12 Chandar P, Somasundaran P & Turro N J, *Macromolecules*, 21 (1988) 950.

Indian Journal of Chemistry
Vol. 31A, July 1992, pp. 436-438

Structure sensitive nitrogen chemisorption on supported ruthenium catalysts†

S Khaja Masthan*, K S Rama Rao,
P S Sai Prasad & P Kanta Rao

Catalysis Section, Indian Institute of Chemical Technology, Hyderabad 500 007, India

Received 21 October 1991; revised and accepted 10 February 1992

Nitrogen chemisorption is studied on promoted and unpromoted supported ruthenium catalysts as a function of both temperature and pressure. Ru/carbon covered alumina (CCA) catalyst does not chemisorb nitrogen at all the temperatures. Addition of promoters enhances the nitrogen chemisorption capacity of the catalysts (Cs-Ru/CCA and Cs-Ru-Ba/CCA) remarkably at and above 250°C. The chemisorption isotherms are characterized by three well defined adsorption steps. These adsorption steps are attributed to the structure sensitive chemisorption of nitrogen on the three low Miller index planes of ruthenium, (101), (100) and (001).

Ammonia synthesis over metal catalysts is shown to be highly structure sensitive by many investigators[1-4]. It is well known that dissociative nitrogen chemisorption is the rate determining step in ammonia synthesis. On conventional Fe catalysts it has been shown that the synthesis gas mixture with a H_2/N_2 mole ratio of 2.5 instead of the reaction stoichiometric mole ratio of 3.0, would produce higher yields of ammonia over the catalyst[5,6]. This is attributed to the higher concentration of chemisorbed nitrogen as a result of lower concentration of chemisorbed hydrogen. Promoted ruthenium catalysts exhibit much higher activity than the conventional Fe catalysts[7]. The ammonia synthesis activity of ruthenium catalysts is found to be influenced by the support and also by the promoter[8-10]. Recently carbon covered aluminas (CCA) are proved to be much superior supports for ruthenium than the conventional supports like active carbon and alumina[11]. In the present communication the results of a study of nitrogen chemisorption on Ru/CCA (wt. ratio 10:100), Cs-Ru/CCA (51:7.7:100) and Cs-Ru-Ba/CCA (51:7.7:5:100) catalysts as a function of both temperature and pressure are presented. Inspired by the fact that dissociative nitrogen chemisorption is the rate determining step in ammonia synthesis, these studies are carried out with a view to get information on the influence of temperature and the morphological structure of ruthenium on the nature of chemisorption on these catalysts.

† IJCT communication no. 2927

Experimental

Three catalysts Ru/CCA (Catalyst 1), Cs-Ru/CCA (Catalyst 2), and Cs-Ru-Ba/CCA (Catalyst 3) were prepared by the stepwise impregnation and reduction method. $CsNO_3$ (Fluka Chemie) and $RuCl_3.3H_2O$ (Aldrich, USA) were used as precursors for Cs and Ru respectively. The details of the method of preparation of the catalysts were given in a previous publication[11]. Carbon covered alumina (CCA) support was prepared by the pyrolysis of ethylene (Matheson, USA) in N_2 (IOLAR-1, India) at 600°C over commercial γ-Al_2O_3 (Harshaw, Al-3996 R, 18/25 BSS mesh)[11]. The flow rates of ethylene and nitrogen were 2 ml min^{-1} and 15 ml min^{-1} respectively per gram of alumina. The procedure followed was similar to that of Vissers *et al.*[12].

3-4 g of each catalyst were taken for nitrogen chemisorption and hydrogen chemisorption studies. The catalysts were reduced at 400°C in H_2 at a flow rate of 10 l h^{-1} till they were free from chloride or nitrate (as judged by testing the exit gases with $AgNO_3$ or with Nessler's reagent), thoroughly degassed at 10^{-6} torr pressure and hydrogen chemisorption was studied on the reduced catalysts at 25°C in a conventional gas adsorption unit. The catalysts were again treated with H_2 at 400°C for 20 h and degassed at 10^{-6} torr pressure. Nitrogen chemisorption was studied on these catalysts in the temperature range from 250°C to 400°C in the same way as hydrogen chemisorption as a function of pressure upto one atmosphere. An equilibration period of one hour was found to be sufficient to attain equilibrium for each adsorption point. Two nitrogen chemisorption experiments were intercepted by hydrogen treatment at 400°C and degassing at 10^{-6} torr pressure in order to remove nitrogen chemisorbed strongly on the catalyst surface.

Results and discussion

It was observed that catalyst 1 (Ru/CCA) without promoter did not adsorb any measurable quantity of

nitrogen at all the temperatures. This catalyst exhibited very low activity in this temperature range[11]. The catalysts 2 and 3 (with promoters) did not chemisorb nitrogen and did not exhibit ammonia synthesis activity at lower temperatures upto 200°C. Addition of the promoters Cs and Ba to catalyst 1 was observed to enhance the adsorption capacity and activity of the catalysts only at and above 250°C. The results indicate the importance of electron donation by the promoter to the metal and the back donation of Ru *d* electrons to the antibonding orbital of nitrogen molecule. Aika *et al.*[8] have attributed the inertness of Ru/AC (or Ru/CCA) to the drift of Ru *d* electrons to the electron deficient graphite lattice of the support. The nitrogen chemisorption isotherms of the promoted catalysts 2 and 3 are presented in Figs 1 and 2. The results of the ammonia synthesis activity studies of these catalysts have been published elsewhere[13,14]. It is clear from Figs 1 and 2 that the N_2 chemisorption isotherms of these catalysts contain three well defined adsorption steps in them. The three steps in nitrogen chemisorption do not show up at 400°C because of the small amount of nitrogen chemisorption on both the catalysts.

The highest N_2 uptake of 43 μ mol g^{-1} was measured on Cs-Ru/CCA catalyst at 350°C and at a pressure of 740 torr (Fig.1). Nitrogen chemisorption was found to increase with rise in temperature upto 350°C and decrease on further rise in temperature. The increase in nitrogen chemisorption with rise in temperature should be attributed to the promotional effect of temperature on the electron donation by the promoter to the metal and also on the electron donation by the metal to nitrogen molecule. Maximum electron transition seems to occur at 350°C. It is clear that temperature has a detrimental effect on the adsorption of nitrogen above 350°C.

Nitrogen chemisorption isotherms are not reported on Fe and Ru catalysts in the literature. Isotopic nitrogen exchange transient response studies on Ru catalysts[15,16] have clearly shown that a major part of adsorbed nitrogen is in the form of activated nitrogen atoms under reaction conditions. Aika and Ozaki[17] have studied nitrogen adsorption as a function of time on K-Ru/AC catalysts and have carried out IR studies of nitrogen adsorbed on these catalaysts[18,19]. They found that the equilibrium nitrogen chemisorption increased proportionately with K loading on the catalyst. It was observed that potassium decreased the vibrational frequency of N≡N bond on the catalyst surface.

The three steps in the N_2 chemisorption isotherms would certainly indicate the heterogeneity of ruthenium surface in the catalysts. Structure sensitivity of nitrogen chemisorption and ammonia synthesis was very well demonstrated on Fe single crystal surfaces. N_2 chemisorption rates and NH_3 synthesis rates were found to decrease in the order: (111) > (110) > (100) for the three low Miller index planes of iron[1,20]. The Fe(111) crystal plane has a less dense and more open structure than the other two crystal planes. Very recently Strongin and Somorjai[3] have demonstrated that on mild treatment with NH_3 at 400°C the less active crystal faces (110) and (100) get transformed into the more active crystal plane (111).

The present experimental results and the information on Fe crystal planes in the literature suggest that the three low Miller index planes of Ru, (101),

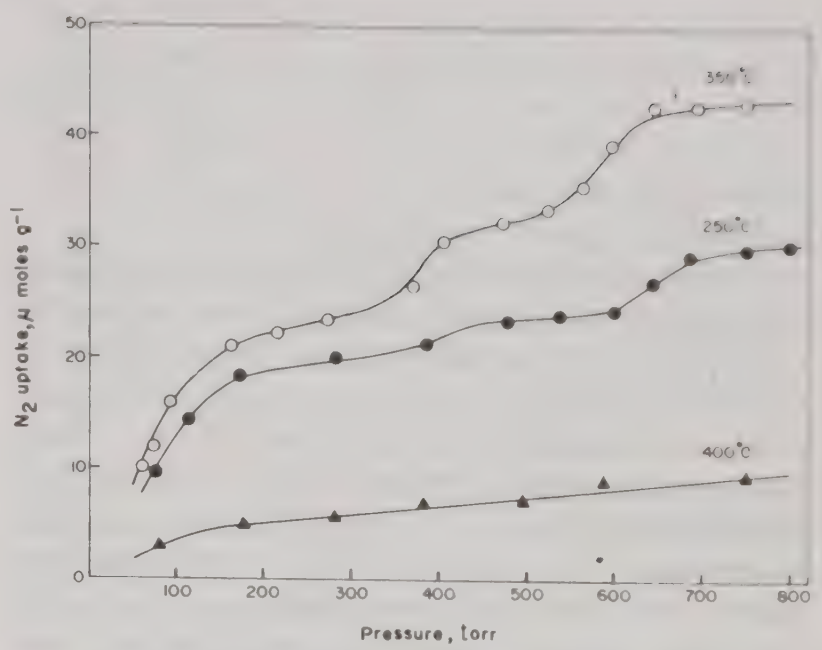

Fig. 1—Nitrogen chemisorption isotherms of Cs-Ru/CCA catalyst at different temperatures ● 250°C; ○ 350°C; ▲ 400°C

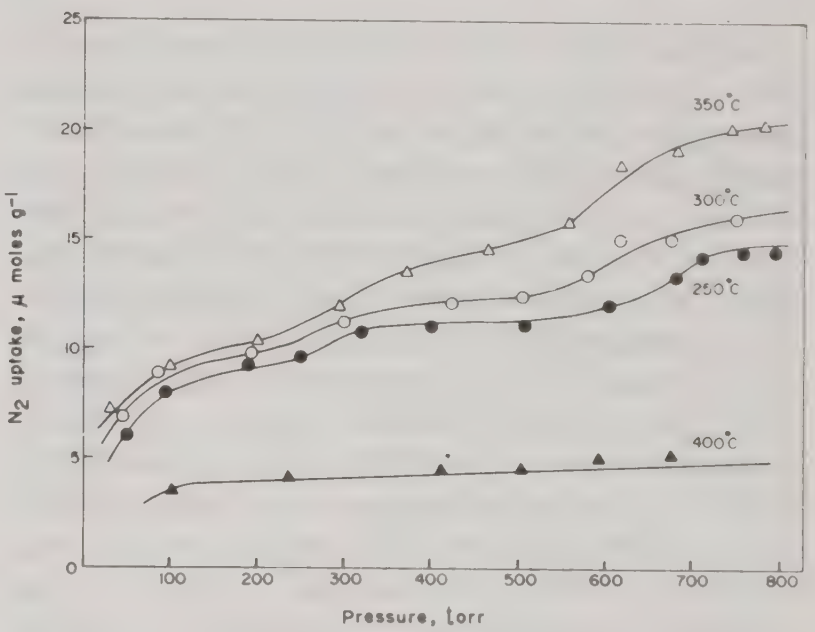

Fig. 2—Nitrogen chemisorption isotherms of Cs-Ru-Ba/CCA catalyst at different temperatures ● 250°C; ○ 300°C; △ 350°C; ▲ 400°C

(100) and (001) also play a prominent role in chemisorption of nitrogen and ammonia synthesis. Therefore, the three adsorption steps in N_2 chemisorption isotherms on these catalysts can certainly be attributed to the structure sensitive nitrogen chemisorption on the three Ru crystal planes.

Transmission electron microscopic studies of ruthenium catalysts derived from $RuCl_3$ and supported on SiO_2 and MgO carried out by Datye *et al.*[21] provide an indirect support to the results of nitrogen chemisorption studies on ruthenium catalysts. They have observed that Ru particles in the catalysts with Ru loadings below 1 wt% are small and spherical in shape. Ru particles in the catalysts with Ru loadings above 1 wt% assume ellipsoidal shapes with diameters above 2 nm. These hexagonal platelets have well developed facets of ruthenium (101), (100) and (001).

Buglass *et al.*[22] have carried out transition electron microscopic studies and ammonia synthesis over active carbon supported Ru catalysts with constant loading of the promoter KNO_2. They have observed that tiny Ru crystallites with well defined faces are surrounded by small islands of the promoter and the turnover frequency of ammonia synthesis increased with Ru loading. This leads to the conclusion that TOF of ammonia synthesis increases with increase in Ru crystallite size and hence that Ru crystal faces play a prominent role in ammonia synthesis. Very recently Masthan *et al.*[14] have invoked the structure sensitivity of Ru crystal planes to ex plain the hysteresis phenomenon observed during ammonia synthesis over these catalysts. They have suggested that the more dense and presumably less active crystal planes (100) and (001) get transformed into less dense and more active crystal plane (101) which has open structure like that of Fe(111) under the influence of nitrogen and ammonia under reaction conditions. So it can be concluded that the three nitrogen adsorption steps undoubtedly demonstrate the structure sensitivity of nitrogen chemisorption on the three dominant crystal faces of ruthenium on supported ruthenium catalysts.

References

1 Spencer N D, Schoonmaker K C & Somorjai G A, *J Catal*, 74 (1982) 129.
2 Dumesic J A, Topsoe H, Khammouma S & Boudart M, *J Catal*, 37 (1975) 503.
3 Richard M A & Vanderspurt T H, *J Catal*, 94 (1985) 563.
4 Strongin D R & Somorjai G A, *J Catal*, 118 (1989) 99.
5 Nielsen A, *Advances in catalysis*, Vol.5 (Academic Press, New York) 1953, p 30.
6 Reddy K V & Hussain A, *Ind Eng Chem Process Des Dev*, 21 (1982)359.
7 Aika K & Kakegawa T, *Catalysis Today*, 10 (1991) 73.
8 Aika K, Hori H & Ozaki A, *J Catal*, 27 (1972) 424.
9 Aika K, Shimazaki K, Hattori Y, Ohya A, Ohshima S, Shirota K & Ozaki A, *J Catal*, 92 (1985) 296.
10 Aika K, Ohya A, Ozaki A, Inoue Y & Yasumori I, *J Catal*, 92 (1985) 305.
11 Rama Rao K S, Kanta Rao P, Masthan S K, Kaluschnaya L & Shur V B, *Appl Catal*, 62 (1990) L19.
12 Vissers J P R, Mercx F P M, Bouwens S M A M, de Beer V H J & Prins R, *J Catal*, 114 (1988) 291.
13 Rama Rao K S, Khaja Masthan S, Sai Prasad P S & Kanta Rao P, *Appl Catal*, 73 (1991) L1.
14 Khaja Masthan S, Sai Prasad P S, Rama Rao K S & Kanta Rao P, *J mol Catal*, 67 (1991) L1.
15 Urabe K, Aika K & Ozaki A, *J Catal*, 32 (1974) 108.
16 Urabe K, Aika K & Ozaki A, *J Catal*, 42 (1976) 197.
17 Aika K & Ozaki A, *J Catal*, 35 (1974) 61.
18 Oh-Kita M, Midorikawa H, Aika K & Ozaki A, *J Catal*, 70 (1981) 384.
19 Oh-Kita M, Aika K, Urabe K & Ozaki A, *J Catal*, 44 (1976) 460.
20 Bozso F, Ertl G & Weiss M, *J Catal*, 50 (1977) 519.
21 Datye A K, Logan A D & Long N J, *J Catal*, 109 (1988) 76.
22 Buglass J G, Tennison S R & Parkinson G M, *Catal Today*, 7 (1990) 209.

Indian Journal of Chemistry
Vol. 31A, July 1992, pp. 439-442

Studies of inorganic precipitate membrane: Evaluation of membrane selectivity from bi-ionic potential and conductivity measurements

R S Kushwah*, Mohd Ayub Ansari, Naheed Akhtar & P Singh

Membrane Research Laboratory, Department of Chemistry
B.B. (P.G.) Science College, Jhansi 284 001

Received 23 September 1991; revised and accepted
15 January 1992

Bi-ionic and multi-ionic potential across parchment supported mercuric sulphide membrane with various combinations of 1 : 1 electrolytes at different concentrations have been measured. Membrane conductivity in contact with a single electrolyte has been experimentally determined to evaluate the selectivity of the membrane with the predetermined values of the intra-membrane mobility ratio. The selectivity sequence of the membrane has been found as $K^+ > Na^+ > Li^+$ which on the basis of the Eisenman-Sherry model of membrane selectivity, points towards the weak field strength of the charge groups attached to the membrane matrix.

Effective fixed charge density of parchment supported membranes[1-7] and duck and hen egg shell membranes[8] has already been demonstrated using Eisenman-Sherry model[9,10] of membrane selectivity and the theories of membrane potential based on non-equilibrium thermodynamics. In this paper bi-ionic potential measurements across a parchment supported mercuric sulphide membrane have been carried out for the evaluation of membrane selectivity of ions. Membrane conductance in contact with various 1 : 1 electrolytes has also been experimentally determined to substantiate our findings.

Experimental

The membrane was prepared by the method of interaction described in part XI of this series[2]. The bi-ionic and multi-ionic potentials were measured by constructing an electro-chemical cell of the following type with a pye precision vernier potentiometer:

$Hg\text{-}Hg_2Cl_2$	Saturated KCl-agar	electrolyte solution AX or (AX + BX)	Membrane
	electrolyte solution BX or (AX + BX)	Saturated KCl-agar	Hg_2Cl_2-Hg

Aqueous solutions of sodium, potassium and lithium chlorides (BDH, AR grade) were used on the two sides of the membrane and were vigorously stirred with a pair of electrically operated magnetic stirrers to remove completely or at least to minimize the effect of the film controlled diffusion[11].

Electrical conductivity of the membrane was determined by setting up a cell of the type shown in Fig. 1 with a conductivity bridge (Cambridge Instrument, England). All measurements were carried out at 25 ± 0.1°C. The error in measurement of membrane potential was within ± 1% whereas electrical conductivity could be measured to better than 99.5% accuracy.

Results and discussion

When an ion exchange membrane of different concentrations is interposed between two solutions of an electrolyte the mobile species penetrate the membrane and various transport phenomena are introduced into the system[12]. If the membrane is used to separate the solutions of the type AX and BX (or AX and AY) electrolytes the steady potential developed is called bi-ionic[13] which is a measure of the selectivity of the membrane for ions of the same sign. Bi-ionic potential has been considered by Helfferich[14], according to the concepts of the TMS theory[15,16] as being the algebraic sum of two interfacial potentials and an internal diffusion potential. For a general case the total bi-ionic potential E for counterions of equal valencies by Wyllie and Kanaan[17] is given by Eq. (1)

$$E = \frac{RT}{F} \ln \frac{a_i \bar{U}_i}{a_j \bar{U}_j} \qquad \ldots (1)$$

where a_i/a_j and $\bar{U}_i/\bar{U}_j$ are the activity ratio of the solutions and mobility ratio of the ions in the mem-

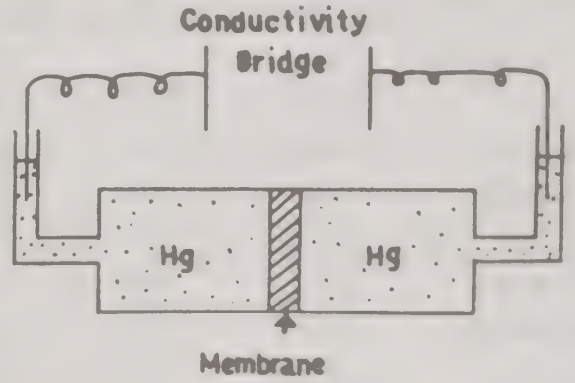

Fig. 1—Experimental cell

brane phase respectively. Wyllie[18] expressed the intramembrane mobility ratio as:

$$\frac{\bar{U}_i}{\bar{U}_j} = \frac{\bar{t}_i}{\bar{t}_j} = \frac{\bar{m}_i \bar{\lambda}_i}{\bar{m}_j \bar{\lambda}_j} \quad \ldots (2)$$

where $\bar{t}_i/\bar{t}_j$ is the intramembrane transference ratio and $\bar{m}_i$ and $\bar{m}_j$ are the steady state equilibrium concentration of i and j in the respective zone; $\bar{\lambda}_i$ is the conductivity of the membrane when it is wholly in i form and $\bar{\lambda}_j$ is the conductivity of the membrane when it is wholly in j form. Furthermore, it was shown that $\bar{m}_i/\bar{m}_j \approx K_{ji}$ is the selectivity. This, on substitution into Eq. (2) gives

$$\frac{\bar{U}_i}{\bar{U}_j} = K_{ji} \left(\frac{\bar{\lambda}_i}{\bar{\lambda}_j}\right) \quad \ldots (3)$$

Thus, the ratios of mobilities were related to the chemical and electrical properties of the membrane.

Bi-ionic potential measurements were also carried out by interposing the membrane between two different electrolyte solutions at the same concentration. The values of bi-ionic potential across parchment supported mercuric sulphide membrane with various 1 : 1 electrolyte combinations at different concentrations are shown in Fig. 2. The values of intramobility ratio $\bar{U}_i/\bar{U}_j$ calculated using Eq. (1) are given in Table 1. An interestng point with regard to the value of $\bar{U}_i/\bar{U}_j$ is that the mobility ratio undergoes considerable change with the concentration of the each electrolyte pair.

To gain knowledge of selectivity K_{ji} from the predetermined values of $\bar{U}_i/\bar{U}_j$ the ratio of electrical conductivities $\bar{\lambda}_i/\bar{\lambda}_j$, demanded by Eq. (3), must be known. Membrane conductance measurements were carried out when it was wholly in form i or from j. The values of membrane conductance (Fig. 3) were relatively more dependent on the concentration of the electrolytes which implies that the membrane has a relatively high Donnan uptake of anion and a low selectivity constant values. The values of selectivity K_{ji} evaluated using the values of electrical conductivity and the intramembrane mobility ratio from Table 1 are given in Table 2. The intramembrane mobility ratio values also refer to the selectivity sequence of the membrane for the cations $K^+ > Na^+ > Li^+$. This order of selectivity on the basis of the Eisemnan-Sherry model of membrane selectivity[9,10] points towards the weak field strength of the charge groups attached to the membrane matrix. Further, it is well known that the bi-ionic potential is a measure of selectivity[19] of a membrane for ions of the same sign. Equation (4) has been found to predict the values of bi-ionic potential reasonably well

Table 1—Values of the intramembrane mobility ratios of various 1 : 1 electrolyte ions pairs

Membrane	Mercuric sulphide		
Electrolyte ion pair Concentration (M)	$\bar{U}_{K^+}/\bar{U}_{Na^+}$	$\bar{U}_{K^+}/\bar{U}_{Li^+}$	$\bar{U}_{Na^+}/\bar{U}_{Li^+}$
0.1/0.1	1.01	1.32	1.17
0.05/0.05	1.04	1.34	1.22
0.02/0.02	1.10	1.53	1.42
0.01/0.01	1.21	1.74	1.75
0.005/0.005	1.27	1.99	1.83
0.002/0.002	1.38	2.21	1.94
0.001/0.001	1.52	2.39	1.97

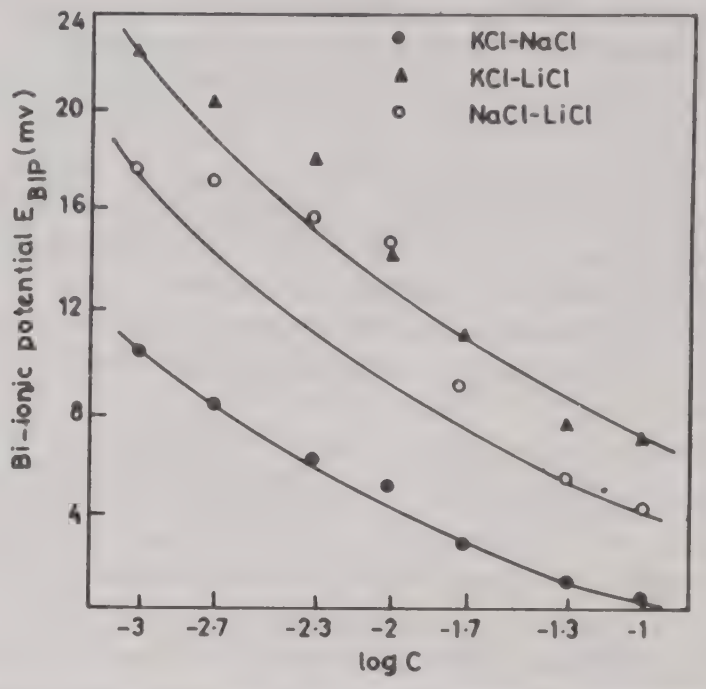

Fig. 2—Plots of bi-ionic potential E_{BIP} (mV) versus log C across mercuric sulphide membrane with 1 : 1 electrolytes

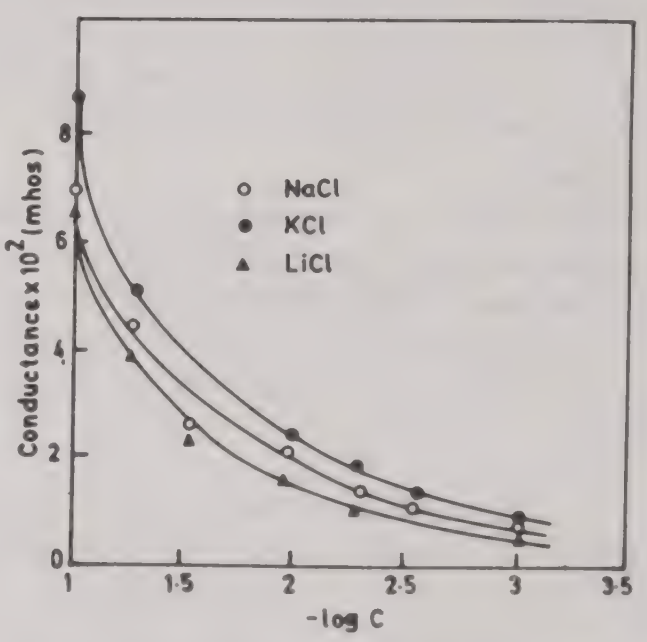

Fig. 3—Plots of conductance $\times 10^2$ (MHOS) versus log C for mercuric sulphide membrane with 1 : 1 electrolytes

Table 2—Values of the selectivity K_{ji} ($1/K_{ij}$) evaluated from the intramembrane mobility ratio and the ratio of electrical conductivities at various electrolyte concentrations

Membrane	Mercuric sulphide						
Concentrations (M)	0.1/0.1	0.005/0.05	0.02/0.02	0.01/0.01	0.005/0.005	0.002/0.002	0.001/0.001
Selectivity							
K_{NaK}	0.83	0.89	0.98	1.10	0.90	1.25	1.38
K_{LiK}	1.00	1.05	1.30	1.58	1.26	1.90	1.65
K_{LiNa}	1.09	1.10	1.30	1.40	1.60	1.80	1.47

provided $\bar{\gamma}_B/\bar{\gamma}_A$ remains constant.

$$E_{BIP} = \frac{RT}{F} \ln \frac{\bar{U}_A a'_A \bar{\gamma}_B}{\bar{U}_B a''_B \bar{\gamma}_A} \quad \ldots (4)$$

Equation (4) can be written as

$$E_{BIP} = \frac{RT}{F} \ln \frac{\bar{U}_A a'_A}{\bar{U}_B a''_B} \quad (\text{if } \bar{\gamma}_A = \bar{\gamma}_B) \quad \ldots (5)$$

$$\text{and} \quad E_{BIP} = \frac{RT}{F} \ln \frac{\bar{t}_A}{\bar{t}_B} \quad \ldots (6)$$

where $$\frac{\bar{t}_A}{\bar{t}_B} = \frac{\bar{u}_A \bar{a}_A \bar{\gamma}_B}{\bar{u}_B \bar{a}_B \bar{\gamma}_A}$$

provided that the Donnan relation $\bar{a}_A/\bar{a}_B = a'_A/a''_B$ is established.

The bi-ionic potentials generated across mercuric sulphide membrane were also measured by keeping the concentration of AX constnat and by varying the concentration of BX, and again by keeping [BX] constant and varying [AX]. These measurements were extended to three solutions, i.e. KCl-NaCl, KCl-LiCl and NaCl-LiCl. The bi-ionic potential values thus masured were plotted in Fig. (4) as a function of log a_{AX}/a_{BX}. Good linear plots as demanded by Eq. (5) were obtained. The point of intersection of the two linear plots at the same activity, i.e., $a_{AX}/a_{BX} = 1$, gives the value of the transport ratio using Eq. (6). The transport ratio thus obtained for different 1 : 1 electrolyte pairs are

$$\bar{t}_{K^+}/\bar{t}_{Na^+} = 1.12, \bar{t}_{K^+}/\bar{t}_{Li^+} = 1.08, \bar{t}_{Na^+}/\bar{t}_{Li^+} = 1.06.$$

These results also point towards the order of selectivity of cations transporting through the membrane as: $K^+ > Na^+ > Li^+$.

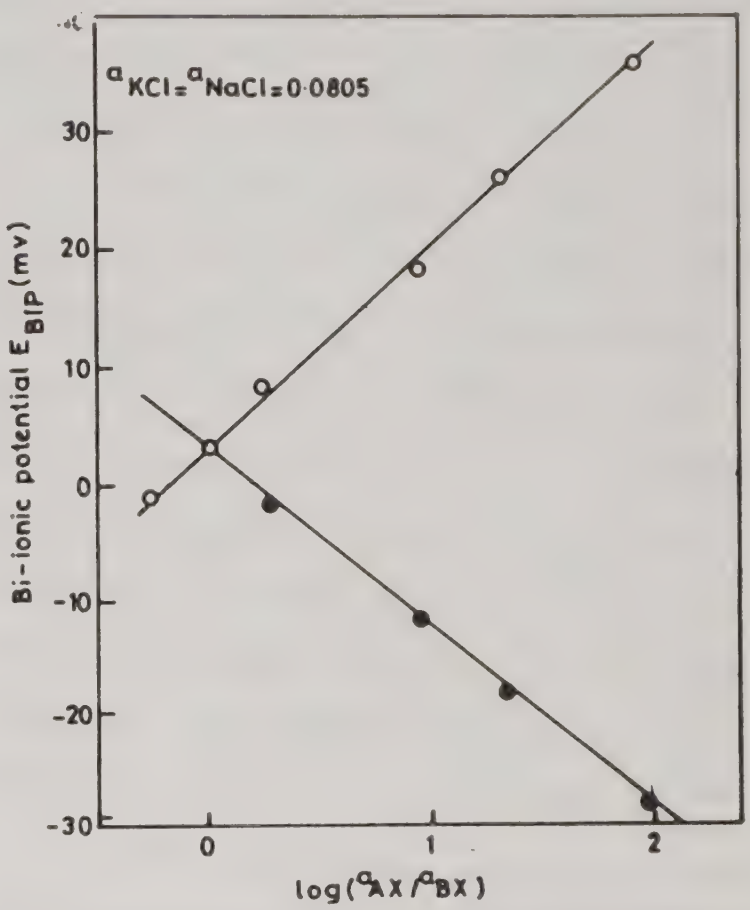

Fig. 4—Plots of log (a_{AX}/a_{BX}) versus bi-ionic potential E_{BIP} (mV) for KCl-NaCl set

Acknowledgement

The authors are grateful to Prof. R.P. Khandelwal, Head, Department of Chemistry, for providing necessary facilities.

References

1 Siddiqi F A, Lakshminarayanaiah N & Beg M N, *J polym Sci*, 9 (1971) 2853, 2869.
2 Beg M N, Siddiqi F A & Shyam R, *Can J Chem*, 55 (1977) 1680.
3 Beg M N, Siddiqi F A, Shyam R & Altaf I, *J electroanal Chem*, 98 (1979) 140.
4 Beg M N, Siddiqi F A, Shyam R & Arshad M, *J memb Sci*, 2 (1977) 365.
5 Siddiqi F A, Beg M N, Singh S P, *J polym Sci*, 15 (1977) 959.
6 Siddiqi F A, Beg M N & Singh S P, *Indian J Chem*, 30 (1991) 335, 339.
7 Siddiqi F A, Beg M N & Singh S P, *J polym Sci*, 15 (1977) 959.
8 Beg M N, Shyam R, Altaf I & Akhtar N, *Acta Chimica Hungarica*, 125(5) (1988) 647, 656.

9 Eisenman G, *Membrane transport and metabolism*, edited by A Kleinzer & A Kotyk, (Academic Press, New York) (1961) 163; *Biophys J Suppl*, 2 (1962) 259.

10 Sherry H, in *Ion exchange*, edited by J A Marinsky (Dekker, New York) (1968, 2.

11 Scatchard G & Helfferich F, *Discuss Faraday Soc*, 21 (1956) 70.

12 Kobatake Y & Kamo N, *Prog Sci Japan*, 5 (1973) 257.

13 Wilson J R, *Demineralisation by electrodialysis*, (Butterworths, London) (1960) 84.

14 Hefferich F, *Ion exchange*, (McGraw Hill, New York) (1962).

15 Teorell T, *Proc Soc Expt Biol Med*, 33 (1935) 282, *Proc Nat Acad Sci (USA)*, 21 (1935) 152, *Z Electrochem*, 55 (1952) 460, *Prog Biophys Chem*, 3 (1953) 385.

16 Meyer K H & Sievers J F, *Helv Chim Acta*, 19, 987 (1936) 649, 665.

17 Wyllie M R J & Kanaan S L, *J phys Chem*, 58 (1954) 73.

18 Wyllie M R J, *J phys Chem*, 58 (1954) 73.

19 Lakshminarayanaiah N, *Transport phenomena in membranes*, (Academic Press, New York) (1969) 170.

Indian Journal of Chemistry
Vol. 31A, July 1992, pp. 443-448

Study on thermodynamics of aqueous solution of sodium tetraphenylborate

Zou Li-Zhuang*, Li Lin-Wei & Wang Xiao-Ling

Department of Chemistry, Shandong Liaocheng Teachers College, Liaocheng, China 252000

Received 23 September 1991; revised and accepted 27 January 1992

Solution enthalpies of $NaBPh_4$ in water measured by precision solution calorimeter, formation enthalpies of $NaBPh_4$ in aqueous solution with different concentrations, standard solution enthalpy, standard formation Gibbs free energy, standard solution entropy of $NaBPh_4$ and a series of thermodynamic properties of BPh_4^- have been given. Activity coefficients and osmatic coefficients of $NaBPh_4$ in aqueous solution with different concentrations have been measured in the temperature range of 288.15-318.15 K by the isopiestic method. The results show that the natural logarithms of activity coefficients of $NaBPh_4$ have a linear relation with temperature, viz $\ln Y_{\pm}(NaBPh_4) = A + BT$. Furthermore, the relative partial molar enthalpies and relative partial molar heat capacities of $NaBPh_4$ under different conditions have been calculated. The results can be expressed as, $\bar{H}r,m(NaBPh_4) = (-930.40 + 6.1446\ T)\ (m)^{1/2}/(0.2734 + (m)^{1/2})$ and $Cr,m(NaBPh_4) = (0.0312 + 0.0204\ T)\ (m)^{1/2}/(0.2734 + (m)^{1/2})$ respectively.

In recent years, to determine and calculate the transfer thermodynamical properties of an ion, the interaction between a typical large negative ion and various kinds of solvents was studied. But, the reports on formation thermodynamical properties of $NaBPh_4$ and BPh_4^- are negligible inspite of the fact that $NaBPh_4$ (sodium tetraphenylborate) is a typical strong electrolyte with a large negative ion and its aqueous solution is fairly stable. Formation thermodynamic properties of crystal of $NaBPh_4$ and other monovalent metallic salts of tetraphenylborate have already been reported by us[1]. In this paper we will give a series of thermodynamic properties of $NaBPh_4$ and BPh_4^- in aqueous solution.

Experimental

$NaBPh_4$ (99.7%, Shanghai First Reagent Factory) was purified[2] and used. NaCl is a spectroscopically pure reagent (99.99%, Shanghai First Reagent Factory). Doubly distilled water treated with ion exchange resin was used, and its electric conductivity was 1.22×10^{-4} S/m.

To determine solution enthalpy of $NaBPh_4$, its aqueous solutions in the concentration range 3.81×10^{-3} to 1.819×10^{-2} mole/kg were prepared by weight. Because $NaBPh_4$ gave off heat to the surrounding while dissolving, the temperature of thermostat was regulated such that it was a little higher than temperature of the final state of solution (298.15 K), in order that the thermal transport conduction might keep in one-way direction and that the uncertainty arising from the positive Newtonian fluid was reduced. The sample was filled in the calorimeter, the temperature of which was slightly lower than experimental temperature (298.15 K), then calorimeter was put into the thermostat, stirred and the initial temperature was recorded after 15-20 min of equilibration. When the initial temperature approaches 298.15 K, the sample was added and final temperature was recorded at the same time.

To determine activity of $NaBPh_4$ in the system of $NaBPh_4 + H_2O$, the aqueous solution of NaCl and $NaBPh_4$ of different concentrations were taken in equilibrium containers, and the equilibrium containers of NaCl and $NaBPh_4$ were connected by tube of polytetrafluoroethylene. The equilibrium containers were evacuated by vacuum pump and vacuum of the equilibrium container was regulated to attain 0.13 Pa. Then the equilibrium containers were thermally equilibrated ($t \pm 0.01$°C). In order to shorten the time for equilibrium, the internal box of the thermostat was fastened to the shaking pole connected with synchronous motor, working voltage was regulated with the transformer in order that it kept at 40 r/min, angle of swaying for the shaking pole kept $\leqslant 10°$. The weight difference of less than 0.0006 g between last two readings was taken as the criterion of equilibrium.

Results and discussion

Solution enthalpies and formation enthalpies of $NaBPh_4$

Solution enthalpies of $NaBPh_4$ in water at different concentrations are given in Table 1. The solution enthalpies (ΔH_s) of $NaBPh_4$ are plotted against the concentration m of $NaBPh_4$ and solution enthalpy $\Delta H_s(\infty)$ of $NaBPh_4$ at infinite dilution was found by extrapolation. From the standard formation enthalpy of $NaBPh_4$ from our earlier work[1] ($\Delta H_f^{\theta}(NaBPh_4, C) = -1009.5$ kJ/mol), the formation enthalpies of $NaBPh_4$ in aqueous solution for different concentrations were calculated (Table 1).

Table 1—Solution enthalpies and formation enthalpies of $NaBPh_4$ in H_2O

$m \times 10^2$ mol/kg	$-\Delta H_s$ (kJ/mol)		$-\Delta H_s$ (kJ/mol)	$-\Delta H_f$ (kJ/mol)
	(1)	(2)		
1.819	19.44	19.41	19.42	1028.92
1.412	19.39	19.42	19.40	1028.90
1.081	19.40	19.43	19.41	1028.91
0.9299	19.43	19.47	19.45	1028.95
0.8115	19.48	19.50	10.49	1028.99
0.6959	19.52	19.54	19.53	1029.03
0.5966	19.56	19.54	19.55	1029.05
0.4999	19.58	19.58	19.58	1029.08
0.4566	19.59	19.59	19.59	1029.09
0.3810	19.65	19.62	19.63	1029.13

$\Delta H_s^\theta(NaBPh_4) = \Delta H_s(\infty) = -19.94$
$\Delta H_f^\theta(aq) = -1029.34$

Standard formation enthalpy of BPh_4^- (aq)

At infinite dilution, formation enthalpy of $NaBPh_4$ in aqueous solution can be considered as the sum of formation enthalpy for Na^+ (aq) and BPh_4^- (aq), therefore, we have

$$\Delta H_f^\theta(BPh_4^-, aq) = \Delta H_f^\theta(NaBPh_4, aq) - \Delta H_f^\theta(Na^+, aq) \quad \ldots (1)$$

From Table 1, $\Delta H_f^\theta(NaBPh_4, aq) = -1029.34$ kJ/mol, $\Delta H_f^\theta(Na^+, aq) = -239.66$ kJ/mol (ref. 3), from Eq. (1), we have $\Delta H_f^\theta(BPh_4^-, aq) = -789.47$ kJ/mol.

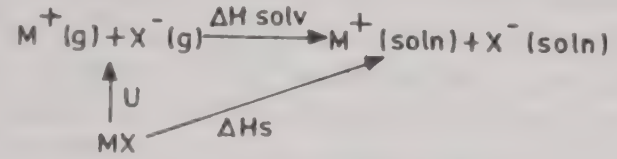

SCHEME 1

Lattice energy of $NaBPh_4$

According to Scheme 1, standard solution enthalpy of ion crystal salt (solution enthalpy of ion crystal at infinite dilution) is equal to the sum of the lattice energy of ion crystal salt and the solvolytic enthalpy of the ion, and the latter can be calculated from standard formation enthalpy of the ion in the solution and gaseous state. Thus

$$\Delta H_s^\theta = U + \Delta H_{solv}(M^+) + \Delta H_{solv}(X^-) \quad \ldots (2)$$

where, U stands for the lattice energy of ion crystal, $\Delta H_{solv}(M^+)$ and $\Delta H_{solv}(X^-)$ respectively stands for the solvolytic energy of the cation and anion. If the solvent is water, then,

$$U = \Delta H_s^\theta - [\Delta H_h(M^+) + \Delta H_h(X^-)] = \Delta H_s^\theta - [\Delta H_f^\theta(M^+, aq) - \Delta H_f^\theta(M^+, g) + \Delta H_f^\theta(X^-, aq) - \Delta H_f^\theta(X^-, g)] \quad \ldots (3)$$

where, $\Delta H_h(M^+)$, $\Delta H_h(X^-)$, $\Delta H_f^\theta(M^+, aq)$, $\Delta H_f^\theta(M^+, g)$, $\Delta H_f^\theta(X^-, aq)$, $\Delta H_f^\theta(X^-, g)$ rspectively stands for the hydration enthalpy and the standard formation enthalpy for the cation and anion in the aqueous solution and gaseous state.

Because of the lack of reference data for $NaBPh_4$, by using standard solution enthalpy ΔH_s^θ of $NaBPh_4$ (−19.94 kJ/mol) and $KBPh_4$ (39.03 kJ/mol, ref. 1), we can carry out the following calculation.

$$U(NaBPh_4) - U(KBPh_4) = \Delta H_s^\theta(NaBPh_4) - \Delta H_s^\theta(KBPh_4) - [\Delta H_f^\theta(Na^+, aq) - \Delta H_f^\theta(Na^+, g)] + [\Delta H(K^+, aq) - \Delta H_f^\theta(K^+, g)] \quad \ldots (4)$$

Using $\Delta H_f^\theta(Na^+, aq)$, $\Delta H_f^\theta(Na^+, g)$, $\Delta H_f^\theta(K^+, aq)$, $\Delta H_f^\theta(K^+, g)$ is respectively −239.65, 610.93, −251.21, 514.92 kJ/mol (ref. 3) in Eq. (4), we get

$$U(NaBPh_4) - U(KBPh_4) = 25.68 \text{ kJ/mol} \quad \ldots (5)$$

Because $NaBPh_4$ is ion crystal[4], from the approximate calculation, equation of lattice energy for ion crystal is

$$U = 1201.6[\Sigma n Z^+ Z^- / (r_+ + r_-)] \times [1 - 0.345/(r_+ + r_-)] \quad \ldots (6)$$

where, n stands for the number of ion constituing the molecule, Z^+, Z^- and r_+, r_- respectively stands for the electric charge and radius of the cation and anion. Substituting Eq. (6) in Eq. (5), we get Eq. (7).

$$1201.6\left[\frac{\Sigma n Z^+ Z^-}{r_+ + r_-}\left(1 - \frac{0.345}{r_+ + r_-}\right) - \frac{\Sigma n Z^+ Z^-}{r_+ + r_-}\left(1 - \frac{0.345}{r_+ + r_-}\right)\right] = 25.68 \text{ kJ/mol} \quad \ldots (7)$$

Since $r_{Na^+} = 0.098$ nm, $r_{K^+} = 0.133$ nm (ref. 3), substituting them in Eq. (6), we get $r_{BPh_4^-} = 4.16$ nm. Further, Eq. (6) can be solved to give $U(NaBPh_4) = 436.16$ kJ/mol.

$\Delta H_f^\theta(BPh_4^-, g)$, $\Delta H_h(BPh_4^-)$, $\Delta G_f^\theta(BPh_4^-, aq)$, $\Delta S_f^\theta(BPh_4^-, aq)$ and $\Delta S_s^\theta(BPh_4^-)$

Hydration enthalpy $[\Delta H_h(Na^+)]$ of Na^+ is −407 kJ/mol (ref. 5), substituting it in Eq. (2), we get the hydration enthalpy of BPh_4^-, viz. $\Delta H_h(BPh_4^-) = -49.10$ kJ/mol. Since,

$\Delta H_h(BPh_4^-) = \Delta H_f^\theta(BPh_4^-, aq) - \Delta H_f^\theta(BPh_4^-, g)$, then, the standard formation $[\Delta H_f^\theta(BPh_4^-, g)]$ of BPh_4^- at gaseous state is -415.99 kJ/mol [$\Delta H_f(H^+, aq)$ value used is 422.58 kJ/mol, see ref. 6].

Combining the standard formation Gibbs free energy of $KBPh_4$ and $RbBPh_4$ and the change of standard Gibbs free energy for the reaction (8),

$$M^+(aq) + BPh_4^-(aq) = MBPh_4\downarrow \quad \ldots (8)$$

with the standard formation Gibbs energy of K^+ and Rb^+, we calculated the standard formation Gibbs free energy of BPh_4^- (aq), as -433.18 kJ/mol and -430.73 kJ/mol respectively. Taking the mean value, $\Delta G_f^\theta(BPh_4^-, aq) = -431.96$ kJ/mol. Further combining with $\Delta H_f^\theta(BPh_4^-, aq)$, we get $S_f^\theta(BPh_4^-, aq) = 315.51$ J/mol.K.

Latimer[7] pointed out that a given ion entropy made little difference in different lattices, and could be regarded as irrelevant to the ion. Accordingly, Cox[8] inferred that a given ion solution entropy was irrelevant to the other ions included in the lattice, then,

$$\Delta S_s^\theta(M^+) + \Delta S_s^\theta(X^-) = \Delta S_s^\theta(MX) \quad \ldots (9)$$

and, change of standard solution enthalpy of BPh_4^- is

$$\Delta S_s^\theta(BPh_4^-) = \Delta S_s^\theta(Ph_4As^+) \quad \ldots (10)$$

Given, change of standard solution Gibbs free energy and standard solution enthalpy for Ph_4AsBPh_4 as $\Delta G_s^\theta(Ph_4AsBPh_4) = 99.16$ kJ/mol (ref. 2) and $\Delta H_s^\theta(Ph_4AsBPh_4) = 66.11$ kJ/mol (ref. 9), the change of standard solution entropy for Ph_4AsBPh_4 and BPh_4^- is respectively $\Delta S_s^\theta(Ph_4ASBPh_4) = -110.86$ J/mol.K and $\Delta S_s^\theta(BPh_4^-) = -55.43$ J/mol.K. The literature data[2] based on Eq. (11) is -57.17 J/mol.K.

$$\Delta S_s^\theta(BPh_4^-) = \tfrac{1}{2}\Delta S_s^\theta(Ph_4AsBPh_4)$$
$$= \tfrac{1}{2}[\Delta S_s^\theta(Ph_4AsI) + \Delta S_s^\theta(KBPh_4) - \Delta S_s^\theta(KI)] \quad \ldots (11)$$

$\Delta H_f^\theta(NaBPh_4, C)$, $\Delta G_f^\theta(NaBPh_4, C)$, $\Delta S_f^\theta(NaBPh_4, C)$, $\Delta S_s^\theta(NaBPh_4)$, $\Delta G_f^\theta(NaBPh_4, aq)$, $\Delta S_f^\theta(NaBPh_4, aq)$

Given, change of standard solution entropy of Na^+ is 36.80 J/mol.K (ref. 5), $\Delta S_s^\theta(NaBPh_4) = \Delta S_s^\theta(Na^+) + \Delta S_s^\theta(BPh_4^-) = -18.68$ J/mol.K. The standard solution enthalpy and standard solution Gibbs free energy is respectively $\Delta H_s^\theta(NaBPh_4) = -19.94$ kJ/mol and $\Delta G_s^\theta(NaBPh_4) = -14.37$ kJ/mol. Because, the standard formation entropies of Na^+ (aq) and BPh_4^- (aq) are respectively $\Delta S_f^\theta(Na^+, aq) = 60.3$ J/mol.K (ref. 3), $\Delta S_f^\theta(BPh_4^-, aq) = 315.51$ J/mol.K, from the Latimers rule and Cox's inference, we have the standard formation entropy of BPh_4^- (C) and Na^+ (C)

$$S_f^\theta(BPh_4^-, C) = S_f^\theta(BPh_4^-, aq) - \Delta S_s^\theta(BPh_4^-) = 370.94 \text{ J/mol.K}$$

$$S_f^\theta(Na^+, C) = S_f^\theta(Na^+, aq) - \Delta S_s^\theta(BPh_4^-) = 23.4 \text{ J/mol.K}.$$

Therefore, $\Delta S_f^\theta(NaBPh_4, C) = 394.36$ J/mol.K, and because $\Delta H_f^\theta(NaBPh_4, C) = -1009.5$ kJ/mol, its standard formation Gibbs free energy is $\Delta G_f^\theta(NaBPh_4, C) = -679.67$ kJ/mol. From reason given $\Delta G_f^\theta(NaBPh_4, aq) = -698.35$ kJ/mol and $\Delta S_f^\theta(NaBPh_4, aq) = 374.42$ J/mol.K. The thermodynamic function of BPh_4^- and $NaBPh_4$ are given in Table 2.

The mean activity coefficients of $NaBPh_4$

The mean activity coefficients of $NaBPh_4$ in aqueous solution can be calculated using Eq. (12) (ref. 10).

$$\ln Y_{\pm NaBPh_4} = \ln Y_{\pm NaCl} + \ln(m_{NaCl}/m_{NaBPh_4}) + \int_0^{m_{NaCl}} [(\nu m)_{NaCl}/(\nu m)_{NaBPh_4} - 1] d\ln(Y_{\pm} m)_{NaCl} \quad \ldots (12)$$

where, m_{NaCl}, m_{NaBPh4}, $Y_{\pm NaCl}$, $Y_{\pm NaBPh4}$, ν_{NaCl},

Table 2—The thermodynamic functions of BPh_4^- and $NaBPh_4$

	ΔH_f^θ(aq)	ΔG_f^θ(aq)	S_f^θ(aq)	ΔH_s^θ	ΔG_s^θ	ΔS_s^θ
BPh_4^-	-789.47	-431.96	315.51	–	–	55.43
$NaBPh_4$	-1029.34	-698.42	374.42	-19.94	-14.37	-18.68
	ΔH_f^θ(C)	ΔG_f^θ(C)	S_f^θ(C)	ΔH_f^θ(g)	ΔH_h	
BPh_4^-	–	–	370.94	-415.99	-49.10	
$NaBPh_4$	-1009.5	-679.67	394.36	–	–	

note: ΔH, ΔG in kJ/mol, S, ΔS in J/mol.K

ν_{NaBPh4}, are respectively the equilibrium concentration, the mean activity coefficients of NaCl and $NaBPh_4$ and the number of ions that make up the molecule, the third term at the right side of the equation can be figured out by grpahical integration. The results of the experiment and calculations are given in Table 3.

The natural logarithm of inserted value of mean activity coefficients of $NaBPh_4$ at different temperatures and concentrations are given in Table 4. We used $\ln Y_{\pm NaBPh4}$ in Table 4 to thermodynamic temperature (T) to carry out linear regression on microcomputer, the results show that dependence of natural logarithm of mean activity coefficients of $NaBPh_4$ on temperature (T) can be expressed by following equation

$$\ln Y_{\pm NaBPh4} = A + BT \quad \ldots (13)$$

the linear correlation coefficients k are all above 0.99, value of A and B for different concentrations are shown in Table 4.

Osmatic coefficients and excess Gibbs free energies of $NaBPh_4$ aqueous solution

For aqueous solution, calculation formula for osmatic coefficient is

$$\phi = (-55.55/\nu m) \ln a_{H_2O} \quad \ldots (14)$$

under equilibrium condition, activity of H_2O in NaCl aqueous solution is equal to activity of H_2O in the $NaBPh_4$ aqueous solution, hence can deduce by Eq. (14)

$$\phi_{NaBPh_4} = (\phi . m)_{NaCl} / m_{NaBPh_4} \quad \ldots (15)$$

We calculated osmatic coefficients of $NaBPh_4$ aqueous solution at different equilibrium concentrations using Eq. (15), and osmatic coefficients of NaCl aqueous solution from ref. 11. From Eq. (16), excess Gibbs free energies of $NaBPh_4$ aqueous solution at different conductions can be calculated (see Table 5).

$$G^{ex}(NaBPh_4) = (\nu m) \cdot RT (1 - \phi + \ln Y_{\pm}) \quad \ldots (16)$$

Table 3—Equilibrium concentrations (m, m_1) and mean ion activity coefficients ($Y_{\pm}$, $Y_{\pm I}$) of $NaBPh_4$ and NaCl from 288.15 to 318.15 K

				T = 288.15 K				
$m \times 10^2$	10.130	7.8010	5.7790	3.9360	2.5860	1.4760	0.6561	0.1781
$m_1 \times 10^2$	10.340	7.9410	5.8680	3.9940	2.6210	1.4901	0.6602	0.1793
$Y_{\pm}$	0.8174	0.8294	0.8431	0.8590	0.8776	0.8997	0.9289	0.9591
$Y_{\pm I}$	0.7806	0.7977	0.8161	0.8484	0.8606	0.8869	0.9195	0.9523
				T = 298.15 K				
$m \times 10^2$	10.250	7.9210	5.8990	4.0560	2.7060	1.5950	0.7742	0.1763
$m_1 \times 10^2$	10.450	8.8060	5.9870	4.1130	2.7401	1.6090	0.7783	0.1772
$Y_{\pm}$	0.8150	0.8266	0.8399	0.8564	0.8735	0.8944	0.9193	0.9564
$Y_{\pm I}$	0.7767	0.7938	0.8123	0.8345	0.8568	0.8829	0.9128	0.9544
				T = 308.15 K				
$m \times 10^2$	10.210	7.8610	5.8390	3.9960	2.6470	1.5350	0.7171	0.1654
$m_1 \times 10^2$	10.380	8.0010	5.9280	4.0520	2.6820	1.5470	0.7212	0.1664
$Y_{\pm}$	0.8126	0.8244	0.8380	0.8549	0.8725	0.8941	0.9204	0.9569
$Y_{\pm I}$	0.7744	0.7913	0.8101	0.8328	0.8556	0.8828	0.9141	0.9551
				T = 318.15 K				
$m \times 10^2$	10.270	7.8710	5.8490	4.0060	2.6540	1.5450	0.6861	0.1698
$m_1 \times 10^2$	10.460	8.0080	5.9350	4.0610	2.6860	1.5570	0.6898	0.1707
$Y_{\pm}$	0.8093	0.8216	0.8353	0.8524	0.8702	0.8920	0.9203	0.9556
$Y_{\pm I}$	0.7703	0.7878	0.8066	0.8298	0.8530	0.8804	0.9142	0.9536

note: m in mol/kg, $Y_{\pm I}$ see ref. (14)

where, ν, m, $Y_{\pm}$ is respectively number of ions of $NaBPh_4$, equilibrium concentration and mean activity coefficient of $NaBPh_4$ in the system of $NaBPh_4 + H_2O$.

Relative partial molar enthalpies and relative partial molar heat capacities of $NaBPh_4$

From Eqs (17) and (18), combined with Eq. (13), the relative partial molar enthalpies and relative partial molar heat capacities of $NaBPh_4$ in aqueous solution at different temperatures and concentrations can be calculated (see Table 6).

$$\bar{H}_{r,m}(NaBPh_4) = -\nu RT^2 (\ln Y_{\pm}/\partial T)_{m,p} \quad \ldots (17)$$

$$\bar{C}_{r,m}(NaBPh_4) = -\nu R (T^2 \partial^2 \ln Y_{\pm}/\partial T^2 + 2T\partial \ln Y_{\pm}/\partial T)_{m,p} \quad \ldots (18)$$

To comprehensively survey the dependence of $\bar{H}_{r,m}$ and $\bar{C}_{r,m}$ of $NaBPh_4$ in aqueous solution on temperature and molality, the temperature was kept fixed, we used $\bar{H}_{r,m}(NaBPh_4)$ and $\bar{C}_{r,m}(NaBPh_4)$ to $(m)^{1/2}$, by curve fitting on microcomputer, the relationship between the experimental constant in the model and temperature (T) was found out. The experimental equation of $\bar{H}_{r,m}$ and $\bar{C}_{r,m}$ for $NaBPh_4$ in aqueous solution at experimental temperature and concentration can be expressed as, respectively

Table 4—Values of natural logarithm of inserted value of mean ion activity coefficients of $NaBPh_4$ in the system of $NaBPh_4 + H_2O$ from 288.15 to 318.15 K

	288.15 K	298.15 K	308.15 K	318.15 K			
$(m)^{1/2}$		$-\ln Y_{\pm}$			$-A$	$-B \times 10^4$	K
0.3200	0.2016	0.2045	0.2078	0.2115	0.1063	3.30	0.997
0.2800	0.1870	0.1898	0.1929	0.1962	0.0984	3.07	0.998
0.2400	0.1706	0.1732	0.1761	0.1792	0.0878	2.87	0.998
0.2000	0.1520	0.1543	0.1569	0.1597	0.0778	2.57	0.997
0.1600	0.1305	0.1326	0.1348	0.1373	0.0653	2.26	0.998
0.1200	0.1057	0.1074	0.1093	0.1113	0.0517	1.87	0.999
0.0800	0.0766	0.0778	0.0792	0.0807	0.0370	1.37	0.998
0.0400	0.0419	0.0426	0.0434	0.0443	0.0188	0.80	0.998

Table 5—Osmatic coefficients and excess Gibbs free energies of $NaBPh_4$ aqueous solution for different temperature and concentration

				288.15 K				
$m \times 10^2$	10.130	7.8010	5.7790	3.9360	2.5860	1.4760	0.6561	0.1781
ϕ	0.9511	0.9526	0.9557	0.9621	0.9676	0.9726	0.9796	0.9908
$-G^{ex}$	74.128	52.198	34.991	21.515	12.163	5.537	1.677	0.338
				298.15 K				
$m \times 10^2$	10.250	7.9210	5.8990	4.0560	2.7060	1.5950	0.7742	0.1763
ϕ	0.9494	0.9517	0.9545	0.9604	0.9651	0.9706	0.9759	0.9887
$-G^{ex}$	78.239	55.815	37.718	23.208	13.462	6.501	2.304	0.291
				308.15 K				
$m \times 10^2$	10.210	7.8610	5.8390	3.9960	2.6470	1.5350	0.7171	0.1654
ϕ	0.9472	0.9515	0.9543	0.9599	0.9650	0.9692	0.9769	0.9889
$-G^{ex}$	80.861	58.243	39.204	23.888	13.752	6.382	2.199	0.279
				318.15 K				
$m \times 10^2$	10.270	7.8710	5.8490	4.0060	2.6540	1.5450	0.6861	0.1698
ϕ	0.9474	0.9504	0.9529	0.9589	0.9642	0.9682	0.9764	0.9873
$-G^{ex}$	86.377	61.168	41.111	25.134	14.494	6.742	2.158	0.294

note: m in mol/kg, G^{ex} in J

Table 6—Relative partial molar enthalpies and relative partial molar heat capacities of $NaBPh_4$ in the system $NaBPh_4 + H_2O$ at 288.15-318.15 K

	288.15 K		298.15 K		308.15 K		318.15 K	
$(m)^{1/2}$	$\bar{H}_{r,m}$	$\bar{C}_{r,m}$	$\bar{H}_{r,m}$	$\bar{C}_{r,m}$	$\bar{H}_{r,m}$	$\bar{C}_{r,m}$	$\bar{H}_{r,m}$	$\bar{C}_{r,m}$
0.3200	455.61	3.162	487.78	3.272	521.05	3.382	555.41	3.491
0.2800	423.85	2.942	453.78	3.044	484.73	3.146	516.70	3.248
0.2400	396.24	2.750	424.22	2.845	453.15	2.941	483.04	3.036
0.2000	354.82	2.463	379.97	2.548	405.79	2.643	432.55	2.719
0.1600	312.02	2.166	334.05	2.241	356.84	2.316	380.37	2.391
0.1200	258.18	1.792	276.41	1.854	295.26	1.916	314.73	1.978
0.0800	189.15	1.312	202.50	1.358	216.31	1.404	230.58	1.449
0.0400	110.45	0.766	118.24	0.793	126.31	0.820	134.65	0.846

note: $\bar{H}_{r,m}$ in J/mol, $\bar{C}_{r,m}$ in J/mol.K

$$\bar{H}_{r,m}(NaBPh_4) = (-930.40 + 6.1446\,T)(m)^{1/2}/[0.2734 + (m)^{1/2}] \quad \ldots (19)$$

$$\bar{C}_{r,m}(NaBPh_4) = (0.0312 + 0.0204\,T)(m)^{1/2}/[0.2734 + (m)^{1/2}] \quad \ldots (20)$$

Temperature and concentration of this experiment are substituted into Eqs (19) and (20), the calculated results of $\bar{H}_{r,m}(NaBPh_4)$ and $\bar{C}_{r,m}(NaBPh_4)$ in aqueous solution are identical to those in Table 6.

References

1 Zhuang Z-H, Zou L-Z, Xu G-D & Qu S-S, *Wuji Huaxue Xuebao*, 7 (1991) 486.

2 Cox B G, Hedwig G R, Parker A J & Watts D W, *Aust J Chem*, 27 (1974) 477.

3 Rossini F D, *Selected values of chemical thermodynamical properties*, Natl. Bur. Stand. Circ. 1952, p 500.

4 Arnott S, Abrahams S C, *Acta Cryst*, 11 (1958) 501.

5 Marcus Y, *Ion-solvation*, (John Wiley, New York), 1985, p 107.

6 Tung C-H, Ten T-C & Tao H – H, *Wuhan Daxue Xuebao*, 2 (1963) 84.

7 Latimer W M, *The oxidation states of the elements and their potentials in aqueous solution*, (Prentice-Hall, N.J.), 1952.

8 Cox B G & Parker A J, *J Am chem Soc*, 95 (1973) 6879.

9 Choux G, Benoit R L, *J Am chem Soc*, 91 (1969) 6221.

10 Wu D-Q, Sun X-M & Qu S-S, *Gaodeng Xuexiao Huaxuc Xuebao*, 8 (1987) 1305.

11 Robinson R A & Stokes R H, *Electrolyte solution*, (Butterworths, London), 1959, p 474.

Indian Journal of Chemistry
Vol. 31A, July 1992, pp. 449-451

A new catalyst for the preparation of oleate of glycerin

Li Rongsheng*, Yang Hua & Zhang Wuyang
Department of Chemistry, Jilin University, Chagchun 130 023 China, P.R.
Wei Quan
Testing Center, Jilin University, Chagchun 130 023 China, P.R.
and
Wei Naixiang
Jilin Plastics Institute, Chagchun 130 023, China, P.R.

Received 29 October 1991; revised and accepted 7 January 1992

In this investigation sulfate promoted titanium oxide (SPTO) is used to prepare oleate of glycerin, an excellent internal lubricant for manufacturing transparent sheet materials of polyvinylchloride (PVC). Experimental results show that the occasional saponification caused by the conventional sodalye catalyst for preparing oleate of glycerin can be avoided completely. SPTO can be used repeatedly without any special treatment. Its activity is comparable with that of sodalye. Also the use of SPTO can produce the desirable product composition. SPTO is likely to become a new catalyst for the production of oleate of glycerin.

Oleate of glycerin is an excellent lubricant for manufacturing transparent sheet materials of PVC. Usually oleate of glycerin is produced by the esterification of glycerin with oleic acid, with sodalye as the catalyst. The use of sodalye, however, may occasionally cause saponification, leading to waste of raw materials. For this reason the plant has to use the raw materials of high purity and to severely control the operating conditions. In turn, the cost of producing oleate of glycerin is raised. Sulfate promoted titanium oxide (SPTO) is a new kind of catalytic material developed in recent years[1]. Besides the high activity, it does not corrode the equipment and is recovered easily and the whole process is economically cheaper. This investigation tries to replace SPTO for sodalye to prepare oleate of glycerin.

Experimental

The samples of SPTO were prepared[2] by treating ammonium sulfate-titanium oxide at different temperatures, and designated SPTO (K), where K refers to the temperature at which the sample was obtained. The esterification temperature was 453 K; The molar ratio of oleic acid to glycerin, 2.0; the dose of the catalyst, 0.5 wt. % of the whole raw materials. The conversion of oleic acid was used to represent the activity of the catalyst. The water formed during the esterification was taken away from the reaction system by nitrogen flow. Nitrogen flow also prevented oleic acid from being oxidized.

Sodalye was taken as the partner in the contrast experiment, with the same dose as that of SPTO being used. The samples and KBr were mixed in the weight ratio of 1 to 300, milled and tabletted in order to measure IR spectra. Spectra were recorded at room temperature on Nicolet 5DX FI-IR spectrometer. Analysis of the esterification product was performed by high performance liquid chromatography (Shimadzu L-5A).

Results and discussion

The data of catalytic activity of the samples are presented in Table 1. From Table 1 it is seen that all the samples, with the exception of SPTO (432), have the catalytic activity for the esterification. The very low activity of (423) is due to the intrinsic activity of titanium oxide. Below 573 K the activity of the samples increases gradually as the treatment temperature.

Based on the work of Yamaguchi and Tanabe[1,3], the catalytic activity of SPTO was attributed to the S-Ti species formed by the interaction of ammonium sulfate with TiO_2. The structure of the proposed S-Ti species can be expressed as (I).

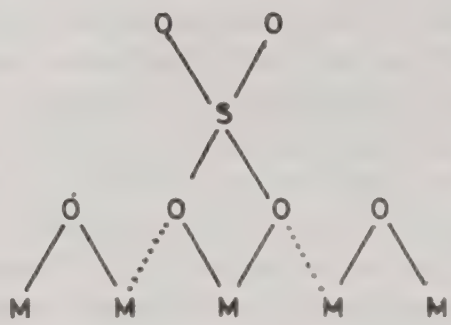

(I)

The anchored sulfate ion contained in S-Ti species has been proved to have the characteristic IR absorptions at 974, 1048, 1138, 1240 cm^{-1} (refs 1, 4). These absorptions are observed in IR spectra of some of SPTO samples prepared in this investigation (Fig. 1).

SPTO (423) only gives IR absorption bands at 1400 and 1113 cm^{-1}. By comparison with the IR

Table 1—Activity of sulfate promoted titanium oxide
Reaction time = 2h; reaction temperature = 453K; molar ratio of oleic acid to glycerin = 2.0

Samples	Conversion of oleic acid %	Samples	Conversion of oleic acid %
TiO_2	12.1	SPTO(573)	73.1
SPTO(423)	12.0	SPTO(673)	68.7
SPTO(473)	30.0	SPTO(773)	66.0
SPTO(523)	55.4	SPTO(873)	63.7

spectrum of ammonium sulfate these two absorption bands should be attributed to ammonium sulfate, 1113 cm^{-1} to SO stretching frequency and 1400 cm^{-1} to NH bending frequency. Clearly, this means that no interaction between ammonium sulfate and titanium oxide has taken place in this sample.

However, for the samples of SPTO obtained at the increased temperatures new bands at 974, 1048, 1138, 1240 and 1327 cm^{-1} have appeared in IR spectra. The band at 1327 cm^{-1} was associated with the adsorbed water[5]. The appearance of bands at 974, 1048, 1138 and 1240 cm^{-1} means that the S-Ti species has been formed in these samples.

SPTO (423) having no catalytic activity does not give IR absorptions, either, characteristic of the anchored sulfate ion. Samples which have catalytic activity give the characteristic IR absorptions. Still, when the catalytic activity of the samples increases the intensities of characteristic IR absorptions of them also do. All these facts suggest that the active species responsible for the catalysis of the esterification of glycerin with oleic acid would be the one proposed by Yamaguchi and Tanabe.

Above 573 K the intensities of IR absorptions characteristic of the anchored sulfate ion decrease with further increase in the treatment temperature. This means the decrease of the amount of S-Ti species in the samples. Since it is responsible for the catalysis of the esterification, the activity drops with the increase in the treatment temperature. Evidently, the decrease in the amount of S-Ti species is due to its decomposition at the temperature higher than 573 K. An additional X-ray photo electron spectroscopic measurement indicates that above 573 K with the further increase in treatment temperature the surface atom percentage of S does decrease gradually.

The results of the contrast experiments with SPTO and sodalye catalysts are listed in Table 2. From Table 2 it is clear that the sample SPTO (573) has the activity almost the same as that of sodalye.

Above all, SPTO can be repeatedly used without

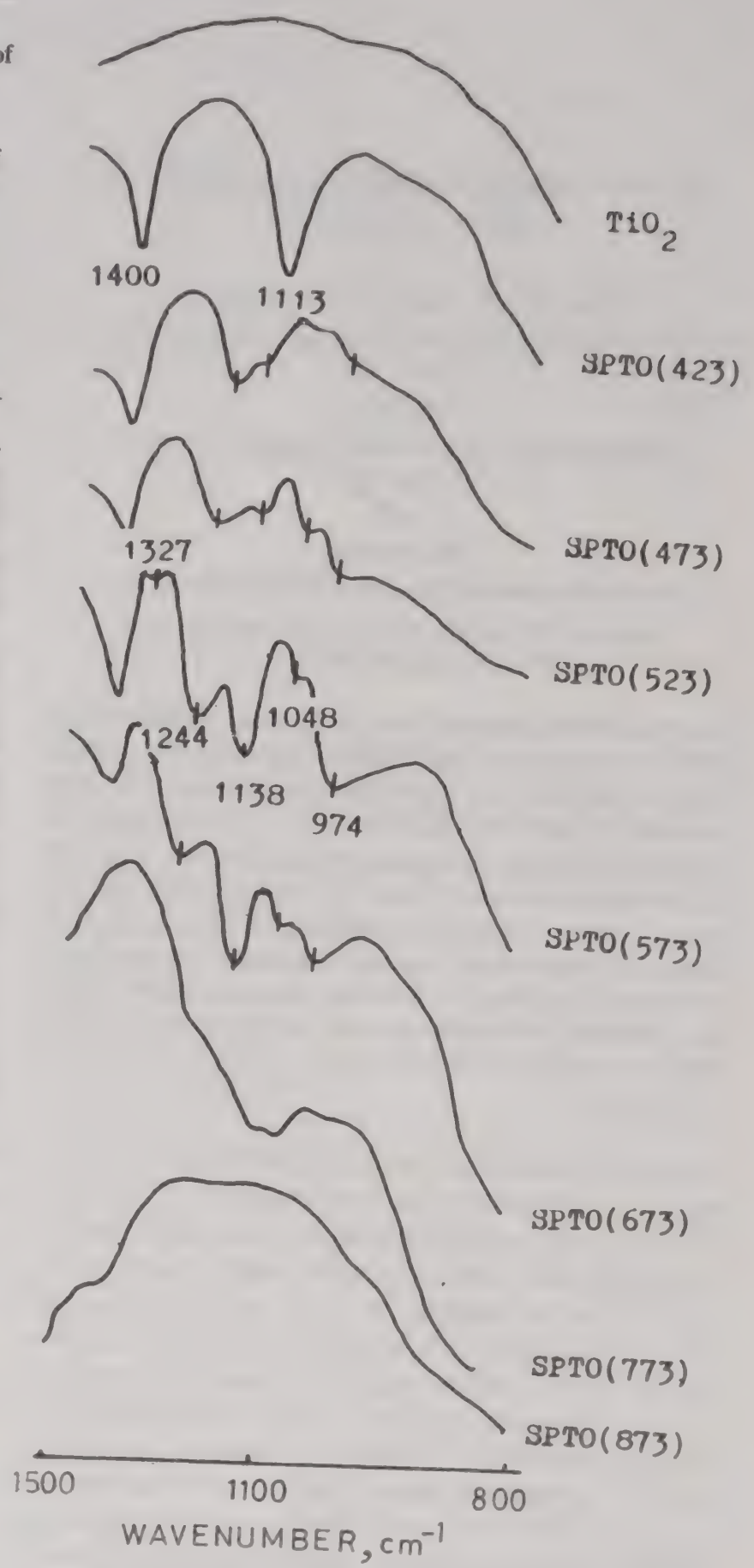

Fig. 1—IR spectra of sulfate promoted titanium oxide

any special treatment. After being used successively five times, for 8 h each time, for example, the activity of a sample of SPTO decreases only by 1-2%.

Owing to the substitution of SPTO for sodalye the occasional saponification will not happen any longer in the esterification.

For good lubrication effect during milling PVC resin appropriate esterification product distributions are needed. Such distributions can be obtained

Table 2—Activity comparison between sulfate promoted titanium oxide and sodalye

Sample used is SPTO(573); esterification temp. = 453K; molar ratio of oleic acid to glycerin = 2.0.

Reaction time (h)	Conversion of oleic acid(%)	
	sodalye	SPTO
2	75.1	73.1
4	88.5	86.8
6	94.0	92.3
8	96.8	96.0

when SPTO is used to catalyze the esterification of glycerin with oleic acid. The content of three esters in the esterification product, given by analyzing the products, varies in the ranges: triolein, 48-55; diolein (β), 21-27; diolein (α), 16.12; monoolein, 1-4 (wt%).

The operational performance tests of oleate of glycerin have shown that the above esterification product compositions can have as good lubricating effect as oleate of glycerin from sodalye catalyzed esterification.

References

1 Yamaguchi T, *Appl Catal*, 61 (1990) 1-25.

2 Tanabe K, in *Proc Symp Ind Coop Chem Program of Heterogeneous Catalysis*, edited by B L Shapiro (Texas A & M University Press, Texas) (1984) p. 71.

3 Tanabe K & Yamaguchi T, in *Successful design of catalysts, Studies in surface science and catalysis*, edited by T. Inui (Elsevier, Amsterdam) Vol. 44 (1988) p. 99.

4 Nakamoto K, *IR spectra of inorganic and coordination compounds* (Wiley, New York) (1970).

5 Khadzhiivanov K I & Davidov A A, *Kinetika i Kataliz*, 29 (1988) 460-465.

Indian Journal of Chemistry
Vol. 31A, July 1992, pp. 452-456

Conductivity, viscosity and ultrasonic studies of rubidium caprylate

K N Mehrotra* & Mamta Jain

Department of Chemistry, Institute of Basic Sciences, Khandari (Agra University), Agra 282 002 (India)

Received 12 August 1991; revised and accepted 22 January 1992

Rubidium caprylate behaves as a moderate electrolyte in dilute aqueous solutions. The CMC, degree of dissociation and dissociation constant of rubidium caprylate have been evaluated from conductometric measurements. The viscosity results have been explained on the basis of equations proposed by Einstein, Vand, Thomas, Moulik and Jones-Dole. The values of molar volume calculated by using equations of Einstein, Vand and Thomas are in agreement. The values of CMC for rubidium caprylate obtained from the conductivity and viscosity measurements are in agreement with the results obtained from ultrasonic measurements. The results show that the soap-soap interactions are weaker than soap-solvent interactions.

The alkali metal soaps are being widely used in many industries as detergents, catalysts, candle hardners, cosmetics, medicines, insecticides and water-proofing agents. Inspite of wide applications of alkali metal soaps in industries, the properties of rubidium soaps have not been thoroughly investigated. Trzebowski *et al.*[1,2] and Mehrotra *et al.*[3-6] studied the structure of rubidium caprate, laurate and stearate using infrared spectra and thermal analysis techniques. Gallot and Skoulios[7,8] established the presence of two types of lameller structure by studying the structure of all phases present in rubidium soaps between room temperature and their melting points. Massorotti and Spindo[9] investigated the powder patterns of propionates of rubidium soaps while Gallot *et al.*[10] studied the liquid crystal structure of the aqueous solutions of rubidium soaps. Sarin[11] used the X-ray diffraction technique to study the crystal structure of rubidium compounds. Mehrotra *et al.*[6,12] determined the CMC of rubidium soaps by conductometric, viscometric and *p*H-metric measurements. Mehrotra *et al.*[13] also determined the molecular weight and aggregation number of rubidium and caesium soaps in aqueous solutions by light-scattering measurements.

The present work deals with the study of conductivity, molar volume, viscosity and ultrasonic measurements of aqueous solutions of rubidium caprylate. The soap possesses limited solubility at lower temperatures and so the studies were carried out in aqueous solutions at 40 ± 0.05°C. The work has been initiated with a view to study the micellar behaviour and evaluate various parameters.

Experimental

The chemicals used were of AnalaR grade. Rubidium caprylate was prepared by the direct reaction of aqueous solution of rubidium chloride with slight excess of caprylic acid. The excess of caprylic acid was removed by washing with benzene, soap was purified by recrystallization in methanol and its purity was checked by determining its m.p. (210°C) and IR spectrum.

Toshniwal CL 01.10A digital conductivity meter, dipping type conductivity cell with platinized electrodes, dilatometer, Ostwald's type viscometer and ultrasonic pulse ECO Interferometer type: SDU I-003 were used for conductance, viscosity and ultrasonic velocity measurements, at a constant temperature, (40 ± 0.05°C).

The apparent molar volume, (ϕ_v), viscosity, (η), adiabatic compressibility, (β), and solvation number, (S_n), were calculated by using the relationships (1-4)

$$\phi_v = \frac{1000}{C\rho_0}(\rho - \rho_0) + \frac{M}{\rho_0} \quad \ldots (1)$$

$$\frac{\eta}{\eta_0} = \frac{\rho.t}{\rho_0.t_0} \quad \ldots (2)$$

$$\beta = U^{-2}.\rho^{-1} \quad \ldots (3)$$

$$S_n = \frac{n_1}{n_2}\left[1 - \frac{VB}{n_1 V_0 B_0}\right] \quad \ldots (4)$$

where M is molecular weight of soap, and C is

molar concentration of solution: η_0, η, ρ_0, ρ and t_0, t are viscosity, density and time of flow for solvent and solution, respectively, v. is ultrasonic velocity, V is molar volume of solution containing n moles of solute and V_0 is molar volume of solvent.

Results and discussion

(A) Conductivity

The specific conductance, k of aqueous solutions of rubidium caprylate increases with increase in soap concentration and this may be due to the ionization of rubidium caprylate into simple metal cations, Rb^+ and the fatty acid anions, $C_7H_{15}COO^-$ and due to the formation of micelles at higher soap concentration. The plot of specific conductance, k versus soap concentration, C (Fig. 1) is characterized by an intersection of two linear plots at 0.040 mol dm^{-3} (40°C) which corresponds to the CMC of soap. The result is in agreement with the value of CMC (0.043 mol dm^{-3}) for caesium oleate by conductometric measurement at 35°C (ref. 6).

The decrease in equivalent conductance, with increase in soap concentration may be due to the combined effects of ionic atmosphere, solvation of ions, decrease of mobility and ionization with the formation of micelles.

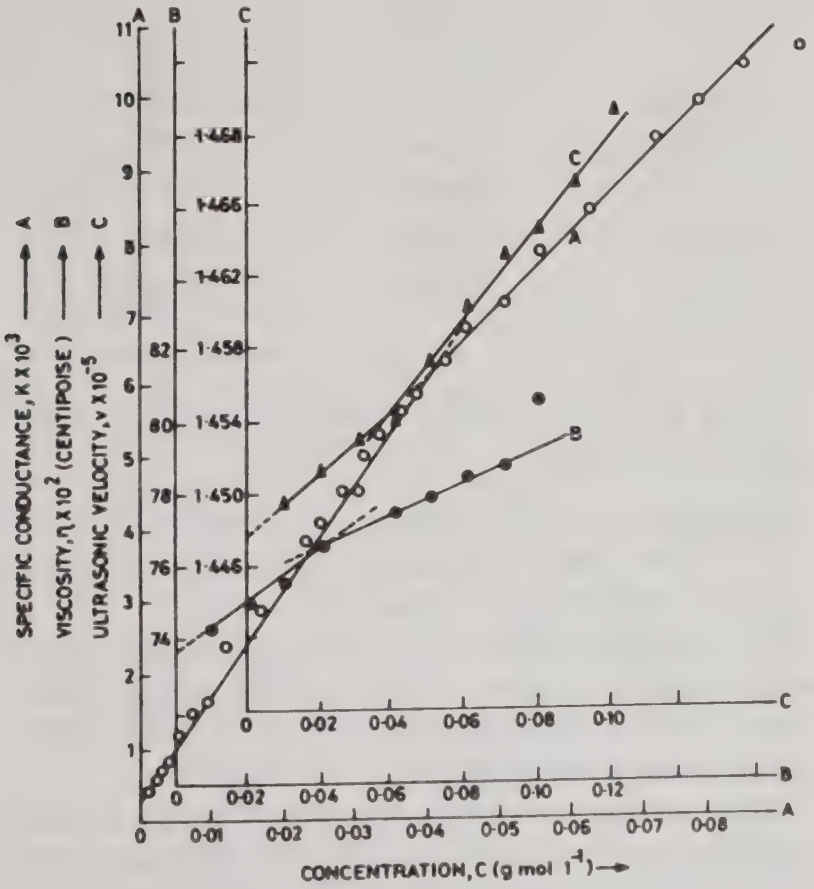

Fig. 1 – (A) Plot of specific conductance versus soap concentration C; (B) plot of viscosity versus C and (C) plot of ultrasonic velocity versus C

An expression for dissociation of rubidium caprylate can be developed using Ostwald's method (5)

$$\underset{C(1-\alpha)}{C_7H_{15}COORb} \rightleftharpoons \underset{C\alpha}{C_7H_{15}COO^-} + \underset{C\alpha}{Rb^+}$$

where C and α are the concentration (mol dm^{-3}) and degree of dissociation, respectively. The dissociation constant, K can be represented as:

$$K = \frac{[Rb^+][C_7H_{15}COO^-]}{[C_7H_{15}COORb]} = \frac{C\alpha^2}{1-\alpha} \qquad \ldots (5)$$

Since the ionic concentrations are low and the interionic effects being almost negligible, the solutions will not deviate appreciably from the ideal behaviour and therefore the activity of ions can be taken as almost equal to their concentrations. The degree of dissociation, α may be replaced by conductance ratio, λ/λ_0 where λ and λ_0 are the equivalent conductances at finite and infinite dilution. On substituting the value of α and rearranging, Eq. (5) can be expressed as Eq. (6)

$$\lambda.C = \frac{K\lambda_0^2}{\lambda} - K\lambda_0 \qquad \ldots (6)$$

The values of K and λ_0 have been obtained from the slope and intercept of the linear portion of the plot of λC versus $1/\lambda$ and are found to be 2.2×10^{-3} and 419.9, respectively.

The values of α lie in the range of 0.2786 to 0.7162 (Table 1) indicating that the soap behaves as a simple moderate electrolyte in aqueous solutions. The values of dissociation constant, K have been calculated using Eq. (5) and lie between 1.8×10^{-3} to 10.7×10^{-3}.

(B) Molar volume and viscosity

The density of aq. solutions of rubidium caprylate increases with increase in soap concentration and the results have been explained in terms of Root's equation (7)

$$\rho = \rho_0 + AC - BC^{3/2} \qquad \ldots (7)$$

where ρ and ρ_0 are densities of soap solution and solvent, respectively. The constants A and B

Table 1 – Conductance for aqueous solutions of rubidium caprylate at 40 ± 0.05°C

Concentration C (g mol dm^{-3})	Specific conductance k × 10^3 (mhos cm^{-1})	Equivalent conductance (mhos)	$\lambda.C$	Degree of dissociation	Dissociation constant $K \times 10^3$
0.0013	0.40	300.75	0.39	0.7162	2.350
0.0017	0.46	267.44	0.45	0.6369	1.899
0.0021	0.56	260.46	0.54	0.6203	2.128
0.0024	0.63	257.89	0.61	0.6142	2.346
0.0028	0.70	247.90	0.68	0.5904	2.383
0.0038	0.86	224.54	0.85	0.5347	2.335
0.0057	1.18	207.01	1.17	0.4932	2.736
0.0075	1.50	198.01	1.48	0.4716	3.156
0.0096	1.66	172.64	1.65	0.4111	2.755
0.0120	2.41	192.80	2.31	0.4591	4.677
0.0170	2.91	175.30	2.98	0.4175	5.087
0.0230	3.84	168.28	3.68	0.4008	6.165
0.0250	4.13	165.20	4.13	0.3934	6.379
0.0280	4.53	163.53	4.58	0.3893	6.951
0.0310	5.00	160.00	4.96	0.3810	7.271
0.0330	5.31	159.46	5.26	0.3797	7.672
0.0360	5.59	156.58	5.63	0.3729	7.983
0.0380	5.86	152.60	5.79	0.3634	7.884
0.0420	6.36	152.66	6.41	0.3636	8.723
0.0450	6.76	148.90	6.70	0.3546	8.768
0.0500	7.12	144.40	7.22	0.3439	9.012
0.0550	7.82	142.16	7.81	0.3385	9.527
0.0620	8.48	135.67	8.41	0.3231	9.563
0.0710	9.37	131.23	9.31	0.3125	10.087
0.0770	9.88	128.48	9.89	0.3060	10.387
0.0830	10.40	124.85	10.36	0.2973	10.442
0.0910	10.62	116.83	10.51	0.2782	9.760
0.1000	11.70	117.00	11.70	0.2786	10.762

refer to the soap-solvent and soap-soap interactions, respectively. The values of constants A (0.17) and B (0.14) have been obtained from the intercept and slopes of plot of $(\rho-\rho_0)/C$ versus $\sqrt{C}$. The results confirm that the soap-solvent interaction is larger than the soap-soap interaction in dilute aqueous solutions of soap.

The calculated values of apparent molar volume, ϕ_v were found to vary linearly with the square root of soap concentration in conformity with the Masson's equation[14]

$$\phi_v = \phi_v^0 + S_v\sqrt{C} \quad \ldots (8)$$

where ϕ_v^0 is apparent molar volume of solvent and S_v is a constant.

The values of ϕ_v^0 (399.6 ml mol^{-1}) and S_v (−147) have been calculated from the intercept and slopes of plot of ϕ_v versus $\sqrt{C}$.

The negative value of S_v shows that the soap-soap interactions are weak in dilute soap solutions. This is in agreement with the results obtained from Root's equation.

The viscosity, η and specific viscosity, η_{sp} of the aqueous solutions of rubidium caprylate increase with increase in soap concentration (Table 2). The plot of η versus C is characterized by an intersection of two linear plots at a definite soap concen-

Table 2 – Molar volume and viscosity data for aqueous solutions of rubidium caprylate at 40 ± 0.05 °C

Concentration C (g mol dm^{-3})	Density ρ (g ml^{-1})	Apparent molar volume ϕ_v (ml mol^{-1})	$\frac{\rho-\rho_0}{C}$	Viscosity (Centipoise) $\eta\times10^2$	Specific viscosity η_{sp}	Reduced viscosity $\eta_{sp}/\sqrt{C}$	$\left(\frac{\eta}{\eta_0}-1\right)\Big/C$	$(\eta/\eta_0)^2$	$\frac{1}{\log(\eta/\eta_0)}$
0.01	1.0013	378.7	0.150	74.30	0.011	0.110	1.088	1.022	212.69
0.02	1.0027	373.7	0.145	74.99	0.020	0.143	1.014	1.041	114.73
0.03	1.0042	375.4	0.147	75.49	0.027	0.159	0.902	1.055	86.79
0.04	1.0056	373.7	0.145	76.59	0.042	0.210	1.051	1.086	55.01
0.05	1.0077	386.7	0.158	78.07	0.062	0.281	1.243	1.128	38.17
0.06	1.0082	368.7	0.140	77.38	0.053	0.220	0.880	1.108	44.79
0.07	1.0086	354.3	0.126	77.87	0.059	0.226	0.849	1.122	39.86
0.08	1.0099	355.0	0.126	78.44	0.067	0.240	0.840	1.139	35.39
0.09	1.0112	355.4	0.127	78.67	0.070	0.233	0.781	1.146	33.87
0.10	1.0116	346.2	0.118	80.62	0.098	0.300	0.969	1.203	24.90

tration (0.040 mol dm^{-3}) (Fig. 1) which corresponds to the CMC of soap. The values of CMC for aqueous solutions of rubidium caprate and laurate are 0.043 and 0.042, respectively at 35 ± 0.05°C (ref. 12). The viscosity results confirm that there is no appreciable aggregation below the CMC and there is a sudden increase in aggregation at this soap concentration. The viscosity results have been interpreted on the basis of equations proposed by Einstein[15], Vand[16], Thomas[17], Moulik[18] and Jones-Dole[19].

The plot of specific viscosity, η_{sp} versus [soap] C is linear below the CMC with intercept almost equal to zero indicating that the Einstein's equation is applicable to dilute aqueous solutions of rubidium caprylate. The value of molar volume of soap obtained from the slope of Einstein's plot is in agreement with the values obtained from Vand's and Thomas' equations are 0.40, 0.44 and 0.38 dm^3 mol^{-1}, respectively. The results are in agreement with the values of molar volume of rubidium caprate and laurate[12] (0.51 and 0.68 dm^3 mol^{-1}), respectively.

The values of constant A and B of the Jones-Dole's equation calculated from the intercept and slope of the plot of $\eta_{sp}/\sqrt{C}$ versus $\sqrt{C}$ below the CMC are 0.11 and 0.95, respectively. The smaller value of constant A (soap-soap interaction) than B (soap-solvent interaction) confirms that the molecules of soap do not aggregate appreciably below the CMC and there is a sudden change in aggregation at the CMC. The values of Moulik's constants M and K obtained from the intercept and slope of the plot of $(\eta/\eta)^2$ versus C^2 for aq. soap solutions are 1.02 and 40.8, respectively. The values of M and K for solutions in methanol are 1.09 and 12.5, respectively[12]. The values of M and K for aqueous solutions of rubidium caprate and laurate are 1.04 & 20.7 and 1.13 & 20.8, respectively[12]. The values of M show approximate constancy whereas the values of K exhibit a change with the change in the nature of solvent. The results are in agreement with the results for solutions of manganese dicaporate in organic solvents[20].

(C) Ultrasonic measurements

The relationship for the variation of ultrasonic velocity with concentration, $v = v_0 + GC$ (where G signifies for Garnsey's constant and v and v_0 represent ultrasonic velocity in solution and solvent, respectively) facilities the evaluation of G (1.56×10^4) for aqueous solutions of rubidium caprylate. The ultrasonic velocity increases with increase in [soap] (Table 3) and the extrapolated value of ultrasonic velocity (1.4480×10^5 cm s^{-1}) is in agreement with the velocity of solvent (1.4482×10^5 cm s^{-1}) which confirms that the soap molecules do not aggregate to an appreciable extent below the CMC.

The adiabatic compressibility of aqueous solutions decreases with [soap] (Table 3) and this decrease may be attributed to the fact that the soap molecules in dilute aqueous solutions are considerably ionized into rubidium cations, (Rb^+) and fatty acid anions, ($C_7H_{15}COO^-$). These ions are

Table 3 – Ultrasonic velocity and acoustic parameters for aqueous solutions of rubidium caprylate at 40 ± 0.05°C

Concentration C (g mol dm^{-1})	Density ρ (g ml^{-1})	Velocity $v \times 10^{-5}$ (cm s^{-1})	Adiabatic compressibility $\beta \times 10^{11}$ (cm^2 dyne^{-1})	$-(\beta-\beta_0)/C \times 10^{11}$	Solvation number S_n
0.01	1.0013	1.4495	4.753	1.70	15.3
0.02	1.0027	1.4513	4.735	1.75	15.6
0.03	1.0042	1.4529	4.717	1.77	22.0
0.04	1.0056	1.4540	4.704	1.65	14.6
0.05	1.0077	1.4573	4.673	1.94	18.7
0.06	1.0082	1.4602	4.652	1.99	20.7
0.07	1.0086	1.4632	4.631	1.98	17.3
0.08	1.0099	1.4647	4.615	1.94	16.9
0.09	1.0112	1.4671	4.594	1.96	17.0
0.10	1.0116	1.4712	4.567	2.33	17.5

surrounded by a layer of solvent molecules, firmly bound and oriented towards the ions. The orientation of solvent molecules around the ions is due to the influence of the electrostatic field of ions and results in the increase in internal pressure and decrease in the compressibility of solutions.

The adiabatic compressibility, β of the soap solutions is found to obey Bachem's relationship:

$$\beta = \beta_0 + AC + BC^{3/2} \quad \ldots (9)$$

where β_0 is the compressibility of solvent, C is the molar concentration and A and B are constants. The values of constants A (-1.48×10^{-11}) and B (-1.8×10^{-11}) were obtained from the intercept and slope of the plot of $(\beta-\beta_0)/C$ versus $\sqrt{C}$.

The values of solvation number lie in the range 15.3-22.0 (Table 3).

References

1 Trzebowski N & Kasch H, *Freiberger Forschungsh*, 251A (1962) 14360.

2 Trzebowski N & Dunken S, *Wiss Z Friedrich Schiller-Univ Jena Math Naurwiss Reihe*, 10 (1960/61) 45.

3 Mehrotra K N & Saroha S P S, *J Indian Chem Soc*, 56 (1979) 466.

4 Mehrotra K N, Rajpurohit M S & Godara V K, *J macromol Sci Chem*, A19 (1983) 181.

5 Mehrotra K N, Saroha S P S & Kachhwaha R, *Tenside Detergents*, 18 (1981) 1.

6 Mehrotra K N & Godara V K, *Tenside Detergents*, 19 (1982) 5.

7 Gallot B & Skoulios A, *Mol Crystals*, 1 (1966) 263.

8 Gallot B & Skoulios A, *Kolloid Z Z Polym*, 222 (1968) 51.

9 Massorotti V & Spindo G, *J appl Crystallogr*, 13 (1980) 622.

10 Gallot B & Bernard R, *Liq Cryst Inst Liq Cryst Conf (Rap, 3rd,)* 1 (1970) (pub 1972) 507.

11 Sarin V A, Dudarev V Va & Dobrolynboya M S, *Kristallografia* 19 (1974) 74.

12 Mehrotra K N, Saroha S P S & Godara V K, *Tenside Detergents*, 18 (1981) 3.

13 Mehrotra K N, Godara V K & Bohra K K, *Tenside Detergents*, 20 (1983) 5.

14 Masson D O, *Phil Mag*, 8 (1928) 218.

15 Einstein A, *Ann Physik*, 19 (1906) 289; 34, (1911) 591.

16 Vand V, *J phys colloid Chem*, 52 (1948) 277.

17 Thomas D G, *J colloid Sci*, 20 (1965) 267.

18 Moulik S P, *J phys Chem*, 72 (1968) 4682.

19 Jones G & Dole M, *J Am chem Soc*, 51 (1929) 2950.

20 Mehrotra K N & Rawat M K, *Indian J pure appl Phys*, 29 (1991) 131.

21 Bachem C A, *Physik*, 101 (1936) 541.

Indian Journal of Chemistry
Vol. 31A, July 1992, pp. 457-459

Voltammetry of [Ru(Hedta)(OH_2)] at HMDE

M M Taqui Khan*, G Ramachandraiah & A B Boricha

Discipline of Coordination Chemistry & Homogeneous Catalysis, Central Salt and Marine Chemicals Research Institute, Bhavnagar 364 002

Received 6 September 1991; revised and accepted 10 January 1992

Electrochemical reduction of [Ru^{III}(Hedta)(OH_2)] has been studied at HMDE in different electrolytes in the *p*H range 1-11.2 by employing cyclic voltammetry, chronoamperometry and chronopotentiometry. Kinetic parameters such as diffusion coefficient, transfer coefficient and heterogeneous electron transfer rate constants have been evaluated. A mechanism for the electrochemical reduction of the ruthenium centre is proposed.

The earlier electrochemical investigations of [Ru(Hedta)(OH_2)] (where Hedta is ethylenediaminetriacetatoacetic acid) have included polarographic[1] and cyclic-voltammetric estimates of formal potentials for the Ru(III)/Ru(II) couple, attachment of the complex to the surfaces of electrodes[3,4] and measurements[5] of the absorption of the complex on mercury electrodes. Also there are a few studies[6-9] on electrochemical characterisation of the chemically/electrochemically oxidized products of [Ru(Hedta)(OH_2)] or its chlorosubstituted form. In the present note we report the determination of kinetic parameters in electrochemical reduction of [Ru^{III}(Hedta)(OH_2)] at HMDE by cyclic voltammetry, chronoamperometry and chronopotentiometry techniques.

Experimental

The complex [Ru^{III}(Hedta)(OH_2)] was prepared[10] from $RuCl_3.xH_2O$ via $K_2[RuCl_5(OH_2)]$ and K[Ru(Hedta)Cl]$2H_2O$ by the synthetic procedure described earlier[6,11]. The supporting electrolytes (AR grade) were prepared in doubly distilled water. A digital *p*H meter (model DI707, Digisun Electronics) was used for *p*H measurements. A 5 ml solution of the electrolyte was deaerated with nitrogen and then a weighed amount of the title compound added. The *p*H of this solution was maintained earlier with acetate or phosphate buffers. The ionic strength of the final solution was adjusted to 0.2 *M* with sodium perchlorate. Cyclic voltammograms were recorded with EG&G models PAR 174A, Polarographic analyser and PAR 175 universal programmer coupled with Houstan Instruments X-Y recorder. The chronoamperometric and chronopotentiometric experiments were performed with PAR 175 universal programmer connected to PAR 173 potentiostat through an interface model PAR 306 and a current to voltage converter model PAR 176. A three electrode assembly of model PAR 303 SMDE/HMDE provided with HMDE (0.017 cm^2) as working, platinum wire as auxillary and SCE as reference electrodes was used.

Results and discussion

At *p*H 2.1, the complex [Ru^{III}(Hedta)(OH_2)] gave two cathodic peaks during cyclic voltammetric scans at scan speeds (ν) greater than 50 mV/s. The first peak at -0.213 V is for the reduction[6] of Ru(III) to Ru(II), while the second peak at -0.84 V which appears only in acidic region and merges with hydrogen wave is assigned for Ru(II)/Ru(I) couple. The second peak is irreversible in nature and not considered in the present studies. There is one anodic peak at -0.15 V and is a counterpart to the Ru(III)/Ru(II) reduction peak at -0.213 V. The cathodic and anodic peaks of Ru(III)/Ru(II) couple took a broad shape with slight shifts in peak positions as the scan speeds is decreased below 0.2 V/s. Further, the ratio of anodic to cathodic currents is always less than unity and the difference between the cathodic and anodic peak potentials, (ΔE_p) is greater than 0.059 V which is suitable for one electron process. All these observations clearly indicate that the one electron reduction of [Ru^{III}(Hedta)(OH_2)] at mercury electrode is not completely reversible. The nature of CV is almost same at all other *p*H values studied between 1-11.2. A cathodic shift in both the processes and a little variation in peak currents are observed with the rise in *p*H values. The plots of *ip* versus $\nu^{1/2}$ are found to be linear. This shows that the electrode process is diffusion controlled. However, these lines, almost at all *p*H values studied do not pass through the origin. This may be due to weak adsorption of the complex species[5]. At *p*H 2.1, a split in the plateau of Ru(III)/Ru(II) due to adsorption effect was observed at scan speeds less than 50 mV/s. Figure 1 differentiates the cyclic voltammetric responses at $\nu = 20$ mV/s at three selected *p*H values. The plots of *ip* versus $\nu^{1/2}$ in acidic and basic medium are shown in Fig. 2. Relatively large peak currents were observed at $4 < pH < 8$.

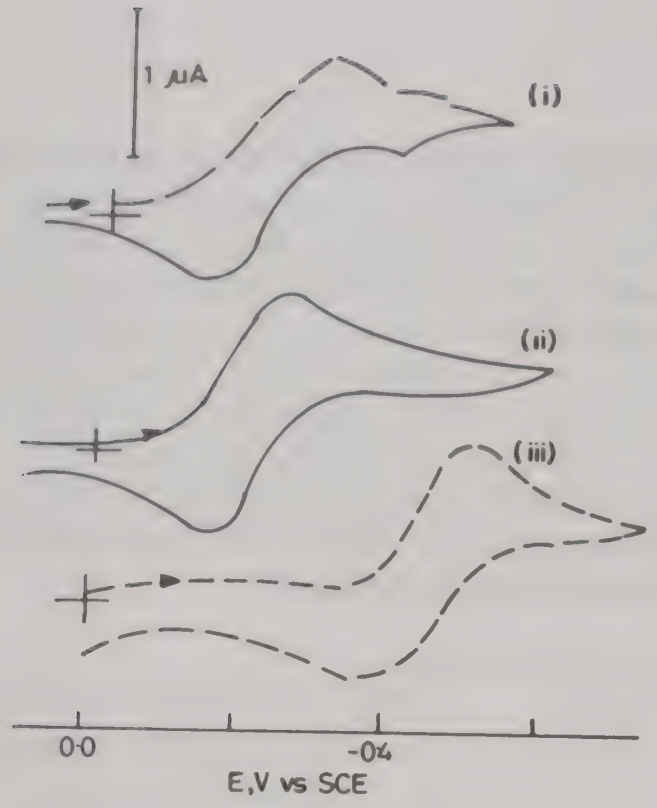

Fig. 1—Cyclic voltammograms of $[Ru(III/II)(Hedta)(OH_2)]^{0/-}$ couple at *p*H (i) 2.1, (ii) 4.5 and (iii) 11.2; scan speed, 20 mV/s.

The current time data were obtained at *p*H 2.1, 4.5, 8.0 and 11.2. The plots of $it^{1/2}$ versus t, from this data, were horizontal showing the charge transfer process to be diffusion controlled. The linear portion of these plots were extrapolated to zero time, $(it^{1/2})_{t=0}$, from which the diffusion coefficient of the electroactive species was evaluated using Cottrell equation[12]. The data is presented in Table 1.

The chronopotentiograms for the above solutions were obtained by changing the current densities between 2-4 μA. In acidic medium, there are two curves in the chronopotentiogram. At *p*H 2.1, the first curve rises at -0.17 V and reaches a limiting value at ~ -0.3 V. The limiting value is not discrete; immediately further reduction follows. The $it^{1/2}$ values, at all *p*H values studied, were found to be constant indicating further the reduction process as diffusion controlled. The diffusion coefficient for $[Ru^{III}(Hedta)(OH_2)]$ has also been calculated using Sand equation[13] (Table 1). The diffusion coefficients obtained by both the methods are in very close agreement.

The peak separation values, ΔE_p were used to calculate the standard reaction rate constant k_s^0 using Eq. (1) as suggested by Nicholson[14],

$$\psi = \gamma^{\alpha} k_s^0/(\pi nFR\,T\,D_{ox}\nu)^{1/2} \quad \ldots (1)$$

where ψ is a function of ΔE, $D_{ox}\nu$ is the ratio of diffusion coefficients of the reduced and oxidized forms of the electroactive species, $(D_{ox} \sim D_{red})$, α is

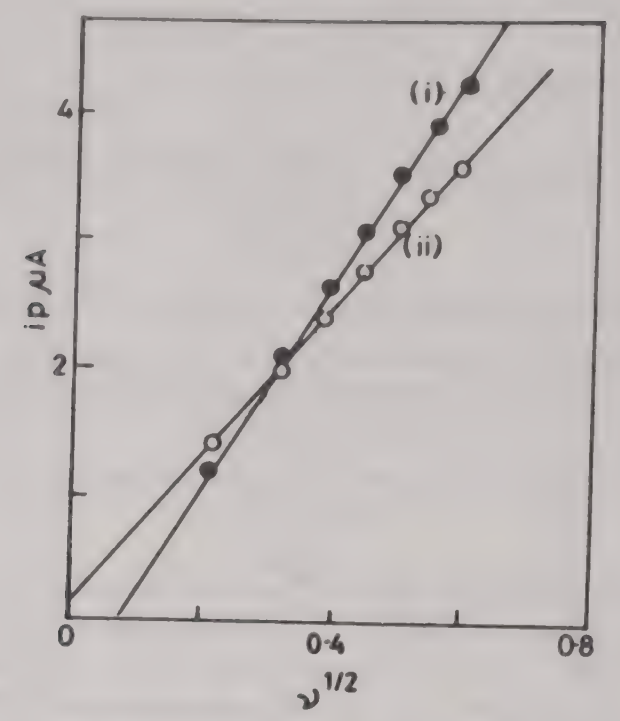

Fig. 2—Plots of *ip* versus $\nu^{1/2}$ at *p*H (i) 2.1 and (ii) 11.2; concentration of the complex 1 m*M*

Table 1—Kinetic parameters of the reduction of $[Ru^{III}(Hedta)(OH_2)]$, (1 m*M*) in different buffer solutions

[Scan speed = 0.12 V/s; W.E. = HMDE, R.E. = SCE]

*p*H	$D_{ox} \times 10^6$ cm²/sec		*αn	$k_{fh}^0 \times 10^8$ cm/s	ψ	**$k_s^0 \times 10^2$ cm/s
	CA	CP				
2.1	3.75	4.15	1.02	3.29	1.32	0.98
4.5	6.19	4.12	1.15	6.65	1.26	1.20
8.0	5.88	5.70	0.91	0.30	1.86	1.73
11.2	4.01	4.70	0.59	0.09	0.53	0.41

*from chronopotentiometry data.
**calculated by using diffusion coefficient data from chronoamperometry.

the transfer coefficient and all other symbols have their usual meaning. From chronopotentiometric data, E_t versus $\log[1(t/T)^{1/2}]$ plots (Eq. 2, under linear diffusion condition)[15] are obtained. By using intercept and slope values of these plots, the forward rate constants k_{fh}^0 at *p*H 2.1, 4.5, 8.0 and 11.2 have also been calculated.

$$E_t = \frac{RT}{\alpha nF} \ln \frac{nFC_{ox}^* k_{fh}^0}{i} + \frac{RT}{\alpha nF} \ln \left[1 - \left(\frac{t}{T}\right)^{1/2}\right] \quad \ldots (2)$$

where the symbols have their usual meanings.

The values of k_s^0 and k_{fh}^0 thus obtained are presented in Table 4. The values of k_s^0 suggest that the electrode process[16] at all *p*H values studied is quasireversible in nature. It is found that the forward

rate constant k_m^0 at all the four *p*H values is about 6-8 orders of magnitude less than that of k_s^0 value.

The cyclic voltammetric data at different *p*H values indicate that the formal potential of Ru(III)/Ru(II) couple is almost independent of *p*H between 3.5-7.5. However, this couple showed a small anodic shift with decreasing *p*H less than 3.5 and cathodic shift at 0.057V/*p*H with an increase in *p*H above 7.5. Our earlier potentiometric data[6] indicate that the complex $[Ru^{III}(Hedta)(OH_2)]$ can exist as $[Ru^{III}(edta)(OH_2)]^-$ at *p*H 3.5-7.5, $[Ru^{III}(edta)(OH_2)]^{2-}$ at *p*H 7.5-9 and $[Ru^{III}(edta)(OH_2)]^{3-}$ at *p*H 9-10.5. Thus the anodic shift at *p*H < 3.5 is accounted for the weak interaction of protons with one/two free carboxylate groups[11,17,18] of EDTA while the cathodic shift is located in the basic medium for the hydrolysis of metal complex. Therefore the electrode reaction at *p*H 2.1, 4.5, 8.0 and 11.2 are considered for the involvement of the species $[Ru^{III}(Hedta)(OH_2)]$, $[Ru^{III}(edta)(OH_2)]^-$, $[Ru^{III}(edta)(OH_2)]^{2-}$ and $[Ru^{III}(edta)(OH_2)]^{3-}$, respectively as shown below:

$$[Ru^{III}(Hedta)(OH_2)] + e \rightleftharpoons [Ru^{II}(Hedta)(OH_2)]^- \quad (pH\ 2.1) \quad \ldots (3)$$

$$[Ru^{III}(edta)(OH_2)]^- + e \rightleftharpoons [Ru^{II}(edta)(OH_2)]^{2-} \quad (pH\ 4.5) \quad \ldots (4)$$

$$[Ru^{III}(edta)(OH)]^{2-} + e + H^+ \rightleftharpoons [Ru^{II}(edta)(OH_2)]^{2-} \quad (pH\ 8.0) \quad \ldots (5)$$

$$[Ru^{III}(edta)(OH_2)]^{3-} + e + H^+ \rightleftharpoons [Ru^{II}(edta)(OH)(OH_2)]^{3-} \quad (pH\ 11.2) \quad \ldots (6)$$

According to k_s^0 values in Table 4, it is clear that the reduction processes involvng $[Ru^{III}(Hedta)(OH_2)]$ and $[Ru^{III}(edta)(OH_2)]^{3-}$ have a higher irreversible tendency than those of $[Ru^{III}(edta)(OH_2)]^-$ and $[Ru^{III}(edta)(OH_2)]^{2-}$ species.

References

1 Shimizu K, Matsubara T & Sato G P, *Bull chem Soc Japan*, 47 (1974) 1651.
2 Matsubara T & Creutz C, *Inorg Chem*, 18 (1979) 1956.
3 Oyama N & Anson F C, *J electroanal Chem*, 88 (1978) 289; *J Am chem Soc*, 101 (1979) 739, 1634, 3480.
4 Scott N S, Oyama N & Anson F C, *J electroanal Chem*, 110 (1980) 303.
5 Gonzalez S & Anson F C, *J electroanal Chem*, 129 (1981) 243.
6 Taqui Khan M M, Hussain A, Ramachandraiah G & Moiz M A, *Inorg Chem*, 25 (1986) 3023.
7 Ezerskaya N & Solovykh T P, *Zh neorg Khim*, 11 (1960) 2569; 13 (1968) 186.
8 Ikeda M, Shimizu K & Sato G P, *Bull chem Soc Japan*, 55 (1982) 797.
9 Baar R B & Anson F C, *J electroanal Chem*, 187 (1985) 265.
10 Taquikhan M M, Bajaj H C, Shirin Z & Venkatasubramanian K, *Indian J Chem*, (in press).
11 Diamantis A A & Dubrawski J V, *Inorg Chem*, 20 (1981) 1142.
12 Adams R N, *Electrochemistry at solid electrodes* (Interscience, New York), 1966.
13 Sand H J S, *Phil Mag*, 1 (1901) 45.
14 Nicholson R S, *Analyt Chem*, 37 (1965) 1351.
15 Charlot G, Bodoz Lambling J & Tremillon B, *Electrochemical reactions—The Electrochemical methods of analysis* (Elsevier Publishing Company, Amsterdam, New York), 1962.
16 Matsuda H & Ayabe Y, *Z Electrochem*, 59 (1955) 494.
17 Okamoto K I, Hidaka J, Iida I, Hino K H & Kanamori K, *Acta Crystallogr*, 46 (1990) 2327.
18 Taqui Khan M M, Venkatasubramanian K, Bhadbhade M M, Siddiqui M R H, Bajaj H C & Shirin Z, *Acta Crystallogr*, A46 (1990) C227, (Supplement containing International Union of Crystallography XVth International Congress, Bordeaux, France, Abstracts).

Indian Journal of Chemistry
Vol. 31A, July 1992, pp. 460-462

Synthesis & multinuclear NMR studies of some 2-(2′-pyridyl)phenyl substituted organotellurium(IV)/mercury(II) compounds

Tarlok S Lobana* & William R Mcwhinnie
Department of Chemical Engineering & Applied Chemistry, Aston University, Aston Triangle, Birmingham B4 7ET, U.K.

Received 3 October 1991; revised and accepted 6 February 1992

The synthesis and spectral properties of 2-(2′-pyridyl)--phenyltellurium(IV) trichloride and 2-(2′-pyridyl)phenyl mercury(II) iodide as well as reactions of 2-(2′-pyridyl)phenyltellurium(IV) halides ($RTeX_3$, X = Cl, Br) with methyl iodide or 2-(2′-pyridyl)-phenylmercury(II) chloride are described. The attempt to metallate $TeBr_4$ with 2-phenylpyridine ended with the formation of an adduct. The compounds are studied using analytical data, IR and multinuclear NMR (^1H, ^{13}C, ^{125}Te and ^{199}Hg) data.

In view of the importance of Group II-VI elements in the development of semiconductors, there is a considerable interest in the chemistry of organotellurium compounds and their reactivity towards metal salts for understanding the mechanism of the metallorganic vapour phase epitaxy (MOVPE) of tellurium semiconductors[1-9].

In this paper, we report the synthesis of some new organotellurium/mercury compounds and reactions of 2-(2′-pyridyl)phenyltellurium halides with methyl iodide or organomercury (II).

Experimental

The substrates, 2-(2′-pyridyl)phenyltellurium (IV) tribromide and 2-(2′-pyridyl)phenylmercury (II) chloride were prepared by the literature method[6]. Methyl iodide, tellurium metal, tellurium tetrahalides and organic solvents were procured from BDH or Aldrich and used as such.

Elemental analyses were performed by Elemental Micro-analysis Ltd., Exeter Road, Oakhampton, Devon EX 20, 1QA, U.K. The melting points (uncorrected) were determined with a Gallenkamp electrically heated apparatus. NMR data were obtained with a Bruker AC 300 spectrometer at 300, 35.4, 94.7 and 53.7 MHz for ^1H, ^{13}C, ^{125}Te and ^{199}Hg nuclei respecively. References were tetramethylsilane (^1H, ^{13}C), bis(*p*-ethoxyphenyl)ditelluride (with ^{125}Te chemical shifts cited relative to Me_2Te) and external $HgCl_2$ in water (for ^{199}Hg).

(1) *Preparation of 2-(2′-pyridyl)phenyltellurium (IV) trichloride* ($RTeCl_3$)

A solution of 2-(2′-pyridyl)phenylmercury(II) chloride (0.60g) in dry dioxane (15 ml) was added to a solution of tellurium (IV) tetrachloride (0.43 g) in dioxane (10 ml). The contents were refluxed for 2.5 h and then filtered to remove any unreacted material. The filtrate was allowed to cool slowly when a creamy light yellow compound was formed. The compound was filtered and dried *in vacuo*. It was then recrystallised from dioxane-methanol (1:1, v/v) mixture; yield 60%, melting point (°C) 265-70d. Analytical data: found (%), C, 33.96; H, 2.04: N, 3.51; required for $C_{11}H_8NCl_3Te$: C, 34.01: H, 2.06; N, 3.61.

(2) *Preparation of 2-(2′-pyridyl)phenylmercury (II) iodide* (*RHgI*)

To a solution of 2-(2′-pyridyl)phenylmercury(II) chloride (0.30 g) in dry dioxane (15 ml) was added an excess of methyl iodide (2 ml). The contents were refluxed for 5 h and filtered to remove any suspended material. The solution was evaporated to dryness when a light yellow sticky mass was left. This mass was extracted with diethyl ether (15 ml) and the extract was allowed to evaporate when a light yellow needle shaped compound was formed. The compound was dried *in vacuo*; yield, 75%; melting point (°C), 102-4. Analytical data: found (%): C, 28.42: H, 1.56; N, 2.94; required for $C_{11}H_8N\,I\,Hg$; C, 27.38; H, 1.63; N, 2.90.

(3) *Reaction of tellurium tetrabromide with 2-phenylpyridine*

A solution of tellurium(IV) tetrabromide (2.87 g) in dioxane (20 ml) was added to a solution of 2-phenylpyridine (5 ml) in dioxane (10 ml). The contents were refluxed for 1 h when a brick red product was formed. The product was filtered and washed with 10 ml of ethanol. It was dried *in vacuo*; yield, 80%; melting point (°C), 205-8. Analytical data, found (%): C, 27.00; H, 2.13; N, 2.81. required for $C_{16.5}H_{15.5}N_{1.5}OBr_4Te$: C, 27.98, H, 2.19; N, 2.96.

(4) *Reaction of 2-(2′-pyridyl)phenyltellurium(IV) tribromide with 2-(2′-pyridyl)phenylmercury(II) chloride* (*RHgCl*)

A solution of 2-(2′-pyridyl)phenyltellurium(IV) tribromide (0.90 g) in dioxane (10 ml) was added to the solution of 2-(2′-pyridyl phenylmercury(II) chloride

† Address for correspondence: Department of Chemistry, Guru Nanak Dev University, Amritsar-143 005.

(0.60 g) in dioxane (10 ml). The contents were refluxed for 3 h and on cooling a light yellow product was formed. It was filtered, washed with ethanol and then recrystallised from acetonitrile-ethanol mixture (1:1, v/v); yield, 60%, melting point (°C), 230-32. Analytical data, found (%): C, 29.69; H, 1.78; N, 3.80: required for $C_{23}H_{17.5}N_{2.5}Br_4Te_2$: C, 30.54; H, 1.93: N, 3.87.

(5) *Reaction of* 2-(2′-*pyridyl*)*phenyltellurium*(*IV*) *trichloride with* 2-(2′-*pyridyl*)*phenylmercury*(*II*) *chloride*

A solution of 2-(2′-pyridyl)phenyltellurium trichloride (0.20 g) in dioxane (10 ml) was added to the solution of 2-(2′-pyridyl)phenylmercury(II) chloride (0.20 g) in dioxane (10 ml). The contents were refluxed for 3 h followed by the evaporation of the excess solvent. The addition of a few ml of cyclohexane formed a light yellow product. It was recrystallised from dioxane-cyclohexane (1:1, v/v) mixture; yield, 65%, melting point (°C), 165-70. Analytical data, found (%): C, 37.73; H, 2.94; N, 3.21; required for $C_{26.8}H_{25.6}N_2Cl_6Te_2$; C, 38.18; H, 3.03; N, 3.32.

Table 1—The ^{13}C NMR data (ppm, relative to TMS) for $RTeCl_3$ and RHgI

Compound (Solvent)	δ values					
	C_1 C_7	C_2 C_8	C_3 C_9	C_4 C_{10}	C_5 C_{11}	C_6
$RTeCl_3$	145.1	132.3	144.5	122.7	152.5	146.8
(DMSO-d_6)	133.1	133.6	128.8	127.8	126.5	
RHgI	147.9	129.9	138.1	120.3	155.9	141.9
($CDCl_3$)	—	137.8	128.7	127.0	123.5	
$RTeBr_3$[a]	145.1	122.7	133.6	126.4	151.5	
(DMSO-d_6)	144.3	132.2	129.3	131.1	127.9	
($RHgCl$[a])	149.5	120.9	138.3	123.4	155.9	141.3
(DMSO-d_6)	147.9	137.8	128.2	129.2	127.1	

(a) From ref. 6

Results and discussion

The reaction of 2-(2′-pyridyl)phenylmercury(II) chloride (RHgCl) with tellurium(IV) tetrachloride formed the *trans*-metallated product, $RTeCl_3$ (compound 1), analogous to $RTeBr_3$ reported earlier[6]. Thus RHgCl is able to *trans*-metallate easily both the tellurium (IV) tetrahalides, contrary to the earlier[6] contention that $TeCl_4$ might pose some difficulty due to its hygroscopic nature. Similarly, the reaction of RHgCl with methyl iodide was expected to give the N-methylated product, $[C_{11}H_8(NMe)HgCl]^+I^-$. However, the exchange of anions between them formed RHgI (compound 2). This exchange of anions can be explained easily in terms of the HSAB principle according to which mercury(II) would prefer iodide over chloride.

The IR data for the compounds (1) and (2) showed peaks characteristic of 2-(2′-pyridyl)phenyl group whose presence was confirmed by the ^1H NMR [compound, δ (ppm versus TMS): $RTeCl_3$ (DMSO-d_6) 7.403 (m, C_4, C_9, C_{10}, C_{11}), 8.609 (2 t, C_2, C_3), 8.751 (d, C_8), 9.304 (d, C_1); RHgI($CDCl_3$), 7.403 (m, C_3, C_9, C_{10}), 7.511(d, C_{11}), 7.851(t, C_2), 7.972 (d, C_4), 8.059(d, C_8), 8.578(d, C_1)] and ^{13}C NMR data (Table 1). In compound (1), the lowest field doublet is at δ 9.304 ppm·and in compound (2), this doublet is at δ8.578 ppm. Both these doublets are due to the proton at carbon (1) (see structure I for numbering scheme) bonded to nitrogen. The N→Te coordination would affect C_1 proton more as compared to N→Hg coordination because Te is tetravalent and attached to three electronegative chlorides ($RTeCl_3$), as compared to Hg which is bonded to the less electronegative iodide. The protons attached to other carbons are at higher field and peaks are doublets, triplets or multiplets (see data above).

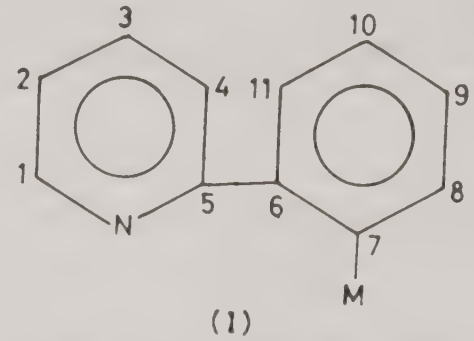

(1)

The ^{13}C NMR data for $RTeCl_3$ and RHgI are similar to those obtained for $RTeBr_3$ and RHgCl respectively (Table 1)[6]. Interestingly, the lowest field carbon is the tertiary carbon C_5 in all the four cases. The ^{125}Te NMR spectrum of $RTeCl_3$ gave a single peak at δ1213.42 ppm (relative to Me_2Te) which is in the range of values observed in other tellurium compounds[4b,7].

Reaction of $RTeBr_3$ with MeI was complicated and no N-methylated product, $[C_{11}H_8(NMe)TeBr_3]^+I^-$ was formed. Similarly, an attempt to *trans*-metallate tellurium tetrabromide using 2-phenylpyridine resulted in the formation of an adduct of stoichiometry, $TeBr_4(1.5L).H_2O$ (L = 2-phenylpyridine). Thus *trans*-metallation process would require the use of RHgCl. A reverse-*trans*-metallation phenomenon was observed for the first time when RR′Te was reacted with $HgCl_2$ (ref. 8). Here R′ group migrated to Hg and Cl group migrated to Te forming RTeCl and R′HgCl [R′ = *p*-ethoxyphenyl-, R = 2-(2′-pyridyl)-phenyl-].

Reactions of $RTeX_3$ ($X=Cl,Br$) with RHgCl

A reaction of $R'TeCl_3$ ($R'=p$-ethoxyphenyl-) with RHgCl gave $[RR'TeCl][HgCl_3]$ as confirmed by NMR and X-ray data[4b,6]. Similarly, reaction of $RTeBr_3$ with RHgCl is reported to give $[R_2TeBr][HgClBr_2]$[6]. However, in the present work it has been established (on the basis of analytical data and absence of ^{199}Hg NMR signals) that reactions of $RTeX_3$ (X = Cl, Br) with RHgCl do not form the above type of ionic products, rather the products of the type; $R_2Te_2Br_4(0.5CH_3CN)$ (compound 4) and $R_2Te_2Cl_6(0.8C_6H_{12})$ (compound 5) are indicated. This difference in reactivity is attributed to the low stability of $[Re_2TeX]^+$ (X = Cl, Br) compared to that of $[RR'TeCl]^+$ due to the higher steric requirements of the two bulky R groups.

Acknowledgement

One of the authors (TSL) thanks the Indian National Science Academy, Delhi; Royal Society, London and Guru Nanak Dev University, Amritsar for financial support and study leave.

References

1 Gysling H G, *Coord chem Rev*, 42 (1982) 133.
2 McWhinnie W R, in Patai S & Rapport Z (eds), *The chemistry of organic selenium & tellurium compounds*, Vol 2 (Wiley, Chichester), 1988, p 495.
3 Gysling H G, in Patai S & Rapport Z (Eds), *The chemistry of organic selenium & tellurium compounds*, Vol 1 (wiley, Chichester), 1986, p 679.
4 (a) Al-Salim N I & Mc Whinnie W R, *Inorg chim Acta*, 155 (1989) 213.
(b) Lobana T S, Mbogo S A, McWhinnie W R, Patalinghug W C & White A H, *J organometal Chem*, 390 (1990) 29.
5 Mullin J B, Irvine S J C, Geiss J & Royle A, *J cryst Growth* 72 (1985) 1.
6 Al-Salim N I, West A A, Mc Whinnie W R & Hamor T A, *J chem Soc Dalton Trans*, (1988) 2363.
7 Mbogo S A, Mc Whinnie W R & Lobana T S, *J organometal Chem*, 384 (1990) 115.
8 Mbogo S A, McWhinnie W R & Lobana T S, *Inorg chim Acta*, 172 (1990) 221.
9 Mbogo S A, Mc Whinnie W R & Lobana T S, Inorg chim Acta, (in press) 1991.

Indian Journal of Chemistry
Vol. 31A, July 1992, pp. 463-465

Synthesis and characterization of Co(II) and Ni(II) complexes of 2-substituted benzimidazoles

S B Balaji Rao & N M Nanje Gowda*
Chemistry Department, Central College, Bangalore 560 001

Received 1 October 1991; revised 11 December 1991; accepted 18 February 1992

Thiocyanates of cobalt(II) and nickel(II) react with 2-alkyl substituted benzimidazoles to give complexes of the type $M(NCS)_2(R\text{-}BzlH)_2$ (where M = Co or Ni; R = Et, *n*-Pr, *i*-Pr or *n*-Bu). Perchlorates of the above metals also react with benzimidazole and its derivatives to yield $Ni(i\text{-}PrBzlH)_2)(ClO_4)_2$, $M(R\text{-}BzlH)_3(ClO_4)_2$ (where M = Co or Ni; R = H or Et; M = Co, R = *i*-Pr) and $M(R\text{-}BzlH)_4(ClO_4)_2$ (where M = Co or Ni, R = Me or *n*-Pr; M = Ni, R = *n*-Bu). On the basis of elemental analyses, conductivity measurements, magnetic moments, infrared and electronic spectral studies, the cobalt complexes have been assigned a distorted tetrahedral stereochemistry and the nickel complexes, a square-planar geometry. Thermal studies of a few thiocyanate complexes have also been carried out.

Benzimidazole and its derivatives are of considerable importance because of their biological properties. They have been found to serve as herbicides and antivirus agents[1,2]. The coordinating ability of benzimidazole and its methyl derivative towards several metal ions has been investigated by Goodgame *et al.*[3,4] and a few other workers[5,6]. A number of halo complexes of cobalt(II) and nickel(II) containing 2-substituted benzimidazoles have been reported earlier from these laboratories[7,8]. The influence of 2-alkyl substituents (ethyl, *n* or *i*-propyl or *n*-butyl) on the coordinating ability of benzimidazole towards thiocyanates and perchlorates of cobalt and nickel is reported in the present work.

Experimental

The metal thiocyanates were prepared by metathesis reaction between the corresponding metal nitrate and potassium thiocyanate in dried acetone. The metal perchlorates were obtained by dissolving the metal carbonate in hot 1:1 perchloric acid followed by filtration and careful evaporation of the filtrate nearly to dryness. The benzimidazole derivatives were prepared according to literature methods[9]. Elemental analyses were carried out using Perkin Elmer 240B elemental analyzer. Infrared spectra were recorded on a Carl Zeiss Specord 75IR spectrophotometer and electronic spectra on Hitachi 150-20 and U-3400 spectrophotometers. Magnetic susceptibilities were measured employing a Gouy balance with $Hg[Co(NCS)_4]$ as the calibrant. Molar conductivities were measured using a Toshniwal CL01.02 conductivity bridge. Thermogravimetric analyses were carried out in air using Mettler TAHE20 with a heating rate of 6°C/min.

Diisothiocyanate bis(alkyl benzimidazole) metal (II) complexes $M(NCS)_2(R\text{-}BzlH)_2$ [*M = Co or Ni; R = Et, n-Pr, i-Pr or n-Bu*]

A solution of the metal thiocyanate (1 mmol) in ethanol was refluxed with R-BzlH (2 mmol) for ~ 1 h. The contents were filtered and concentrated under reduced pressure. Overnight cooling precipitated blue or red solids which were washed successively with dichloromethane and water and dried *in vacuo*.

Tris/tetrakis(alkyl benzimidazole) cobalt (II) perchlorate $Co(R\text{-}BzlH)_x(ClO_4)_2$ ($x = 3$; *R = H, Et, i-Pr*, $x = 4$, *R = Me or n-Pr*)

Cobalt(II) perchlorate (1 mmol) was dissolved in triethylorthoformate-ethylacetate (1:4; ~ 25 ml) and refluxed for about 15 min. To the pale pink solution was added benzimidazole derivative (4 mmol) when the solution turned deep blue. Refluxing was continued for another 4 h and the solution filtered. The filtrate was concentrated under reduced pressure. Overnight cooling yielded the desired products as blue crystals which were washed with ethyl acetate-triethylorthoformate mixture and dried *in vacuo*.

Bis/tris/tetrakis (alkyl benzimidazole) nickel (II) perchlorate $Ni(R\text{-}BzlH)_x(ClO_4)_2$ ($x = 2$, *R = i-Pr*; $x = 3$, *R = H or Et*; $x = 4$, *R = Me, n-Pr or n-Bu*)

Nickel(II) perchlorate (1 mmol) was dissolved in triethylorthoformate-acetone (1:3; ~ 12 ml) and refluxed for ~ 15 min. To the resultant red solution was added benzimidazole derivative (4 mmol) and refluxing was continued for another 2 h. It was filtered and the solvent was removed under reduced pressure to obtain a yellow or orange solid. The solid was washed with cold acetone-triethylorthoformate mixture and dried *in vacuo*.

Results and discussion

Thiocyanate complexes

Thiocyanates of cobalt(II) and nickel(II) react with R-BzlH (R = Et, *n*-Pr, *i*-Pr or *n*-Bu) in 1:2 molar ratio in ethanol to yield coloured complexes of the composition $M(NCS)_2(R\text{-}BzlH)_2$ (M = Co or Ni). The complexes are non-electrolytes in nitrobenzene. The cobalt(II) complexes are blue and paramagnetic while the nickel analogs are red and weakly paramagnetic. In the infrared spectra of the complexes the presence of a broad band ~ 3200 cm^{-1} due to νNH suggests the coordination of benzimidazole group *via* the pyridine nitrogen[10,11]. An intense band around 2075 cm^{-1} and a less intense but sharp band ~ 840 cm^{-1} are characteristic of terminal N-bonded thiocyanate[12,13]. In the case of nickel complexes containing *n*-PrBzlH and *n*-BuBzlH, the νCN values are greater than 2100 cm^{-1} indicating S-bonded or bridging thiocyanate groups[14]. However, there are a few reports on nickel(II) complexes with N-bonded thiocyanate which exhibit νCN values ~ 2110 cm^{-1} (refs 15,16).

The magnetic moment values (Table 1) of the cobalt complexes are in the expected range (4.2-4.7 B.M.) for tetrahedral stereochemistry[17]. The halo analogs also possess magnetic moment values in this range[7]. In the case of nickel complexes the magnetic moment values (0.7-1.9 B.M.) are intermediate between those of planar and the tetrahedral complexes[18,19]. The halo isologs are paramagnetic and have been assigned a tetrahedral stereochemistry[8].

The electronic spectra of the cobalt complexes in acetone exhibit bands around 6000, 8000 and 17000 cm^{-1} typical of a tetrahedral CoN_4 chromophore. The former two bands may be ascribed to $^4A_2 \rightarrow {}^4T_1(F)$ and the latter to $^4A_2 \rightarrow {}^4T_1(P)$ transitions[17]. The nickel complexes appear to decompose in solution. In the solid state spectra (in nujol mull), they exhibit a broad band around 20000 cm^{-1}, assignable to square planar nickel(II)[18].

Thermogravimetric analyses have been carried out for some of the complexes in an atmosphere of air. The cobalt complexes and the nickel complex containing ethyl benzimidazole are quite stable and decompose in the ranges 215-340; 340-550 and 170-292; 292-550°C respectively at elevated temperatures in two steps involving the loss of the heterocycle and the thiocyanates, and eventually to the metal oxide. The nickel complexes containing propyl benzimidazoles however appear to sublime after the first step as evidenced by the sharp weight loss.

Perchlorate complexes

Cobalt(II) perchlorate under anhydrous conditions reacts with R-BzlH in 1:2 molar ratio in ethyl acetate to yield two types of dark blue complexes $Co(R\text{-}BzlH)_3(ClO_4)_2$, (R = H, Et or *i*-Pr) and $Co(R\text{-}BzlH)_4(ClO_4)_2$, (R = Me or *n*-Pr). Under the above conditions for R = *n*-Bu, the complex could not be isolated in the solid state. In the case of R = H, Goodgame and Cotton[16] have isolated a tetrakis complex, $Co(R\text{-}BzlH)_4(ClO_4)_2$ as a purple solid in ethanol medium. The reaction of nickel(II) perchlorate with R-BzlH in acetone under anhydrous conditions produces orange or yellow solids of the compositions, $Ni(i\text{-}PrBlH)_2(ClO_4)_2$, $Ni(R\text{-}BzlH)_3(ClO_4)_2$

Table 1—Characterization data of Co(II) and Ni(II) complexes of 2-substituted benzimidazoles

	Complex Colour, m.pt (°C)	Found (Calcd), %		
		C	H	N
1	$Co(NCS)_2(EtBzlH)_2$ Blue, 275	51.7 (51.4)	4.3 (4.3)	18.0 (18.0)
2	$Co(NCS)_2(n\text{-}PrBzlH)_2$ Blue, 218-19	53.9 (53.3)	5.0 (4.9)	17.1 (17.0)
3	$Co(NCS)_2(i\text{-}PrBzlH)_2$ Blue, 298-99	53.9 (53.3)	5.0 (4.9)	17.1 (17.0)
4	$Co(NCS)_2(n\text{-}BuBzlH)_2$ Blue, > 300	53.4 (55.1)	4.9 (5.4)	17.0 (16.1)
5	$Ni(NCS)_2(EtBzlH)_2$ Red, 286	51.3 (51.4)	4.3 (4.3)	18.0 (18.0)
6	$Ni(NCS)_2(n\text{-}PrBzlH)_2$ Red, 270-1	52.8 (53.4)	4.9 (4.9)	16.9 (17.0)
7	$Ni(NCS)_2(i\text{-}PrBzlH)_2$ Red > 315	53.8 (53.4)	4.7 (4.9)	16.8 (17.0)
8	$Ni(NCS)_2(n\text{-}BuBzlH)_2$ Blue, > 315	52.3 (55.1)	4.8 (5.4)	16.8 (16.1)
9	$Co(BzlH)_3(ClO_4)_2$ Blue, 153-4	41.9 (41.2)	3.6 (3.0)	13.3 (14.1)
10	$Co(MeBzlH)_4(ClO_4)_2$ Blue, 213-5	48.3 (48.3)	4.6 (4.1)	13.6 (13.1)
11	$Co(EtBzlH)_3(ClO_4)_2$ Blue, 122-4	45.2 (46.5)	4.4 (4.3)	12.1 (12.1)
12	$Co(n\text{-}PrBzlH)_4(ClO_4)_2$ Blue, 183-5	52.4 (53.4)	5.4 (5.4)	12.0 (12.5)
13	$Co(i\text{-}PrBzlH)_3(ClO_4)_2$ Blue, 230-2	48.2 (48.8)	4.9 (5.0)	11.3 (10.2)
14	$Ni(BzlH)_3(ClO_4)_2$ Yellow, > 320	41.1 (41.2)	3.1 (2.9)	13.6 (13.7)
15	$Ni(MeBzlH)_4(ClO_4)_2$ Yellow, 172-4	48.1 (48.8)	4.3 (4.2)	14.1 (14.3)
16	$Ni(EtBzlH)_3(ClO_4)_2$ Yellow, 210	45.2 (46.5)	4.4 (4.3)	12.1 (12.7)
17	$Ni(n\text{-}PrBzlH)_4(ClO_4)_2$ Yellow, 264-5	52.5 (53.4)	5.3 (5.4)	12.1 (12.5)
18	$Ni(i\text{-}PrBzlH)_2(ClO_4)_2$ Yellow, 222-3	40.9 (41.6)	4.7 (4.2)	9.4 (9.7)
19	$Ni(n\text{-}BuBzlH)_4(ClO_4)_2$ Orange, 247-9	55.4 (55.4)	6.3 (5.9)	11.4 (11.7)

(R = H or Et) and $Ni(R\text{-}BzlH)_4(ClO_4)_2$ (R = Me, *n*-Pr or *n*-Bu).

The complexes are sparingly soluble in nitrobenzene but freely soluble in acetonitrile showing 1:2 electrolytic behaviour. The cobalt complexes are paramagnetic while those of nickel are diamagnetic. The magnetic moment values of the cobalt complexes (4.2-4.6 B.M.) correspond to a tetrahedral stereochemistry around cobalt ions[17]. The diamagnetic nature of nickel complexes is suggestive of a square planar geometry[18]. The IR spectra of the complexes display a weak band ~ 3200 cm^{-1} due to νNH of the coordinated benzimidazole groups. Further evidence for the coordination of the heterocycle arises from the band ~ 1600 cm^{-1} in the spectra due to C = C and C = N stretching frequencies of the benzimidazole groups[10]. The spectra of the bis and tris ligand complexes exhibit splitting of the band ~ 1100 cm^{-1} and also display a weak band ~ 920 cm^{-1} suggesting the coordination of at least one of the perchlorates[20]. The electrolytic behaviour of the complexes in acetonitrile may be attributed to the displacement of the coordinated perchlorate(s) by the solvent molecule(s). The IR spectra of the tetrakis complexes clearly reflect the ionic nature of the perchlorate groups[21].

The electronic spectra of the cobalt complexes (in nujol mull) display a band ~ 17500 cm^{-1} assignable to $^4A_2 \rightarrow {}^4T_1(P)$ transition of tetrahedral cobalt(II)[17]. For the tetrakis complexes, the ligand field parameter (10 Dq), the Racah parameter (B′) and the nephelauxetic parameter have been calculated according to the method of Billing and Underhill[22]. The magnitude of 10 Dq is indicative of a strong ligand field around the metal ion[17]. The ligand field spectra of the nickel complexes exhibit two broad bands one ~ 12000 and the other ~ 22500 cm^{-1} supporting the proposed planar arrangement.

References

1 Isikdag I & Noyanalapan N, *Doga Bilim Derg Seri C*, 9 (1985) 183; *Chem Abstr*, 103; 210881j.
2 Isikdag I, Zitouni C & Demirayak S, *Doga Bilim Derg Seri C*, 9 (1985) 277; *Chem Abstr*, 104; 104257w.
3 Goodgame M, Holt S D, Piggot B & Williams D J, *Inorg chim Acta*, 49 (1985) 107.
4 Goodgame D M L, Goodgame M & Rayner Canhamn G W, *Inorg chim Acta*, 6 (1972) 245.
5 Artemenko M V & Slyusarenko K F, *Russ J Inorg Chem*, 15 (1970) 1616.
6 Garnovskii A D, Skopenko V V, Knyazhanskii M J, Osipov O A, Gilyanovskii P V & Artyukhovich T D, *Zh obshch Khim*, 42 (1972) 2068; *Chem Abstr*, 78, 21996e.
7 Shashikala N, Leelamani E G & Reddy G K N, *Indian J Chem*, 21A (1982) 743.
8 Shashikala N, Nanje Gowda N M & Reddy G K N, *J Indian chem Soc*, 62 (1985) 928.
9 Hein D W, Alhurn A I & Liquitt J J, *J Am chem Soc*, 79 (1957) 427.
10 Bellamy L J, *Infrared spectra of complex molecules* (Methuen, London) 1966.
11 Massacessi M, Pinn a R, Devoto G, Barni E, Savarino P & Erre L S, *Trans Met Chem*, 9 (1984) 351.
12 Norbury A H, *Adv Inorg Chem Radio Chem*, 17 (1975) 231.
13 Singh P P, *Coord chem Rev*, 32 (1980) 33.
14 Singh P P & Srivastava B, *Indian J Chem*, 25A (1986) 1109.
15 Goodgame M, Piggot B & Thorpe S D, *Inorg chim Acta*, 67 (1982) 91.
16 Goodgame M & Weeks M J, *J chem Soc(A)*, 1156 (1966).
17 Goodgame M & Cotton F A, *J Am chem Soc*, 84 (1962) 1543.
18 Campbell M J M, Card D W, Grzeskowiak R & Goldstein M, *J chem Soc (Dalton)*, (1972) 1687.
19 Sharpe A G, *Inorganic chemistry* (ELBS Edition, England) 1986.
20 Gowda N M N, Naikar S B & Reddy G K N, *Adv Inorg Chem Radiochem*, 28 (1984) 255.
21 Naikar S B, Gowda N M N & Reddy G K N, *Indian J Chem*, 23A (1984) 133.
22 Underhill A E & Billing D E, *Nature*, 210 (1966) 834.

Indian Journal of Chemistry
Vol. 31A, July 1992, pp. 466-468

Complex peroxovanadates(V) containing chelated cysteinate as the co-ligand: Synthesis and spectroscopic studies

Mihir K Chaudhuri* & Pradip C Paul
Department of Chemistry, North-Eastern Hill University, Shillong 793 003

Received 14 October 1991; revised and accepted 15 Jsanuary 1992

Synthesis of oxoperoxo (L-cysteinato)vanadate(V), $A_2[V_2O_2(O_2)_3(cysH)_2].H_2O$ (A= NH_4 or K), by the reaction of vanadium(V) with H_2O_2 and L-cysteine at *p*H 2.5 to 3, is reported. The compounds have been characterized by chemical analyses and spectral studies. The co-ligand occurs in the complex as cysteinate and binds the metal bidentately through O and S atoms. A comparison of the complex with that of its glycine analogue has been made.

A system containing vanadium, peroxide (O_2^{2-}), and cysteine [$cysH_2$, $HSCH_2CH(NH_2)COOH$] in its non-ionic or deprotonated ionic ($cysH^-$) form is expected to constitute an interesting combination since the metal as well as the two chosen ligands are of acknowledged bio-relevance. Although co-ordination of an amino acid to an oxoperoxovanadium(V) core has not always been successful[1], such a possibility under an appropriate experimental condition cannot be ruled out as evidenced by the very recent successful synthesis of glycine coordinated oxoperoxovanadium(V) systems[2].

The salient difference between glycine and cystein ligands are that while the former acts as a mono- or a bi-dentate ligand[3], the latter may occupy one, two, or three coordination sites[4]. Moreover, in its bidentate form cysteine offers three different sets of binding sites, −O N−, −S N−, or −O S−, with any one of them being operative in a given situation.

Experimental

Commercially available reagent grade chemicals were used. Infrared spectra were recorded on a Perkin-Elmer Model 983 spectrophotometer. Magnetic susceptibilities were measured by Gouy method, using $Hg[Co(NCS)_4]$ as the calibrant. *p*H values of the reaction solutions were measured by using Systronics Type 335 digital *p*H meter. The ESR measurements were made on a Varian E 109, X band ESR spectrometer with 100 Kc field modulator. The UV-visible spectra were recorded in water on a Hitachi Model 330 spectrophotometer.

Vanadium, peroxide, and potassium were estimated by methods mentioned earlier[5]. The C, H and N analyses were carried out at the Micro-Analytical Laboratory, Department of Chemistry, NEHU, Shillong.

Synthesis of $A_2[V_2O_2(O_2)_3(cysH)_2].H_2O$ (A= NH_4 *or K*)

A sample of V_2O_5 (1.0 g, 5.5 mmol) was mixed with 1.33 g (10.98 mmol) of cystein followed by slow addition of 30% H_2O_2 (15 cm^3, 132.35 mmol) with stirring, maintaining the V: cysteine:H_2O_2 ratio as 1:1:24. The mixture was stirred for 10 min in an ice-bath keeping the temperature below 5°C, whereupon a red solution resulted. The *p*H of the solution was raised to 2.5-3 by careful addition of potassium hydroxide solution (25%) or aqueous ammonia (sp. gr. 0.9). The solution was stirred for 15 min and an addition of ethanol precipitated an orange coloured compound. The product was filtered, washed 2-3 times with ethanol, and dried *in vacuo* over conc. H_2SO_4.

The yield of $(NH_4)_2[V_2O_2(O_2)_3(cysH)_2].H_2O$ was 2.3 g (79%) and that of $K_2[V_2O_2(O_2)_3(cysH)_2].H_2O$ was 2.2 g (71%). *Anal. Calc.* for $(NH_4)_2[V_2O_2(O_2)_3(cysH)_2].H_2O$: V, 19.43; O_2^{2-}, 18.31; C, 13.74; N, 10.69; H, 4.24. Found: V, 19.81; O_2^{2-}, 18.06; C, 13.86; N, 10.71; H, 4.2%. IR(cm^{-1}): 952s ($\nu V=O$), 838s ($\nu O-O$), 820m ($\nu O-O$), 637m ($\nu V-O_2$, ν_2), 533m ($\nu V-O_2$, ν_3), 1605s (NH_3^+ deg. deform.), 1510s (NH_3^+ sym. deform.) 393m ($\nu V-S$), 1648s (ν_{asym} COO^-), 1382s (ν_{sym} COO^-), 440m ($\nu V-O$), 1405s (ν_2 mode of NH_4^+).
Anal. Calc. for $K_2[V_2O_2(O_2)_3(cysH)_2].H_2O$: V, 17.99; O_2^{2-}, 16.95; C, 12.72; N, 4.95; H, 2.5; K, 13.81. Found: V, 18.18; O_2^{2-}, 16.81; C, 12.76; N, 5.91; N, 2.41; K, 13.72%. IR (cm^{-1}): 950s ($\nu V=O$), 841s ($\nu O-O$), 818m ($\nu O-O$), 641m ($\nu V-O_2\nu_2$), 530m ($\nu V-O_2\nu_3$), 1600s (NH_3^+ deg. deform). 1515s (NH_3^+ sym. deform), 393m ($\nu V-S$), 1652s ($\nu_{asym}COO^-$), 1380s (ν_{sym} COO^-), 437m ($\nu V-O$).

Results and discussion

In order to bring about coordination of both peroxide and cysteine with vanadium(V), the reaction among V_2O_5, $cysH_2$ and 30% H_2O_2 was conducted in aqeous medium. The appropriate *p*H value for the success was ascertained to be 2.5-3, and the alkali used for the purpose also provided the counter cations (NH_4^+ and K^+). Notably, the *p*H not only controlled the V:O_2^{2-} ratio (below 1:2) but also per-

mitted ionisation of cysteine to cysteinate enabling synthesis of the compounds $A_2[V_2O_2(O_2)_3(cysH)_2].H_2O$ (A=NH_4 or K), as obtained. Unlike in the cases of glycine[2], cysteine occurs in its ionic form, and the sequence of addition of H_2O_2 and cysteine to vanadium(V) does not seem to have any apparent effect on the formation of the product. The composition of the complex, $[V_2O_2(O_2)_3(cysH)_2]^{2-}$, and a preferred hexacoordination of V(V) point to a possibility of $cysH^-$ occurring as a chelated ligand, while the O_2^{2-} ligands might be present in structurally two different forms namely chelated O_2^{2-} and $\mu-O_2^{2-}$.

The $A_2[V_2O_2(O_2)_3(cysH)_2].H_2O$ compounds are EPR-inactive, and in addition the magnetic susceptibility measurements showed them to be diamagnetic in nature. Thus, it is clear that no reduction of the metal took place. Incidentally, both the cysteinate (present work) and glycine[2] containing heteroligand peroxovanadium(V) complexes are hygroscopic in nature and undergo a slow decomposition in water. Determination of active oxygen contents in such complexes is very crucial and this was emphasized in our earlier work[6]. The atom ratio of $V:O_2^{2-}$ was unequivocally ascertained to be 1:1.5 in agreement with the formulation of the complex species as $[V_2O_2(O_2)_3(cysH)_2]^{2-}$.

As in the case of $[V_2O_2(O_2)_3(glyH)_2(H_2O)_2]^2$, the electronic spectra of $A_2[V_2O_2(O_2)_3(cysH)_2].H_2O$, recorded immediately after making their solution, display only a single broad LMCT band at 310-320 nm due to the $\pi_v^* \rightarrow d\sigma$ transition[7,8] originating from coordinated O_2^{2-}. A close analogy between the electronic spectra of the glycine[2] and the cysteinate complexes suggests that the peroxovanadium interaction in the two different complexes is apparently similar. Unfortunately, another transition (σ) $\pi_v^* \rightarrow d\sigma^*$, expected of a terminally bonded peroxometal unit[7,8], has not been encountered in the present case. Incidentally, this transition is very rarely observed[7,8] and thus it is not really very unusual.

The free ligand cystein exists in zwitter ionic form and can bind a metal to form a 5-membered chelate ring through its N and S or N and O atoms; alternatively, it can also form a 6-membered chelate involving its S and O atoms. Incidentally, non-interference of cysteinate modes with V=O or coordinated peroxo bands enabled clear identification[5,9,10] of $\nu(V=O)$ at ~950s cm^{-1}, and $\nu(O-O)$ at ~840s and ~820m cm^{-1}. The appearance of two $\nu(O-O)$ bands causes us to believe that the complex has structurally two different types, viz., terminal chelated and bridging bidentate, of peroxo ligands. Consequent upon the presence of chelated O_2^{2-} ligand, the expected ν_2 and ν_3 modes of $V-O_2$ vibrations have been observed at ~ 640m and ~530m cm^{-1}, respectively[10].

The pattern originating from the coordinated amino acid residue shows that the NH_3^+ degenerate deformation at ~1600s cm^{-1}, and the NH_3^+ symmetric deformation at ~1515s cm^{-1} have not undergone any change in their positions and shapes[4]. Accordingly, the coordination through N is ruled out. Owing to the presence of lattice water, the NH_3^+ stretching region was obscured. Significant is the absence of S−H stretching (at ~2565s cm^{-1}) suggesting deprotonation of the sulphhydryl group[4]. This indicates the involvement of S in coordination and consequently the $\nu(V-S)$ has been observed at 393m cm^{-1}. Equally important is the shift of ν_{asym} mode of COO^- to a higher frequency, ~1650s cm^{-1}, and lowering of ν_{sym} vibration of COO^- to ~1380s cm^{-1}, compared to those of the corresponding modes of uncoordinated COO^- (Ref. 4). This is a clear indication of coordination of COO^- in the present case. The corresponding (V−O) mode appears at ~439m cm^{-1}.

The IR spectra of $A_2[V_2O_2(O_2)_3(cysH)_2].H_2O$, therefore, provide very convincing support for the presence of V=O, two different types of coordinated peroxo ligands, viz., terminal and bridging, and the occurrence of cysteinate co-ligand as a chelated one coordinating with the metal through −S and −O atoms forming a 6-membered ring[4]. These results are consistent with structure I of the complex ion.

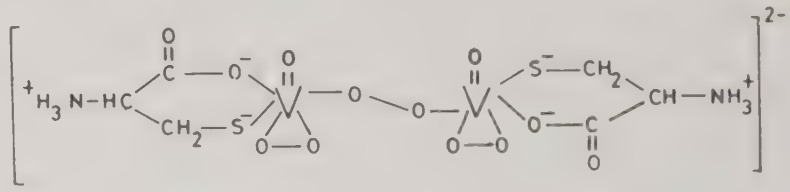

A comparison of the IR spectral features of the newly synthesized compounds with those of the corresponding glycine complexes[2] enables us to state that while in both the types of complexes the ligands occur in their zwitterionic form without involving the −N atoms, the former contain chelated co-ligand ($cysH^-$) involving −S− and −O− atoms and in the latter the co-ligand (glyH) acted as a monodentate ligand being coordinated through its −O− atom only. Both $cysH^-$ and glyH containing peroxovanadium(V) systems are not very stable, however.

References

1 Djordjevic C, Vuletic N & Sinn E, *Inorg chim Acta*, 104 (1985) L7.

2 Bhattacharjee M, Chaudhuri M K, Islam N S & Paul P C, *Inorg chim Acta*, 169 (1990) 97.
3 Kieft J A & Nakamoto K, *J inorg nucl Chem*, 29 (1967) 2561; Herlinger A W & Long II T V, *J Am chem Soc*, 92 (1970) 6481.
4 Shindo H & Brown T L, *J Am chem Soc*, 87 (1965) 1904; Chandrasekhar M, Udupa M R & Arvamudan G, *Inorg chim Acta*, 7 (1973) 88.
5 Chaudhuri M K & Ghosh S K, *Inorg Chem*, 23 (1984) 534; *J chem Soc Dalton Trans*, (1984) 507.
6 Chaudhuri M K, Ghosh S K & Islam N S, *Inorg Chem*, 24 (1985) 2706; Bhattacharjee M, Chaudhuri M K & Dutta Purkayastha R N, *Inorg Chem*, 25 (1986) 2354.
7 Lever A B P & Gray H B, *Acc Chem Res*, 11 (1978) 348.
8 Lever A B P, *Inorganic electronic spectroscopy*, 2nd Edn (Elsevier, Amsterdam) 1984, p. 287, 294.
9 Selvin J, *Chem Rev*, 65 (1965) 153.
10 Griffith W P & Wickins T D, *J chem Soc A* (1968) 397.

Indian Journal of Chemistry
Vol. 31A, July 1992, pp. 469-471

Seven coordinated organotin(IV) complexes of 1,3-dihydro-1,3-dioxo-α-(substituted)-2H-isoindole-2-acetic acids

A K Saxena, S Saxena & A K Rai*

Department of Chemistry,
University of Rajasthan, Jaipur 302 004, India

Received 1 October 1991; revised and accepted 16 December 1991

Some butyltin(IV) complexes of the type $BuSn(L)_3$ where $LH = \overline{C(O)C_6H_4C(O)N}CHRCOOH$ [R = H, $-CH_3$, $-CH_2C_6H_5$, $-CH(CH_3)_2$, $-CH_2CH_2SCH_3$ and $-CHR- = -(CH_2)_2-$] have been prepared. Pentagonal bipyramidal geometry has been proposed for complexes on the basis of molecular weight measurements and IR, ^1H, ^{13}C and ^{119}Sn NMR spectral studies.

Organotin(IV) carboxylates with penta- and hexa-coordinated tin are known[1-7]. In this paper, we report the synthesis and spectral characterization of some seven coordinated tin complexes of 1,3-dihydro-1,3-dioxo-α-(substituted)-2H-isoindole-2-acetic acids (N-phthaloylamino acids).

Experimental

Precautions were taken to exclude moisture throughout the experiment. Butyltin(IV) trichloride was distilled (92°C/10 mm) before use and ligands, N-phthaloylamino acids, were synthesized according to reported procedure[8]. Sn and N analyses were carried out as per the procedure described elsewhere[9]. Molecular weights were determined on a Knauer vapour pressure osmometer at 45°C. IR and NMR spectra were recorded on NICOLET FTIR and JEOL FX 90Q multinuclei spectrometers, respectively.

Synthesis of butyl tris(1,3-dihydro-1,3-dioxo-α-(methyl)-2H-isoindole-2-acetato)tin(IV); $(C_4H_9)Sn[O_2CCH(CH_3)\overline{NC(O)C_6H_4C(O)}]_3$:

N-Phthaloyl-DL-alanine (0.97 g, 4.42 mmol) was added to a solution of sodium methoxide [prepared from 0.10 g (4.34 mmol) of sodium in minimum amount of methanol] and the mixture was refluxed for ~2 hr. To this was added a calculated amount of butyltin trichloride (0.42 g, 1.49 mmol) and refluxing was continued for another 6 hr to ensure the completion of the reaction. A precipitate of sodium chloride formed, was removed by filtration. The filtrate was evaporated under reduced pressure to get the product which on recrystallization from chloroform-hexane produces a white solid.

A similar procedure was adopted for the preparation of the rest of the complexes. Analytical data along with melting points of the complexes are summarized in Table 1.

Results and Discussion

Butyltin(IV) complexes of N-phthaloylamino acids were prepared by the reaction of butyltin trichloride with sodium salt of ligands in 1:3 molar ratio in refluxing benzene:

$$MeONa + \overline{C(O)C_6H_4C(O)N}CHRCOOH \rightarrow \overline{C(O)C_6H_4C(O)N}CHRCOONa + MeOH$$

$$BuSnCl_3 + 3\overline{C(O)C_6H_4C(O)N}CHRCOONa \rightarrow BuSn[O_2CCHR\overline{NC(O)C_6H_4C(O)}]_3 + 3NaCl$$

R = H, $-CH_3$, $-CH_2C_6H_5$, $-CH(CH_3)_2$, $-CH_2CH_2SCH_3$ and $-CHR- = -CH_2CH_2-$

The complexes are freely soluble in common organic solvents. Osmometric molecular weight measurements of the complexes in chloroform show their monomeric nature.

IR spectra of the complexes (nujol mull) show a medium intensity band around 600 cm^{-1} due to $\nu Sn-O$[10]. A band around 1760 cm^{-1} corresponding to νCO_{as} of imido $-C=O$ group is unshifted as compared to that of free ligands indicating the nonparticipation of this group in bonding. However, the band around 1700 cm^{-1} in the spectra of the ligands [$\nu CO_s + \nu COO_{as}$] is split into two after complexation[11]. A sharp band at ~1700 cm^{-1} may be assigned to νCO_s and the medium intensity band at 1600-1570 cm^{-1} to νCOO_{as}. Lowering of νCOO_{as} frequency by 100-145 cm^{-1} in the complexes indicates the bidentate coordination of carboxylic group. The appearance of only one band for νCOO_{as} suggests the equivalent nature of the three coordinated ligand moieties. $\nu Sn-C$ vibration[2] has been identified at ~550 cm^{-1}.

Proton NMR spectra (in $CDCl_3$) of the complexes (Table 2) display the expected multiplicity of the signals and are not shifted relative to their positions in the spectra of the corresponding ligands[11,12]. Butyl protons exhibit a complex reson-

ance pattern in the region δ 1.7-0.2 ppm.

^{13}C NMR spectra (in $CHCl_3$) of the complexes (Table 3) display a downfield shift of $-COO$ carbon signal as compared to that in the free ligand owing to bidentate nature of this moiety. Imido carbon signal around δ 167 ppm remains unshifted implying the non-participation of $>C=O$ group in bonding to the metal. Other signals are also unshifted after complexation. Butyl carbon resonances are in the range $\rightsquigarrow \delta$ 28.0-13.0 ppm.

As the complexes are monomeric, bridging of ligands is ruled out. IR and ^{13}C NMR spectra of the complexes support the bidentate chelating nature of the carboxylic group. Hence the com-

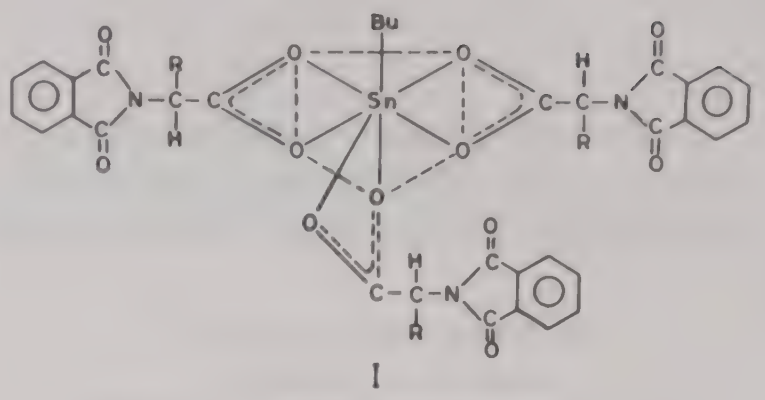

I

Table 1 – Synthetic and analytical data

Sl. No.	Reactants in g			Product %	Found (calc.),			M.P. (±1°C)
	Na	LH	$BuSnCl_3$	yield	% Sn	% N	Mol. wt.	
1.	0.15	L_1H	0.62	$BuSn(L_1)_3$	14.92	5.30	795	120
		1.35		92	(15.06)	(5.33)	(788)	
2.	0.22	L_2H	0.89	$BuSn(L_2)_3$	14.20	5.00	843	105
		2.09		95	(14.29)	(5.06)	(830)	
3.	0.10	L_3H	0.42	$BuSn(L_3)_3$	14.22	4.95	842	114
		0.97		90	(14.29)	(5.06)	(830)	
4.	0.12	L_4H	0.48	$BuSn(L_4)_3$	11.18	3.92	1050	72
		1.52		88	(11.22)	(3.97)	(1058)	
5.	0.17	L_5H	0.70	$BuSn(L_5)_3$	12.95	4.50	923	94
		1.82		90	(12.98)	(4.59)	(914)	
6.	0.16	L_6H	0.66	$BuSn(L_6)_3$	11.63	4.08	1012	77
		1.97		90	(11.75)	(4.16)	(1010)	

$L_1H = \overline{C(O)C_6H_4C(O)N}CH_2COOH$; $L_2H = \overline{C(O)C_6H_4C(O)N}CH_2CH_2COOH$; $L_3H = \overline{C(O)C_6H_4C(O)N}\underset{CH_3}{C}HCOOH$;

$L_4H = \overline{C(O)C_6H_4C(O)N}\underset{CH_2C_6H_5}{C}HCOOH$; $L_5H = \overline{C(O)C_6H_4C(O)N}\underset{CH(CH_3)_2}{C}HCOOH$; $L_6H = \overline{C(O)C_6H_4C(O)N}\underset{CH_2CH_2SCH_3}{C}HCOOH$;

Table 2 – ^1H NMR spectral data (in δ, ppm)

Complex	C_6H_4/C_6H_5	CH	CH_2	CH_3	C_4H_9
1	8.05-7.69 m	—	4.47 s	—	1.43-0.31 m
2	8.00-7.60 m	—	4.00 t 2.77 t	—	1.60-0.36 m
3	8.05-7.73 m	5.05 q	—	1.75 d	1.65-0.31 m
4	8.05-7.53 m/ 7.24 s (5p)	5.66 t	3.62 d	—	1.56-0.22 m
5	8.05-7.64 m	4.60 d 2.90-2.46 m	—	*	1.70-0.36 m
6	8.05-7.73 m	5.14 b	2.50 s (4 p)	2.10 s	1.38-0.36 m

* = mixed with C_4H_9-Sn

Table 3 – ^{13}C and ^{119}Sn NMR spectral data (in δ, ppm)

Complex	COO	CO	C_6H_4	CH	CH_2	CH_3	C_4H_9-Sn	^{119}Sn
1	177.5	167.2	133.7, 131.5 123.0	—	40.3	—	28.5, 26.4 25.3, 13.0	—
2	177.4	167.5	133.0, 131.1 122.4	—	33.8 32.6	—	28.8, 26.7 25.1, 13.3	−552
3	177.8	167.2	133.7, 131.7 123.0	48.6	—	15.2	27.6, 26.5 25.1, 12.9	−547
4*	177.3	167.5	133.7, 131.7 123.0	53.1	34.4	—	28.4, 26.5 25.3, 13.1	−544
5	175.2	167.7	133.8, 131.7 123.3	58.5 28.6	—	20.9 19.4	28.6, 26.6 25.4, 13.1	—
6	175.3	167.2	133.7, 131.5 123.1	50.5	30.7 28.1	14.9	28.1, 26.3 25.2, 12.8	−545

* Phenyl carbons appeared at ~ δ 138, 129, 128 and 126 ppm

plexes may be assigned a pentagonal bipyramidal geometry (I).

^{119}Sn NMR spectra (in $CHCl_3$) of a few of these complexes exhibit a sharp ^{119}Sn resonance in the region δ −552 to −544 ppm (Table 3). The data are in close agreement with those reported[13] for seven coordinated butyltin(IV) complexes, $BuSn[oxinate]_3$ and $BuSn[tropolonate]_3$.

Acknowledgement

The authors are thankful to the CSIR, New Delhi, for the financial assistance.

References

1 Ho B Y K & Zuckermann J J, *Inorg nucl chem Lett*, 9 (1973) 849.
2 Hall W T & Zuckermann J J, *Inorg Chem*, 16 (1977) 1239.
3 Silvestri A, Duca D & Huber F, *Appl organometal Chem*, 2 (1988) 417.
4 Roge G, Huber F, Preut H, Silvestri A & Barbieri R, *J chem soc Dalton Trans*, 4 (1983) 595.
5 Sandhu G K, Gupta R, Sandhu S S, Parish R V & Brown K, *J organometal Chem*, 279 (1985) 373.
6 Sandhu G K, Gupta R, Sandhu S S & Parish R V, *Polyhedron*, 4 (1985) 81.
7 Mesubi M A, Eke U B & Bamgboye T T, *Appl organometal Chem*, 2 (1988) 121.
8 Sheehan J C, Chapman D W & Roth R W, *J Am chem Soc*, 74 (1952) 3822.
9 Vogel A I, *A text book of quantitative inorganic analysis*, (Longman, London) 1978.
10 Butcher F K, Gerrard W, Mooney E W, Ress R G & Wilis H A, *Spectrochim Acta*, 20 (1964) 51.
11 Saxena A K, Saxena S & Rai A K, *Indian J Chem*, 29A (1990) 255.
12 Saxena A K, Saxena S & Rai A K, *Synth React inorg metal-org Chem*, 20 (1990) 21.
13 Otera J, Kusaba A, Hinoishi T & Kawasaki Y, *J organometal Chem*, 228 (1982) 223.

Indian Journal of Chemistry
Vol. 31A, July 1992, pp. 472-474

Synthesis, characterization and fungitoxicity of Cu(II), Ni(II), Zn(II), Co(II), Fe(III) and Mn(III) chelates with (5-phenyl-1,3, 4-oxadiazol-2-yl)-N-benzoyl dithiocarbamate

H Singh*, V K Srivastava†, S N Shukla & M K Upadhyaya
Department of Chemistry, Gorakhpur University, Gorakhpur 273 009

Received 6 September 1991; revised 12 December 1991; accepted 10 February 1992

The metal chelates of (5-phenyl-1, 3, 4-oxadiazol-2-yl)-N-benzoyl dithiocarbamate, (POBDC) with Cu(II), Ni(II), Co(II), Zn(II), Fe(III) and Mn(III) have been synthesized and characterized on the basis of analytical, conductance, magnetic and spectroscopic techniques. Fungicidal screening against *Aspergillus niger* and *Fusarium oxysporum* shows that Mn(III) and Zn(II) chelates exhibit fungicidal activity of the order of Dithane M-45 at 1000 ppm.

The dithiocarbamate fungicides, e.g. maneb, zineb, ziram, and vapam have wide applications in agriculture[1,2]. Likewise, 1, 3, 4-oxadiazole moiety has also been associated with a broad spectrum of pesticidal activity[3-6]. In view of the above facts our desire to develop new antifungal compounds of high potency prompted us to couple the biolabile 1, 3, 4-oxadiazole and dithiocarbamate moieties and synthesize their metal chelates.

Additional features of interest in the present investigation were: (i) the formation of six-membered metal chelates involving nitrogen of the oxadiazole ring and sulphur of the dithiocarbamate grouping as coordination centre[2], instead of four-membered chelates with S, S-coordination as reported earlier for a number of dithiocarbamate chelates[7-9], and (ii) the formation of only Mn(III) and Fe(III) chelates, even when their salts in M^{2+} oxidation state were used[2]. This was probably due to steric and thermodynamic/kinetic reasons[10].

Experimental

The solvents were dried and distilled before use in the usual manner. All the metal salts used were of BDH(AR) quality. Infrared spectra were measured on a Perkin-Elmer-580 spectrophotometer in nujol mull/KBr in the range 200-3600 cm^{-1}. ^1H NMR spectra were measured on Jeol FX-100 NMR spectrometer in DMSO-d_6/acetone-d_6 using TMS as internal and external standards. Electronic spectra in DMF were recorded on a Cary-170 double beam recording spectrophotometer. Carbon, hydrogen and nitrogen were analysed with a Coloman automatic analyzer, and metal ions were estimated by standard procedure[17]. Conductance measurements of dilute solutions ($\sim 10^{-3}$ *M*) in DMF, were measured with the help of Elico-conductivity bridge, type CM82T and magnetic susceptibilities were determined by Gouy's method using $Hg[Co(NCS)_4]$ as standard. Melting points were determined in open capillaries and are uncorrected.

Preparation of ligand

2-Mercapto-5-phenyl-1, 3, 4-*oxadiazole*: This was prepared using the method of Young and Wood[18].

(5-Phenyl-1, 3, 4-*oxadiazol*-2-*yl*)-*N*-*benzoyl dithiocarbamate* (*POBDC*): An equimolar mixture of 2-mercapto-5-phenyl-1, 3, 4-oxadiazole (0.08 *M*), NaOH (0.08 *M*) and benzoyl isothiocyanate (0.08 *M*) was refluxed in ethanol for 5-6 hr. The reaction mixture was reduced to half of its volume, diluted with water followed by acidification with HCl. The desired product (LH) thus precipitated was recrystallised from ethanol to obtain yellowish needles; yield 80%. Its m.p. and analytical data are recorded in Table 1.

Preparation of chelates

The requisite amount of metal salts of Co(II), Ni(II), Cu(II), Zn(II) in the ratio 1:2 and Mn(III) and Fe(III) in the ratio 1:3 and LK (prepared by dissolving equimolar quantity of ligand and KOH in ethanol) were refluxed in ethanol for 2 hr. The chelates thus formed were filtered, washed several times with hot water followed by ethanol and dried over P_4O_{10}. It was noteworthy to see that Mn(III) and Fe(III) chelates were formed, even when their salts in +2 oxidation states were used (Table 1).

Results and discussion

The stoichiometry of the complexes are confirmed by the elemental analysis. The lower value of molar conductance in DMF indicates their

† Department of Chemistry, M G Degree College, Gorakhpur 273 001

Table 1—Characterization data of (5-phenyl-1, 3, 4-oxadiazol-2-yl)-N-benzoyl dithiocarbamate and its metal chelates

Compound (colour, yield)	M.P. (°C)	Found (Calc.), %				
		M	C	H	N	S
$C_{16}H_{11}N_3O_2S_2$ (Dark yellow, 80%)	198-200	—	56.32 (56.30)	3.25 (3.23)	12.40 (12.32)	18.50 (18.77)
$Mn(C_{16}H_{10}N_3O_2S_2)_3$ (Blackish brown, 70%)	156[d]	5.10 (5.12)	53.66 (53.58)	2.80 (2.79)	11.70 (11.72)	17.90 (17.86)
$Fe(C_{16}H_{10}N_3O_2S_2)_3$ (Reddish brown, 68%)	227-229	5.20 (5.21)	53.55 (53.51)	2.70 (2.74)	11.75 (11.71)	17.85 (17.84)
$Co(C_{16}H_{10}N_3O_2S_2)_2(H_2O)_2$ (Blue, 72%)	275	7.50 (7.61)	49.60 (49.55)	3.25 (3.10)	10.70 (10.83)	16.45 (16.53)
$Ni(C_{16}H_{10}N_3O_2S_2)_2(H_2O)_2$ (Light brown, 65%)	149[d]	7.80 (7.61)	50.10 (49.60)	2.90 (3.10)	10.95 (10.80)	16.50 (16.61)
$Cu(C_{16}H_{10}N_3O_2S_2)_2$ (Dirty green, 74%)	165[d]	9.01 (8.72)	51.90 (51.68)	2.50 (2.69)	11.50 (11.31)	17.50 (17.23)
$Zn(C_{16}H_{10}N_3O_2S_2)_2$ (white, 66%)	210-212	9.01 (8.72)	51.70 (51.54)	2.90 (2.68)	11.50 (11.28)	17.10 (17.18)

d = decomposed.

non-electrolytic nature. The thermogravimetric analysis indicate that the hydrated complexes, $CoL_2(H_2O)_2$ and $NiL_2(H_2O)_2$, lose two water molecules in the temperature range 150-170°C indicating that the water molecules are coordinated and not lattice held[11].

A comparison of the IR spectrum of the ligand with those of the metal chelates revealed that in the case of metal complexes νNH band (3200 cm^{-1}) was absent, the cyclic νC=N band (1610 cm^{-1}) was shifted to a lower frequency by 10-30 cm^{-1}, and a new sharp band appeared in the region 1650-1670 cm^{-1} assignable to exocyclic νC=N. This suggests that in the ligand both the tautomeric forms are present in equilibrium mixture with the C=S from predominating. Coordination through −C−S−H moiety shifts the equilibrium towards the other side leading to predominance of −C−S−H. The other coordination centre is the nitrogen of the oxadiazole ring. This is also supported by the consideration of ring size: the proposed N, S-coordination is more likely since it gives a six-membered chelate ring, whereas S, S-coordination will result in a less stable four membered ring, on the other hand the lesser availability of sulphur atom for coordination is also responsible.

The chelates of Co(II) and Ni(II) exhibited two extra bands around 660 and 820 cm^{-1} attributable to wagging and rocking modes of coordinated water[12]. In the far-IR spectra of chelates, new bands were observed in the range 515-530 cm^{-1} and 380-405 cm^{-1} compatible with ν(M−N) and ν(M−S) respectively[13,14]. Electronic spectra and magnetic susceptibility studies suggest octahedral

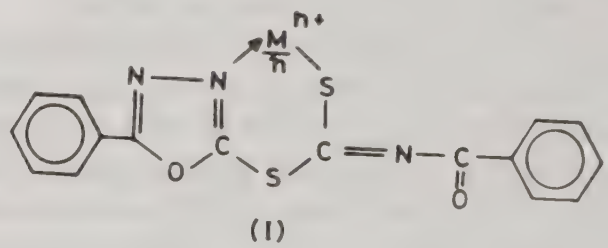

(I)

environment around Mn(III), Fe(III), Co(II) and Ni(II) ions in their chelates[15]. However, ligand field parameters of Co(II) and Ni(II) chelates have also been calculated and B and β values thus obtained are indicative of substantial covalent character[15]. Electronic spectra and magnetic moment values also suggest square planar and tetrahedral environment around Cu(II) and Zn(II) ions in their chelates respectively. ^1H NMR spectra shows multiplets observed at δ 6.76-8.28 for phenyl protons in the ligand and its complexes. In the ligand, a broad signal for −NH proton appears at δ 9.98, which however disappears in the corresponding complexes indicating the removal of −NH proton during the course of chelation. This is in agreement with our suggestion made on the basis of IR spectra.

In view of the above studies, the most probable structure assigned to these metal chelates is shown in (I) where $n=3$ for M=Mn(III), Fe(III); and $n=2$ for M=Co(II), Ni(II), Cu(II), Zn(II). Two molecules of water are also coordinated in the case of Co(II) and Ni(II) chelates.

Fungicidal screening

The antifungal activity was evaluated against *Aspergillus niger* and *Fusarium oxysporum* by the

Table 2—Fungicidal activity of POBDC and its metal chelates

Compound	Average percentage inhibition *in vitro* after 96 hr					
	A. niger at			*F. oxysporum* at		
	1000 ppm	100 ppm	10 ppm	1000 ppm	100 ppm	10 ppm
$C_{16}H_{11}N_3O_2S_2$	71.9	44.9	24.12	69.2	42.6	16.7
$Mn(C_{16}H_{10}N_3O_2S_2)_3$	83.6	53.3	36.1	83.7	56.9	34.0
$Fe(C_{16}H_{10}N_3O_2S_2)_3$	80.1	65.3	29.8	70.1	45.2	19.6
$Co(C_{16}H_{10}N_3O_2S_2)_2(H_2O)_2$	78.6	54.1	34.0	74.8	52.5	23.5
$Ni(C_{16}H_{10}N_3O_2S_2)_2(H_2O)_2$	76.5	45.2	26.0	70.5	50.8	20.2
$Cu(C_{16}H_{10}N_3O_2S_2)_2$	77.0	47.0	34.5	76.1	46.2	28.3
$Zn(C_{16}H_{10}N_3O_2S_2)_2$	90.1	75.2	43.2	89.2	71.3	41.8
Dithane M-45 (Commercial fungicide)	100.0	79.8	62.5	95.2	76.5	60.5

Number of replicates in each case = 3.

usual agar-plate technique[16] at 1000, 100 and 10 ppm concentrations as described earlier[2].

All the tested compounds had significant fungitoxicity at 1000 ppm but their toxicity decreased markedly on dilution (at 100 and 10 ppm). The metal chelates were more potent against both the test fungi than their parent dithiocarbamate (Table 2). This is understandable in the sense that chelation reduces considerably the polarity of the metal ion in the complex, mainly due to partial sharing of its positive charge with the donor groups and possible π-electron delocalization over the whole chelate ring system through dπ-dπ or pπ-dπ interactions of the ligand orbital and the metal ion. This in turn increases the hydrophobic character of the metal chelate favouring its permeation through lipoid layers of fungal membranes. It was interestingly observed that Mn(III) and Zn(II) chelates exhibited fungicidal activity of the order of Dithane M-45 at 1000 ppm, and inhibited ~40% growth of both the fungal species even at 10 ppm.

Acknowledgement

The authors are thankful to the Head, Dept. of Chemistry, Gorakhpur University, Gorakhpur for providing necessary laboratory facilities and to CDRI, Lucknow for elemental analyses. Thanks are also due to Dr R S Srivastava, Departmento Di Scienze Chimiche, Universita Di Trieste, Trieste Italy, for recording IR, NMR and UV spectra.

References

1 Green M B, Hartley G S & West T F, *Chemicals for crop protection and pest control* (Pergamon Press Ltd, UK) 1979.
2 Singh H, Yadav L D S & Mishra S B S, *J inorg nucl Chem*, 43 (1981) 1701.
3 Dutta M M, Goswami B N & Kalaky J C S, *J heterocycl Chem*, 23 (1986) 793.
4 Sinnur K H, Siddappa S, Hiremath Shivayogi P & Purohit M G, *Indian J Chem*, 25B (1986) 716.
5 Mistubishi Chemical Industries Co Ltd, Japan Kokai Tokkyo Koho, JP60 (1985) 85, 109; *Chem Abstr*, 103 (1985) 178266z.
6 Singh H, Mishra A R & Yadav L D S, *Indian J Chem*, 26B (1987) 1000.
7 Martiz B S & Van Eldik R, *Inorg chim Acta*, 17 (1976) 21.
8 Chatt J, Duncansan L A & Vananzi L M, *Nature*, 177 (1956) 1042.
9 Martin R L & White A H, *Trans met Chem*, 4 (1968) 113.
10 Newton M D, *J phys Chem*, 90 (1986) 3734-9; *Chem Abstr*, 105 (1986) 678298h.
11 Sharma V K, Pandey O P & Sengupta S K, *Trans Met Chem*, 14 (1989) 263.
12 Camo I, *Bull chem Soc Japan*, 34 (1961) 760.
13 Adams D M, *Metal-ligand and related vibrations* (Edward Arnold, London) 1967.
14 Nakamoto K, *Infrared spectra of inorganic and coordination compounds* (Interscience, New York) 1970.
15 Lever A B P, *Inorganic electronic spectroscopy* (Elsevier, New York) 1968 p 318, 328, 333.
16 Horsfall J G, *Bot Rev*, 11 (1945) 357.
17 Vogel A I, *A text book of quantitative inorganic analysis* (ELBS and Longmans Green and Co, London) 1978.
18 Young R W & Wood K H, *J Am chem Soc*, 77 (1955) 400.

Indian Journal of Chemistry
Vol. 31A, July 1992, pp. 475-477

Reactions of triarylantimony with some carboxylic acids

Ashok K S Chauhan*, Rita Sharma & Ramesh C Srivastava*
Department of Chemistry, Lucknow University,
Lucknow 226 007

Received 4 July 1991; revised 9 December 1991;
accepted 13 January 1992

Triarylantimony compounds are directly converted to the corresponding triarylantimony(V) dicarboxylates, $Ar_3Sb(OOCR)_2$ [$R = CH_2I$, CH_2Br, CH_2Cl, CCl_3, CF_3, 3,5-$(NO_2)_2C_6H_3$] by a number of carboxylic acids under mild conditions. Iodoacetic acid reacts more readily than chloro- or bromo-acetic acid. There is no evidence of any Sb-Ar bond cleavage.

Several methods for obtaining triorganoantimony(V) dicarboxylates, $R_3Sb(OOCR')_2$, have been reported in the literature[1-5]. Comparatively very little[6] is known about organoantimony(III) carboxylates, $R_2SbOOCR$ and $RSb(OOCR)_2$. The direct reaction between triarylbismuth, Ar_3Bi, and carboxylic acids leads to Bi-C bond(s) cleavage to give $Ar_nBi(OOCR)_{3-n}$ (ref. 7). Extension of this reaction to triarylantimony, as a possible route to organoantimony(III) carboxylates, therefore, appeared worthwhile.

In this note, results of the interaction of triarylantimony with a number of carboxylic acids are described.

Experimental

The Ar_3Sb compounds were prepared by Wurtz's method[8]. Ar_3SbCl_2 were obtained by an improved method involving the reaction of Ar_3Sb with methanol solution of HCl [produced by adding acetyl chloride (~ 3 ml) to methanol]. The solid carboxylic acids (BDH) were used as such and the liquids were freshly distilled. Solvents were dried by conventional methods. IR spectra (4000-400 cm^{-1}) were recorded on a Perkin-Elmer 337 spectrophotometer. ^1H NMR spectra (using TMS as internal standard) were recorded on A-90D spectrometer at the RSIC, Lucknow.

Reactions of triarylantimony with carboxylic acids

(i) Tri-*p*-tolylantimony (1.0 g, 2.5 mmol) and iodoacetic acid (0.94 g, 5.06 mmol) were dissolved in benzene (15 ml) and heated to ~ 100° for 5 hr. After removing the solvent by distillation, the residue was crystallized from benzene/hexane to obtain pale yellow crystals of tri-*p*-tolylantimony(V) diiodoacetate.

Other dicarboxylates were prepared in the same way except that the reactions with CX_3COOH (X = F, Cl) were carried out in dichloromethane at 0°.

(ii) Tri-*p*-tolylantimony (1.0 g, 2.5 mmol) and bromoacetic acid, freshly distilled, (0.70 g, 5.06 mmol) were dissolved in benzene (15 ml) and heated to 100° for 8 hr. After removing the solvent by distillation, the residue was crystallized from benzene/hexane to get crystals of tri-*p*-tolylantimony(V) dibromoacetate (0.47 g, 34%), m.p. 98°C. Unreacted tri-*p*-tolylantimony (0.5 g) was also recovered from hexane.

Preparation of $(p\text{-}MeC_6H_4)_3Sb(OOCCH_3)_2$

Attempts to prepare this compound by the direct reaction of $(p\text{-}MeC_6H_4)_3Sb$ with acetic acid failed. It was, however, prepared as follows:

Silver acetate (0.60 g, 3.6 mmol) and tri-*p*-tolylantimony dibromide (1.0 g 1.8 mmol) were stirred together in benzene (~ 20 ml) for ~ 6 hr. After filtering off the silver bromide the filtrate on concentration gave $(p\text{-}CH_3C_6H_4)_3Sb(OOCCH_3)_2$ (0.85 g, 66%), m.p. 202°C.

Results and discussion

Triarylantimony(III) reacted with a number of carboxylic acids under mild conditions to give the corresponding triarylantimony dicarboxylates (Eq. 1).

$$Ar_3Sb + 2HOOCR \rightarrow Ar_3Sb(OOCR)_2 + H_2 \quad \ldots (1)$$

(Ar = Ph, $p\text{-}CH_3C_6H_4$)

Nearly quantitative yields were obtained with $R = CH_2I$, CF_3, CCl_3, 3,5-$(NO_2)_2C_6H_3$, but surprisingly, reaction with $R = CH_2Cl$ or CH_2Br was sluggish under similar conditions. At present we are unable to explain this difference in the reactivity between iodoacetic acid and chloro- or bromo-acetic acid. Acetic acid, benzoic acid, *p*-chlorobenzoic acid and phenylacetic acid did not react probably due to comparatively weaker protonic character of these acids (see Eq. 2).

Unlike triarylbismuth(III), there was no evidence of a Sb-aryl bond cleavage. A solution of tri-*p*-tolylantimony and iodoacetic acid in deutrated chloroform did not show the presence of free tolu-

Table 1—Analytical, IR and NMR spectral data of triarylantimony(V) dicarboxylates

S.No.	$Ar_3Sb(OCOR)_2$		m.p. (°C)	Yield (%)	Found (Calc) %		Chemical shifts (δ)			
	Ar	R			C	H	Aromatic CH			
							ortho	meta	CH_3	CH_2
1.	Ph	CH_2I[a]	116	82	36.18 (34.14)	2.65 (2.60)	7.9m	7.4m	—	3.4s
2.	*p*-tolyl	CH_2I[b]	138	85	40.00 (39.18)	3.41 (3.41)	7.8d	7.2d	2.4s	3.28s
3.	*p*-tolyl	CF_3	240d	60	49.01 (48.32)	3.68 (3.40)	—	—	—	—
4.	*p*-tolyl	$C_6H_3(NO_2)_2$[c]	227	66	51.91 (51.41)	3.48 (3.32)	7.8d	7.24d	2.3s	—
5.	*p*-tolyl	$CHCHOC_4H_3(NO_2)$	176	67	55.92 (55.20)	4.60 (4.10)	7.76d	7.16d	2.36s	—
6.	*p*-tolyl	CH_3	202	66	59.22 (58.58)	5.72 (5.30)	7.78d	7.2d	2.34s 1.8s[d]	—

[a]I, Found 34.98; Cal. 35.10%
[b]I, Folund 32.80; Cal. 33.11%
[c]N, Found 6.52; Cal. 6.85%
[d]Acid Me protons

ene (in ^1H NMR) even after being refluxed for ~5 hr. This difference in the reactivity of Bi—aryl and Sb—aryl bonds towards electrophiles is not wholly unexpected and has been observed earlier in the case of IX (X=Cl, CN)[9] and 3,5-$(NO_2)_2C_6H_3COCl$[10] and may be attributed to the lower basicity of triarylbismuth(III) and overriding preference of Bi for oxidation state (III).

The direct formation of the dicarboxylates $Ar_3Sb(OOCR)_2$ may involve initial oxidative addition of the acid followed by the reaction of Sb-H bond with a second molecule of the acid (Eq. 2). This derives support from the facts that (i) carboxylic acids readily undergo oxidative addition/protonation reaction with tertiary phosphines[11] as well as coordinatively unsaturated transition metal complexes[12] and (ii) Sb—H bond is very unstable[13].

$$Ar_3Sb + HOOCR \longrightarrow [Ar_3Sb \rightarrow H^+][OOCR]^- \rightleftharpoons Ar_3Sb(OOCR)(H) \xrightarrow{HOOCR} Ar_3Sb(OOCR)_2 + H_2 \quad \cdots (2)$$

Eq. (1) is particularly interesting in the case of iodoacetic acid as attempts to prepare triarylantimony(V) diiodoacetates by other established methods[2] failed due to the liberation of free iodine.

The dicarboxylate were characterized by comparing their m.p. and IR spectra with those reported earlier and the ones which have been prepared for the first time by elemental analysis, IR and ^1H NMR spectra (Table 1). The ν(COO) frequency for triorganoantimony(V) dicarboxylates has been discussed[1,14] before and interpreted in terms of ester type RCOO groups arising from C_{2v} symmetry of $-CO_2-$ group and our results are no different.

The ^1H NMR spectra of tri-*p*-tolylantimony(V) dicarboxylates are interesting. Thus, $(p\text{-}CH_3C_6H_4)_3Sb(OOCCH_2I)_2$ shows two singlets at δ 3.38 and δ 2.4 ppm due to methylene and methyl protons respectively. The aryl protons appear as two doublets centred at δ 7.8 and δ 7.2 ppm due to *ortho* protons [$^3J(H-H)=8$ Hz] and *meta* protons [$^3J(H-H)=8$ Hz] respectively. Both the doublets show a downfield shift with respect to $(p\text{-}CH_3C_6H_4)_3Sb$; the former being more deshielded, shifts more than the latter. Thus, the ^1H NMR spectra of (*p*-tolyl)antimony derivatives may be used to follow the reations of $(p\text{-}CH_3C_6H_4)_3Sb$ as both $(p\text{-}CH_3C_6H_4)_3SbX_2$ and $(p\text{-}CH_3C_6H_4)_nSbX_{3-n}$ derivatives show[15] considerable lower field shifts of the *ortho* and *meta* protons.

Acknowledgement

We are thankful to Dr (Miss) Anju Asthana for carrying out the initial experiments with iodoacetic acid. We are also grateful to the Department of Atomic Energy, Bhabha Atomic Research Centre, Bombay for awarding Dr K.S. Krishnan Fellowship to one of the authors (R.S.) and the CSIR, New Delhi for financial assistance.

References

1 Goel R G, Maslowsky (Jr) E & Scnoff C V, *Inorg nucl Chem Lett*, 6 (1970) 833; *Inorg Chem*, 10 (1971) 2572.

2 Bajpai K, Singhal R & Srivastava R C, *Indian J Chem*, 18A (1979) 73.

3 Havranek J & Mleziva J, *J organometal Chem*, 157 (1978) 163.

4 Ladochnikova V J, Panov E M & Kocheshkov K A, *Zh obsnch Khim*, 34 (1964) 946.

5 Challenger F & Wilon V K, *J chem Soc*, (1927) 209.

6 Weiber M & Fetzer Kremling I, *Z Naturforsch*, 39*b* (1984) 754; Bone S P & Sowerby D B, *J organometal Chem*, 184 (1980) 181.

7 Freedman L D & Doak G O, *Chem Rev*, 82 (1982) 22.

8 Olifirenko S P, Visn & Lvivs'k, *Chem Abstr*, 63 (1965) 8401.

9 Wilkinson J F & Challenger F, *J chem Soc* (1924) 854; Bhattacharya S N & Singh M, *Indian J Chem*, 16A (1978) 778.

10 Asthana A & Srivastava R C, *J organometal Chem*, 366 (1989) 281.

11 Allman T & Goel R G, *Can J Chem*, 60 (1982) 716.

12 Collman J P & Hegedus L S, *Principles and applications of organotransition metal chemistry* (University Science Book, California) 1980.

13 Haiduc I & Juckerman J J, *Basic organometallic chemistry* (Walter de Gruyter, Berlin) 1985, p. 208.

14 Goel R G & Ridley D R, *J organometal Chem*, 38 (1972) 83.

15 Deacon G B, Roy Jackson W & Pfeiffer J M, *Aust J Chem*, 37 (1984) 527.

Indian Journal of Chemistry
Vol. 31A, July 1992, pp. 478-479

Mixed ligand complex formation of Cu^{2+} ion with 6-aminopenicillanic acid in the presence of bipyridine, glycine and adenine

G N Mukherjee* & T K Ghosh
Department of Chemistry, University College of Science,
92 Acharya Prafulla Chandra Road, Calcutta 700 009

Received 29 April 1991; revised and accepted
9 September 1991

A *p*H-metric study of the mixed ligand complex formation of Cu^{2+} ion with 6-aminopenicillanic acid (apaH) and bipyridine/glycine/adenine (L) has been carried out at 37°C in aqueous solution ($I = 0.1\,M\,NaNO_3$). The results show the evidence of formation of ternary complexes of the type Cu(apa)(L), in addition to the binary complexes Cu(apa) and Cu(L). Quaternary hydroxo complexes, Cu(apa)(L)(OH) and Cu(apa)(L)$(OH)_2$ have been identified at *p*H > 7. Complexation equilibria are evaluated with the aid of the computer programme, SCOGS, and correlated with the modes of bonding of the ligand.

Penicillin group of drugs, because of their ability to inhibit protein synthesis in the ribosome, are widely used in medicine as broad spectrum antibiotics[1]. A study on the chemical equilibria in the metal-drug-ligand systems may be of importance in exploring the molecular mechanism of action of these drugs. In this note we describe the results of our *p*H metric study, on the mixed ligand complex formation of Cu^{2+} ion with 6-aminopenicillanic acid, hereafter, apaH (I) in the presence of some typical ligands of biological importance, viz., bipyridine, glycine and adenine in aqueous solution at 37 ± 0.1°C at a fixed ionic strength ($I = 0.1\,M\,NaNO_3$).

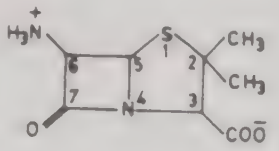

Experimental

AR quality 6-aminopenicillanic acid, bipyridine, glycine and adenine, obtained from Aldrich Chemical Company, Inc. (USA), were used as such. For the determination of binary Cu^{2+}-ligand stability constants, the Cu^{2+}: ligand ratios in the experimental solutions were kept 1:1, 1:5 and 1:10. For studying the mixed ligand complexation equilibria the Cu^{2+}: apaH:L ratios were 1:1:1 and 1:2:1.

Stability constants, β_{pqrs}, of ternary $[Cu_p(L)_q(apa)_r(OH)_s]$ complexes as defined below:

$$pCu + qL + rapa + sOH \rightleftharpoons Cu_pL_q(apa)_r(OH)_s$$

$$\beta_{pqrs} = \frac{[(Cu)_p(L)_q(apa)_r(OH)_s]}{[Cu]^p[L]^q[apa]^r[OH]^s} \quad \ldots (1)$$

were calculated with the aid of SCOGS programme[2] run on a PC-XT computer system. Proton-ligand and Cu^{2+}-ligand binary stability constants[3-8], supplied to the computer as input data, were also determined under identical conditions.

Results and Discussion

The ligand species $apaH_2^+$ titrates as a biprotic acid and acts as a (N,O) and (N,S) bidentate chelating agent towards Cu^{2+} to form only 1:1 binary complexes using the amino nitrogen and carbonyl oxygen or thiazolidine sulphur atoms[3]. Binary Cu(L) and Cu(apa) species are predominant at *p*H values lower than 5. The region between *p*H 5 and 8 is dominated by the ternary Cu(L)(apa) complexes, which are formed according to the following equilibria:

$$Cu + LH + apaH \rightleftharpoons Cu(apa)(L) + 2H \quad \ldots (ii)$$

$$Cu(apa) + LH \rightleftharpoons Cu(apa)(L) + H \quad \ldots (iii)$$

$$Cu(L) + apaH \rightleftharpoons Cu(apa)(L) + H \quad \ldots (iv)$$

$$Cu(L) + Cu(apa) \rightleftharpoons Cu(apa)(L) + Cu \quad \ldots (v)$$

where, L = bipy, gly^- and ad^-. These equilibria are supported by the species distribution curves (Fig. 1). Charges are omitted for clarity. The stability constants of ternary complexes, $\beta^{Cu}_{Cu(L)(apa)}$, were directly

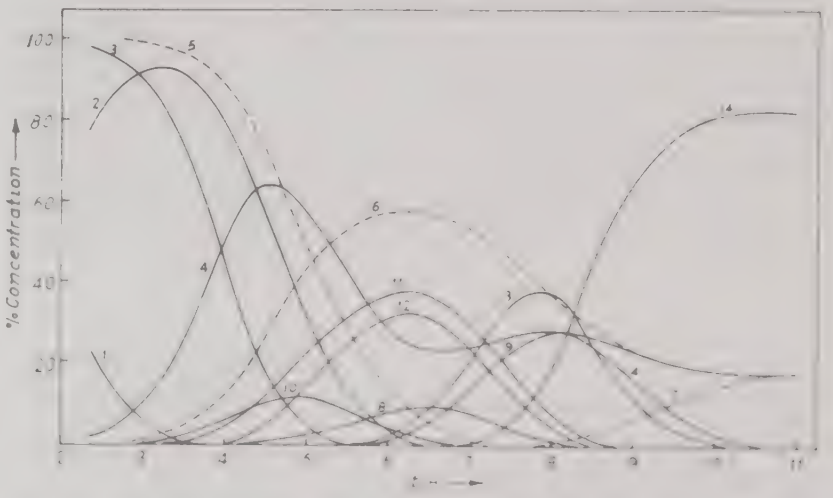

Fig. 1—Species distribution curves of Cu^{2+}-ad-apa system [1. $apaH_2^+$; 2. $apaH^+$; 3. adH_2^+; 4. adH; 5. Cu^{2+}; 6. apa^-; 7. ad^-; 8. $Cu(OH)^+$; 9., $Cu(OH)_2$; 10. $Cu(apa)^+$; 11. $Cu(ad)^+$; 12. Cu(apa)(ad); 13. Cu(apa)(ad)$(OH)^-$; 14. Cu(apa)(ad)$(OH)_2^{2+}$]

Table 1—Cu^{2+}/L/apa ternary constants, β_{pqrs}, with L = bipy, gly and ad at 37 ± 0.1°C in aqueous solution (I = 0.1 M $NaNO_3$)

$\log\beta_{pqrs}$	L		
	bipy	gly	ad
$\log\beta^{Cu}_{Cu(L)(apa)}$	12.54	12.86	13.17
$\log\beta^{Cu}_{Cu(L)(apa)(OH)}$	6.04	6.21	6.12
$\log\beta^{Cu}_{Cu(L)(apa)(OH)_2}$	−2.16	−2.84	−2.13
$\log K^{Cu(L)}_{Cu(L)(apa)}$	4.72	4.74	4.52
$\log K^{Cu(apa)}_{Cu(apa)(L)}$	8.44	8.76	9.07
$pK^{H}_{Cu(L)(apa)}$	6.50	6.65	7.05
$pK^{H}_{Cu(L)(apa)(OH)}$	8.65	9.05	8.25
$\Delta\log K_{Cu}$	0.62	0.64	0.42

Ionic product of water pK_w (at 37°C), 13.65; limits of error in the constants ± 0.02- ± 0.05 log units.

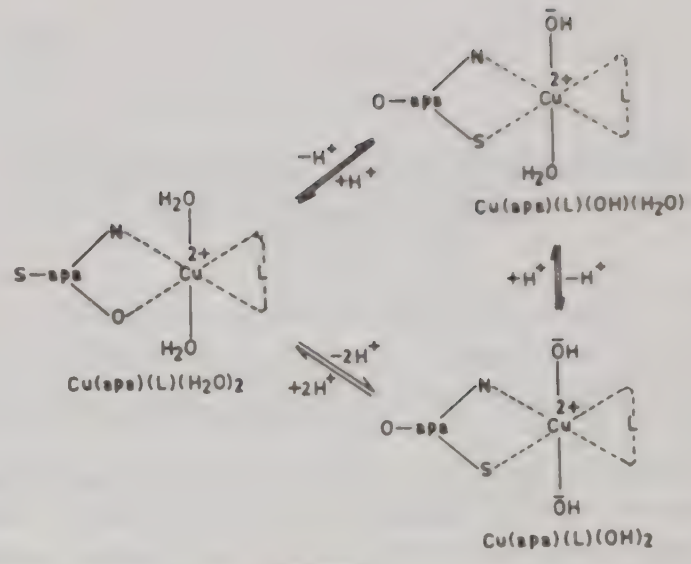

Scheme 1

computed from which the other constants, viz., $K^{Cu(apa)}_{Cu(apa)(L)}$, $K^{Cu(L)}_{Cu(L)(apa)}$ and $\Delta\log K_{Cu}$ were calculated using standard relations[9] (Table 1).

$\Delta\log K_{Cu}$ values are positive suggesting favoured formation of the ternary Cu(L)(apa) complexes.

With rise of pH, all these ternary Cu(L)(apa) complexes disappear and two quaternary hydroxo complexes, $Cu(L)(apa)(H_2O)(OH)^-$ and $Cu(L)(apa)(OH)_2^{2-}$ are formed, obviously due to successive deprotonation of the two coordinated H_2O molecules in these complexes. Intramolecular rearrangement involving the replacement of the carbonyl oxygen atom from the copper coordination sphere by the thiazolidine sulphur atom, according to the following equilibria (Scheme 1), possibly provides the driving force leading to the deprotonation of coordinated H_2O molecules. Such transformation of apa^- from (N, O) bidentate to (N, S) bidentate ligand within the coordination complex increases electronegativity of the Cu^{2+} ion as a consequence of delocalization of metal ion $d\pi$ electrons over to the vacant $d\pi$ orbitals of the sulphur atom, resulting in an increase in acidity of coordinated H_2O molecules. Such π-electron delocalization, however, is not possible when apa^- acts as a bidentate (N, O) chelating agent to Cu^{2+} ion, due to the absence of any π-acceptor orbitals on the oxygen atom. Deprotonation constants, $pK^{H}_{Cu(L)(apa)}$, $pK^{H}_{Cu(L)(apa)(OH)}$ are 5 to 7 log units lower than the pK_w of water. This indicates the extent of π-electron delocalization, Cu^{2+} $(d\pi) \rightarrow S(d\pi)$, in these ternary complexes.

Cu(L)(apa)(OH) complexes for L = bipy and gly contain about 80% of total copper at pH 8-9 and $Cu(L)(apa)(OH)_2$ contribute more than 90% at pH ≥ 10, whereas the $Cu(ad)(apa)(OH)^-$ and $Cu(ad)(apa)(OH)_2^{2-}$ complexes dominated at pH values greater than 7.

References

1 Egorov N S, *Antibiotics* (MIR Publishers, Moscow) 1985, 311.
2 Saycee I G, *Talanta*, 15 (1968) 1397.
3 Mukherjee G N & Ghosh T K, *J Indian chem Soc*, 68 (1991) 194.
4 Condike G F & Martell A E, *J inorg nucl Chem*, 31 (1969) 2455.
5 Israeli J & Volpe R, *Inorg chim Acta*, 6 (1972) 5.
6 Reinert H & Weiss R, *Hoppe Seyler's z physiol Chem*, 350 (1969) 1310.
7 Taquikhan M M & Krishnamoorthy C R, *J inorg nucl Chem*, 33 (1971) 1417.
8 Martin R B & Mariam Y H, *Metal ions in biological systems* (Marcel Dekker, New York), 8 (1979) 57
9 Sigel H, *Angew Chem (Internat Edn)*, 14 (1975) 394.

Indian Journal of Chemistry
Vol. 31A, July 1992, pp. 480-481

Spectrophotometric determination of molybdenum in steel

Atamjyot, Ashok Kumar Malik & A L J Rao*
Department of Chemistry, Punjabi University, Patiala147 002

Received 1 *October* 1991; *revised and accepted* 29 *January* 1992

A method has been developed for determining microamounts of molybdenum (VI) using cyclohexyl xanthate and thiocyanate after extraction with isobutyl methyl ketone in 2.0-7 *M* hydrochloric acid medium. The apparent molar absorptivity is 5.2×10^4 l mol^{-1} cm^{-1} at 500 nm. The method has been used for the rapid determination of molybdenum in alloy steels.

Molybdenum (VI) has been determined with thiocyanate after reduction, but the reduction is not quantitative[1]. In this note we report the reaction of molybdenum (VI) with cyclohexyl xanthate and ammonium thiocyanate in 2.0-7 *M* hydrochloric acid medium which forms a red coloured complex extractable into isobutyl methyl ketone. The method is sensitive and some of the trace elements like tungsten (VI), chromium (III) and vanadium (V) do not interfere. The method has been applied for the spectrophotometric estimation of molybdenum in alloy steels.

Experimental

Sodium cyclohexylxanthate was prepared by the method of Dewitt *et al.*[2]. A 0.1% solution of this reagent was prepared in distilled water and standardised titrimetrically using diphenylcarbazone as an internal indicator. Standard solutions of sodium molybdate[3] and ammonium thiocyanate solution (5%) were prepared in distilled water. Stock solutions (0.1%) of diverse metal ions and anions were prepared in distilled water for the interference studies. An SP-20 spectrophotometer was used for absorbance measurements.

Procedure

To an aliquot of the molybdenum (VI) solution, was added hydrochloric acid (2 ml, 10 *M*) cyclohexyl xanthate solution (1 ml) and ammonium thiocyanate solution (1 ml) and the contents diluted to 10 ml with distilled water. The resulting solution was stirred with 10 ml of isobutyl methyl ketone and the absorbance was measured at 500 nm against a reagent blank prepared under similar conditions.

Results and discussion

The observations indicated that the complex absorbs strongly at 500 nm, when the acidity of the reaction medium was kept in the range 2.0-7 *M* with hydrochloric acid. The mixed ligand complex was intensely coloured and stable for more than 70 hr in isobutyl methyl ketone.

Sodium cyclohexylxanthate (1 ml, 0.1%) and ammonium thiocyanate (1 ml, 5%) were sufficient for the maximum absorbance.

The mixed ligand complex was extractable in chloroform, isoamyl alcohol, ethyl acetate, butyl acetate, acetophenone, carbon tetrachloride and isobutyl methyl ketone. Since the maximum absorbance was observed in isobutyl methyl ketone, this solvent was chosen for further study.

The calibration curve was linear over the concentration range 2.4-14.5 μg of Mo(VI) in 10 ml of final solution. The molar absorptivity and the Sandell's sensitivity were calculated to be 5.2×10^4 l mol^{-1} cm^{-1} and 0.0018 μg/cm^2 at 500 nm respectively.

For interference studies, the determination of molybdenum was carried out in the presence of various anions and cations. Li^+, Mg^{2+}, Ca^{2+}, Na^+, K^+, Ba^{2+}, Al^{3+}, La^{3+}, Sn^{2+}, Pb^{2+}, Ti^{4+}, Zr^{4+}, Cr^{3+}, Mn^{2+}, Fe^{2+}, Cl^-, Br^-, I^-, SO_4^{2-}, F^-, CO_3^{2-}, HCO_3^-, NO_2^-, NO_3^-, citrate, borate, oxalate, tartrate (20-25 mg) are tolerable.

Cyclohexyl xanthate reacts with copper, cobalt and nickel under neutral conditions but in acidic media these metal ions fail to react. The metal ions V(V) and W(VI) are tolerated in the presence of ascorbic acid.

Determination of molybdenum in steel alloys

The validity of the method was checked by the determination of molybdenum (VI) in steel alloys. A 1-2 g of the alloy sample was dissolved in 10 ml of hydrochloric acid by heating gently and then evaporating to dryness. The residue was dissolved in 5 ml of concentrated nitric acid and evaporated again to dryness. The residue was dissolved in 1-2 ml of 4 *M* hydrochloric acid and diluted to 100 ml in a standard flask. To an aliquot of this solution was added 1 ml of 10% ascorbic acid solution and determined by general procedure. The following values were obtained: BHO 501 (Mo 0.47%) gave 0.465% and BHO 502 (Mo 0.77%) gave 0.768% Mo (average of five dererminations).

The proposed method has been found to be sensitive, selective and simple. There is no need of reducing agent, heating or pre-extraction. The sensitivity of the present method is comparable with other methods reported in literature[4-13].

References

1 Sandell E, *Colorimetric determination of traces of metals*, (Wiley Interscience, New York), 1959.
2 Dewitt C & Roper E, *J Am chem Soc*, 54 (1932) 444.
3 Vogel A I, *Quantitative inorganic analysis*, (Longmans, London), 1968, p 506.
4 Gupta U & Rao A L J, *Inst Chemists (India)*, 62 (1990) 183.
5 Willians D A, Holcomb I J & Baltz D F, *Analyt Chem*, 47 (1975) 20.
6 Chakrabarti A K & Bag S P, *Talanta*, 23 (1976) 736.
7 Singh A K & Kumar D, *Analyst*, 110 (1985) 75.
8 Desiva M E M S, *Analyst*, 100 (1975) 517.
9 Pilipenko A T, Samchuk A I & Zulfigarov O S, *Zh analit Khim*, 40 (1985) 1262.
10 Mitra M & Mitra B K, *Talanta*, 24 (1977) 689.
11 Gowda A T & Gowda N M M, *Analyst*, 110 (1985) 743.
12 Salinas F, Berzas-Nevado J J & Acedovalenzuela M I, *Talanta*, 32 (1985) 63.
13 Chakrabarti A K, *Indian J Chem*, 25A (1986) 884.

Indian Journal of Chemistry
Vol. 31A, July 1992, p. 482

Letter to Editor

Additions and corrections to the paper entitled, "Mössbauer studies on tin bearing catalysts used for hydrogenation of coal".

The manuscript of the paper entitled "Mössbauer studies on tin bearing catalysts used for hydrogenation of coal" [*Indian J Chem*, 29A (1990) 1118-21] of which I am a coauthor, was not shown to me prior to publication by Dr B K Sharma, the Indian coauthor. Some of the reported results need correction, specially the tin Mössbauer results as Dr Sharma was not fully aware of the parameters of the experimental set-up.

First of all, the linewidths, W, in Table 2 should be doubled, since the corresponding parameters supplied by the program, MOSFIT, are W/2. This results in three consequences:

(i) In the right hand side of page 1120, the lines 9 to 14 should be deleted.

(ii) $\Delta = 0$ for SnO_2 in samples CHS-11 and CHS-14 now are joined to too large values of the true W: this is often observed as mathematical alternative fitting solution when Δ is small enough. The higher values of Δ for SnO_2 reported in reference 7 of the title paper were shown to originate in very small particles. This statement should replace the lines 9 to 15 on the left hand side of page 1120.

(iii) The penultimate sentence of "Conclusion" should be deleted.

As to SnS, which appears as a minor component in the spectra and for which δ and Δ are not far from their usual values, the comparison between CHS-7, and CHS-14 is not easy. Contrary to the statement in the last lines of the left hand side of page 1120 in the title paper, the linewidths are nearly the same since in the original listing W/2 for CHS-14 is 0.518, instead of 0.578 which is given in Table 2.

Iron Mössbauer spectroscopy brings a little more information (but the isomer shifts refer to α-Fe and not to SNP as stated in "Experimental"). CHS-11, CHS-7 and CHS-14 samples clearly exhibit differences in the vacancy structure of their pyrrhotites, as indicated by the hyperfine magnetic fields, in pyrrhotite content and in the ratio Fe^{2+}/Fe^{3+}, which would require further investigation.

19 February 1992

P. Bussière
Institut de Recherches
sur la catalyse
69626 Villeurbanne
Cedex-France

C.F.T.R.I. REGIONAL CENTRE
6 JUL

Biotechnology has taken rapid strides in recent years and has emerged as one of the most promising branches of science. Committed to rooting out hunger by the creation of high-yielding, disease-resistant crops and pledged to resurrect the earth's verdant green cover, plant biotechnology holds the key to the world of tomorrow. Digging out closely guarded secrets from the inner recesses of the vault of life, and unleashing and channelizing nature's power of self-renewal, this particular brand of biotechnology has virtually rewritten the story of botanical genesis and prospects.

This attractive, profusely illustrated book written in a popular language highlights human creativity and imagination in coaxing life to spring from non-conventional sources and takes the reader on a trip down the woods of tomorrow.

Lovely, dark and deep forests fashioned in
test tubes by scientists who laboured
long because they had promises
to keep.

TEST TUBE FORESTS

A.F.MASCARENHAS
RAJANI NADGAUDA

Pages : 72
Price : Rs. 10.00

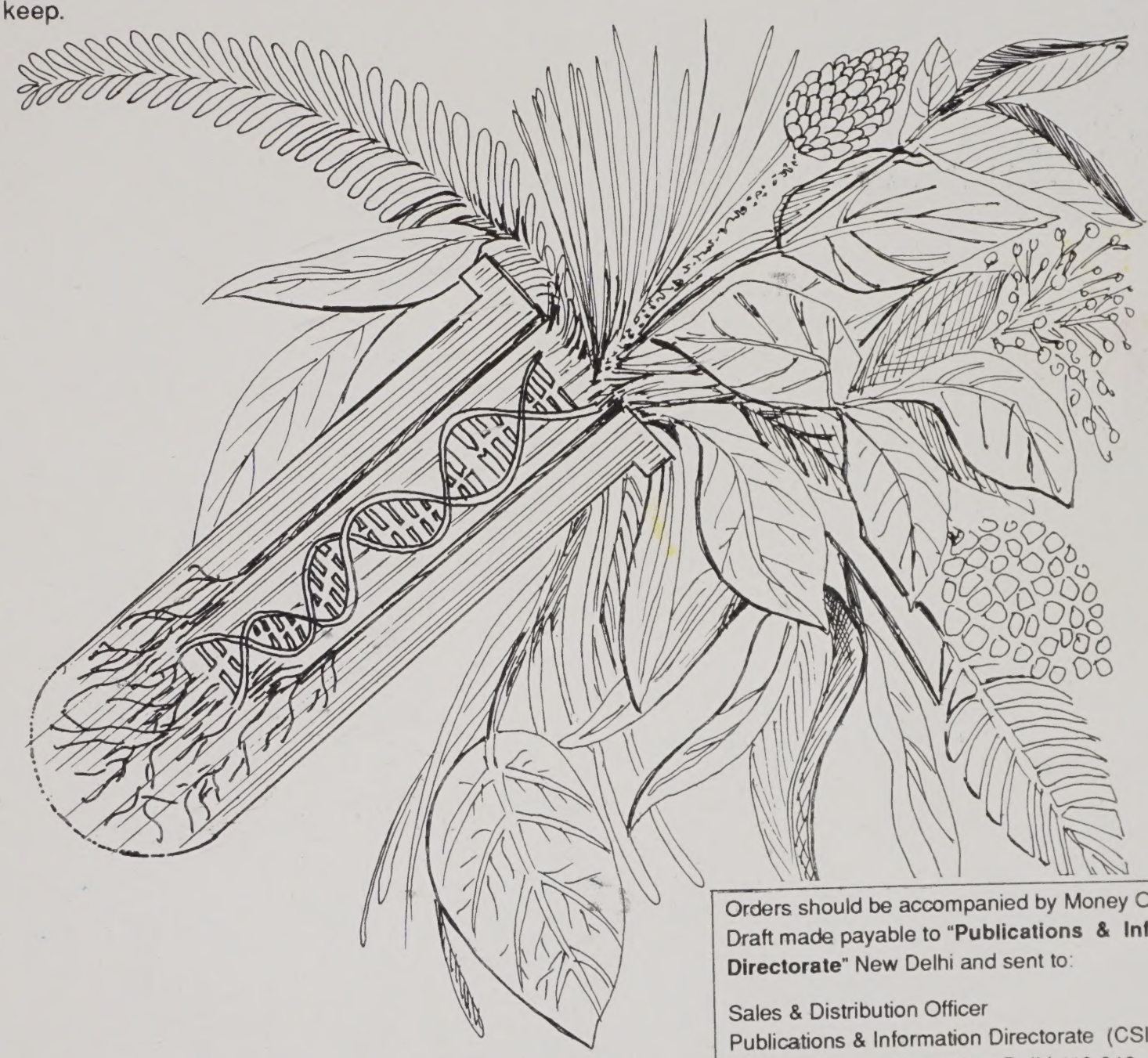

Orders should be accompanied by Money Order or Demand Draft made payable to "**Publications & Information Directorate**" New Delhi and sent to:

Sales & Distribution Officer
Publications & Information Directorate (CSIR)
Dr K.S.Krishnan Marg, New Delhi 110 012

Printed & Published by Dr. G.P. Phondke, Director, Publications & Information Directorate (PID)
Dr. K.S. Krishnan Marg, New Delhi 110 012, at PID.

BENSON & HEDGES
WORLD CUP 1992
The only official world cup Indian shoes

The most extravagant collection of SHOES with an unbeatable blend of contemporary STYLES and ultimate in COMFORT.

action® SHOES

DL-18023/92
RN 7090/63